Bilag 39

FINAL REPORT

Bioavailability and Methylation Potential of Mercury Sulfides in Sediments

SERDP Project ER-1744

August 2014

Heileen Hsu-Kim
Marc Deshusses
Duke University

SERDP
DOD ▪ EPA ▪ DOE

REPORT DOCUMENTATION PAGE

Form Approved
OMB No. 0704-0188

PLEASE DO NOT RETURN YOUR FORM TO THE ABOVE ORGANIZATION.

1. REPORT DATE *(DD-MM-YYYY)*	2. REPORT TYPE	3. DATES COVERED *(From - To)*
08-2014	Final Report	11-2009-08-2014

4. TITLE AND SUBTITLE
Bioavailability and Methylation Potential of Mercury Sulfides in Sediments

5a. CONTRACT NUMBER

5b. GRANT NUMBER

5c. PROGRAM ELEMENT NUMBER

6. AUTHOR(S)
Heileen Hsu-Kim

5d. PROJECT NUMBER
ER-1744

5e. TASK NUMBER

5f. WORK UNIT NUMBER

7. PERFORMING ORGANIZATION NAME(S) AND ADDRESS(ES)
Duke University
Department of Civil & Environmental Engineering
121 Hudson Hall, Box 90287 Durham, NC 27708

8. PERFORMING ORGANIZATION REPORT NUMBER
ER-1744

9. SPONSORING/MONITORING AGENCY NAME(S) AND ADDRESS(ES)
SERDP/ESTCP
4800 Mark Center Drive, Suite 17D08
Alexandria, VA 22350-3605

10. SPONSOR/MONITOR'S ACRONYM(S)
SERDP/ESTCP

11. SPONSOR/MONITOR'S REPORT NUMBER(S)

12. DISTRIBUTION/AVAILABILITY STATEMENT
Unlimited

13. SUPPLEMENTARY NOTES

14. ABSTRACT

In this project, we investigated the geochemical processes that control the bioavailability of mercury to methylating bacteria in contaminated sediments. The research tested the hypothesis that kinetically-limited mercury sulfide mineralization reactions, rather than equilibrium porewater chemistry, controls the concentration of bioavailable mercury to sediment bacteria that convert it to methylmercury, the form that bioaccumulates in food webs (Figure E.1). We studied the relationship between mercury speciation and biouptake/methylation in sediments, a relationship that remains poorly understood. The work focused specifically on the microbial methylation potential of nanoparticulate HgS in relation to bulk scale HgS and dissolved Hg-sulfide species. The aim was to establish a premise that links the 'age' and chemical form of Hg in sediment porewater to the rate of MeHg formation. The kinetic data was incorporated in a conceptual model describing the fate of mercury.

15. SUBJECT TERMS

16. SECURITY CLASSIFICATION OF:			17. LIMITATION OF ABSTRACT	18. NUMBER OF PAGES	19a. NAME OF RESPONSIBLE PERSON
a. REPORT	b. ABSTRACT	c. THIS PAGE		134	Stuart Strand
					19b. TELEPHONE NUMBER *(Include area code)* 916-660-5109

Reset

Standard Form 298 (Rev. 8/98)
Prescribed by ANSI Std. Z39.18

Table of Contents

List of Tables

List of Figures

Acronyms and Abbreviations

1pr3	Desulfobulbus propionicus 1pr3strain
AVS	Acid volatile sulfide
CLE-SPE	competitive ligand exchange – solid phase extraction
DEDC	diethyl dithiocarbamate
DGT	diffusive gradient in thin-film
DLS	dynamic light scattering
DMSP	dimethylsulfoniopropionate
DOC	dissolved organic carbon
DOM	dissolved organic matter
EDX	energy dispersive X-ray spectroscopy
FWHM	full width at half maximum of the peak
GSH	glutathione
HEPES	4-(2-hydroxyethyl) piperazine-1-ethanesulfonate
HgS	mercuric sulfide
MeHg	methylmercury
MeHgCl	methylmercury chloride
ND132	Desulfovibrio desulfuricans ND132 strain
nHgS	nanoparticulate HgS
NOM	natural organic matter
OD_{660}	optical density at 660 nm
PBS	phosphate buffer solution
SAED	selected area electron diffraction
SAXS	small angle X-ray scattering
SFEI	San Francisco Estuary Institute
SRB	sulfate-reducing bacteria
SRHA	Suwannee River humic acid
SSRL	Stanford Synchrotron Radiation Laboratory
TEM	transmission electron microscopy
TOC	total organic carbon
XAS	X-ray absorption spectroscopy
XRD	X-ray diffraction
XPS	X-ray photoelectron spectroscopy

Keywords
mercury, methylmercury, sulfide, sediment, methylation potential, bioavailability, nanoparticles

Abstract

Objectives. Mercury is a potent neurotoxin for humans, particularly if the metal is in the form of methylmercury. Mercury is widely distributed in aquatic ecosystems as a result of anthropogenic activities and natural earth processes. A first step towards bioaccumulation of methylmercury in aquatic food webs is the methylation of inorganic forms of the metal, a process that is primarily mediated by anaerobic microorganisms that are abundant in sediments. The production of methylmercury in the environment is controlled in part by the bioavailability of inorganic mercury Hg(II) to methylating microbes. In sediment porewater, mercury associates with sulfide and organic matter to form chemical species that include organic-coated mercury sulfide nanoparticles as reaction intermediates of heterogeneous mineral precipitation.

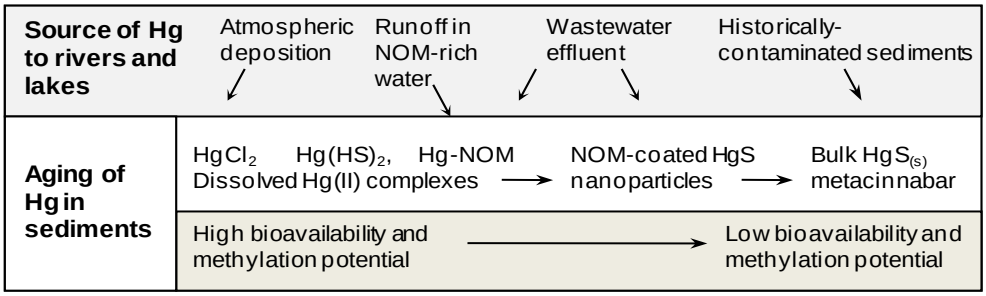

Figure A.1. Framework that links speciation and methylation potential through rate-limited chemical transformations of mercury, sulfide and dissolved organic matter (DOM) in sediments.

In this project, we investigated the geochemical processes that control the bioavailability of mercury to methylating bacteria in contaminated sediments. The research tested the hypothesis that kinetically-limited mercury sulfide mineralization reactions, rather than equilibrium porewater chemistry, controls the concentration of bioavailable mercury to sediment bacteria that convert it to methylmercury, the form that bioaccumulates in food webs (Figure E.1). We studied the relationship between mercury speciation and biouptake/methylation in sediments, a relationship that remains poorly understood. The work focused specifically on the microbial methylation potential of nanoparticulate HgS in relation to bulk scale HgS and dissolved Hg-sulfide species. The aim was to establish a premise that links the 'age' and chemical form of Hg in sediment porewater to the rate of MeHg formation. The kinetic data was incorporated in a conceptual model describing the fate of mercury. The overall goals of SERDP project #ER-1744 were to assess the importance of nanoscale mercuric sulfides for methylation potential in sediments and to develop a conceptual model that links mercury geochemical speciation to methylation potential in sediments.

Research Approach. The research involved four major tasks and is described in this report in Chapters 2 – 4 (Figure E.2). Tasks 1 and 2 (described in Chapter 2) involved pure culture studies in which the net production of MeHg was compare in bacterial cultures exposed to dissolved Hg and sulfide, nanoparticulate HgS, and bulk scale HgS. Research for Task 3 (Chapter 3) involved kinetic modeling of the Hg speciation and net MeHg production rate of the pure culture

experiments. The objective of the model calculation was to determine if the methylation of mercury originating from nanoparticles could be explained by dissolution of the particles and dissolved phase speciation. This model utilized kinetic expressions for complexation reactions involving dissolved Hg-ligand complexes and precipitation and dissolution reactions involving nanoparticles and microparticles of HgS. All dissolved forms of Hg were presumed to be bioavailable and rates of methylation and demethylation were fitted to previous methylmercury production experiments in which bacteria were exposed to dissolved mercury sulfides. The final component (Chapter 4) involved sediment slurry microcosm experiments in which the aim was to better capture the complexity of sediment settings in ways that could not be achieved with pure culture studies. The study involved sediment slurry microcosms that represented a spectrum of salinities in an estuary and were each amended with different forms of mercuric sulfides: dissolved Hg and sulfide, nanoparticulate HgS, and microparticulate HgS.

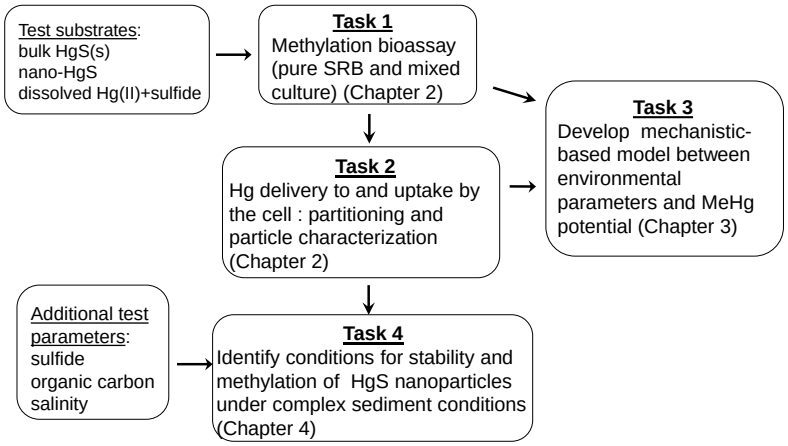

Figure A.2. Schematic of the research approach to evaluate the bioavailability of mercuric sulfides in contaminated sediments.

Results. The results of the pure culture studies demonstrated that bacteria cultures exposed to HgS nanoparticles methylated mercury at a rate slower than cultures exposed to dissolved forms of mercury. However, methylation of the nanoparticles was considerably faster than larger microscale HgS particles, even when normalized to specific surface area. Furthermore, the methylation potential of HgS nanoparticles decreased with storage time of the nanoparticles in their original stock solution, suggesting that crystal ripening of the nanoparticles reduced their methylation potential. The methylation of mercury derived from nanoparticles (in contrast to the larger particles) would not be predicted by traditional models of mercury bioavailability and was probably caused by the disordered structure of nanoparticles that facilitated release of chemically labile mercury species immediately adjacent to cell surfaces. Overall these findings add new dimensions to the understanding of mercury methylation potential by demonstrating that bioavailability is related to the geochemical intermediates of rate-limited mercury sulfide precipitation reactions.

In kinetic models of the pure culture experiments, the enhancement of methylmercury production in cultures exposed to HgS nanoparticles relative to HgS microparticles could be simulated by assigning larger dissolution rates for the nanoparticles. However, the model showed that calculation of dissolved mercury through dissolution of HgS particles provided an incomplete picture of the overall bioavailability. The simulations were improved if a fraction of the nanoparticulate phase was assumed to be directly bioavailable, either through direct uptake of nanoparticles or the immediate uptake of Hg dissolving from the nanoparticles directly outside the cell. Our results point to a new approach for modeling mercury speciation and bioavailability that considers the dynamic nature of mercury sulfide interactions in anaerobic environments.

In the sediment slurry microcosm experiments, the results indicated that net MeHg production was influenced by both the activity of sulfate-reducing microorganisms and the bioavailability of mercury. In the presence of abundant sulfate and carbon sources (resulting in relatively high microbial activity), net MeHg production in the slurries amended with dissolved Hg was greater than in slurries amended with nano-HgS, similar to previous experiments with pure bacterial cultures. However, in cases of minimal microbial activity (such as low sulfate reduction rate), the addition of either dissolved Hg or nano-HgS resulted in similar amounts of net MeHg production. For slurries receiving micro-HgS, MeHg production did not exceed abiotic controls. In slurries amended with dissolved and nano-HgS, mercury was mainly partitioned to bulk-scale mineral particles and colloids, such as iron sulfides, indicating that Hg bioavailability was not simply related to dissolved Hg concentration or speciation. Therefore, assessments of Hg bioavailability in sediments need to consider not only the dissolved phase speciation in pore water, but also the speciation of particle-bound Hg, including nanostructured species that may be weakly sorbed or more soluble than bulk mineral phases.

Benefits and Implications. The overall results of this work demonstrated that dissolved phase speciation alone is inadequate for understanding and predicting Hg bioavailability to methylating microorganisms. The transformation reactions involving these mercury species, such as cluster formation, monomer aggregation and crystal ripening, are often times kinetically-hindered in the presence of DOM[1]. Therefore, the bioavailability and methylation potential of mercury is most likely related to the ‘slow’ kinetics of these processes that control the relative abundance of various mercury species (i.e., those falling through a 0.2-μm filter), rather than the equilibrium chemistry. Future modeling efforts for predicting mercury bioavailability will need to consider the rate of transformations involving mercury species. Such an approach would require a series of rate constants for the geochemical reactions that dictate the concentration of the available forms of inorganic mercury for microbial methylation.

Chapter 1

Critical Review of Mechanisms Regulating Mercury Bioavailability for Methylating Microorganisms in the Aquatic Environment

This chapter was published as the following:
Hsu-Kim, H.; Kucharzyk, K.H.; Zhang, T.; Deshusses, M.A. (2013). Mechanisms regulating mercury bioavailability for methylating microorganisms in the aquatic environment: A critical review. *Environ. Sci. & Technol*. 47(6), 2441-2456. DOI: 10.1021/es304370g.

1.1 Introduction

Mercury (Hg) is a global pollutant that is released from both natural and anthropogenic sources[2]. Molecules and materials containing this trace element can spread widely in the nature (even in remote areas) through a complex web of transformation and transport processes. In most environmental settings, mercury exists as the elemental form Hg^0, inorganic divalent Hg(II), and organomercury compounds such as monomethylmercury (MeHg). Each form of mercury can impart health hazards, depending on the dose and route of exposure. MeHg is the species of most concern for humans[3], due to the highly bioaccumulative nature of this organomercurial compound[4]. The neurotoxic effects of MeHg to humans, particularly during early stages of brain development, have been well-documented[5,6]. Moreover, exposure rates to vulnerable portions of the population (maternal age women and newborn children) can be considerable. In the U.S. for example, maternal exposure rates suggest that10,000's to 100,000's of children are born each year with *in utero* MeHg exposures exceeding health guidelines[6,7]. Maternal consumption of fish is believed to be the major route of exposure for newborns. Because of the health risks, millions of river miles and lake acres in the U.S. have been placed under fish consumption advisories[8], indicating the widespread prevalence and persistence of methylmercury contamination in the environment.

The methylation of mercury in the aquatic environment is a critical step towards accumulation of this toxic metal in the aquatic food chain. MeHg is produced in the environment primarily by anaerobic bacteria that exist in most natural settings. MeHg levels in aquatic systems vary widely and do not necessarily correlate to the total amount of mercury in water or sediments[9]. Instead, mercury methylation rates generally depend on the productivity of the anaerobic microorganisms that can methylate mercury and the bioavailability of inorganic Hg(II) that can be taken up by these bacteria[10-12].

The processes that result in elevated methylmercury concentrations in the environment have received much attention in the last three decades, yet much is unknown concerning the forms of inorganic mercury that are available for methylation and the biochemical mechanisms by which microorganisms mediate this process. This information is needed to determine how methylmercury 'hotspots' occur in the environment and to predict the response of ecosystems that are directly or indirectly altered. For example, we have a limited ability to predict how an

ecosystem may respond to changes in the source and flux of mercury inputs from atmospheric deposition. Moreover, efforts to remediate contaminated soil and sediment are stymied by our poor understanding of factors controlling methylmercury production. Finally, longer term hydrological and ecological disturbances (such as those induced by climate change) are expected to alter mercury biogeochemistry in ways that remain unknown.

In this chapter, we review our current understanding of the mechanism of microbial mercury methylation and the research needed to address this problem. This review is particularly focused on assessing Hg(II) bioavailability – i.e., the geochemical forms of inorganic Hg(II) that can be taken up and methylated by anaerobic microorganisms. In most settings including the water column, aquatic sediments, and extracellular and intracellular matrices, the dissolved aqueous cation Hg^{2+} is a very small portion of total Hg(II)[13,14]. Rather, Hg(II) is predominantly coordinated to other molecules (e.g. natural organic matter, chloride, sulfide) or adsorbed to particle surfaces. The species of Hg(II) to which methylating microorganisms are exposed will govern rates of uptake and biotransformation (i.e. methylation). Therefore, in this review we evaluate the conventional approach for estimating Hg(II) bioavailability for methylating microorganisms, particularly in light of recent discoveries that point to a different approach. Much progress has been made to delineate the speciation and fractionation of Hg(II) in environments where methylation occurs. This recent work includes studies describing the nanoscale products of reactions involving mercury, sulfide, and dissolved organic matter and the contribution of these species to bioavailability for methylating bacteria [15-19]. Other active research areas include efforts to characterize the diversity of methylating microorganisms and identify the mechanisms of biouptake and methylation. Ultimately, an understanding of the factors influencing mercury methylation potential will inform risk assessments of emission sources and also lead to appropriate strategies for remediating contaminated ecosystems.

1.2 Sources and transformations of mercury in the environment

Mercury is released to the environment from a wide array of sources and cycles through all the compartments of the biosphere (e.g., atmospheric, aquatic, terrestrial), as described in review papers by others[12,20-22]. Natural sources of mercury include volcanic eruptions, forest fires, biomass burning, and low-temperature volatilization[23]. Anthropogenic sources to the biosphere include fossil fuel combustion, mining, waste disposal, and chemical production[23]. All of these sources release mercury to the atmosphere or mobilize the metal from terrestrial settings, leading to deposition or accumulation in aquatic ecosystems.

In the gaseous elemental form (Hg^0), mercury is capable of traveling across regional and global distances[2,24]. In the atmosphere, divalent forms of mercury Hg(II) partition more easily to water and particles (compared to Hg^0), resulting in much shorter distances over which Hg(II) travels in the lower troposphere . Thus, oxidative processes in the atmosphere strongly influence overall residence times[2]. In the aquatic environment, the major form of Hg is inorganic Hg(II), and redox reactions in surface waters can result in loss of gaseous elemental Hg^0 to the atmosphere. While MeHg is typically a small proportion of the total Hg in water and sediments, MeHg is the most toxicologically important species in regards to human health risks[4]. MeHg is better retained

by higher-level organisms than other Hg species and is the predominant form of mercury that biomagnifies in the aquatic food chain[25]. Previous evidence suggests that nearly all of the mercury (>85%) in the muscle tissue of fish occurs as MeHg[26-28]. Because of the large biomagnification factors of MeHg, fish body burdens for MeHg can be as high as 10^6 times the MeHg concentration in the surrounding water[3,29].

The accumulation of MeHg in biota is largely dependent on the MeHg concentration in water[10,12,14], which is controlled by multiple transport and transformation processes involved in the mercury biogeochemical cycle[20,21]. In particular, the balance between MeHg production and degradation, namely the rate of Hg(II) methylation relative to MeHg demethylation, determines the amount of MeHg in an aquatic system. Methylmercury can be generated from abiotic processes, particularly through pathways involving sunlight[30,31]. Likewise, sunlight degradation is believed to be a major pathway for the decomposition of MeHg at the surface of the water column[32-35]. However, in most freshwater and coastal aquatic settings, anaerobic microorganisms thriving in anoxic zones (such as benthic sediments, saturated soil, stratified water column, periphyton biofilms) are the dominant producers of MeHg. MeHg concentrations in these settings are typically a reflection of production and degradation processes that are occurring simultaneously and are mediated by a variety of microorganisms.

1.3 Microbial methylation and demethylation of mercury

In low oxygen aquatic settings, the production and degradation of methylmercury is predominantly a microbial process. The biological mechanisms of mercury methylation and demethylation in the environment have been described in recent review papers[11,36]. Thus, this section aims to summarize our current understanding of the microbiology of MeHg production/degradation, particularly in light of advances in the past few years.

1.3.1 Microbial production of methylmercury

Microbial Methylators. The methylation of mercury by microorganisms in water, soils, sediments, and even the human intestinal tract has been broadly reported in the literature[37-42]. To date, the isolated environmental strains that are capable of mercury methylation have fallen mostly in the delta-*proteobacteria* classification[11,43,44], with a few exceptions[45]. The most studied methylators of inorganic Hg(II) for environmental settings belong to sulfate-reducing bacteria (SRB), a group of obligate anaerobes that utilize sulfate as their terminal electron acceptor for energy generation[46]. Methylmercury production by iron-reducing bacteria and methanogens has also been observed in several instances[47-49]. Nevertheless, the dominant role of SRB in Hg(II) methylation is supported by extensive experimental evidence obtained with numerous pure SRB strains isolated from environmental settings[11] and in microcosm experiments with mixed microbial communities derived from sediments, low oxygen regions of the water column, and periphyton [46,50,51] . Evidence supporting the mercury methylating role of SRB in mixed communities generally stem from experiments where the addition of sulfate resulted in enhanced MeHg production (in sulfur-limited settings[52]) and the addition of molybdate, a selective inhibitor of sulfate reduction in SRB, suppressed Hg(II) methylation[46,51]. However, the ability of mercury

methylation does not appear to correspond with the phylogeny of SRB. For example, not all SRB can methylate mercury[30]. Also, the capacity to generate MeHg amongst SRB was found to depend on the strain rather than species or genus[44].

Among the non-SRB strains that can produce MeHg, researchers have isolated dissimilatory iron-reducing *Geobacter* spp. which are phylogenetically close to some methylating SRB within the class of delta-*proteobacteria*[47,49]. The ability to methylate Hg is not common to all iron-reducing bacteria, as indicated by the absence of mercury methylation capabilities by several *Shewanella* spp.[49] Methanogenic activity in macrophytic periphyton has also recently been linked to the methylation of mercury[48]. While the researchers of this study were not able to identify the individual methanogens responsible for mercury methylation[48], the researchers did identify sequences of methanogens among the active microorganisms in the biofilms, including those in the archeal orders *Methanococcales*, *Methanobacteriales*, and *Methanosarcinales* [48]. The very recent discovery and characterization of a two-gene cluster, *hgcA* and *hgcB*, that correlates with the ability of bacteria to methylate mercury[53] will certainly open new possibilities for the identification of methylating organisms in complex environments.

Pathways of Mercury Biouptake. Microbial methylation of mercury is likely to be an intracellular reaction[43,53-56]. Thus, transport of inorganic mercury from the microorganism's extracellular surroundings and through the inner and outer membranes is an important step leading to its biomethylation[43,56-58]. A few possibilities exist for membrane transport of Hg(II) in microorganisms (Figure 1.1). For those with the *mer*-resistance system, the uptake of divalent inorganic Hg(II) is believed to be mediated by transport proteins, among which MerC, MerP and MerT play an important role (Figure 1.1A).

In addition to the Mer-based transporters, alternative mercury transport pathways must exist since the known bacterial isolates that produce MeHg, including all obligatory anaerobic microorganisms, do not have the *mer* sequence in their genomes[11]. Most of the isolates capable of mercury methylation are Gram negative bacteria[43,44]. Thus in Figure 1.1B-D, we summarize the possible inorganic Hg(II) uptake mechanisms for these types of microorganisms. For Gram positive microorganisms, the possible uptake pathways would be similar except these microorganisms lack an outer membrane lipid bilayer and possess a thicker peptidoglycan layer outside the cytoplasmic membrane.

One possible transport pathway is passive diffusion of lipophilic, neutrally-charged complexes of Hg(II) across the cell membrane (Figure 1.1B). Evidence for a passive diffusion-based transport mechanism is generally limited to studies[59-61] with aerobic microorganisms that are not known to produce MeHg. In these studies, the organisms appeared to take up neutrally-charged Hg-chloride complexes, forms of Hg(II) that are not expected in high abundance in anaerobic and organic matter-rich settings (described further in Section 4). The concept of passive uptake of neutrally-charged Hg(II) complexes has been applied to SRB in anaerobic settings[62-64], but as we discuss later, assumptions regarding the geochemistry of Hg(II)-sulfides must be made for this approach to work.

More recent studies have directly focused on methylating microorganisms (both iron- and sulfate-reducers) in identifying the rates of Hg(II) associations with cells and mechanisms of

biouptake[56,57,65,66]. While it is difficult to distinguish between Hg adsorption to cells and transmembrane uptake, some of these studies[49,50] indicated that Hg(II) uptake did not occur through passive diffusion, but rather through another process such as facilitated and/or active uptake with membrane transport proteins (Figure 1.1C and 1.1D). This body of work demonstrated that mercury added to cultures as Hg-complexes with low molecular weight-thiols resulted in association of Hg with the cellular fraction in the cultures and subsequent production of methylmercury [56,57]. While one could conclude that the Hg-thiol complexes were directly taken up by methylating microorganisms, an alternative explanation could be that the thiols prevented the formation or adsorption of Hg(II) to suspended particles in anaerobic culture media[18,19,43]. Other evidence also points to an active transport mechanism for Hg uptake, particularly for the iron-reducing strain *G. sulfurreducens* where the disruption of microbial metabolism resulted in decreased Hg uptake and methylation[56]. The importance of an active uptake mechanism is less clear for SRB[56,65]. In experiments with the same SRB strain, methylation rates and microbial metabolism was demonstrated to be linked in one study[54] and poorly correlated in another[63]. If facilitated and active transport processes are indeed the major pathways for Hg uptake, it is likely that the membrane transporters are intended for a non-specific function (e.g. trace metal uptake) and fortuitously mediate Hg(II) uptake[56,67].

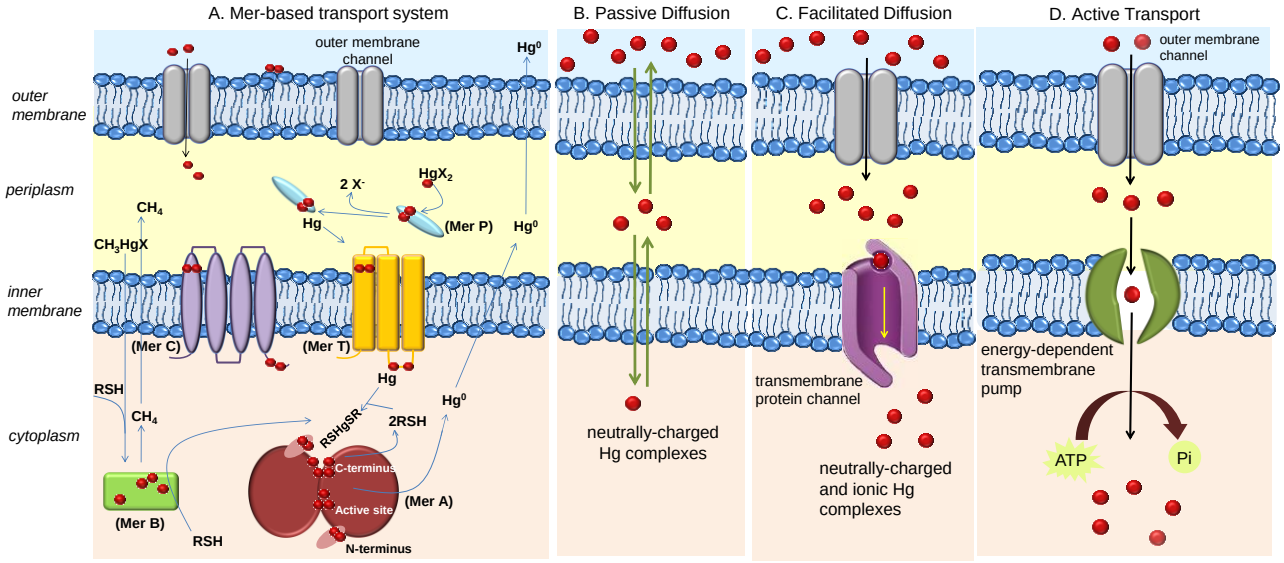

Figure 1.1. Possible mechanisms of inorganic Hg(II) uptake for Gram negative microorganisms (relevant to most of the methylating strains isolated from aquatic ecosystems). Hg(II) first enters the periplasmic space, likely by passive diffusion of lipophilic Hg(II) species through the outer membrane or by facilitated diffusion of hydrophilic Hg species and other Hg complexes (e.g. Hg-thiols) through outer membrane channels. Transport across the inner membrane could occur through: (A) Mer-based transport system where MerP binds Hg(II) in the periplasm, passes the mercury to MerT, and then transfers the element to MerA for reduction. (Adapted from Barkay *et al.*[68]); (B) Passive diffusion of lipophilic, neutrally-charged complexes (e.g. $HgCl_2$, $Hg(HS)_2$); (C) Facilitated diffusion of neutrally-charged and/or ionic species through a transmembrane protein channel. (D) Active transport of mercury via an energy-dependent transmembrane protein pump. In all cases, dissolved Hg(II) species (indicated by red circles) could comprise of a variety of Hg-ligand complexes, depending on local composition directly outside the outer cell membrane, in the periplasm, and in the cytoplasm. The species of Hg(II) that can be taken up depend on the mode of transport (passive, facilitated, or active) and binding affinities to membrane receptors (for facilitated and active pathways).

Biochemical Mechanism of Methlyation. Until very recently, little was known regarding the biochemical pathway of methylation after Hg(II) crosses the cytoplasmic membrane[11,36]. The enduring absence of identified genetic systems[37-42] for mercury methylation and lack of clear correlations of taxonomy of methylating microorganisms and methylation rates[44,46-49,69] have long been major obstacles for advancing our knowledge of this phenomenon. However, at the time this review went to press, a two-gene cluster *hgcA* and *hgcB* was reported to be required for mercury methylation in *Desulfovibrio desulfuricans* ND132 and *Geobacter sulfurreducens* PCA. The gene cluster encodes a putative corrinoid protein facilitating methyl transfer, and a ferredoxin carrying out corrinoid reduction, resulting in mercury methylation[53] consistent with a pathway proposed earlier[55]. It is not yet known whether this gene cluster is universal to all mercury methylators. In any case, there is consensus that The biochemical reactions causing methylation of mercury are strictly intracellular, followed by a rapid transport or diffusion of MeHg outside the cell[43,56,57,65]. The ability to produce MeHg is constitutive rather than induced by exposure to mercury[43], and as mentioned above, it appears to be closely linked to the *hgcA* and *hgcB* two-gene cluster. Since MeHg production is primarily associated with the activity of sulfate-reducing organisms, it has been proposed that the organism's ability to methylate mercury is most likely associated with substrate specificity of its enzymes[55]. Prior to the recent identification of *hgcAB* system, microbiologists have postulated that methylmercury production could be linked to a specific methyl-transferase pathway, to a Hg-specific uptake pathway, or to the biochemistry of Hg binding within the cell[11,43,70,71].

It now appears likely that one mechanism of mercury methylation follows one that has been first described for the sulfate-reducing bacterium *Desulfovibrio desulfuricans* LS, a dissimilatory incomplete oxidizer of short-chain fatty acids[39,69,55]. Methylation of inorganic Hg(II) occurred through methylcobalamin compounds and the acetyl-coenzyme A (acetyl-CoA) pathway. This biochemical pathway for mercury methylation is largely consistent with the recent report[53] on the genetic basis for bacterial methylation of mercury. This mechanism is likely to be relevant for other SRB strains that utilize the acetyl-CoA pathway for major carbon metabolism [70,71].However, several SRB strains have been observed to methylate mercury even though they either lacked detectable activities of acetyl-CoA enzymes or were exposed to acetyl-CoA inhibitors that blocked MeHg production in complete oxidizers[70,71]. Therefore, more than one biochemical pathway of Hg methylation may exist in SRB.

Future studies on the biochemistry of mercury methylation will build on the recent discovery of the *hgcAB* system and follow on mechanistic studies that could not be imagined before. The search for other possible biochemical pathways could perhaps target other enzymatic pathways that involve methyl transfer steps. An example is the synthesis of methionine, a process that is well-characterized for the fungus *Neurospora crassa*[72], and likely occurs within most microorganisms[73]. Another possibility introduced by Larose *et al.*[74] is the biological degradation of dimethylsulfoniopropionate (DMSP), an organosulfur compound that is especially abundant in marine microorganisms and is best known as a protection agent against osmotic stress[75]. Decomposition of DMSP results in the generation of methyl donors that could be relevant for

mercury methylation[74,76]. One could propose many other metabolic functions generating methyl donors, and more in-depth research is needed to determine their potential roles for MeHg production. Since these proposed pathways could occur in a wide variety of microorganisms, including both aerobes and anaerobes[75], future work would also need to address why the methylation of mercury seems to occur only with anaerobic microorganisms and mainly sulfate reducers in the aquatic environment.

1.3.2 Microbial degradation of MeHg

Biological demethylation is a major pathway of methylmercury degradation below the photic zone in the aquatic environment. A vast majority of the microorganisms identified as Hg methylators also have the ability to degrade MeHg[58]. Thus, microbial demethylation of MeHg should be considered in the overall assessment of mercury methylation potential in anaerobic settings. Compared to the progress made in identifying microorganisms that can methylate Hg(II), less work has been done to identify microorganisms that demethylate MeHg. Nevertheless, the capability for mercury demethylation does appear to be a widespread attribute amongst microbial communities in anaerobic settings[77].

Microbiologists have described two pathways by which microorganisms degrade methylmercury[77] . The first is reductive demethylation mediated by the *mer*-operon system leading to the formation of Hg^0 and CH_4. The second is oxidative demethylation in which MeHg is degraded to inorganic Hg(II), CO_2, and small amounts of CH_4 as a cometabolic by-product of methylotrophic metabolism[77]. Oxidative demethylation is mediated by anaerobic bacteria and may be somewhat analogous to monomethylamine degradation by methanogens or to acetate oxidation by sulfate-reducing bacteria[36,77].

The specific biodegradation pathway for methylmercury in anaerobic settings has relevance to the global mercury cycle since reductive demethylation to elemental Hg^0 can result in evasion of gaseous mercury from water, soil, and sediments[11,36]. In contrast, inorganic Hg(II) as the product of the oxidative demethylation can be available for methylation within the anaerobic microbial community. Thus, a cycle of methylmercury production and degradation may exist among anaerobic communities that do not have the *mer* operon, such as those identified microorganisms that can both methylate and demethylate mercury[58].

1.4 Geochemical factors affecting net production of methylmercury

Numerous microbial studies on mercury methylation have indicated that cellular uptake is a limiting step for MeHg production[9,18,56]. The uptake of Hg(II) may involve specific Hg(II) complexes and/or forms of mercury that can bind to a non-specific transmembrane transport system[56] as shown in Figure 1.1. Therefore, the geochemical speciation of mercury in environment will be critical towards determining the bioavailability of mercury for methylating microorganisms. As discussed in the previous section, the precise mechanism(s) of uptake remain largely unknown, and a few possibilities exist. Therefore, our ability to directly relate geochemical speciation and bioavailability remains limited.

1.4.1 Geochemical speciation of inorganic Hg(II) in the aquatic environment

The determination of the bioavailable forms of mercury for methylating microorganisms first requires an understanding of the forms of inorganic Hg(II) to which the methylators are exposed. A wide variety of Hg compounds exists in anaerobic settings, yet only a small portion of the total inorganic mercury is likely to be available for cellular uptake. In natural waters, inorganic divalent mercury generally persists in the form of aqueous mercury-ligand complexes (e.g., Hg^{2+} complexes with chloride, inorganic sulfide, or dissolved organic matter) or Hg(II) associated with particles (mercury-bearing minerals or Hg^{2+} adsorbed to particle surfaces). The relative partitioning of inorganic Hg(II) in various dissolved and particulate forms will govern the overall mobility of Hg in aquatic systems and the bioavailability of Hg to methylating microorganisms in anaerobic settings. One can deduce the partitioning of Hg(II) into different chemical forms based on experimental assays, such as size separation (i.e. filtration with a particular pore size or molecular weight cutoff) or metal-ligand complexation from experimentally determined thermodynamic binding strengths of 'dissolved' Hg complexes.

Size fractionation of Hg(II) generally involves filtration of aqueous samples with filters of various pore size. While dissolved Hg(II) is often defined by the amount of the metal that can pass through a 0.2 or 0.45 μm filter, 20% to 80% of this fraction may comprise of colloidal-bound Hg(II)[78-80]. The lower end of this range generally occurs in saline water while the higher proportion of colloidal Hg occurs in freshwater[78-80], consistent with the flocculation of colloids in saline water. In the water of anoxic settings where methylation occurs (e.g. sediments, bottom waters, periphyton), the proportion of mercury in the colloidal fraction is not as well documented. However, the presence of colloidal Hg could be expected in light of evidence showing that nanoparticulate forms of Hg can persist as by-products of metal sulfide precipitation occurring in the presence of dissolved organic matter (DOM)[15-17,81].

The size ranges that define dissolved, colloidal, and particulate mercury are based on the pore size or the molecular weight cut-off of filtration units employed in the experiment. The size distinctions are nominal, indeed, as there is no natural cut-off to distinguish between dissolved molecules, nanoparticles, and larger particles[1]. Furthermore, dissolved Hg(II) (with its sticky tendencies) can adsorb to filters, resulting in fractionation data that is difficult to decipher. To avoid potential artifacts, researchers must employ proper controls, such as filtration of a simulated water or an ultra-filtered natural water sample that has been spiked with dissolved Hg(II) to mimic the dissolved forms of mercury at the study site[82]. Ultrafiltration is often presumed to capture all forms of particles[82,83]. However, colloids that comprise of aggregates of smaller particles can potentially pass through filter membranes (especially under high pressure[84]) as a result of disaggregation at the membrane surface and re-aggregation after the primary particles are forced through the membrane pores. Moreover, nanostructured particles (e.g. dendritic aggregates of nanoparticles) are likely to have different levels of reactivity toward dissolution in comparison to larger crystalline particles. The subtleties of these experimental artifacts are often overlooked and further complicate interpretation of size fractionation data.

Diffusive gradient thin film (DGT) passive sampling devices are another approach for fractionating inorganic Hg(II) species in anaerobic water and sediments[85-89]. The DGT device

consists of a membrane or gel layered over a functionalized resin. When deployed in water or sediments, Hg(II) compounds (presumably only aqueous dissolved complexes of Hg) diffuse through this membrane/gel layer and accumulate on the resin through direct chelation of functional groups (e.g., thiolate ligands). This technique is typically used to estimate the 'chemically labile' Hg(II) concentration, presumed to be dissolved species, over a specific deployment time. However, the approach requires assumptions regarding the diffusional properties of Hg(II) compounds into the sampler: the diffusion coefficients for low molecular weight species (e.g. $HgCl_2$ complexes) can be two times greater than coefficients for Hg(II)-DOM complexes[88]. Diffusion coefficients are also related to the stability of dissolved Hg-ligand complexes[88,] Therefore, further development of these passive samplers will need to address how Hg flux is altered by multiple Hg-binding site affinities on DOM and the wide range of molecular weight and aggregation states that can occur for Hg-DOM and polynuclear Hg-sulfide compounds. It is also unclear if DGT samplers are capturing Hg(II) originating from particles in the sampling matrix (i.e. through dissolution or desorption reactions).

The chemical species of Hg(II) in the aquatic environment can also be deduced based on binding strength of distinct dissolved Hg(II)-ligand complexes. Trace metal complexation has been studied extensively in the past using a wide variety of methods that include electrochemical, competitive ligand exchange, and chromatographic approaches[90]. Thiol-functionalized DGT resins could also be interpreted as a form of *in-situ* competitive ligand exchange. Complexation of 'dissolved' Hg(II) compounds has been quantified by competitive ligand exchange with a Hg^{2+}-binding ligand, typically a chelating agent or a low molecular weight thiol[91-97]. Hg(II) complexes with these competing ligands are then separated from the sample (e.g. with an ion exchange or hydrophobic resin, or via dialysis) and quantified. In general the competitive ligand exchange experiment involves a titration of the sample with either dissolved Hg(II) or the competing ligand. From the titration data, researchers then calculate the thermodynamic stability of the Hg-ligand complex that is native to the sample (often modeled as a single homogeneous ligand binding site). Hg-ligand binding strength has also been quantified based on reactivity towards a reductant (i.e. stannous chloride), a method that is analogous to voltammetric techniques for other trace metals such as copper.

When all of these dissolved Hg(II) complexation techniques were applied to streams, rivers, estuaries and municipal wastewater effluent[91,92,96,98], the results generally demonstrated that the stability constants for Hg-ligand complexes resembled those for Hg-sulfhydryl (i.e., thiol) complexes, consistent with spectroscopic studies of Hg coordination to DOM isolates[99-102]. It is important to note that these Hg(II) complexation studies assume that only dissolved forms of Hg(II) are being probed in the experiments. This presumption could be particularly erroneous in settings such as municipal wastewater effluent that contain nanoscale metal sulfides as potential binding 'ligands' for Hg(II)[91,103].

Overall, previous assessments of mercury geochemistry demonstrated that in most natural waters, Hg(II) exists as a mixture of dissolved, colloidal and particulate phases. Furthermore, dissolved (and possibly colloidal) forms of mercury are associated with natural organic matter (NOM), particularly via specific binding with sulfhydryl functional groups on the NOM. In certain

settings located near a source of sulfide, this Hg(II) can also be complexed by inorganic sulfides such as dissolved or nanoparticulate entities.

1.4.2 Predicting Hg methylation potential: Chemical equilibrium speciation

Methylmercury production rates in water and sediments do not always correlate with the amount of total mercury (in filtered or unfiltered water)[21,64,104-106]. Moreover, researchers have hypothesized that only a small proportion of the inorganic mercury in anaerobic settings is available for uptake by methylating bacteria[9,20,21]. To that end, bioavailability models have been devised to link the geochemical speciation of inorganic mercury to methylmercury production in anaerobic settings. The most established approach for modeling mercury bioavailability assumes that biouptake occurs through a passive diffusion mechanism[62,107]. In this case, one would presume that lipophilic mercury species, such as small, neutrally-charged dissolved Hg(II) complexes, can be taken up by methylating microorganisms (Figure 1.2). From these assumptions, the concentration of bioavailable forms of Hg(II) (i.e. neutrally charged Hg-sulfide complexes) are subsequently estimated from thermodynamic equilibrium models of Hg(II) complexes[62,107].

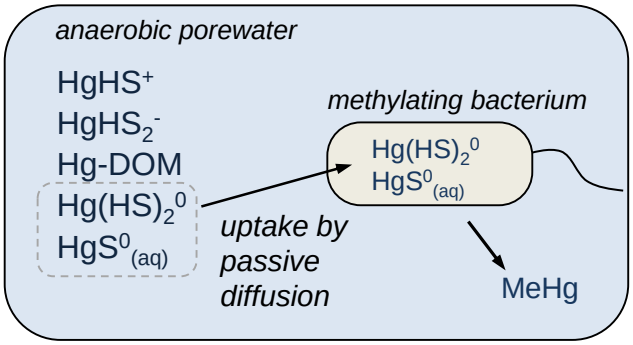

Figure 1.2. The neutral mercury-sulfides bioavailability model postulates that only the neutrally-charged forms of Hg(II) are able to passively diffuse into methylating bacteria. The model also presumes that the speciation of dissolved inorganic mercury in porewater has reached chemical equilibrium. From this basis, equilibrium chemistry predicts that aqueous mercury-sulfide complexes are the predominant form of dissolved mercury in porewater, and the net production of methylmercury (MeHg) is related to the concentration of neutrally-charged Hg-sulfide complexes. (Originally postulated by Benoit *et al.*[62].)

In this modeling approach, the inputs are the concentrations of dissolved Hg(II), the concentrations of other aqueous constituents that can potentially complex Hg^{2+}, and the thermodynamic stability constants for the formation of these complexes (Table 1). This approach has been utilized by several others in attempts to draw correlations between observed MeHg concentrations in environmental samples and the calculated concentrations of neutrally-charged forms of dissolved Hg(II)[64,105,108-111]. The use of equilibrium speciation to predict mercury bioavailability relies on assumptions that the input parameters for the model (i.e. the stability constants) are accurate, that a clear distinction can be made between fully dissolved and particulate Hg(II) concentrations in the model system (e.g. with filtration or DGT techniques), and that the partitioning of mercury between various chemical species can be represented by equilibrium

chemistry. Much work has been performed to address the first of these assumptions through studies that seek to improve the accuracy of Hg-ligand binding constants. The latter two assumptions bring many uncertainties for this approach. As discussed earlier, colloidal phases of Hg(II) could be an important fraction of mercury in 0.2-μm filtered water. The question of whether or not chemical equilibrium is reached under environmentally-relevant conditions has not yet been firmly answered.

The general consensus emerging from this thermodynamic equilibrium approach is that dissolved mercury is mainly complexed to reduced sulfur-containing ligands such as inorganic sulfides (H_2S/HS^-, polysulfides) and organic sulfhydryls (e.g. dissolved organic matter) in anaerobic settings relevant to biomethylation. Much effort has been devoted towards quantifying stability constants for Hg-DOM complexes[91-97]. The values for stability constants vary widely and depend on empirical factors such as the reaction stoichiometry used to model the Hg-DOM interaction, the type of DOM, the method used to measure Hg-DOM constants, and the composition of the sample used to perform the measurement (e.g. Hg:DOM concentration ratio). Overall, most agree that at environmentally relevant dissolved Hg(II) concentrations (typically less than 1 nM), complexation of Hg^{2+} by DOM involves reduced-S functional groups.

While much of the focus in the last decade has been on elucidating the Hg-DOM interaction, thermodynamic predictions of dissolved Hg(II) complexation by inorganic sulfides are equally challenging. The difficulty lies with large discrepancies in binding constants and the identity of the major forms of Hg-sulfides. For example, there is much uncertainty concerning the dissolved $HgS^0_{(aq)}$ (or $HgOHSH_{(aq)}$) complex, a species that was incorporated into a bioavailability model by Benoit *et al.*[62] (summarized in Figure 1.2). In developing this model, the researchers needed to include the neutrally-charged $HgS^0_{(aq)}$ molecule as a form of dissolved Hg(II) in order to fit field data that included MeHg concentrations observed over a large sulfide concentration gradient. In the original paper citing the $HgS^0_{(aq)}$ compound[112], the authors Dryssen and Wedborg extrapolated the intrinsic solubility of $HgS^0_{(aq)}$ ($K_{sp1} = 10^{-10}$ for the reaction: $HgS_{(s)} \Leftrightarrow HgS^0_{(aq)}$) (Table 1.1) from data on Zn- and Cd-sulfides. Dryssen and Wedborg also discussed the uncertainty of this *K* value and noted that this form of mercuric sulfide was probably colloidal HgS rather than a mononuclear aqueous complex. Experimental measurements with photon scattering seemed to indicate that this HgS^0 'aqueous'complex, which was originally presumed to be lipophilic based on partitioning into octanol[63], was more likely to be nanoparticles of HgS that could also partition into octanol[15]. Likewise, Skyllberg[113] postulated that the formation of $HgS^0_{(aq)}$ from $HgS_{(s)}$ should be represented by the smaller value estimated by Dryssen and Wedborg ($K_{sp1} = 10^{-22.3}$).

The decision to incorporate $HgS^0_{(aq)}$ (and the appropriate stability constant) into equilibrium models for mercury speciation dramatically alters the outcome of the calculation and the predicted concentration of neutrally-charged mercury species. For example, we calculated the equilibrium speciation of dissolved Hg(II) in a solution that would be representative of 0.2 μm-filtered water from an anaerobic setting (Figure 1.3). In calculations that utilized the Hg-DOM binding constant corresponding to aquatic humic acid (Fgiure 3A and 3B), the result indicated that the use of the larger intrinsic solubility K_{sp1} of 10^{-10} leads to an estimation that $HgS^0_{(aq)}$ is the dominant form of dissolved Hg(II) in anaerobic porewater at relatively low sulfide concentrations ($<10^{-4}$M total

sulfide) and that other forms of dissolved mercury such as $HgS(HS)^-$ are important only at high sulfide levels (i.e. $>10^{-4}$ M, Figure 1.3A). This transition coincided with observations that net MeHg production and Hg partitioning into octanol was reduced at high sulfide levels, leading researchers to believe that mercury bioavailability is related to passive diffusive transport of lipophilic Hg(II) complexes[62,63]. In contrast, if the smaller solubility constant for $HgS^0_{(aq)}$ is used in the speciation calculation ($K_{sp1} = 10^{-22.3}$), $HgS^0_{(aq)}$ concentration is negligible, and $HgS(HS)^-$ is the major form of dissolved mercury, regardless of sulfide concentration (Figure 1.3B). The need to fit a bioavailability model is a somewhat unsatisfactory basis for the choice of one stability constant over the other. In this case, the assumptions for the neutral mercury sulfide bioavailability theory need to be reexamined.

Table 1.1. Stability constants for $HgS_{(s)}$ solubility and Hg(+II)-ligand complexation reactions relevant to natural waters.

	log K (I = 0 M, 25°C)	Reference
β-$HgS_{(s)} + H^+ \Leftrightarrow Hg^{2+} + HS^-$	log K_{s0} = -38.7 ± 2	114
$HgS_{(s)} \Leftrightarrow HgS^0_{(aq)}$	log K_{s1}= -10 or -22.3	112
$HgS_{(s)} + (n\text{-}1)S^0_{(s)} + HS^- \Leftrightarrow Hg(S_n)HS^-$	-3.97 ± 0.17	115
$Hg^{2+} + HS^- \Leftrightarrow HgSH^+$	30.2	62
$Hg^{2+} + 2HS^- \Leftrightarrow Hg(SH)_2{}^0$	37.7	112
$Hg^{2+} + 2HS^- \Leftrightarrow HgHS_2{}^- + H^+$	31.5	112
$Hg^{2+} + 2HS^- \Leftrightarrow HgS_2{}^{2-} + 2H^+$	23.2	112
$Hg^{2+} + RS_2{}^{2-} \Leftrightarrow Hg(RS_2)$	log $K_{Hg\text{-}DOM}$ = 38.3 (peat humic)	95
	log $K_{Hg\text{-}DOM}$ = 28.7 (aquatic humic)	116
$RS_2{}^{2-} + H^+ \Leftrightarrow RS_2H^-$	8.4	95
$RS_2H^- + H^+ \Leftrightarrow RS_2H_2$	8.4	95
$Hg^{2+} + H_2O \Leftrightarrow HgOH^+ + H^+$	-3.4	114
$Hg^{2+} + 2H_2O \Leftrightarrow Hg(OH)_2{}^0 + 2H^+$	-6.2	114
$Hg^{2+} + 3H_2O \Leftrightarrow Hg(OH)_3{}^- + 3H^+$	-21.1	114
$Hg^{2+} + Cl^- \Leftrightarrow HgCl^+$	7.3	114
$Hg^{2+} + 2Cl^- \Leftrightarrow Hg(Cl)_2{}^0$	14.0	114
$Hg^{2+} + 3Cl^- \Leftrightarrow Hg(Cl)_3{}^-$	15.0	114
$Hg^{2+} + Cl^- + H_2O \Leftrightarrow HgOHCl^0 + H^+$	4.2	114
$Hg^{2+} + HS^- \Leftrightarrow HgS^0_{(aq)} + H^+$	28.7 ± 2 (log K_{s1}= -10)	Calculated: log $K_{HgS(aq)}$ = logK_{s1}–logK_{s0}
	16.4 ± 2 (log K_{s1}= -22.3)	
$H_2S \Leftrightarrow HS^- + H^+$	7.0	114

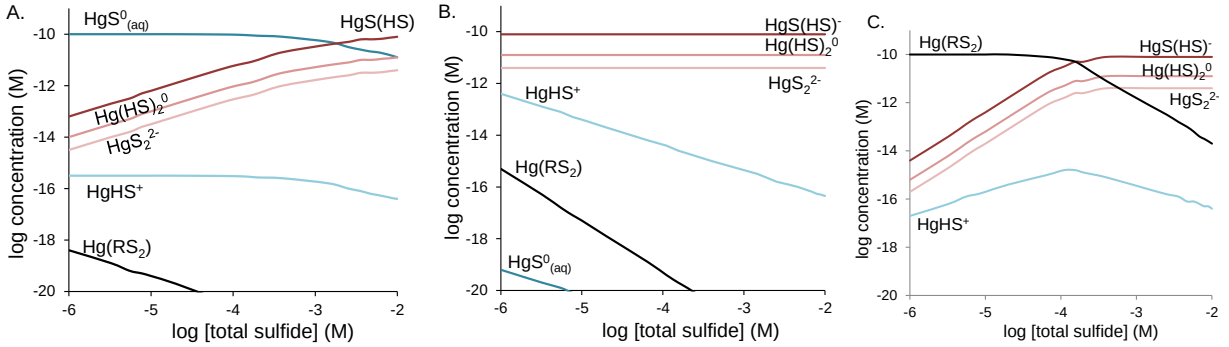

Figure 1.3. Predicted equilibrium speciation of dissolved Hg(II) in a solution representative of filtered anaerobic water: 10^{-10} M dissolved Hg(II), 10^{-6} M sulfhydryl concentration associated with DOM, 0.5 M Cl^-, pH 7. Calculations were performed used the stability constants listed in Table 1, assuming no precipitation of $HgS_{(s)}$ and two different stability constants for the formation of Hg-DOM and $HgS^0_{(aq)}$ complexes: (A) $K_{Hg\text{-}DOM} = 10^{28.7}$, $K_{HgS(aq)} = 10^{28.7}$; (B) $K_{Hg\text{-}DOM} = 10^{28.7}$, $K_{HgS(aq)} = 10^{16.4}$; and (C) $K_{Hg\text{-}DOM} = 10^{38.3}$, $K_{HgS(aq)} = 10^{16.4}$.

The choice of the Hg-DOM stability constant is another source of uncertainty for speciation models. The calculations in Figures 1.3A and 1.3B are based on Hg binding with aquatic humic substances ($K_{HgDOM} = 10^{28.7}$), which we believe is a better representation of DOM in aquatic settings occupied by methylating microorganisms[15]. If the larger Hg-DOM binding constant $K_{HgDOM} = 10^{38.3}$, which is derived from a soil organic matter, is used in the calculation, then Hg-DOM species are predicted to control Hg speciation for dissolved sulfide concentration less than 0.1 mM. The merits of one Hg-DOM binding constant over another have been extensively reviewed in previous papers[13,15,93,113,117], and we defer to these for detailed analysis. A key point to recognize, though, is that Hg-DOM ligand complexation reactions shown in Table 1 are vastly simplified representations of Hg interactions with DOM. The binding of Hg^{2+} ions to the 'strong' ligands in DOM appears to be slow (e.g. ~1 day or longer[118]), suggesting that perhaps the kinetics of Hg-DOM interactions, rather than stability at a presumed equilibrium state, need greater consideration. The identity of these strong binding sites is further complicated by evidence for polynuclear metal-sulfide clusters as part of the reduced-S pool in natural organic matter isolates[119,120]. These type of S(-II) groups could be expected to have a very high affinity for Hg(II) through metal exchange reactions, ultimately resulting in Hg(II) species that better resemble mixed metal-sulfide clusters infused within the organic matter matrix rather than Hg-sulfhydryl coordination[99,120].

In addition to the binding interactions between dissolved Hg-sulfides and Hg-organic matter, a third source of uncertainty for the speciation model is the solubility products K_{s0} for minerals such as metacinnabar and cinnabar, which vary by orders of magnitude in the NIST database for critically selected stability constants[114] (Table 1.1). Depending on the value used for the solubility of metacinnabar (K_{s0} for β-$HgS_{(s)}$), the saturation state of this mineral is near, below, or above saturation in our calculations shown in Figure 1.3. Whether metacinnabar is undersaturated or oversaturated particularly depends on the solubility product for $HgS_{(s)}$. The development of the

neutral mercury-sulfide bioavailability model required the selection of a relatively large $HgS_{(s)}$ solubility constant ($K_{s0}= 10^{-36.5}$, Table 1.1) in conjunction with a large formation of $HgS^0_{(aq)}$ so that the transition of the predominant dissolved Hg-sulfide species (e.g. $HgS^0_{(aq)}$ versus $HgS(HS)^-$ in Figure 1.3A)) could be matched to field data showing a decrease of MeHg with an increase of sulfide concentration[62]. The selection of this relatively large K_{s0} value caused the equilibrium calculations to predict undersaturation (with respect to metacinnabar $HgS_{(s)}$,) for dissolved Hg concentration less than 10^{-10} M. Because of these assumption, one could conclude that the formation of Hg-sulfide particles is not thermodynamically favored in most anaerobic settings [64,83], a notion that conflicts with direct observations of $HgS_{(s)}$ in soil and sediments[121,122].

1.4.3 Hg-sulfide-organic matter speciation at non-equilibrium

The Benoit et al. [60,105] approach to estimating mercury bioavailability heavily relies on the assumption that Hg speciation in anaerobic waters can be represented by chemical equilibrium, and perhaps it is this assumption that should be given greatest consideration. Previous measurements to deduce the forms of mercury in environmental samples (whether the characterization involves metal-ligand stability or fractionation of particulate vs. dissolved) are difficult to interpret because of the heterogeneity of mercury-containing compounds in natural waters, particularly in anaerobic settings. The constituents that comprise an anoxic surface water, sediment porewater or biofilm extracellular matrix include a continuum species: from dissolved molecules to polynuclear clusters, amorphous nanoparticles, and larger (perhaps crystalline) particles (Figure 1.4). This mixture of compounds would not be predicted from chemical equilibrium (with or without the incorporation of mineral phases) and likely represent intermediates of metal-ligand complexation, mineral precipitation and dissolution processes at non-equilibrium. Several studies have pointed to the importance of rate-limited processes (e.g. $HgS_{(s)}$ dissolution, precipitation, mass transfer across depth) for influencing Hg geochemistry in sulfidic settings[18,19,81,108,123-125].

As more studies are emerging to highlight the importance and unique reactivities of colloidal or nanoscale HgS, the use of $HgS^0_{(aq)}$ to represent a single bioavailable form of mercury presents a few problems. First, the basis for the neutral mercury bioavailability model is that particles have no bioavailability (i.e. they cannot be directly taken up by cells). Thus, these nanoscale materials are supposed to provide the same contribution of bioavailable Hg as macrocrystalline $HgS_{(s)}$ (via dissolution or desorption), even as experiments show differences in methylation between microorganisms exposed to nanoparticulate and microparticulate HgS[19]. Second, HgS and other metal nanoparticles themselves can vary widely in terms of their degree of crystallinity, aggregation state, and composition. Thus, one term to represent colloidal HgS is inadequate for describing a complex array of compounds that are changing in composition and structure over time. Moreover, recent evidence has demonstrated that the primary mode of mercury biouptake is not a passive diffusion mechanism, but rather involves a facilitated or active transport mechanism[56,57,65].

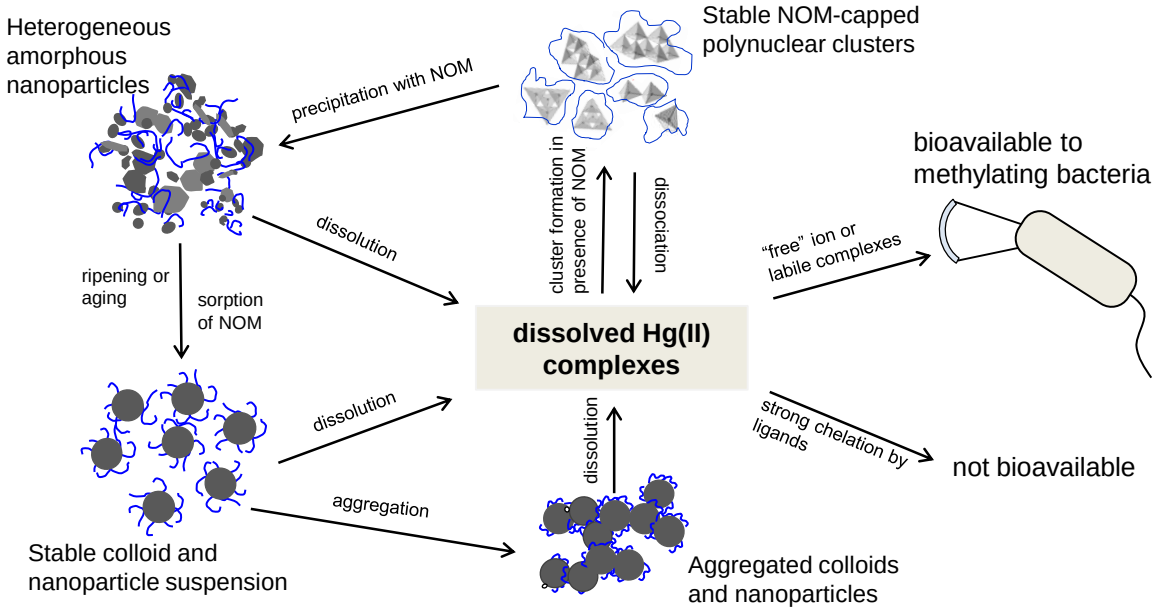

Figure 1.4. The transformations of mercuric sulfides in anoxic settings involve a diverse collection of species, many of which are intermediates of metal-ligand complexation reactions and precipitation and dissolution of $HgS_{(s)}$. Natural organic matter (NOM) is expected to play an important role in modifying reaction rates and the composition of metastable intermediates. If uptake of Hg(II) involves a facilitated mechanism (e.g. via metal transporter), then bioavailability will be governed by the propensity of Hg(II) to bind to a receptor site. Nanoscale phases could also cross membrane boundaries, but these would presumably need to dissolve or dissociate inside the organism prior to methylation. Modified from Aiken *et al.*[1].

Improvements to models of methylation potential will need to consider the contribution of natural organic matter. Equilibrium speciation calculations indicate that the concentration of Hg(II)-DOM complexes are negligible for sulfidic settings (Figure 1.3A and 1.3B)[15,18]. However, field and experimental data have demonstrated correlations between organic carbon concentration and MeHg production[10,18,126,127]. NOM could contribute to Hg bioavailability and methylation potential in two ways. First, complexation of Hg(II) by DOM had been hypothesized to decrease the amount of Hg(II) available to the methylating bacteria due to the difficulty for the large macromolecular and hydrophilic Hg-DOM complexes to diffuse through the cell membranes[128,129]. On the other hand, in most settings MeHg concentration was observed to increase with organic carbon content in sediments[127,130,131]. This positive correlation was typically attributed to a stimulating effect of the labile carbon on microbial growth. Neither of these two theories fully captures the inter-related roles of natural organic matter and sulfide for inorganic Hg(II) bioavailability and methylation. Exceptions to the correlation between MeHg and organic matter have been reported[132] in which the co-existence of sulfide and DOM appeared to yield a favorable geochemical environment for microbial Hg(II) uptake[18,132]. Therefore, the explicit

mechanism through which DOM influences mercury methylation needs to be investigated in conjunction with other environmental variables, especially sulfide.

While Hg^{2+} preferentially coordinates to inorganic sulfides over organic thiols associated with DOM, organic matter can influence Hg(II) speciation in other ways, particularly if the coordination reactions involving Hg are at a non-equilibrium status. DOM is known to enhance the dissolution rate of cinnabar and inhibit the precipitation rate of metacinnabar[81,123,133]. Moreover, macromolecular characteristics of the organic matter such as molecular weight and aromatic carbon content correlate with precipitation rates of metal sulfides [17,134] and possibly the bioavailability of mercury for methylating bacteria[18,104]. The occurrence of an aqueous ternary DOM-Hg-sulfide complex is a possible explanation[83]. However, more recent studies have demonstrated that organic matter plays a significant role in slowing the growth and aggregation of HgS nanoparticles as they precipitate in aqueous suspension[15,16]. These nanoparticles are likely to consist of a metacinnabar-like material (in terms of Hg-S coordination structure) that result in amorphous or nanocrystalline Hg-S-DOM nanoparticles[16,17].

These recent findings on the chemistry of mercury, sulfide, and organic matter highlight the inadequacies of an equilibrium-based approach. Perhaps a rate-based approach is needed to model mercury speciation and bioavailability, just as a rate-based approach is used to model microbial growth and biotransformations. The main challenge with a kinetics-based approach is that an understanding of chemical reaction mechanisms is needed, particularly in systems involving heterogeneous materials (dissolved, colloidal and particulate). In this case, recent advances in the nanogeosciences may provide a path forward towards improving assessments of mercury speciation and bioavailability.

1.4.4 Nanogeochemistry of mercury

In the last decade, geochemists and aquatic chemists have realized that nanoscale particles are ubiquitous in the environment[135-137]. Much of this work to document the presence of naturally-occurring nanoparticles has involved metal elements that are much more abundant than mercury (e.g. iron, aluminum, manganese, titanium, zinc). Nanoparticles and polynuclear clusters of metal sulfides such as ZnS and CuS have been observed in settings such as the biofilms of sulfate-reducing (and sulfide-generating) bacteria and in wastewater effluent[138-141]. (The term 'polynuclear clusters' refers to aqueous molecules with multiple metal centers[142] that are the precursors to more crystalline phases during nanoparticle synthesis.) Because of the high affinity between Hg(II) and inorganic sulfide, a portion of mercury in anaerobic settings could be expected to associate with metal sulfide clusters or nanoparticles, possibly through sorption of Hg^{2+} ions or coprecipitation of HgS on sulfide nanoparticle surfaces[143]. Discrete nanoparticles of HgS have been detected directly in soil, sediment, and biofilms on plant roots[122,144,145]. However, these examples were highly contaminated settings, such as mining and industrial sites where mercury-enriched materials were actively processed. Methods to directly detect nanoparticles (e.g. electron microscopy) generally require high concentrations of the target element in the sample (e.g. greater than one part-per-million). Most natural settings have much more dilute mercury

concentrations. Therefore, we expect that nanoscale mercuric sulfides will likely comprise of a mixture of metal sulfides, such as Hg sorbed to or coprecipitated with FeS[143].

Nanoscale particles are expected to behave differently than the compositionally identical, larger materials due to the high specific surface areas and unique reactivity of materials at the nanoscale[135,137]. Indeed, the defining characteristics of nanoparticles are not only the small size (i.e., at least one dimension smaller than 100 nm) but also size-specific reactivity exhibited by the nanomaterials[146]. Nano-specific reactivity is generally observed in monomer particles smaller than 30 nm and stems from the relatively large specific surface area and crystal lattice imperfections in a material with a large proportion of atoms on the surface. Nano-specific reactivity may include increased sorption capacity (normalized to surface area), enhanced transport, and faster rates of dissolution and re-nucleation[135,146].

The reactivity of nanoparticles can lend them to unique pathways for uptake into organisms, and at the very least, will influence the microbial bioavailability of the metal constituents of the nanoparticle. Clues toward understanding the importance of nano-HgS for microbial uptake and methylation could be gained from more established research on biouptake of iron originating from nanostructured iron oxides. For example, in microbial iron reduction, nanosized iron oxide colloids exhibited up to 100 times greater iron transformation rates than their respective bulk minerals[147]. This observation was attributed to the enhanced solubility[148] and larger mineral particle-bacteria contact for nanoparticulate Fe(III)[149,150]. Moreover, microscopic analysis revealed that iron oxide nanoparticles could penetrate the outer membrane of iron reducing bacteria, *Shewanella putrefaciens*, without collapsing the cells[149], and this bacterium tended to dissolve Fe(III) at the bacteria-mineral interface[151].

Recent work has suggested that mercury derived from HgS nanoparticles is more available to methylating bacteria than bulk minerals (e.g., metacinnabar), even when normalized to surface area[19]. Greater dissolution rates of small, more amorphous particles may account for the observed relationship between MeHg production and the 'age' of the Hg-sulfide species. However in this study, attempts to quantify the 'dissolved' fraction of Hg in the growth media could not fully account for the enhanced MeHg production in cultures exposed to HgS nanoparticles.

In natural aquatic systems, nanoparticles commonly exist as aggregates[135]. Therefore, while nanostructured materials may appear as a larger particle in conventional fractionation methods, they would differ in their reactivity towards transformations such as dissolution and bio-reduction[152-155]. The aggregation of metal sulfide nanoparticles (e.g., HgS, ZnS, CdS) are controlled by various environmental factors, including ionic strength, pH, the concentration and type of natural organic matter, and metal:sulfide ratio[134,156-160]. Humic substances, in particular, are known to interfere with precipitation reactions of minerals. Geochemists have long recognized that polynuclear clusters and nanoparticles are formed as intermediates of heterogeneous precipitation reactions [161], yet the role of NOM for controlling cluster formation, particle nucleation, growth, and aggregation rates remains unclear[1]. Most of the work in this area has involved metal oxides and hydroxides, rather than metal sulfides. For example, the reaction mechanics of metal hydroxide flocculation (e.g., aluminum and iron hydroxides) in the context of organic matter-containing water has been studied using spectroscopic tools[162,163]. This body of work has

led to evidence for the formation of polynuclear clusters and nanoparticle compounds during the initial stages of precipitation. Furthermore, the formation of nanoscale iron hydroxides may be part of a reaction mechanism in which the dissolved metal, Fe^{3+} in this case, can proceed through two pathways: either direct coordination with Fe-binding ligands on the NOM or hydrolysis to form polynuclear Fe-hydroxide clusters that are coated with organic matter or infused in the NOM matrix[162].

For metal sulfides such as metacinnabar, the nanoscale materials produced during the initial stages of precipitation are expected to be structurally different from metal hydroxide minerals. During the early stages of Hg-S polymerization, Hg takes on a 2-coordinate linear structure (-S-Hg-S-Hg-S-) that evolves into four-coordinate cubic HgS structure[164,165]. This transformation is likely to involve polynuclear Hg-S cluster species as intermediates[165], particularly if precipitation is occurring in the presence of dissolved organic matter[16,17] that caps the nanoclusters and prevents them from growing further. HgS nanoclusters also differ from metal hydroxides in the specific interactions with natural organic matter[15]. Because metals such as Hg persist at low levels in surface water and sediment porewater (picomolar to nanomolar), complexation with high affinity, low abundance ligands such as thiols must be considered. Thiol-containing organic compounds are capable of altering the growth kinetics of metal sulfide nanoparticles[15,166]. This phenomena could explain why low molecular weight thiols enhanced the uptake of Hg(II) for sulfate-reducing bacterial cultures[56,65]: the thiols slowed the precipitation of HgS particles as the microorganisms were producing inorganic sulfide at trace levels. The simultaneous interactions between Hg(II), organic matter, and sulfide ultimately determine the collection of species that make up this continuum of dissolved, polynuclear, nanoparticulate, and particulate mercury in anoxic settings. These species could be expected to exhibit differences in Hg^{2+} release rates that may be a limiting step toward biouptake in methylating bacteria.

1.5 Research Needs

Key questions remain to be answered concerning the mechanisms by which microorganisms methylate mercury. An understanding of these mechanisms is critical to the development of models that predict methylation potential in contaminated settings, and particularly in settings altered by remediation or change in mercury deposition. The greatest gaps in knowledge are related to the molecular processes that control the speciation of mercury, the route of Hg(II) uptake into methylating bacteria, and the enzymatic pathways toward methylation. In this respect, recent developments in molecular biology and nanogeochemistry can lend clues to address these questions. The breakthrough discovery of the *hgcAB* system[53] will undoubtedly pave the way for the development of a much greater understanding of mercury methylation mechanisms, the distribution of methylators in the environment and the factors that govern the rate of mercury methylation.

In terms of the geochemical speciation of mercury at biological interfaces, recent developments in the nanogeosciences provide much promise for enabling the understanding of mercury reactivity in complex mixtures such as sediments and sulfidic bottom waters. These developments include not only the realization of unique reactivity associated with nanoparticles

but also new tools and novel applications of older approaches (such as spectroscopy, photon scattering, and microscopy) to help us answer these questions. These methods could be particularly powerful if combined with more 'conventional' tools such as size separation and complexation. For example, synchrotron-based X-ray spectroscopic methods have been widely used for analyzing metal speciation in environmental samples due to their element specificity, minimal sample manipulation and non-destructive nature[167]. However, these techniques generally require samples with at least part-per-million amounts of mercury, a concentration applicable only to highly contaminated settings[168]. This limitation can be alleviated by the application of a pre-concentration step such as a C18 resin[17], a technique that was modified from mercury–ligand competitive exchange experiments. DGT techniques also hold much promise in enabling measurements of the reactive or 'bioavailable' Hg(II), particularly if the devices can mimic the environment immediately surrounding a methylating bacterium. If a kinetics-based approach is developed to assess mercury bioavailability in anaerobic settings, then the DGT probes could be used as proxies for Hg(II) flux at biological interfaces. The utilization of Hg stable isotopes can also be valuable in tracking simultaneous transformation reactions in microcosm studies[44,124,169].

The mechanistic understanding of microbial mercury methylation will be greatly improved if the biogeochemical reactions occurring at the microorganism-mineral interface (e.g., adsorption, complexation, dissolution, precipitation, aggregation) can be directly investigated, rather than indirectly implied by the measurements of bulk samples. The investigation of these interfacial processes requires powerful analytical tools with both high spatial resolution and chemical sensitivity. High-resolution transmission electron microscopy, synchrotron-based X-ray microscopy, and microprobe mapping have been utilized to examine the distribution of mercury and other trace elements and to identify the 'hot spots' of these elements in biological samples[144,170,171]. These techniques can also be coupled with metal speciation analysis, including X-ray absorption spectroscopy, X-ray diffraction, selected-area electron diffraction, and energy dispersive X-ray spectroscopy, and have shown great promise in elucidating the mechanisms of nanoparticle-microorganism transformation processes[19,172].

In addition to the molecular-level speciation of Hg in anoxic settings, we also lack a good understanding of the process by which methylating microorganisms take up inorganic mercury before converting it to methylmercury. Perhaps the characteristics of the microorganisms themselves can provide clues toward the mechanism of uptake. For example, Hg uptake by sulfate-reducers could occur via metal transporters[56], and these organism would need mechanisms for acquiring metabolically necessary soft-sphere metals such as Cu or Zn from their sulfidic surroundings.

Additional questions on the biochemical mechanism of mercury methylation remain to be fully answered. New and faster capabilities in the "-omics" of molecular biology (e.g. genomics, proteomics, metabolomics) could provide assistance to this problem[67]. For example, scientists are now realizing the diversity of yet uncultured microorganisms that are capable of methylating mercury in the environment[43,45,48]. With the ongoing improvements in tools utilized for microbial ecology, this list of organisms will continue to grow. Advances in pyrosequencing are improving the efficiency of large scale DNA sequencing, allowing for a metagenomics approach to

characterizing genetic material recovered from environmental samples[173,174]. The use of comparative metagenomics[175] can potentially provide additional insights into the differences among microbial populations that perform the same biological function (e.g., mercury methylation) but have evolved in different environments. Researchers are also successfully utilizing proteomics tools to characterize the proteins involved in metabolic pathways and to determine the proteome of microorganisms exposed to contaminants and environmental stressors[176,177]. Even with these new advances, however, an unresolved challenge is how to perform these experiments at Hg exposure levels representative of environmental concentrations (e.g., parts-per-billion or less).

While much progress has been made in understanding the multifaceted aspects of mercury methylation in the past decades, many fundamental questions remain. Hopefully, recent advances in the geochemical and biological sciences will help provide insights to those elusive questions. Ultimately, an improved comprehension of the factors that control MeHg production in the environment should enable the development of effective mercury remediation strategies, support the implementation of sound mercury emissions policies, and decrease human exposure to methylmercury.

Chapter 2

Methylation of Mercury by Bacterial Pure Cultures Exposed to Dissolved, Nanoparticulate, and Microparticulate Mercuric Sulfides

This chapter was published as the following:
Zhang, T.; Kim, B.; Levard, C.; Reinsch, B.C.; Lowry, G.V.; Deshusses, M.A.; Hsu-Kim, H. (2012). Methylation of mercury by bacteria exposed to dissolved, nanoparticulate, and microparticulate mercuric sulfides. *Environ. Sci. & Technol*. 46(13), 6950-6958. DOI: 10.1021/es203181m

2.1. Introduction and Objectives

As stated earlier, the overall goals of SERDP project #ER-1744 is to assess the importance of nanoscale mercuric sulfides for methylation potential in sediments and to develop a conceptual model that links mercury geochemical speciation to methylation potential in sediments. In this chapter, we describe research experiments to examine the methylation potential of various forms of mercuric sulfides by exposing fermentatively cultured SRB strains, *Desulfobulbus propionicus* 1pr3 and *Desulfovibrio desulfuricans* ND132, to three forms of mercury: dissolved $Hg(NO_3)_2$ freshly mixed with Na_2S (dissolved Hg+S exposure), humic-stabilized HgS nanoparticles, and commercially-purchased HgS microparticles. These forms of mercury represented three different aging states of mercury in sulfidic sediments. This component of the work is Task 1 of our overall plan. We also performed experiments for Task 2. Here, we characterized the structure of the nanoparticles and assessed the speciation of mercury in the culture media during the incubation experiments.

2.2. Materials and Methods

2.2.1 Methylation of dissolved, nano, and microparticulate mercury in culture

Microorganisms and Culture Conditions. *Desulfobulbus propionicus* 1pr3 (ATCC 33891) and *Desulfovibrio desulfuricans* ND132 (C. Gilmour, Smithsonian Environmental Research Center) were utilized as the test microorganisms. These strains were cultured in Hungate tubes (Bellco Glass) placed in an anaerobic chamber. Cell growth was monitored by optical density (OD_{660}) and protein content [178]. The bacterial cultures were maintained between experiments on sulfate-containing medium. Prior to mercury methylation bioassays, the cultures were transferred for three successive generations in fermentative media that contained 20 mM pyruvate (for 1pr3) or 40 mM fumarate (for ND132) as the organic carbon source and 0.15 mM Ti-nitrilotriacetic acid (NTA) as the reductant, according to previous methods [107,179].

HgS Particle Preparation. The Hg stock solution consisted of $Hg(NO_3)_2$ dissolved in 0.1 N HNO_3. Na_2S stocks were prepared by dissolving freshly washed and dried crystals of $Na_2S{\cdot}9H_2O$ (Fisher Scientific) in N_2-purged water and were utilized within 4 h of preparation. HgS

nanoparticles were synthesized by dissolving 50 μM $Hg(NO_3)_2$ and 50 μM Na_2S with 10 mg-C L^{-1} Suwannee River humic acid (SRHA, International Humic Substances Society) in a solution of 0.1 M $NaNO_3$ and 4 mM sodium 4-(2-hydroxyethyl) piperazine-1-ethanesulfonate (HEPES) (pH 7.5, double-filtered to <0.1 μm). The Hg-S-NOM nanoparticle stock solution was allowed to age for 16 hours to 1 week at room temperature prior to use in the methylation experiments. A microparticulate HgS stock suspension was prepared by adding a commercial metacinnabar powder (β-HgS, Alfa Aesar) into nanopure-filtered water (>18 MΩ-cm). This suspension was mixed end-over-end prior to taking an aliquot for the experiments.

HgS Particle Characterization. The average hydrodynamic diameter of HgS nanoparticles and microparticles were analyzed by light-intensity weighted dynamic light scattering (DLS) (Malvern Zetasizer NS). The diameters of the monomers within the aggregates were analyzed by transmission electron microscopy (TEM). Samples for DLS were directly quantified in their respective stock suspensions. Samples for TEM were prepared by depositing droplets of the particle stocks on a carbon-coated copper grid (200 mesh), wiping the excess liquid with a lint-free tissue, and allowing the grid to air dry under protective cover. Micro- and nano-HgS particles (aged for 16 h or 1 week) were examined by a FEI Technai TEM at 200 keV and characterized with selected area electron diffraction (SAED) to assess crystal structure of the particles. Images of HgS nanoparticles (aged for 3 days) were captured on a Hitachi HF2000 TEM operating at 200 keV and analyzed for elemental composition by energy dispersive X-ray (EDX) spectroscopy (Oxford Inca EDX system).

BET surface areas of HgS nanoparticles and microparticles were determined using the BET N_2 adsorption technique (Beckman Coulter SA3100 Surface Area Analyzer). The geometric surface areas of HgS particles were calculated from the individual particle size obtained from TEM images. The geometric surface area calculations assumed spherical particles with a density of 7.71 g cm^{-3} [180].

The crystallographic structure of HgS nanoparticles and microparticles was analyzed by synchrotron X-ray diffraction (XRD). The HgS nanoparticle stocks were filtered through 0.025 μm pore size mixed cellulose ester membranes (Millipore). The material that deposited on the filter membrane was analyzed by synchrotron XRD performed at the Stanford Synchrotron Radiation Laboratory (SSRL) BL 11-3. Samples were placed in the path of a 12,700 eV beam measuring 0.150 mm^2 and the diffraction pattern was captured using a MAR 345 detector set at a distance of 149.9 mm away from the sample, as determined through calibration with a LaB_6 standard. The diffraction image was integrated and peak matched in a manner similar to Reinsch *et al.* (2010) [181].

The average crystallite diameter *D* of nano-HgS was estimated from the broadening of the X-ray diffraction peaks by the Scherrer formula [182]:

$$D = \frac{K\lambda}{\beta \cos\theta} \qquad (1)$$

where *K* is the constant of proportionality (*K*=0.9), λ is the x-ray wavelength (λ = 0.0977 nm), β is the full width at half the maximum intensity in radians (FWHM) and θ is the Bragg angle.

The HgS particles that deposited on the 0.025 μm mixed cellulose ester filters (Millipore) were also analyzed for elemental composition by X-ray photoelectron spectrometry (XPS). A PHI VersaProbe Scanning XPS Microprobe was used for these measurements. XPS data were calibrated using the binding energy of C(1s) (285.00 eV) as the internal standard. In the XPS spectra, binding energy and peak width of the Hg(4f) and S(2p) transitions were comparable for nano-HgS and micro-HgS, indicating similar local structure.

Mercury Methylation Bioassay. The bacterial cultures were pre-grown in a fermentative medium and incubated until exponential growth phase (19 h for *D. propionicus* 1pr3 and 67 h for *D. desulfuricans* ND132) prior to dosing with mercury. In the dissolved Hg+S exposure, $Hg(NO_3)_2$ and Na_2S were added into the test cultures separately. While we refer to this exposure as "dissolved Hg+S" because of the initial method of dosing, HgS was supersaturated in these cultures and likely consisted of early-stage precipitation products (i.e., HgS clusters and nanoparticles). The cultures were also exposed to humic-associated HgS nanoparticles, representing an intermediate stage of heterogeneous HgS precipitation, and microscale crystalline HgS, representing a mercury-bearing mineral commonly encountered in soil and sediments [122,183]. In the dissolved and micro-HgS treatments, SRHA, $NaNO_3$ and HEPES were also added to the test cultures to account for the chemical carryover from the HgS nanoparticle stock in the nano-HgS treatment. The cultures were continuously mixed end-over-end and stored in an anaerobic chamber during incubation. All mercury methylation bioassays were incubated in the dark at room temperature (25-27°C).

At each time point, triplicate vials were sacrificed and subsampled for measurements of total protein and mercury concentration. After subsampling, the remaining cultures were preserved by adding 0.4% (v/v) concentrated hydrochloric acid (HCl) (trace metal grade) and stored at 4°C prior to methylmercury (MeHg) analysis. Two sets of controls were incubated under the same conditions including: 1) abiotic control consisting of uninoculated media amended with $Hg(NO_3)_2$ and Na_2S; 2) killed control consisting of autoclaved (121°C, 30 min) cultures amended with $Hg(NO_3)_2$ and Na_2S after the autoclave step. MeHg concentrations in all control samples were below the detection limit (≤ 8 pM MeHg) and significantly lower than MeHg in viable cultures amended with $Hg(NO_3)_2$ and Na_2S.

Methylmercury Degradation Bioassay. The microbes tested in this study are known to both methylate and demethylate mercury simultaneous. We tested for the approximately rate of methylmercury degradation by *D. propionicus* 1pr3 by amending the cultures with methylmercury instead of inorganic mercuy. These cultures were first pre-grown in a fermentative medium and incubated until exponential growth phase prior to dosing with methylmercury chloride (MeHgCl). All methylmercury degradation bioassays were conducted under the same conditions as in the mercury methylation bioassays. Abiotic control consisted of uninoculated media amended with MeHgCl.

Chemical Analysis. MeHg concentration was quantified by distillation, aqueous phase ethylation, gas chromatographic separation, and atomic fluorescence spectrometry (Tekran 2600) [184]. Samples for total mercury analysis was first digested with 2 to 4% (v/v) BrCl for at least 12 h

and analyzed by $SnCl_2$ reduction, gold amalgamation, and cold vapor atomic fluorescence spectrometry [185].

2.2.1 Mercury distribution in bacterial cultures

Mercury Fractionation by Filtration. In mercury methylation bioassays, total mercury in a subset of *D. propionicus* 1pr3 cultures was fractionated using filtration. Separate test cultures were filtered with either 0.22 μm polycarbonate (GE Osmonics Labstore) or 0.02 μm aluminum oxide (Whatman) syringe filters. Total mercury concentration in the filtrates was quantified and represented different mercury species: 1) <0.02 μm fraction considered the nominally "dissolved" mercury and likely consisted of aqueous mononuclear mercury complexes (e.g., $Hg(OH)_x^{2-x}$, $Hg(HS)_x^{2-x}$) and possibly polynuclear mercury sulfide clusters; 2) 0.02 to 0.22 μm fraction which contained colloidal mercury (e.g., Hg-S-NOM nanoparticles); and 3) >0.22 μm fraction which contained cell- and/or large particle-associated mercury. Filtration experiments were also performed with bacteria-free media amended with the three forms of mercury (dissolved Hg+S, nano-HgS, and micro-HgS). These solutions were incubated and filtered with 0.02 μm and 0.22 μm filters at multiple time points up to 1 day.

Mercury Fraction by Centrifugation and Ultracentrifugation. In mercury methylation bioassays, total mercury in *D. propionicus* 1pr3 cultures was also fractionated using centrifugation and ultracentrifugation. HgS-treated bacteria were first separated from the bulk medium by centrifugation at 6,700 *g* for 5 min. The pellets (containing mercury associated with bacterial cells and/or large particle aggregates) were washed with 10 mM PBS (pH 7.4) by centrifugation and resuspended in nanopure-filtered water (>18 MΩ-cm). The cells within the washed pellets were then lysed through four freeze-thaw cycles plus 15-min sonication (90 W). This procedure was adequate to fully compromise the cell membrane integrity as determined from the LIVE/DEAD® viability assay (Invitrogen). The mercury released from the lysed cells was collected from the supernatant after centrifugation at 10,800 *g* for 30 min and the cell debris- and/or large particle-associated mercury was collected from the pellets. Total mercury in the supernatant of the centrifuged (6,700 *g*, 5 min) sample was further fractionated by ultracentrifugation at 370,000 *g* for 2 h. After ultracentrifugation, we considered the mercury remaining in the supernatant to be nominally dissolved, while mercury in the pellet after ultracentrifugation consisted of nanoparticulate/colloidal mercury. The applicability of this procedure for separating dissolved, nanoparticulate and microparticulate mercury was demonstrated by (ultra)centrifugation of bacteria-free media that were treated by these different forms of mercury.

TEM Analysis of HgS-Amended Cultures. After 14-h exposure to HgS, cells from 1pr3 cultures were separated by centrifugation, washed with 10 mM phosphate buffered saline (PBS, pH 7.4), and resuspended in a fixative solution containing 4% (v/v) formaldehyde and 2% glutaraldehyde. After storing for 4 h in the fixative, the cells and were washed with high purity deionized water (>18 MΩ-cm). This suspension was deposited on a carbon-coated copper grid (200 mesh) and imaged by FEI Tecnai TEM operating at 80 keV and a JEOL 2000 FX TEM operating at 200 keV with an EDX spectrometer for the element analysis.

Mercury Speciation by Competitive Ligand Exchange. A subset of mercury-treated media solution was analyzed for chemical speciation of mercury using a previously developed competitive ligand exchange-solid phase extraction (CLE-SPE) method [15,91,186]. This technique separates labile mercury species from strongly complexed mercury species based on the chemical reactivity of mercury in the presence of a competing ligand: glutathione (GSH) or diethyl dithiocarbamate (DEDC). GSH and DEDC are both thiol-containing compounds and form strong hydrophilic complexes ($HgH_2(GSH)_2^{2-}$) or hydrophobic complexes ($Hg(DEDC)_2^0$) with mercury that can be differentiated from the original Hg-sulfide or Hg-NOM species using C_{18}-resin solid phase extraction.

Aliquots of the media were sampled at the beginning and end of the 1-day incubation, amended with either 0.1 mM GSH or DEDC for 1 h, and then filtered through a C_{18}-resin packed column. The hydrophobic fraction was defined by mercury retained by the resin, while the hydrophilic fraction was defined as mercury passing through the C_{18}-filter.

2.3. Results and Discussion

2.3.1 Methylation of Mercury Sulfides

The net production of MeHg in the cultures varied depending on the type of HgS added (Figure 2.1). For each SRB strain, the cultures exposed to dissolved $Hg(NO_3)_2$ and Na_2S (and likely to be precipitating HgS *in situ*) demonstrated the highest net MeHg production. MeHg production was observed to a lesser extent in the nanoparticle exposures. In cultures exposed to HgS microparticles, MeHg concentration was less than 8 pM and similar to the autoclaved and abiotic controls. Furthermore, MeHg production by cultures exposed to nanoparticles depended on the age of the nano-HgS stock solutions. The cultures methylated 6% to 10% of the total mercury derived from nanoparticles aged for 16 hours, while cultures methylated a smaller fraction (2% to 4%) if exposed to older nanoparticles (aged 3 days or 1 week) (Figure 2.1a and 2.1b). Consistent results were obtained in replicate experiments employing higher mercury doses (5 nM) and longer incubation time (up to 10 days) (Figure 2.2).

Overall, the results demonstrated that the methylation potential of mercury introduced as HgS nanoparticles was greater than bulk scale HgS particles. These results were not due to differences in cell growth, as the optical density (OD_{660}) and protein content were identical in all HgS exposures (Figure 2.3). However, the diameter of the nanoparticles was smaller (3 to 4 nm) and specific surface area was larger (220 to 260 $m^2\ g^{-1}$) compared to the microparticles (>500 nm, 2.5 $m^2\ g^{-1}$) (Table 2.1, Figure 2.4 and 2.5). While the surface composition of Hg and S was similar for the nano- and micro-HgS, as shown by X-ray photoelectron spectroscopy (Figure 2.6a and 2.6b), the degree of crystallinity varied between nano- and microparticles. As expected, X-ray diffraction and energy dispersive x-ray spectroscopy data suggested that the nanoparticles were poorly crystallized compared to the HgS microparticles (Figure 2.5 and 2.6c). The XRD spectra indicated that the commercial HgS microparticles consisted of a mixture of metacinnabar and cinnabar (approximately 50-50 proportion based on Rietveld analysis of XRD data). The spectra for the humic-HgS nanoparticles indicated metacinnabar-like structure, but peaks were broader

and less defined than the micro-HgS spectrum, signifying that the nano-HgS consisted of smaller crystallite size and less crystallinity (Figure2.6c).

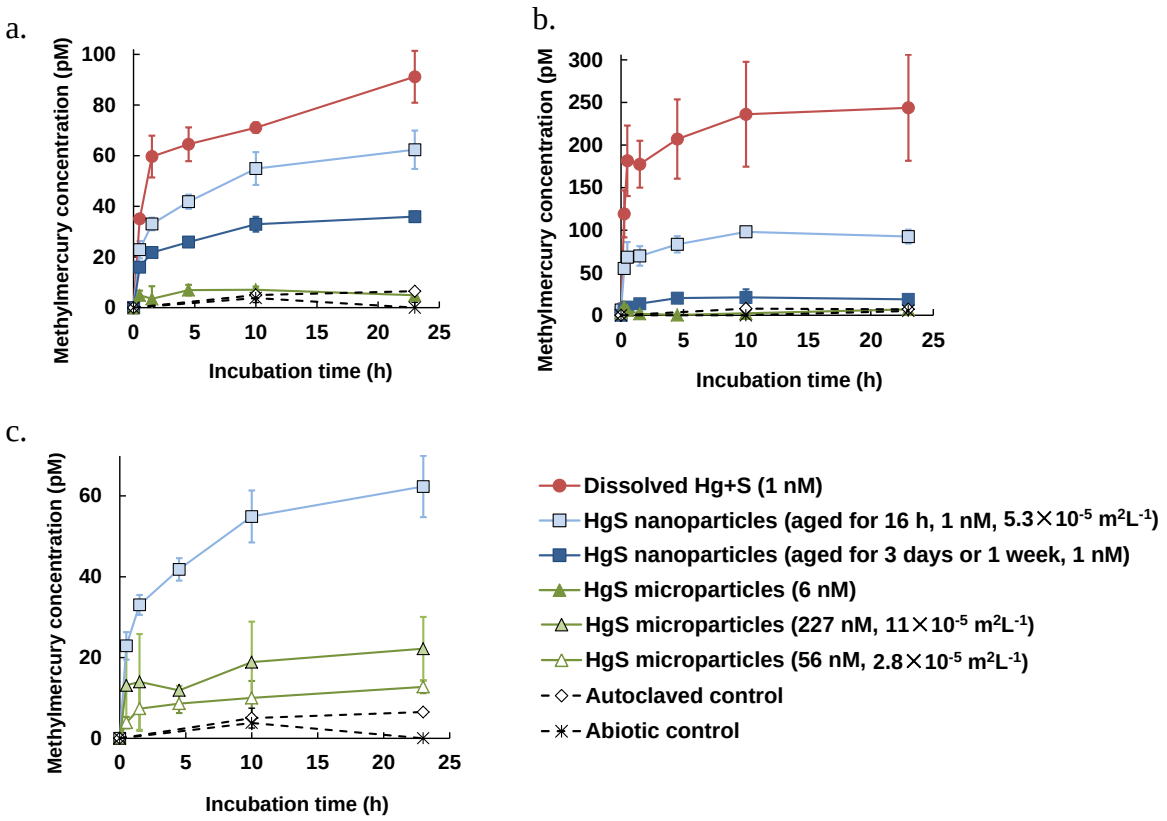

Figure 2.1. Net MeHg production in SRB cultures exposed to different forms of mercuric sulfides. Methylation by **(a)** *D. propionicus* 1pr3 and **(b)** *D. desulfuricans* ND132 cultures that were exposed to 1 nM dissolved $Hg(NO_3)_2$ and Na_2S, 1 nM humic-HgS nanoparticles, and 6 nM HgS microparticles. The HgS nanoparticle stock solution was stored at room temperature for 16 h and a longer period (3 days in Figure 1a and 1 week in Figure 1b) prior to amending to cultures. **(c)** Methylation by *D. propionicus* 1pr3 cultures that were exposed to the similar geometric surface area of HgS nano- and microparticles: 1 nM (5×10^{-5} m^2 L^{-1}) HgS nanoparticles aged for 16 h, 56 nM HgS microparticles (3×10^{-5} m^2 L^{-1}), and 227 nM HgS microparticles (11×10^{-5} m^2 L^{-1}). Control experiments were either autoclaved cultures or abiotic culture media that were amended with 1 nM dissolved $Hg(NO_3)_2$ and Na_2S. All cultures received the same humic acid concentration (0.2 μg-C L^{-1}). MeHg concentrations in all control samples were below the detection limit (8 pM MeHg). The error bars represent ±1 s.d. of duplicate samples for the controls and triplicate samples in all other experiments.

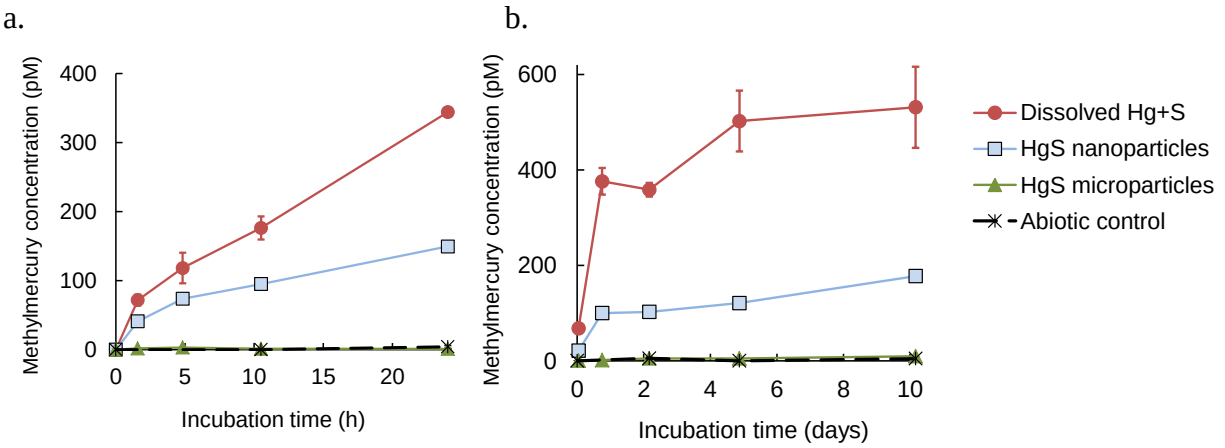

Figure 2.2. Net MeHg production in *D. propionicus* 1pr3 cultures exposed to different forms of mercuric sulfides. Test cultures were exposed to 5 nM dissolved $Hg(NO_3)_2$ and Na_2S, 5 nM humic-HgS nanoparticles (aged for 16 h), and 20 nM HgS microparticles during **(a)** 1-day time course experiments and **(b)** 10-day time course experiments. Abiotic controls were uninoculated medium solutions amended with 5 nM dissolved $Hg(NO_3)_2$ and Na_2S. The error bars represent ±1 s.d. for duplicate samples.

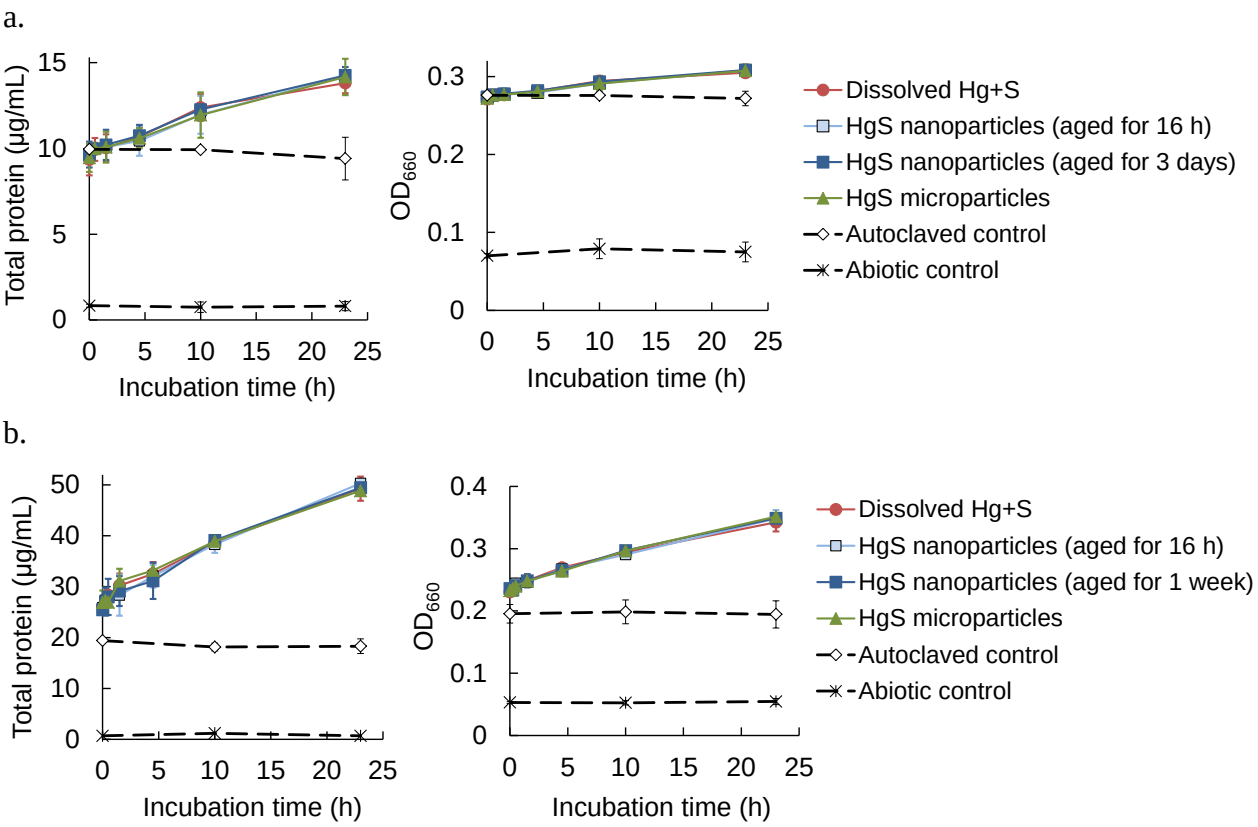

Figure 2.3. Bacterial growth in SRB cultures exposed to different forms of mercuric sulfides. Total protein content and optical density (OD_{660}) of **(a)** *D. propionicus* 1pr3 cultures and **(b)** *D. desulfuricans* ND132 cultures.

Table 2.1. Average size and surface area of humic-HgS nanoparticles and HgS microparticles utilized in methylation bioassays. Diameters and geometric surface areas were compared to the 16-h HgS nanoparticles using an unpaired two-tailed t-test. Values that are statistically different ($p<0.01$) from the 16-h nanoparticles are indicated by an asterisk (*).

HgS particles	Hydrodynamic diameter (nm) [(a)]	Monomer diameter (nm) [(b)]	Crystallite diameter (nm) [(c)]	Surface area (m^2 g^{-1})	
				BET [(d)]	Geometric [(e)]
Nanoparticles (aged for 16 h)	25.8 ± 2.9 (n=10)	3.2 ± 0.8 (n=110)	5.7 ± 0.1 (n=3)	47.9	264 ± 72 (n=110)
Nanoparticles (aged for 3 days)	27.6 ± 3.0 (n=5, p=0.27)	3.3 ± 0.9 (n=110, p=0.14)	5.0 ± 0.3 (n=3, p=0.012)	ND	250 ± 63 (n=110, p=0.13)
Nanoparticles (aged for 1 week)	28.3 ± 4.9 (n=4, p=0.25)	3.6 ± 0.7* (n=110, $p=10^{-5}$)	5.7 ± 0.1 (n=3, p=0.89)	ND	224 ± 47* (n=110, $p=2\times10^{-6}$)
Microparticles	1457 ± 435* (n=7, $p=2\times10^{-8}$)	530 ± 367* (n=78, $p=10^{-25}$)	NA	2.5	2.5 ± 1.8* (n=78, $p=10^{-68}$)

(a) Quantified by light-intensity weighted dynamic light scattering.

(b) Estimated from individual monomers observed in TEM images (Figure 2.5).

(c) Estimated from the broadening of the X-ray diffraction peak widths by the Scherrer formula (Figure 2.6c).

(d) BET surface area quantified by N_2-gas adsorption.

(e) Geometric surface areas (based on approximation of spherical monomers) were calculated from the size of individual particles in TEM images.

NA: Not available

ND: Not determined

a.

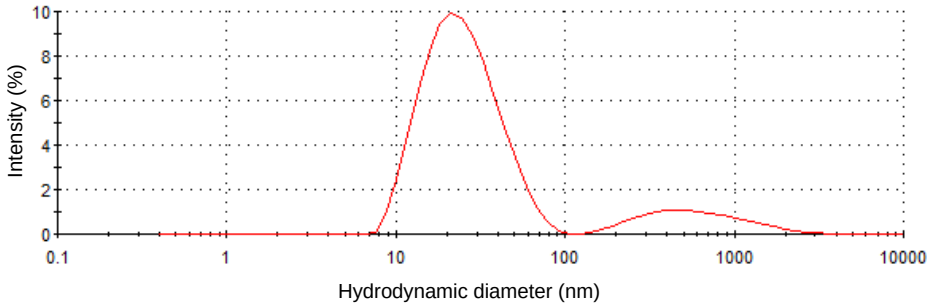

b.

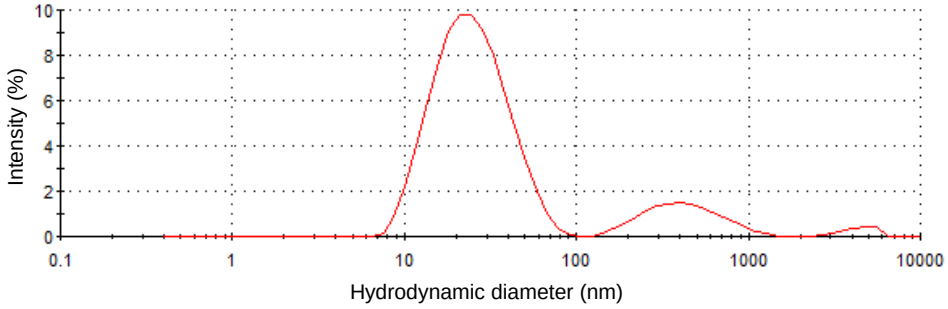

c.

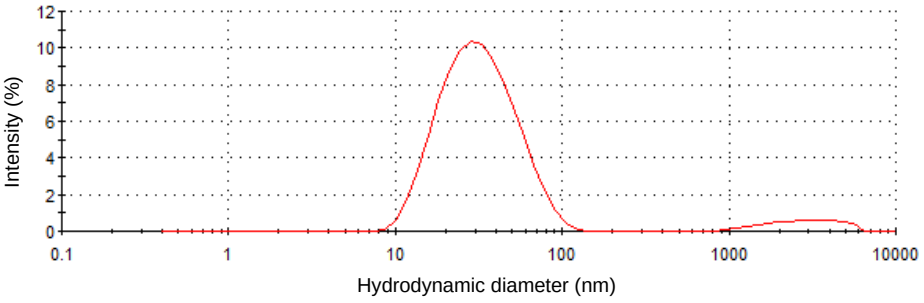

d.

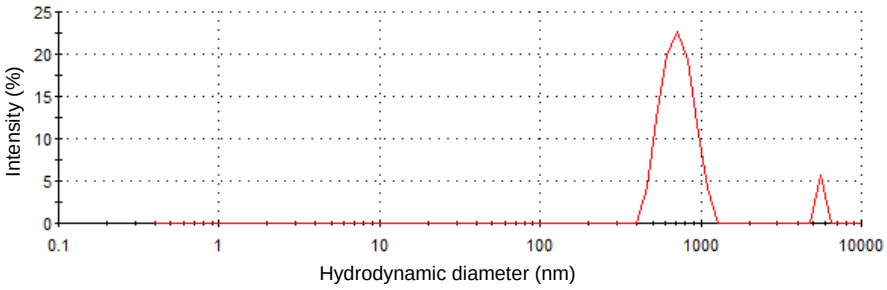

Figure 2.4. Intensity-weighted size distribution of HgS particles measured by dynamic light scattering. **(a)** HgS nanoparticles (aged for 16 h; **(b)** HgS nanoparticles (aged for 3 days); **(c)** HgS nanoparticles (aged for 1 week); **(d)** Commercial HgS microparticles.

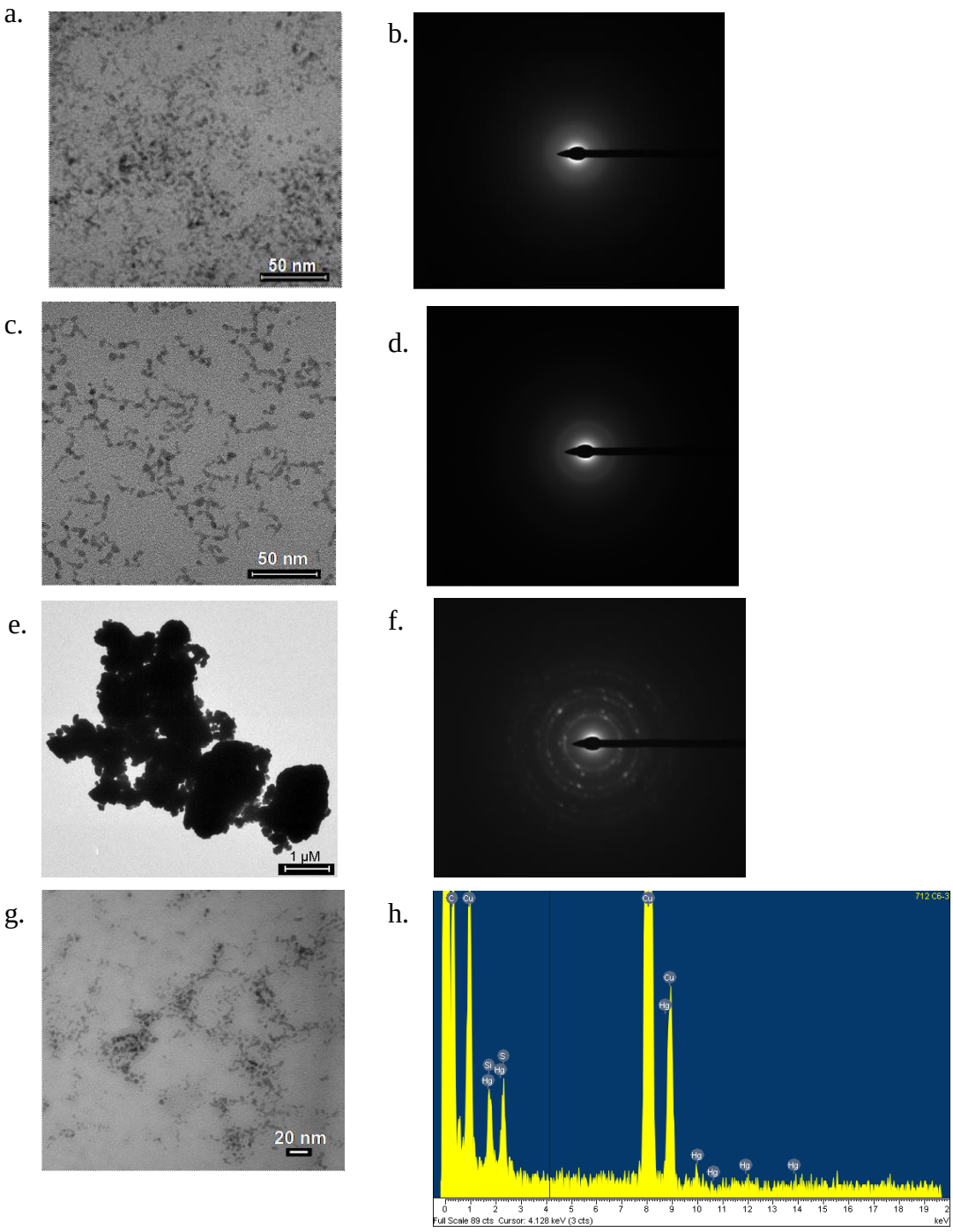

Figure 2.5. TEM and SAED patterns of HgS nanoparticles aged for 16 h **(a,b)**, HgS nanoparticles aged for 1 week **(c,d)**, and commercial HgS microparticles **(e,f)**. The EDX spectra for HgS nanoparticles aged for 3 days **(g)** is shown in **(h)**. EDX spectrum indicated the presence of Hg and S in the nano-HgS sample. In SAED patterns, defined rings indicate long range crystal structure.

a.

b.

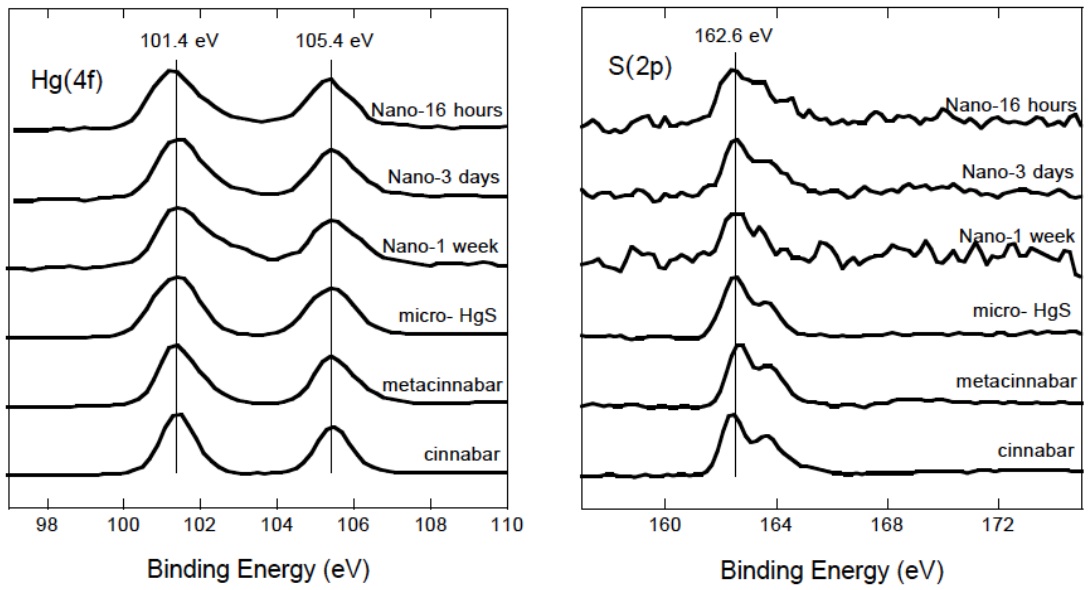

c.

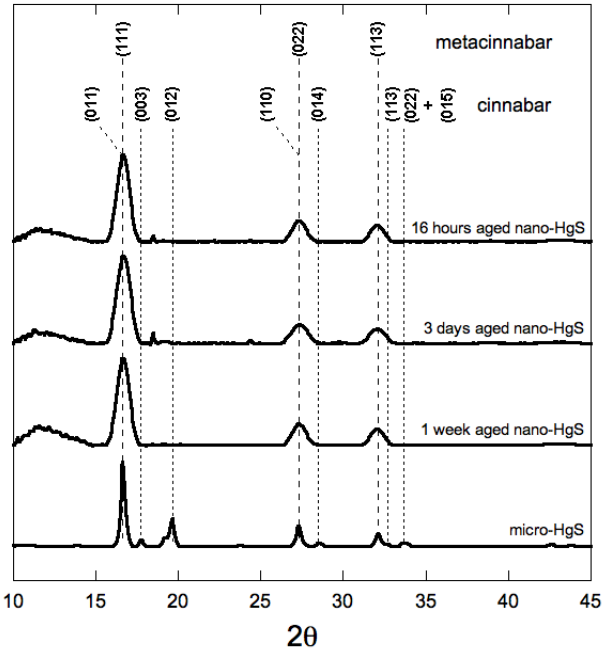

Figure 2.6. X-ray photoelectron spectroscopy (XPS) and X-ray diffraction (XRD) results of HgS particles. XPS data corresponding to **(a)** Hg(4f) and **(b)** S(2p) electrons for the HgS nanoparticles (aged for 16 h, 3 days or 1 week) and HgS microparticles used in methylation experiments. XPS spectra were also collected for pure minerals of metacinnabar and cinnabar. **(c)** XRD spectra of the same samples. Dotted lines correspond to expected peak positions for pure cinnabar and pure metacinnabar. The spectra for humic-HgS nanoparticles indicated metacinnabar-like structure. HgS microparticles consisted of a mixture of metacinnabar and cinnabar.

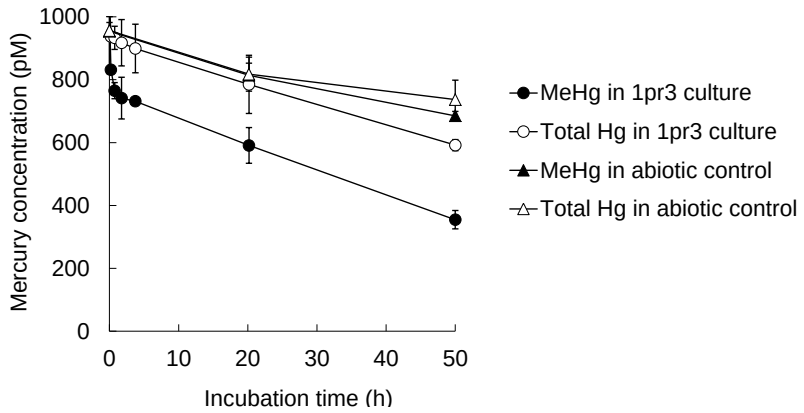

Figure 2.7. MeHg degradation in *D. propionicus* 1pr3 cultures. Test cultures were exposed to 1 nM methylmercury chloride (MeHgCl) during 2-day time course experiments. Abiotic controls were uninoculated medium solutions amended with 1 nM MeHgCl. The error bars represent ±1 s.d. for duplicate samples.

While nanoparticles generally have high specific surface areas relative to their bulk scale analogs, they can also exhibit unique reactivity due to lattice or surface imperfections that occur with nanoscale particles [135,137]. Here, we provide two lines of evidence to demonstrate that biomethylation of HgS nanoparticles did not depend simply on surface area. First, as the HgS nanoparticles were allowed to age for 16 hours and 3 days prior to exposure to *D. propionicus* 1pr3, their methylation potential was considerably reduced (Figure 2.1a) while their size and specific surface area remained similar (Table 2.1). Statistically significant differences in geometric surface area and monomer diameter were observed only with the 1-week old nanoparticles. Second, nano-HgS was more reactive per unit surface area relative to micro-HgS. MeHg generated from nano-HgS (with 5.3×10^{-5} m^2L^{-1} surface area) was 3 times greater than MeHg generated from micro-HgS with 11×10^{-5} m^2L^{-1} surface area (Figure 2.1c) corresponding to a production of MeHg per m^2 of material 6 times higher for nano-HgS compared to micro-HgS (1.13 $\mu mol.m^{-2}$ and 0.18 $\mu mol.m^{-2}$ respectively). The reduced availability of nano-HgS during aging may be due to the structural changes occurring with amorphous nanoparticles or cluster/particles at the small size range (1-2 nm). These changes would not be reflected in the results of TEM or XRD analyses.

The net production of methylmercury was relatively fast in the first few hours and slow after this initial time period (Figure 2.1 and 2.2). This deceleration of MeHg production could not be explained by microbial growth, as we observed a steady increase of cell density throughout the one-day mercury methylation experiments (Figure 2.3). Similar trends were observed in other mercury methylation studies using the same SRB strains [107,179] and estuarine sediment slurries [187]. These results are possibly due to the saturation of enzymes and/or depletion of certain compounds (e.g. methyl donors) that were required for mercury methylation. Furthermore, inorganic Hg speciation may have shifted after the first few hours towards less bioavailable forms for the bacteria. The declining net methylation rate may also be explained by the contribution of a reverse process (i.e. methylmercury degradation) balancing overall methylmercury concentrations in the cultures. *Desulfovibrio desulfuricans* ND132 and *Desulfobulbus propionicus* strains are known to

simultaneously generate and degrade MeHg [179,188,189]. We performed experiments with the 1pr3 strain exposed to methylmercury chloride and observed MeHg degradation in these cultures (Figure 2.7).

2.3.2 Mercury Fractionation in Methylating Cultures

Bacteria are not known to directly take up nanoparticles without compromising their membrane integrity. However, previous works have indicated that they can take up metal constituents of nanoparticles through the accumulation of nanoparticles at cell surfaces [147,149,190]. To test this hypothesis, we fractionated the mercury in the cultures into nominally dissolved mercury (<0.02 μm), colloidal mercury (between 0.02 and 0.22 μm), and particulate or cell-associated mercury (>0.22 μm) using filters with two different pore sizes (0.02 and 0.22 μm) (Figure 2.8). Filtration of bacteria-free media that were amended with dissolved $HgNO_3$, nanoparticulate HgS, and microparticulate HgS (Figure 2.9) indicated that the two filters could be used to distinguish these forms of mercury (Figure 2.9a).We also examined the cultures with transmission electron microscopy (TEM) to further differentiate mercury associated with cells from mercury associated with large aggregates of HgS particles. In the nano-HgS exposures, the filtration results showed that the amount of mercury in the >0.22 μm fraction increased over incubation time (Figure 2.8c). In TEM images, on the other hand, large aggregates of HgS particles (>0.22 μm), as seen in the micro-HgS treated cultures (Figure 2.8f and Figure 2.10c), were not observed in the nanoparticle exposures (Figure 2.8d and Figure 2.10b).

While mercury was quantified in the >0.22 μm fraction, the nanoparticles were likely too dilute to be observed in bacterial cultures that contained a complex mixture of particles (Figure 2.10b). The nanoparticles could also be dissolving into solution, as indicated by a small increase of dissolved mercury (from 0.073 nM to 0.21 nM in one day) in bacteria-free media amended with 1 nM nano-HgS (Figure 2.9c). This concentration range is greater than would be expected from the equilibrium solubility of $HgS_{(s)}$. (Dissolved Hg at equilibrium is 10^{-8} to 10^{-5} nM at pH 7.5, depending on the solubility product for $HgS_{(s)}$ [15]). In media containing both bacteria and nanoparticles, the percent of total mercury in the >0.22 μm fraction was 60% after 1 day and greater than bacteria-free media containing nanoparticles (8%) (Figure 2.8c and Figure 2.9c), indicating that the nanoparticles were either depositing onto cells or releasing dissolved mercury that was immediately adsorbed to or taken up by the cells. Micro-HgS was less accessible for biomethylation, possibly due to the minimal mercury dissolution (<0.02 nM mercury dissolved in the bacteria free experiments, Figure 2.9d).

In the dissolved Hg+S and nano-HgS exposures, the amount of mercury in the >0.22 μm fraction was similar (Figure 2.8a and 2.8c), yet these treatments exhibited markedly different MeHg production (Figure 2.11). While HgS clusters and nanoparticles were likely forming in the cultures receiving dissolved Hg(II) and S(-II), net MeHg production was faster in the dissolved mercury exposure than the nanoparticle exposure. These results agree with recent studies that suggested transmembrane mercury uptake as the rate-limiting step of intracellular mercury methylation [57,189] and imply that HgS nanoparticles are not as bioavailable as their precursors (e.g., dissolved mercury-sulfide complexes and clusters). Similar patterns of mercury size fractionation were observed in replicate cultures processed by ultracentrifugation (Figure 2.12).

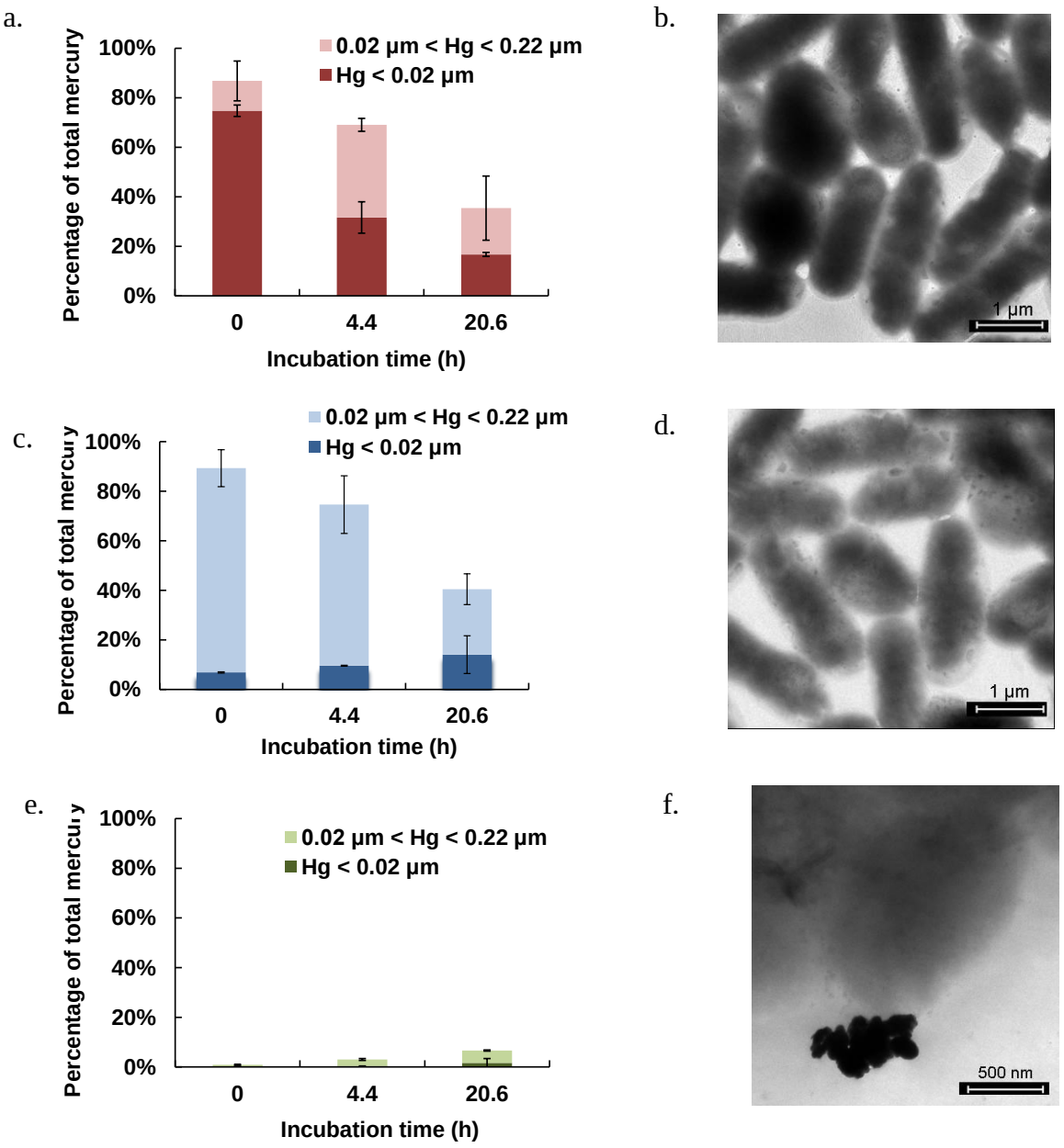

Figure 2.8. Percentages of mercury in solution after filtration of *D. propionicus* 1pr3 cultures and TEM images of the cultures. Cultures were exposed to 1 nM dissolved $Hg(NO_3)_2$ and Na_2S (**a** and **b**); 1 nM humic-HgS nanoparticles (aged for 16 h, **c** and **d**); and 6 nM HgS microparticles (**e** and **f**). "Hg<0.02 μm" represented the fraction of total mercury that passed through 0.02-μm filters. "0.02 μm<Hg<0.22 μm" represented the concentration difference of aliquots filtered by either 0.22-μm or 0.02-μm filters. Cells for TEM image were collected 14 h after exposure to HgS. The error bars represent ±1 s.d. for duplicate samples.

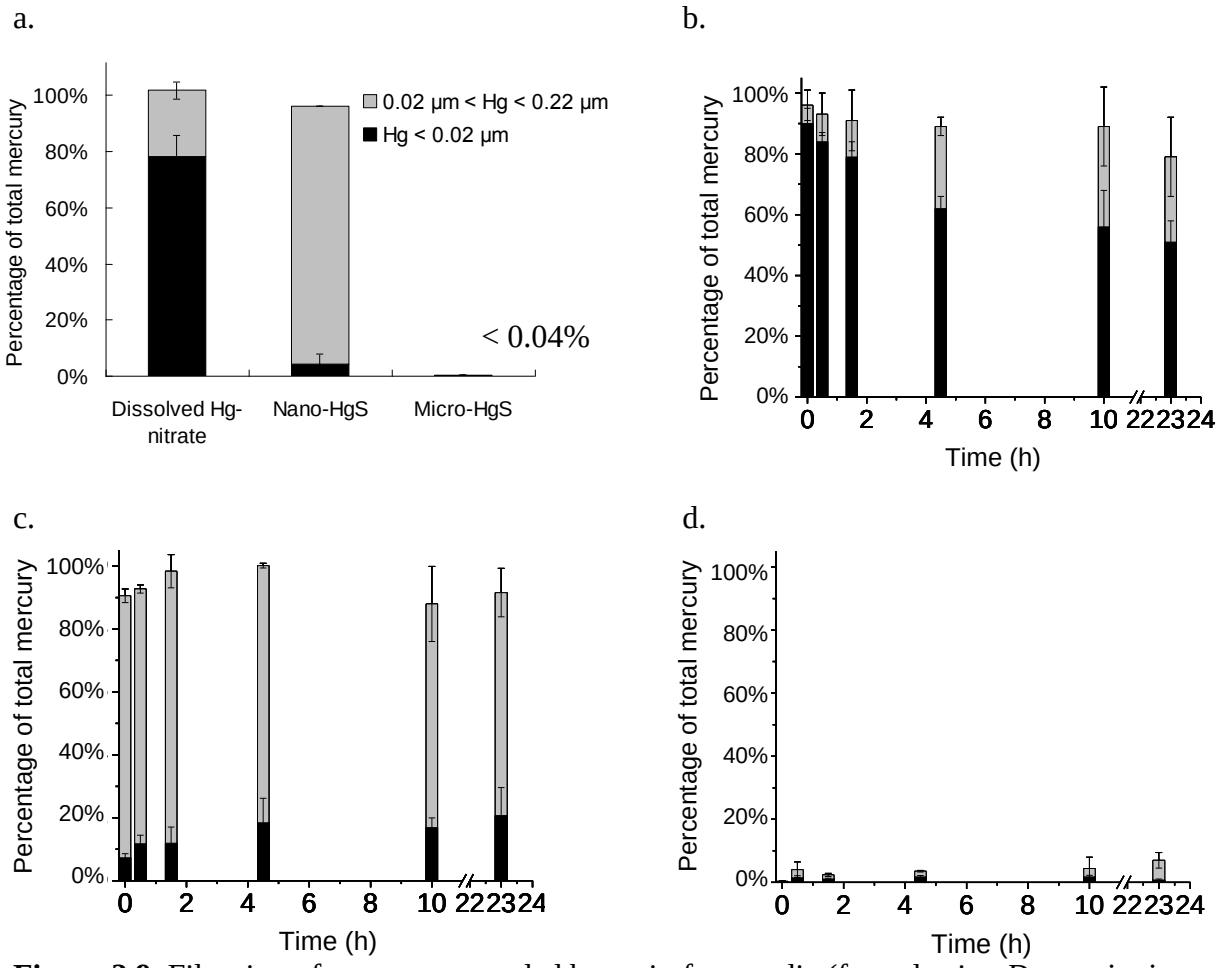

Figure 2.9. Filtration of mercury-amended bacteria-free media (for culturing *D. propionicus* 1pr3). **(a)** Medium solution was amended with 1 nM $Hg(NO_3)_2$, 1 nM humic-HgS nanoparticles (aged for 16 h) or 6 nM HgS microparticles, and filtered immediately (less than 10 min) after mercury addition. Filtration of separate samples at different time points after they were amended with different Hg-sulfide species, including **(b)** 1 nM dissolved $Hg(NO_3)_2$ and Na_2S, **(c)** 1 nM humic-HgS nanoparticles (aged for 16 h), and **(d)** 6 nM HgS microparticles. "Hg<0.02 μm" represented the fraction of total mercury that passed through 0.02-μm filters. "0.02 μm<Hg<0.22 μm" represented the concentration difference of aliquots filtered by either 0.22-μm or 0.02-μm filters. The error bars represent ±1 s.d. for duplicate samples.

a.

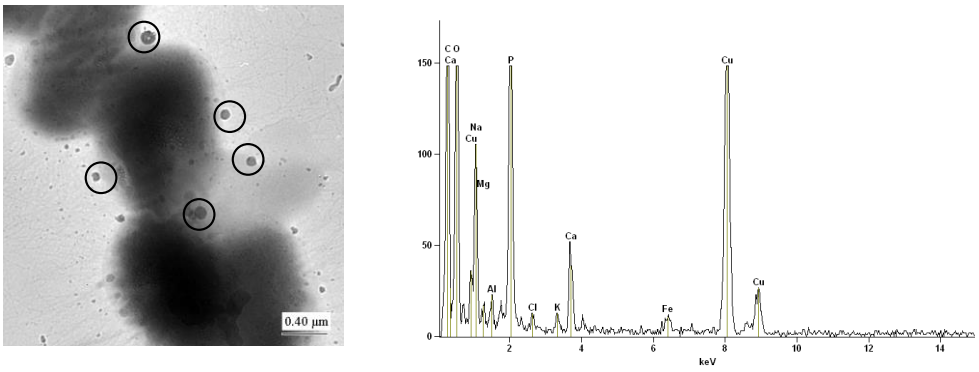

b.

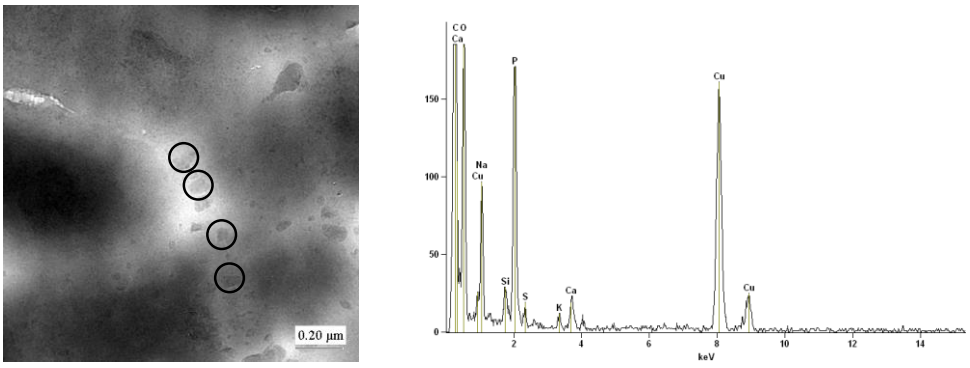

c.

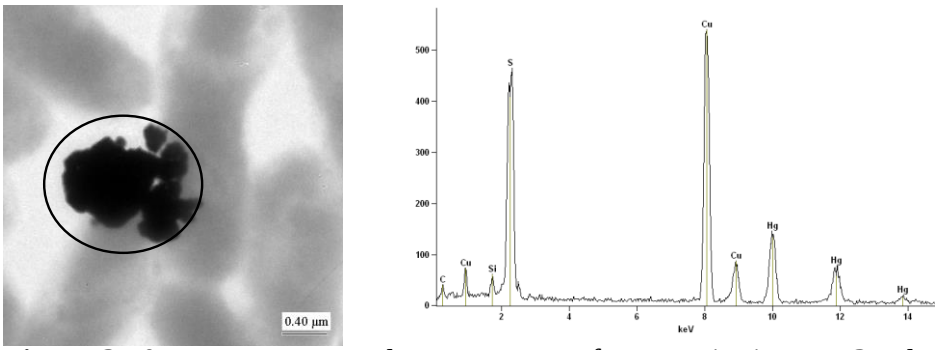

Figure 2.10. TEM images and EDX spectra of *D. propionicus* 1pr3 cultures. Cultures were exposed to **(a)** 1 nM dissolved $Hg(NO_3)_2$ and Na_2S, **(b)** 1 nM humic-HgS nanoparticles (aged for 16 h), and **(c)** 6 nM HgS microparticles. Test cultures for TEM imaging were collected 14 h after exposure to HgS. Elemental composition of the particles around and/or on the bacterial cells (in black circles) was determined by EDX. The Cu, C, O and Si peaks are from the sample grid. Hg-containing particles were not observed in the cultures exposed to dissolved and nanoparticulate mercury; however, other nanoparticles comprising of elements in the culture media were present, highlighting the heterogeneous nature of the bacteria cultures.

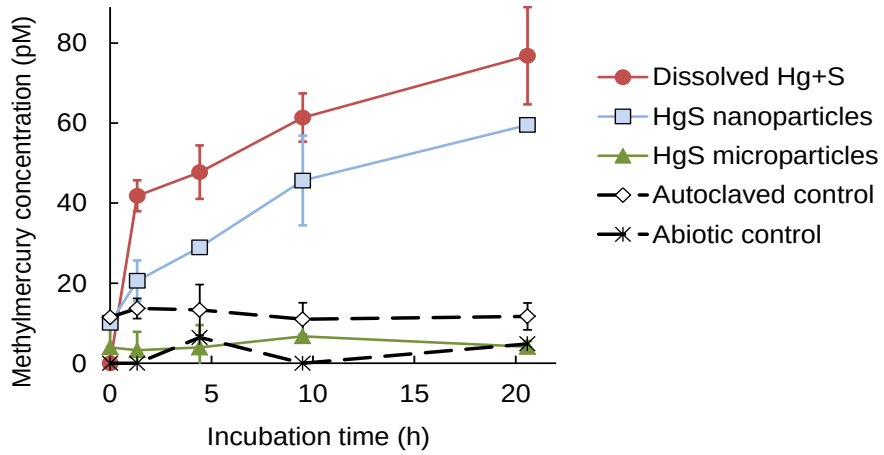

Figure 2.11. Net MeHg production in *D. propionicus* 1pr3 cultures exposed to different forms of mercuric sulfides. Test cultures were exposed to 1 nM dissolved $Hg(NO_3)_2$ and Na_2S, 1 nM humic-HgS nanoparticles (aged for 16 h), and 6 nM HgS microparticles. The error bars represent ±1 s.d. for duplicate samples. Results of Hg fractionation by filtration and (ultra)centrifugation of these samples are shown in Figure 8 and Figure 12, respectively.

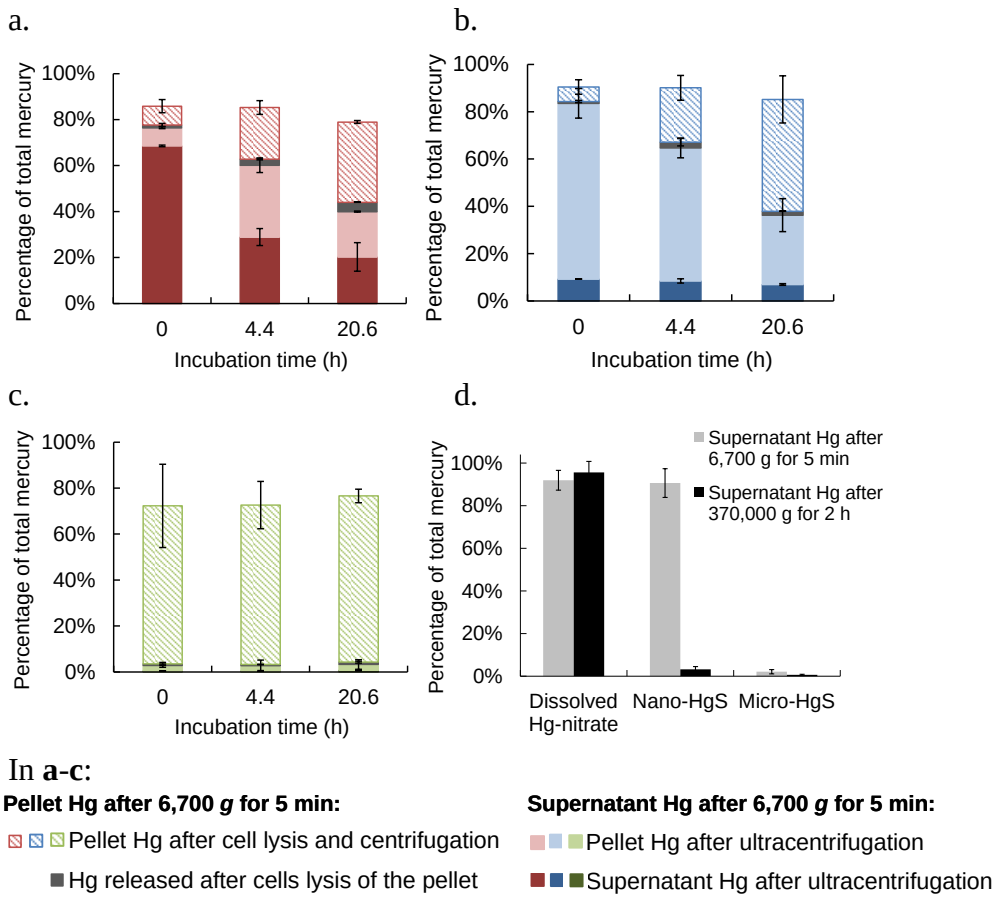

Figure 2.12. Centrifugation and ultracentrifugation of mercury-amended *D. propionicus* 1pr3 cultures. Cultures were treated with different Hg-sulfide species, including **(a)** 1 nM dissolved $Hg(NO_3)_2$ and Na_2S, **(b)** 1 nM humic-HgS nanoparticles (aged for 16 h), and **(c)** 6 nM HgS microparticles. Cultures were incubated at room temperature for up to 1 day after mercury addition. At each time point, cultures were first centrifuged at 6,700 *g* for 5 min. The pellets were lysed through freeze-thaw cycles plus sonication and then centrifuged at 10,800 *g* for 30 min. The supernatant (after 6,700 *g* for 5 min) was ultracentrifuged at 370,000 *g* for 2 h. **(d)** Bacteria-free media were amended with 1 nM $Hg(NO_3)_2$, 1 nM humic-HgS nanoparticles (aged for 16 h) or 6 nM HgS microparticles, and (ultra)centrifuged immediately (less than 10 min) after mercury addition. The error bars represent ±1 s.d. for duplicate samples.

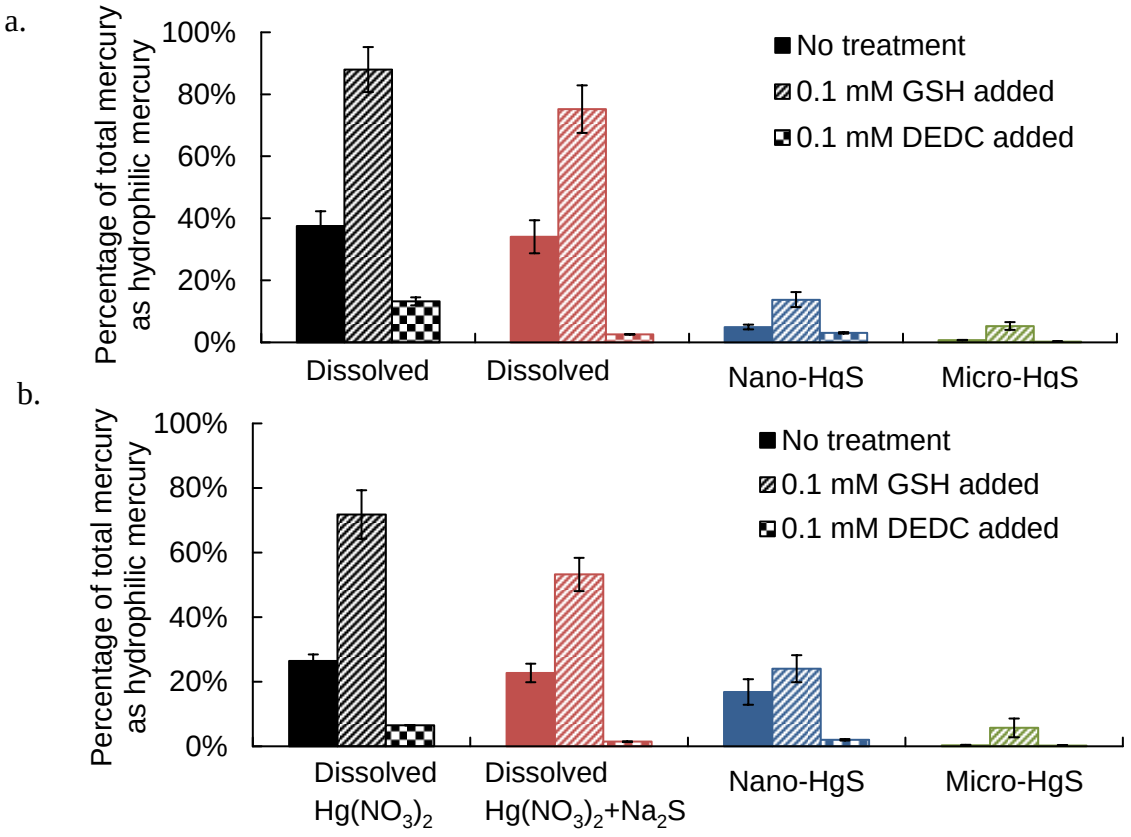

Figure 2.13. Hydrophilic mercury in HgS-amended media after competitive ligand exchange with GSH or DEDC and C_{18} solid-phase extraction. Uninoculated medium solutions (for culturing *D. propionicus* 1pr3) were spiked with 1 nM dissolved $Hg(NO_3)_2$, 1 nM dissolved $Hg(NO_3)_2$ and Na_2S, 1 nM humic-HgS nanoparticles (aged for 16 h), and 6 nM HgS microparticles. Ligand exchange reactions were performed by amending aliquots of these samples with GSH or DEDC at two time points after the mercury amendment: **(a)** Immediately (less than 10 min). **(b)** 23 h. GSH and DEDC were mixed in the samples for 1 h and then filtered through a C_{18} resin. All solutions received the same humic acid concentration (0.2 μg-C/L). Error bars represent ±1 s.d. for duplicate samples.

2.3.3 Mercury Speciation by Competitive Ligand Exchange

We applied competitive ligand exchange-solid phase extraction [91,186] to further examine the speciation of mercury in bacteria-free media. In this method, labile mercury species were replaced by Hg-thiol complexes: either hydrophilic mercury-glutathione (GSH) complexes or hydrophobic Hg-diethyldithiocarbamate (DEDC) complexes. Labile mercury was quantified by the change of mercury in the hydrophilic fraction (defined as mercury passing through a C_{18}-resin filter). In the micro-HgS exposure, mercury speciation remained unchanged after addition of GSH or DEDC (Figure 2.13), indicating that mercury was largely inert. In the media containing nano-HgS, the amount of hydrophilic mercury increased after 1 day, and this fraction was mostly removed by DEDC ligand exchange (Figure 2.13b), indicating the presence of labile mercury. However, in the dissolved Hg+S exposure, the changes in the hydrophilic mercury fraction after addition of GSH and DEDC were both larger than in the nano-HgS treatment. This pattern of decreasing thiol-exchange reactivity between the dissolved, nanoparticulate and microparticulate mercury corresponded to decreasing methylation rates (Figure 2.1). Mercury is believed to bind to bacterial cells through thiol-containing ligands on the membrane surfaces [191], and these complexes may enter the cells as favorable substrates for methylation [57]. Hence, the labile mercury quantified by thiol ligand exchange could signify the available fraction of mercury for microbial uptake and methylation.

2.3.4 Environmental Implications

Our overall results challenge the longstanding view that mercury bioavailability (and methylation potential) can be represented by equilibrium speciation of dissolved mercury in water [62]. Our previous work [15] has indicated that $HgS_{(aq)}^{0}$ (a form of dissolved mercury presumed to be bioavailable [62]) represents HgS nanoparticles rather than a mononuclear aqueous mercury-sulfide complex. We demonstrate here that a single entity to represent nanoparticulate or colloidal HgS is overly simplistic and that the bioavailability of mercury depends on the evolving nanoscale properties of mercury compounds that fall in the fraction typically designated as dissolved and colloidal (less than 0.2 or 0.45 μm). This conclusion could help explain observations that mercury recently deposited to surface waters from the atmosphere (as weak $HgCl_2$ complexes) is more readily transformed to MeHg than older mercury that persists mainly as crystalline $HgS_{(s)}$ in historically contaminated sediments [10,192].

Although the occurrence of nanoparticulate or colloidal HgS has been suggested in a number of studies [15,16,122,145,186,193], our investigation is the first to explore the potential of HgS nanoparticles to serve as an important, but previously unrecognized source of bioavailable mercury for methylating bacteria. Overall, our results points to a new approach for modeling mercury bioavailability that is needed for predicting and mitigating MeHg hotspots in the aquatic environment. Given that mineral nanoparticles are ubiquitous in the environment [135], the importance of nanoscale processes for trace metal bioavailability and toxicity has yet to be fully realized. Our findings provide a new approach that may be applied to other metal-sulfide nanoparticles (e.g., ZnS, CuS, FeS) and their potential roles in biogeochemical metal cycling.

Chapter 3

Kinetic Modeling of Mercury Speciation and Methylation in Bacterial Cultures Exposed to Dissolved and Nanoparticulate Mercuric Sulfides

This chapter has been submitted for publication:
Ticknor, J.L.; Zhang, T.; Deshusses, M.A.; Hsu-Kim, H. Kinetic Modeling of Mercury Speciation and Methylation in Bacterial Cultures Exposed to Dissolved and Nanoparticulate Mercuric Sulfides. Manuscript submitted to *Environmental Modeling*.

3.2 Introduction

Historically, mercury speciation and bioavailability have been predicted using chemical equilibrium models[62,194,195]. With these models, the user enters relevant thermodynamic parameters for Hg(II) species into the program database and then utilizes the model to calculate concentrations of dissolved complexes and mineral phases from measured values of dissolved mercury in the sample. This approach assumes that mercury uptake is controlled by dissolved neutrally charged mercury sulfide species that passively diffuse through the cell membrane of methylating bacteria[62]. Thus, the neutrally charged dissolved complexes calculated at chemical equilibrium will control mercury bioavailability. However, this approach has several problems, including recent evidence pointing towards an active uptake mechanism of Hg(II) by methylating bacteria[56,57,196,197] the requirement for a large presence of an unknown species, $HgS^{(0)}_{(aq)}$, that may be nanoparticulate mercury rather than a dissolved monomeric complex[15]. Mercuric sulfide nanoparticles are known to exist in the environment[122,144,145] and recent work[15-17] has shown the potential for the formation of HgS nanoparticles in conditions typical for anoxic environments. These particles can account for a fraction of mercury passing through either a 0.2 or 0.45 µm filter[198,199], an operational definition of "dissolved" mercury for speciation calculations.

The previous work described in Chapter 2 showed that sulfate-reducing bacteria exposed to nanoparticulate mercury sulfides (nHgS) were capable of producing methylmercury at rates significantly greater than cultures exposed to well-crystalline bulk HgS mineral phases[19]. Based on this observation and the dynamic nature of mercury speciation between dissolved and nanoparticulate phases, a kinetic-based modeling approach may be best suited to accurately predict the speciation and bioavailability of mercury to SRB. Particle formation and dissolution rates tend to be significantly slower than water exchange rates for dissolved complex formation and could control the time required for the system to reach a steady state. Moreover, nanoparticles are expected to exhibit unique reactivity, such as enhanced dissolution rates relative to their bulk mineral counterparts[135]. The unique reactivity of nanoscale materials stems from higher surface area-to-mass ratios and crystal lattice imperfection on nanoparticle surfaces. Therefore, a kinetic mercury speciation model must consider these differences between nanoscale and bulk scale Hg.

The objective of the research in this chapter was to understand why methylmercury production was observed in cultures exposed to nanoparticulate HgS and if this observation could be attributed simply to increased dissolution of the nanoparticles relative to the microscale particles. This analysis involved the development of a rate-based numerical model that considered the kinetics of dissolved mercury complexation, formation and dissolution of HgS nanoparticles and microparticles, biological methylation, and demethylation by SRB. This model was applied

towards experiments conducted with pure cultures of SRB described in previous work in Chapter 2 (and published in Zhang et al.[19]). Rate constants for the model were taken from particle dissolution experiments performed for this study or were fit to methylation data for cultures receiving dissolved Hg. The potential mechanisms by which cultures exposed to HgS nanoparticles could produce methylmercury were tested by making alterations to the model equations by either increasing the rates of dissolution for the nanoparticles or including a unique pathway for enhanced methylation in the presence of HgS nanoparticles . Parametric sensitivity studies were also performed to offer potential avenues for future experimental studies that can link the molecular structure, reactivity, and methylation potential of mercuric sulfide nanoparticles.

3.2 Kinetic Model Framework

The model framework (Figure 3.1) consists of rate equations describing dissolved complex formation, formation and dissolution of nanoparticulate HgS (nHgS) and bulk scale HgS, and mercury methylation/demethylation. The resulting ordinary differential equations (ODE) were solved numerically using a stiff algorithm on Berkeley Madonna software. This approach was required because of the inherent differences in reaction rates, often several orders of magnitude, which often cause simpler methods, like the commonly used Runge-Kutta algorithms, to fail.

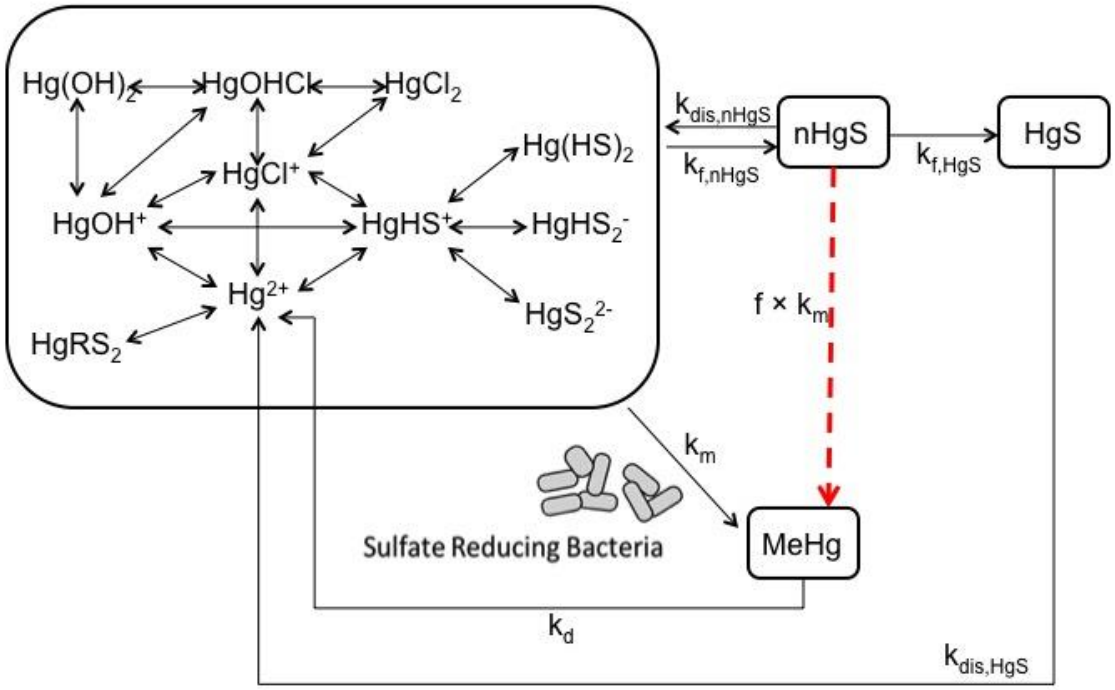

Figure 3.1. Model schematic for rate based model of Hg speciation and methylation by sulfate reducing bacteria. The corresponding rate constants are provided in Table 3.1. Equations describing the calculation of water ligand exchange rates for dissolved Hg-ligand complexes are provided in Supporting Information. The species represented in the far left box are only a subset of all dissolved species, which are provided in Table S1 in their entirety. The dashed red line corresponds to a potential enhanced biomethylation pathway in the presence of nanoparticles (see text).

Table 3.1 Values for the reaction rate constants used in methylation simulations.

Rate constant	Value
[a] nHgS dissolution rate constant, $k_{dis,nHgS}$	
- For dissolved Hg+S treatments	0.012 h^{-1}
- For nHgS treatments	0.0072 h^{-1}
[a] nHgS formation rate constant, $k_{f,nHgS}$	
- For dissolved Hg+S treatments	0.12 h^{-1}
- For nHgS treaments	0.33 h^{-1}
[b] HgS formation rate constant, $k_{f,HgS}$	1.0×10^{-4} h^{-1}
[b] HgS dissolution rate constant, $k_{dis,HgS}$	1.0×10^{-4} h^{-1}
[c]Mercury methylation rate, k_m (1pr3)	0.025 h^{-1}
[c]Mercury demethylation rate, k_d (1pr3)	0.12 h^{-1}
[c] Mercury methylation rate, k_m (ND132)	0.11 h^{-1}
[c]Mercury demethylation rate, k_d (ND132)	0.15 h^{-1}

[a] Dissolution and formation rate constants were calculated by fitting experimental data from Zhang et al.[19], shown in Figure 3.2

[b] HgS refers to microparticulate fraction, generally considered the bulk mineral phase

[c] Determined by model fits of methylation data from Zhang et al.[19] for cultures exposed to dissolved Hg + sulfide.

Dissolved mercury-ligand species (HgL), as shown in Equation 3.1, were modeled by using water exchange reaction kinetics to describe the formation from other dissolved mercury complexes, the dissolution of nHgS, and disappearance as a result of methylation and nHgS formation :

$$\frac{d[HgL]}{dt} = K_{OS}k_w[Hg^{2+}][L] - \frac{K_{OS}k_w}{K_{eq}}[HgL] - \sum(\frac{K_{OS}k_w}{K_{eq}}[HgX][L] - K_{OS}K_{eq}[HgL][X]) + \frac{K_{OS}k_w}{K_{eq}}[HgL_2] - K_{os}k_w[HgL][L] - -k_{f,nHgS}[HgL] + k_{dis,nHgS}[nHgS] - k_m[HgL] \quad (3.1)$$

where ligands L and X are OH^-,Cl^-, or HS^-. The forward ligand complexation reaction rate was calculated by multiplying the water exchange rate constant for mercury (k_w) and the equilibrium constant for outer sphere association (K_{OS}). Consistent with the actual mechanisms of water-ligand exchange reactions, the formation of 1:2 Hg:L complexes was modeled as a two-step process where the first step follows Equation 3.1 and the addition of a second ligand was modeled by Equation 3.2:

$$\frac{d[HgL_2]}{dt} = K_{OS}k_w[HgL][L] - \frac{K_{OS}k_w}{K_{eq}}[HgL_2] - k_{f,nHgS}[HgL_2] + k_{dis,nHgS}[nHgS] - k_m[HgL_2] \quad (3.2)$$

The equilibrium constant (K_{eq}) was obtained for each species from thermodynamic databases[62,112,200] and summarized in Table S1. The constant for outer sphere association (K_{OS}) is related to ionic strength and ionic charges of Hg^{2+} and the ligand L[201], as shown in the Supporting Information.

The formation rate of Hg complexes with thiol functional groups associated with dissolved organic matter (RS_2^{2-}) was modeled as a second order reaction with respect to the

concentration of total dissolved Hg and reduced-S functional groups (RS_2^{2-}) on dissolved organic matter[116], as shown in Equation 3.3.

$$\frac{d(HgRS_2)}{dt} = K_{OS}k_w[Hg^{2+}][RS_2^{2-}] - \frac{K_{OS}k_w}{K_{eq}}[HgRS_2] - k_{f,nHgS}[HgRS_2] + k_{dis,nHgS}[nHgS] - k_m[HgRS_2] \quad (3.3)$$

The total concentration of Hg-binding sites associated with NOM, $[RS_2^{2-}]_T$, was estimated from the NOM concentration utilized by Zhang et al. (0.2 μg-C L^{-1}) and the reduced sulfur content of Suwanee River humic acid (2.3 nmol reduced-S per mg-C [116]). This estimate of $[RS_2^{2-}]_T$ is likely to be a conservatively high concentration, since the strong Hg-binding site content is typically a fraction of the reduced-S pool in NOM. Nevertheless, this uncertainty for $[RS_2^{2-}]_T$ was not consequential in our calculation because in our experiments the dissolved Hg concentration (0.1 nM or greater) exceeded the NOM reduced-S concentration.

To assess the formation of HgS particles in scenarios when dissolved Hg(II) and sulfide are present in solution at concentrations of $HgS_{(s)}$ supersaturation, mineral precipitation was simulated as a two-step process involving the formation of HgS nanoparticles followed by the formation of microparticulate HgS:

$$\frac{d[nHgS]}{dt} = k_{f,nHgS}([Hg^{2+}] + \sum_{i=1}^{2}[HgL_i] + [HgRS_2]) - 11 \times k_{dis,nHgS}[nHgS] - k_{f,HgS}[nHgS] \quad (3.4)$$

$$\frac{d[HgS]}{dt} = k_{f,HgS}[nHgS] - k_{dis,HgS}[HgS] \quad (3.5)$$

The formation of nanoparticulate HgS was modeled as a first order reaction based on the concentration of total dissolved mercury, as shown in Equation 4. Since divalent mercury (Hg^{2+}) cannot be directly measured, a kinetic rate constant ($k_{f,nHgS}$) must be estimated based on the total dissolved mercury concentration that can be measured, thus the need for the summation term in Eq. 3.4. We assumed a first order reaction for nanoparticles formation, similar to a previous study[16]. The constants $k_{dis,nHgS}$ and $k_{dis,HgS}$ correspond to first order dissolution rates of nanoparticles and microparticulate HgS, respectively. The formation of microparticulate HgS (i.e., cinnabar and metacinnabar) was also modeled as a first order process (Eq. 3.5), likely corresponding to aggregation or crystal ripening of nanoparticles formed in earlier time steps. Rate constants for the formation and dissolution of nHgS and HgS were determined in separate dissolution/precipitation experiments in bacteria-free culture media (see Materials and Methods section). The rate constants were estimated by linear least square fitting of dissolved Hg concentration predicted by model equations 3.1 to 3.5.

The rate of mercury methylation and demethylation was determined using Equation 3.6:

$$\frac{d[MeHg]}{dt} = k_m([Hg^{2+}] + \sum_{i=1}^{2}[HgL_i] + [HgRS_2]) - k_d[MeHg] \quad (3.6)$$

where k_m and k_d represent the first-order rate constants for methylation and demethylation, which were fit to previous methylation experiments for *D. propionicus* 1pr3 and *D. desulfuricans* ND132[19]. This formulation is often used to describe mercury methylation processes, particularly

to determine the mercury methylation potential for specific strains of microorganisms[58,107,124,202]. The rate of methylation represents a combination of processes including Hg uptake into the cell and methylation inside the cell. However, these processes are not yet understood enough to parameterize for the model. Therefore we assumed that all dissolved species were bioavailable for methylation with the same rate constant k_m while particles (nano- and microscale) were not bioavailable. Methylmercury demethylation (represented with rate constant k_d) was modeled as a process resulting in the production of Hg^{2+}, which could then react to form other dissolved mercury species via complexation reactions. This is consistent with the oxidative demethylation pathway commonly observed under anaerobic conditions[197].

The monomeric $HgS^0_{(aq)}$ species, was not included in this model because this unknown species most likely includes nanoparticulate mercury[15] which was described as a distinct species in this model. We also did not consider sorption of Hg to cell surfaces that could result in Hg that is unavailable for methylation. If this process were occurring, the rate could be reflected in a shift in the balance between methylation and demethylation (i.e. the relative values of k_m and k_d).

Methylmercury production was determined by numerically solving the above set of linked differential equations (14 total equations in the model and listed in SI). This model was applied to methylation experiments where pure cultures of *D. propionicus* 1pr3 and *D. desulfuricans* ND132 were cultured fermentatively and exposed to 1 nM dissolved Hg and sulfide or 1 nM nHgS.[19] Data for the bulk HgS treatment was not modeled because methylmercury production was no different than in abiotic controls.

In the methylation experiments, total Hg concentration, total sulfide concentration, and growth rate were the same. Only the type of Hg added was varied. The input parameters used for the model were: 1 nM total Hg, 1 μM total dissolved sulfide, pH 7.5, 30 mM Cl^-, and 0.46 pM total RS_2^{2-} (corresponding to the added humic acid concentration). The initial Hg in the calculation was designated as Hg^{2+} or nHgS, depending on the experiment that was modeled. While 1 nM sulfide (either as dissolved Na_2S or nHgS) was added with the mercury, the cultures likely contained approximately 1 μM sulfide resulting from carryover of the bacterial inoculum and trace production of sulfide in fermentatively cultured bacteria[107].

The methylation and demethylation rate parameters k_m and k_d were estimated by fitting the model to experiments involving the addition of dissolved Hg and sulfide to the cultures. The rate constants used from these fits were then used to simulate (without any adjustable parameter) methylation experiments where the same pure cultures were exposed to nHgS.

3.3 Materials and Methods

HgS Nanoparticle Dissolution Experiments. Independent HgS nanoparticle dissolution and formation experiments were performed to determine $k_{dis,nHgS}$ and $k_{f,nHgS}$. The HgS nanoparticles utilized for this experiment were synthesized in the same manner as the procedure used in a previous methylation study[19] (described in the SI). In summary, the nanoparticles had an average hydrodynamic diameter of 29 nm, similar to results reported in our previous study[19] . Our previous work also indicated that these nanoparticles are aggregates of smaller particles (3 ± 1 nm diameter) with metacinnabar-like composition.

The dissolution experiments were performed by amending bacteria-free fermentative growth medium (corresponding to *D. propionicus* 1pr3 cultures)[107] with 1 nM nanoparticulate mercury sulfide (nHgS) or dissolved Hg + sulfide and measuring the evolution of dissolved Hg. Prior to addition of the mercury sulfides, the pH of the medium was adjusted to 7.5 using HCl, filtered to

<0.1 μm, autoclaved to prevent bacterial growth, and then purged with N_2. A subset of samples was amended with 10 μM sulfide (prior to the addition of nHgS) to test the potential impact of microbial generation of sulfide on the dissolution rates. All nanoparticle dissolution and formation experiments were performed in duplicate batch samples prepared with glass vials in an anaerobic chamber (Coy Labs) and held static (i.e., no active mixing) throughout the experiment.

At each time point, aliquots were taken from the batch vials for quantification of dissolved Hg. Each batch vial was first tipped end-over-end prior to sampling 4 mL of the mixture into an 11 × 60 mm Ultra-Clear (Beckman Coulter) centrifuge tube. The sample was then placed in a SW60 Ti swinging bucket rotor and ultracentrifuged for 1 hour at 300,000 g (Beckman Coulter Centrifuge). Following ultracentrifugation, 2 mL of supernatant was pipetted into a pre-cleaned glass vialand digested with 2.2% v/v BrCl (500 μL). The samples were stored at room temperature for one day and then analyzed by $SnCl_2$ reduction, gold amalgamation, and cold vapor atomic fluorescence spectrometry (Brooks Rand Model III). Control experiments were performed to ensure that ultracentrifugation resulted in complete sedimentation of all but dissolved Hg species. Ultracentrifugation of the 50 μM nHgS stock solution resulted in more than 99% removal of Hg from the supernatant while ultracentrifugation of 1 nM $Hg(NO_3)_2$ amended to the culture media solution resulted in >90% of the mercury remaining in the supernatant.

3.4 Results and Discussion

3.4.1 Comparison of Kinetic & Equilibrium Models for Dissolved Hg Speciation.

Simulations of dissolved Hg speciation were first carried out to determine the relative time scale of complexation kinetics for our model. The output of the rate-based model for dissolved species only (i.e. in the absence of solid phases and methylmercury production) was compared to chemical equilibrium calculations performed in MINEQL+ and using equilibrium constants provided in Table S1. Relevant dissolved mercury-sulfide and mercury-chloride species concentrations obtained by the chemical equilibrium model and the proposed rate-based model were compared (Table S2).

The kinetic-based model simulation converged to an effective steady state within 0.1 h of simulation time irrespective of initial conditions. At this time point, the estimated concentrations from the kinetic model were largely in agreement with the equilibrium calculations (Table S2 and Figure S1). Both kinetic and equilibrium models predicted the same major dissolved species ($HgHS^+$, $Hg(HS)_2$, $HgHS_2^-$, and HgS_2^{2-}) as defined by complexes with concentrations greater than 10^{-16} M. The differences in concentrations between the two models for each major species were within a factor of 5.

3.4.2 Particle Dissolution & Formation Rate Constants

Kinetic rate coefficients for nHgS and HgS formation ($k_{f,nHgS}$ and $k_{f,HgS}$) and dissolution ($k_{dis,nHgS}$ and $k_{dis,HgS}$) were determined by fitting Equations 3.4 and 3.5 to data from experiments in which dissolved Hg+S, nanoparticulate HgS, and microparticulate HgS were added to growth media (no bacteria). The dissolved Hg concentration was monitored using two different separation methods: filtration by a 0.02 μm filter[19] or ultracentrifugation (this study), both in anaerobic conditions.

In the dissolution data reported by Zhang et al.[19] (and replotted in Figure 3.2), the apparent steady state Hg concentration for each sample appeared to approach different values, indicating that the re-precipitation of particles in the sample amended with nanoparticulate HgS was occurring by a process separate from the formation of nanoparticles in the sample amended with

dissolved Hg+S. The existence of precursor HgS nanoparticles in the nanoparticle treatment could present an alternate pathway for the loss of dissolved Hg separate from the formation of particles from an initially purely dissolved Hg solution, potentially explaining the discrepancy in equilibrium concentrations shown in Figure 3.2. Therefore, a separate pair of rate constants ($k_{dis,nHgS}$ and $k_{f,nHgS}$) was obtained for each experiment depending on whether mercury was added initially as dissolved Hg or nanoparticulate HgS (Table 3.1).

In order to accurately calculate rate constants for nanoparticle dissolution ($k_{dis,nHgS}$) and formation ($k_{f,nHgS}$), data from cultures spiked with dissolved Hg + sulfide and nanoparticulate HgS were fit separately using a least squares method. The initial dissolved Hg concentration was allowed to adjust during the simulation (between 0 and 1 nM) to allow the error associated with the initial time points to be considered. The reason for a non-zero dissolved Hg concentration in cultures spiked with nHgS was that the stock solution contained some dissolved Hg. Moreover, the nanoparticle stock comprised a mixture of HgS species, a portion of which (especially hydrated multinuclear clusters HgS) are likely to dissolve immediately upon dilution. The starting value for the initial concentration was adjusted multiple times to ensure that a unique solution was obtained. The rate constants were then used in modeling of the corresponding experiment (i.e., constants derived from dissolved Hg addition were used for methylation experiments with dissolved Hg added).

The dissolution of nHgS was determined again for this study using ultracentrifugation to quantify dissolved Hg concentration. These data were compared to filtration data from Zhang et al.[19] (Figure S2). Filtration allowed for precise time resolution because the separation could be performed rapidly. However, the concentration of Hg passing through the filter may not be a good representation of dissolved concentration due to the potential for particle breakthrough, filter malfunction, and sorption of dissolved Hg on the filter[19]. Ultracentrifugation could be an appropriate alternative because of its ability to remove particles of sufficiently small sizes (5 nm or larger)[16]. However, the centrifugation time leads to a very coarse time resolution (see x-axis error bars in Figure S2).

The dissolution experiment using ultracentrifugation resulted in dissolved Hg concentrations that were slightly lower than results from filtration (Figures S2). These differences in the data indicated that the nHgS dissolution rate could be overestimated by the filtration data alone ($k_{dis,nHgS}$ = 0.0072 h^{-1}, Table 3.1). However, the variations in the dissolution experiments do appear to be captured for a range of $k_{dis,nHgS}$ values that are two times greater and lower (Figure S2), indicating a range of dissolution rates to consider for parameter sensitivity analysis.

The potential impact of small amounts of sulfide (i.e. 10 μM) on the dissolution rates of nHgS was compared, as sulfide carryover could occur in bacterial inoculum[107]. However, this sulfide addition did not change the rate of Hg dissolution (Figure S2).

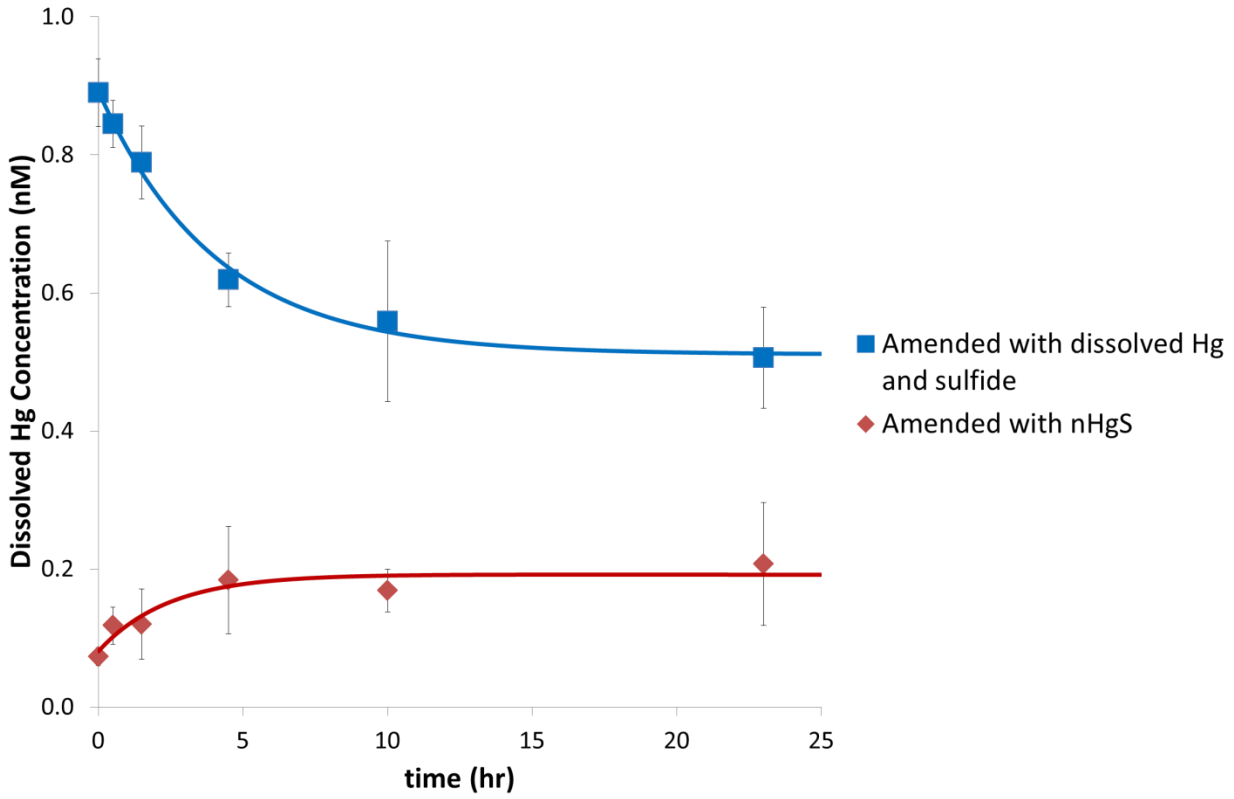

Figure 3.2. Model fits (lines) for dissolution and formation of mercury in experiments[19] in which growth media (no bacteria) was amended with either 1 nM dissolved Hg and 1 nM sulfide or with 1 nM nHgS. The measured dissolved Hg concentration (data points) corresponds to the Hg passing through a 0.02 µm filter. The adjustable parameters in these simulations were nanoparticle dissolution and formation rate constants ($k_{dis,nHgS}$ and $k_{f,nHgS}$), and initial dissolved Hg concentration. Error bars represent ± 1 SD for duplicate samples.

3.4.3 Estimation of Methylation and Demethylation Rate Constants

The dissolution/precipitation rates and the ligand-exchange rates for dissolved complexation were applied to estimate methylation and demethylation rate constants for data corresponding to the dissolved Hg+S treatments. The methylation rate constant k_m values for *D. propionicus* 1pr3 and *D. desulfuricans* ND132 were obtained by fitting the model to methylmercury evolved from dissolved Hg+S exposure[19] using data points within the first 5 hours, during which methylation will be the dominant mechanism compared to demethylation.

A least squares fitting of data for *D. propionicus* 1pr3 resulted in $k_m = 0.025\ h^{-1}$. This value is slightly smaller than the k_m value obtained in similar experiments by Benoit *et al.*[107], where the methylation rate within the first 5 hours was calculated to be $0.047\ h^{-1}$. The basis for this latter rate constant differs slightly from our model in that Benoit *et al.* considered only dissolved inorganic mercury and methylmercury species (and no particles).

The demethylation rate constant k_d for strain 1pr3 was then fit to the experimental incubation data extending to the 24 h time point for the dissolved Hg+S treatment, resulting in a value of $k_d = 0.12\ h^{-1}$. This value is larger than other k_d values ($0.03\text{- }0.09\ h^{-1}$) reported in the literature[58] . The discrepancy of the demethylation rate constant could be due to differences with our model, which

assumes the presence of nanoparticulate HgS that could provide a source of bioavailable Hg (via dissolution).

The methylation and demethylation rate constants for *D. desulfuricans* ND132 were also calculated from the dissolved Hg+S experiments (Figure 3.3), resulting in the estimated values k_m = 0.11 h^{-1} and k_d = 0.15 h^{-1}. To our best knowledge, methylation and demethylation rates for ND132 cultured in these experimental conditions have not been reported in the literature for similar experimental conditions and are not available for comparison purposes.

The rate constants derived from the methylation data in Figure 3.3 and listed in Table 1 were used for models of three separately replicated methylation experiments reported in Zhang et al.[19] (and plotted in Figures S3-S5). Although the microbial growth rates were slightly different between the replicated methylation experiments, the simulations of the dissolved Hg+S amendments in the replicated experiments were within one order of magnitude of the measured methylmercury data (Figures S3-S5).

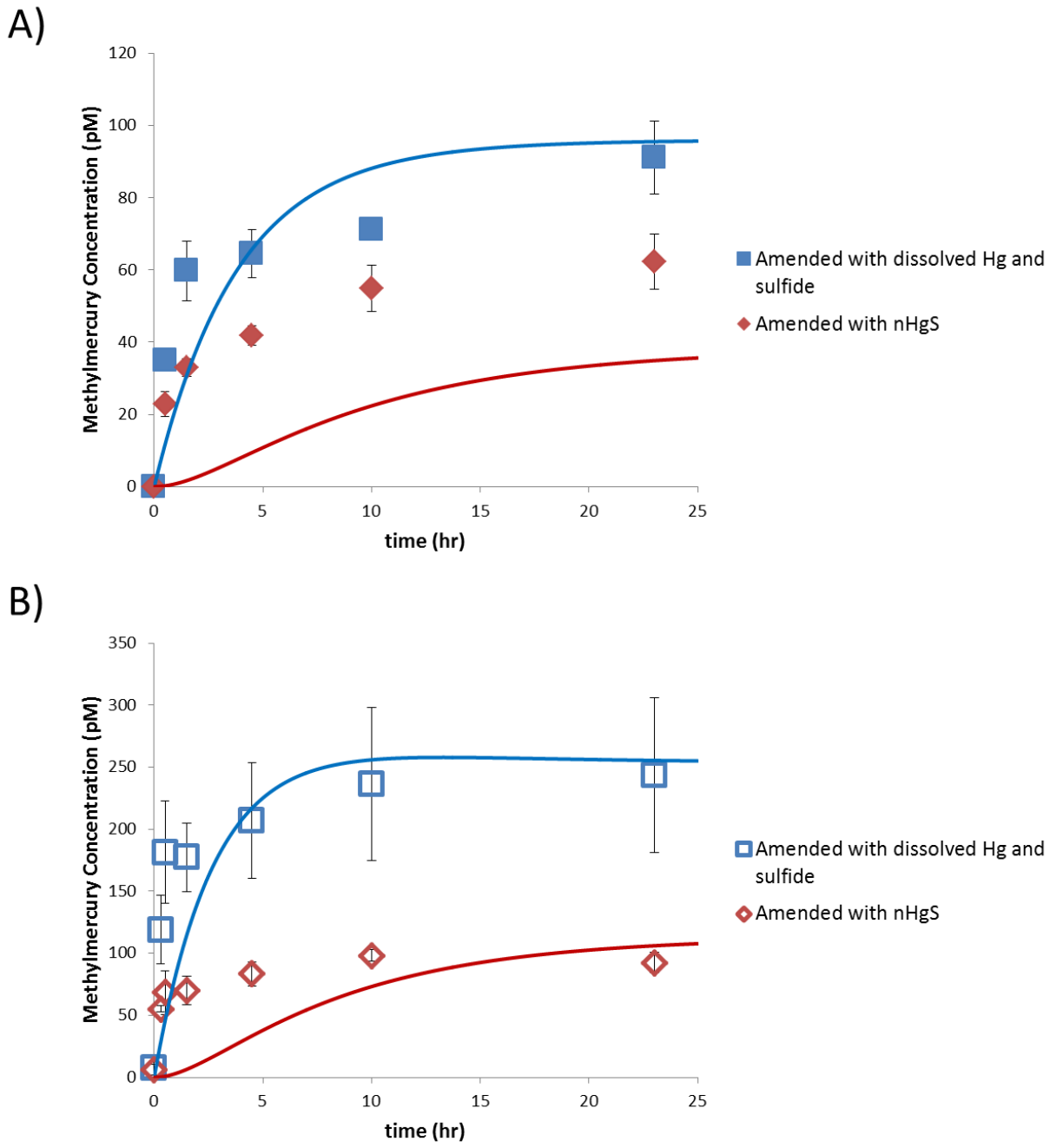

Figure 3.3. Experimental data (symbols, from Zhang et al.[19]) and model simulations (lines) of methylmercury production for: A) *D. propionicus* 1pr3 pure cultures and B) *D. desulfuricans* ND132 pure cultures exposed to dissolved Hg+S and nanoparticulate HgS. Experiments comprised of bacterial inoculum added to fermentative culture media with 1 nM Hg (dissolved or nanoparticulate), 1 nM sulfide, and 0.2 μg-C L^{-1} humic acid.

3.4.4 Simulations of Mercury Methylation in the Presence of Nanoparticles

Methylation simulations were then run for the experiments corresponding to the cultures exposed to 1 nM HgS nanoparticles (Figure 3.3). In the experiment for strain *D. propionicus* 1pr3 (Figure 3.3A), the predicted methylmercury concentration at each time point during the 23 hour experiment was found to be approximately 50% lower than the experimental value. For the experiment with *D. desulfuricans* ND132 (Figure 3.3B), the simulated methylmercury concentration underpredicted the measured concentrations by 20% or more for all time points within the first 10 h.

The model predicted a lag in methylmercury production at early time points (within the first 5 h). However in the experiments, the exposure of SRB to HgS nanoparticles resulted in an immediate production of MeHg. This difference between the model and experimental data at the early time points indicates that the initial bioavailable mercury concentration in the nanoparticle exposures was underestimated by the model. The discrepancy could be due to a fast initial dissolution of HgS nanoparticles immediately after addition to the bacterial cultures, resulting in a dissolution rate that was underpredicted by the rate constant we used ($k_{dis,nHgS}$ = 0.012 h^{-1}). However, if we consider the total dissolved mercury concentrations, defined as the fraction passing through a 0.02 µm filter, in the nanoparticle formation and dissolution experiments (Figure 3.2), we can see that within the first 5 hours there are clear differences in the nominally dissolved Hg concentrations in the cultures with dissolved Hg+S added (0.8 to 1 nM) and in the cultures with nanoparticulate HgS added (0.1 to 0.2 nM) as shown in Fig. 3.2. The curve fittings in Fig. 3.2 show that our model captures this trend, indicating that the discrepancy lies elsewhere in the model system.

The underestimated prediction of methylmercury concentrations in the nanoparticulate HgS exposures relative to experimental results (Figure 3.3) could be due to additional faster dissolution rates of nanoparticles than observed in sterile culture media (Figure 3.2 and S2). For example, the presence of bacteria in culture media could have resulted in an enhancement of dissolution rates for the HgS nanoparticles, perhaps due to the biological production of Hg-binding ligands or other changes in water chemistry that increased rates of dissolution[18]. Additionally, the results of mercury speciation were compared to experimental measurements of dissolved and colloidal mercury measured by Zhang et al.[19] in culture media with bacteria exposed to dissolved and nanoparticulate mercury (Figure S6). Though the values are similar, the loss of dissolved and colloidal mercury (<0.2 µm) from solution along with the transmission electron microscopy (TEM) examination of the Hg-spiked cultures indicated the occurrence of mercury sorption to bacteria rather than the formation of microparticulate mercuric sulfide.

3.4.5 Parametric Sensitivity

The net methylation rate of mercury is controlled by several factors that include the fraction of dissolved mercury to which the bacteria are exposed, Hg uptake rate by the cells, and organism nature and biomethylation rate (possibly related to metabolism or growth rate)[56,203]. Moreover, the dissolution, precipitation, methylation and demethylation rate constants estimated from the data are applicable only to the specific conditions during the experiments (e.g., microbial activity, concentrations of Hg, sulfide, etc.). Nevertheless, investigations on the model parametric sensitivity have the potential to provide greater insight on the relative importance of those individual processes. The model also provides an opportunity to explore various mechanisms that could possibly explain increased mercury methylation in the presence of HgS nanoparticles.

The sensitivity of the model to the nanoparticle dissolution rate constant was analyzed first. Increasing $k_{dis,nHgS}$ by an order of magnitude increased both the rate of mercury methylation during the early transient phase and the steady state methylmercury concentrations (Figure 3.4A & C). However, as the dissolution rate constant was increased, the sigmoidal shape of the methylmercury curve was still present. Thus, the early methylation time points could not be captured by simply adjusting the dissolution rate constant. Figure 3.4 (A & C) shows that small variations of the nanoparticle dissolution rate constant can have profound effects on the availability of mercury. An accurate determination of rate constants in various water chemistry conditions is therefore essential for successfully predicting methylation rates.

Similarly, the model sensitivity to the nanoparticle formation rate constant $k_{f,nHgS}$ was investigated (Figure 3.4 B & D). The sensitivity of the model to the formation rate constant is not as pronounced as for the dissolution rate constant. A decrease in the nanoparticle formation rate has the largest impact because the steady state concentration of dissolved mercury is increased at time points beyond 10 hours, shifting the simulated methylmercury concentration closer to the experimental data at 24 hours for the *D. propionicus* 1pr3 cultures. This finding is important because it indicates that conditions that slow down or prevent particle growth will significantly increase the methylmercury concentration. The sensitivity of the nanoparticle formation and dissolution rate constants highlights the need to better understand the mechanisms of nanoparticle transformations and their kinetics.

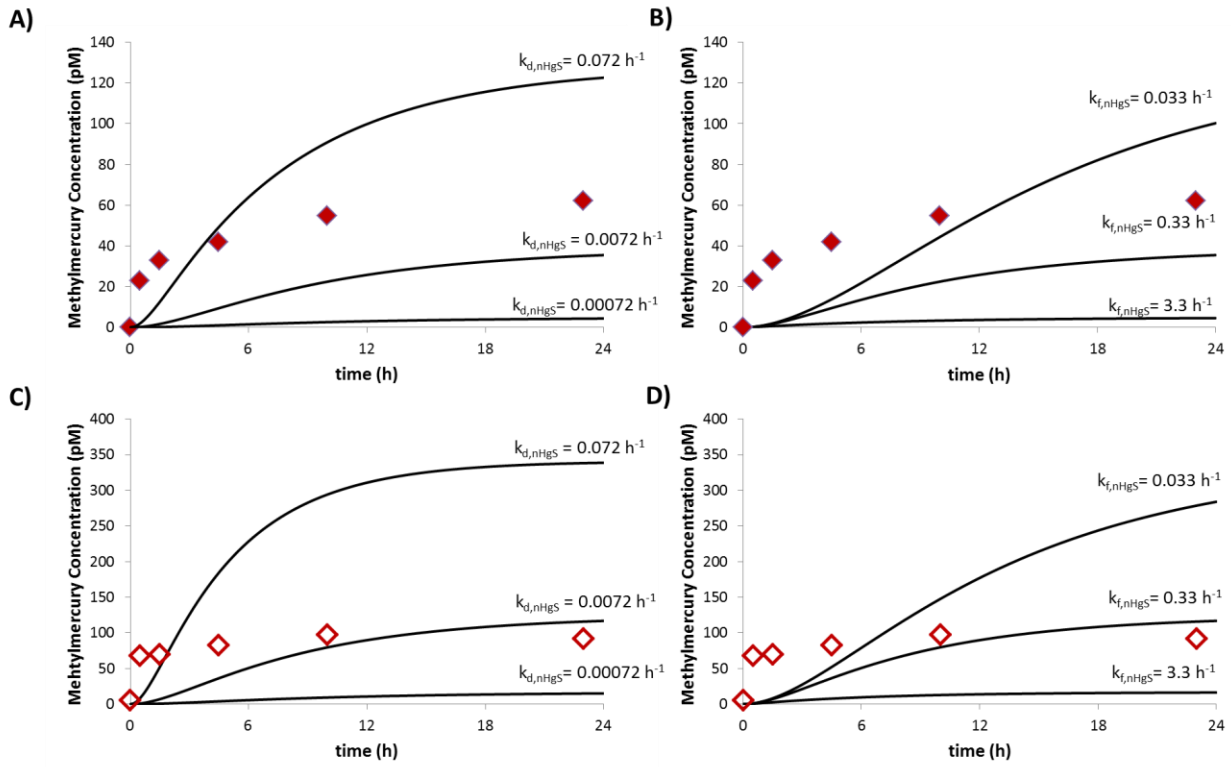

Figure 3.4. Simulations of methylmercury production for *D. propionicus* 1pr3 (A & B) and *D. desulfuricans* ND132 (C & D) cultures amended with HgS nanoparticles. A & C) Simulation where the dissolution rate constant $k_{dis,nHgS}$ was adjusted; B & D) Simulations where the nanoparticle formation rate constant ($k_{f,nHgS}$) was adjusted. Data points correspond to measurements from Zhang et al.[19].

3.4.6 Alternative Mechanisms for Methylation in Nanoparticle Additions

Selected conceptual modifications were made to the model to explore possible mechanisms that may explain enhanced mercury methylation in the presence of HgS nanoparticles. In this respect, we hypothesized that a portion of the nanoparticles may have a more direct pathway towards uptake and methylation (dashed red line in Figure 3.1). This pathway would not involve routing through the dissolved Hg pool. A mechanism that could result in a direct bioavailability pathway for nanoparticles could be explained by one of two distinct processes. The first is the cellular uptake of small HgS nanoparticles that are subsequently dissolved inside the cell and methylated. While the biouptake mechanisms of nanoparticles into bacteria cells are not firmly established, several studies have indicated that some bacteria could be capable of taking up sufficiently small nanoparticles[204,205] even though this uptake is likely to compromise the plasma membrane of the organism[205,206]. We note that in our biomethylation experiments, we found no evidence of nanoparticle uptake in TEM images of bacterial cells[19]. The second possible mechanism is that a portion of the nanoparticles are depositing on the bacteria cells and releasing dissolved mercury directly outside the cell membrane. This dissolved mercury would rapidly be taken up by the bacteria, resulting in the appearance of an enhanced bioavailability of nanoparticles.

Thus, Equation 6 was modified as follows:

$$\frac{d[MeHg]}{dt} = k_m([Hg^{2+}] + \sum_{i=1}^{2}[HgL_i]) + k_m f[nHgS] - k_d[MeHg] \qquad (7)$$

where *f* represents the fraction of nHgS that is available for enhanced methylation. This fraction of nHgS was assumed to methylate at the same rate k_m for dissolved Hg species. Model simulations were performed assuming *f* values between 0 and 0.4 (Figure 3.5A & B). The results indicated that for *f* value approximately equal to 0.2, the predicted methylmercury concentration at the 24 h time point was close to the experimental value. Moreover, the simulated early time points provided a better match to experimental data than the base case (Figure 3.3) or the enhanced dissolution alternative shown in Figure 3.4A. Although methylmercury concentrations at the 0 to 1.5 hour time points were still underestimated, this enhanced biomethylation pathway provided an appropriate curve shape in nanoparticle methylation experiments.

We also considered the possibility where both parameters $k_{dis,nHgS}$ and *f* were adjusted at the same time in order to fit the *D. propionicus* 1pr3 methylation data (Figure 3.3A). The dissolution rate constant, $k_{dis,nHgS}$, was allowed to move within the range 0.0072 h^{-1} to 0.072 h^{-1}, while the range for *f* was 0 to 0.5. In this case, the best fit was for the nominal dissolution rate measured by our dissolution experiments (Figure 3.2) and a *f* value of 0.2 (the same result as the enhanced bioavailabilty alternative in Figure 3.4B). This finding indicated that an enhanced biomethylation pathway may be the more likely explanation for the fast initial methylation rates in pure cultures with nHgS addition.

While the potential bioavailability of nanoparticulate HgS needs to be considered in future models of methylation potential, neither of the proposed modified models successfully predicted methylmercury concentrations at the early time points. A more fundamental understanding of mercury methylation mechanisms is needed to properly quantify and predict net methylmercury production.

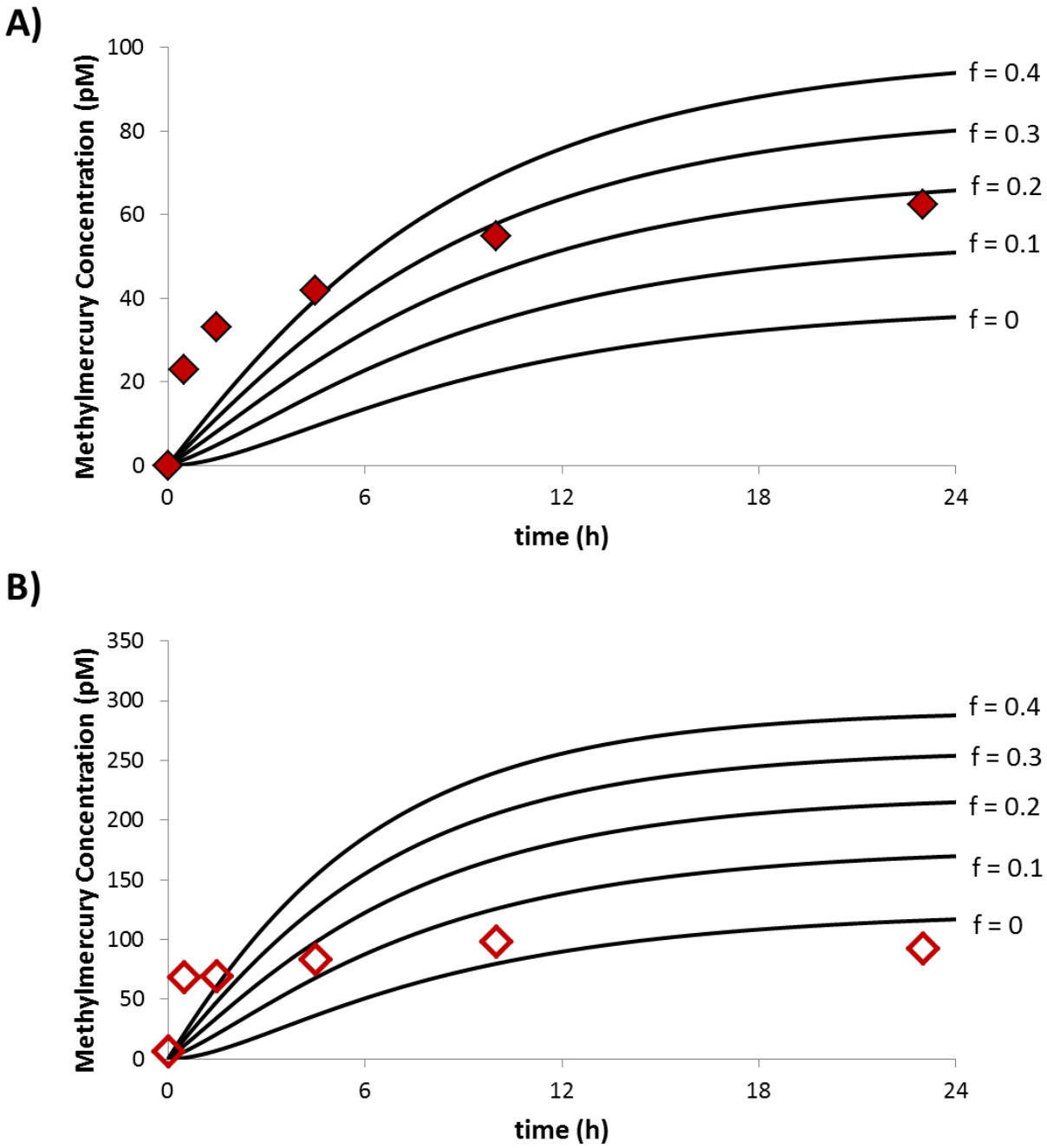

Figure 3.5. Simulation incorporating an enhanced biomethylation pathway for a fraction (f) of the HgS nanoparticles for A) *D. propionicus* 1pr3; and B) *D. desulfuricans* ND132 cultures. The data points correspond to measurements for cultures amended with HgS nanoparticles.[19].

3.6 Environmental Implications

The proposed model framework represents steps towards an alternative to the neutral mercury sulfide approach postulated by Benoit *et al.*[62] for the determination of mercury bioavailability and methylation potential. The results of the proposed model indicated that the longstanding view on bioavailability of mercury may be incomplete. The use of a chemical equilibrium model to estimate Hg speciation and bioavailability cannot explain the production of methylmercury over the incubation time. Instead, results presented and discussed herein indicated that a kinetic-based approach was better suited to link Hg speciation and methylation .

The results of this study also highlight the need to consider reaction kinetics in explaining the enhanced methylation of mercury in cultures exposed to HgS nanoparticles relative to cultures exposed to microscale HgS. The inclusion of a higher dissolution rate for nanoparticles than for mineral phase HgS was not sufficient to explain the methylation rates observed in experiments of Zhang et al.[19]. Rather, the nanoparticle fraction likely represented a heterogeneous mixture of nanoscale HgS species and probably presented a continuum of bioavailability that has yet to be considered. Moreover, previous work showed that the age of the HgS nanoparticle stock solutions influenced mercury methylation potential[19], and this effect was not considered in the modeling efforts described here. More detailed mechanistic concepts not yet discovered will need to be incorporated into the model to accurately describe the bioavailability and methylation of nanoscale mercury sulfides.

Overall, a kinetic-based approach for mercury speciation and methylation potential allows scientists and engineers to make time-based predictions of methylmercury formation. While the model described in this study was able to provide insights into methylation experiments comparing different forms of added Hg, the scope of the model is limited to those experiments because some model parameters are specific to the experimental conditions. In order to expand this approach to environmental samples, kinetic studies involving nanoscale species will need to be performed in a variety of environmentally relevant conditions to increase the applicability of the model. For example, nanoparticle dissolution and formation rates will need to be studied under a range of pH, dissolved sulfide and organic carbon concentrations. The sorption of Hg to cells, the Hg uptake rate into methylating microorganisms, demethylation, and the productivity of these organisms, particularly in mixed communities, will also need to be considered. Our findings provide a new approach to analyzing methylation experiments and highlight the important mechanisms that must be researched to improve our understanding of nanoscale processes and mercury bioavailability.

Chapter 4

Net Methylation of Mercury in Estuarine Sediment Microcosms Amended with Dissolved, Nanoparticulate, and Microparticulate Mercuric Sulfides

This chapter was published as the following:
Zhang, T.; Kucharzyk, K.H.; Kim, B.; Deshusses, M.A.; Hsu-Kim, H. (2014). Net methylation of mercury in estuarine sediment microcosms amended with dissolved, nanoparticulate, and microparticulate mercuric sulfides. *Environ. Sci. & Technol*. DOI: 10.1021/es500336j

4.2 Introduction

The previous work indicated that the bioavailability of mercury for methylation decreased during the aging of mercuric sulfides in anaerobic settings, a process in which mercury is expected to comprise a mixture of dissolved, nanoparticulate and microparticulate forms of Hg-sulfides that represent different reaction products during the precipitation and dissolution of HgS. Our results demonstrated that cultures exposed to nanoparticulate HgS produced MeHg at significantly higher rates relative to cultures receiving micro-crystalline HgS. Dissolved mercury species (i.e., mercury that passed through 0.02 μm filters or remained in the supernatant after ultracentrifugation) was most susceptible to methylation by pure cultures of sulfate-reducing bacteria (SRB) grown under fermentative conditions.

While this previous work highlighted the importance of Hg-sulfide speciation for MeHg production and the previously unrecognized role for nanoparticles, natural sediments are much more complex than pure bacterial cultures growing suspended in aqueous media. For example, natural sediments contain a diverse group of microorganisms that can simultaneously generate and degrade MeHg[207-209]. Non-methylating microorganisms may also compete with methylating bacteria for labile carbon for cellular growth, possibly resulting in limitations to MeHg production rates. The geochemistry of mercury in sediments is also much more complex than can be tested in pure culture experiments. Sediments consist of a mixture of the mineral particles, some coated with natural organic matter, that can scavenge mercury from pore water via adsorption, complexation, and aggregation[168,210,211]. Therefore, results from pure culture studies may not directly apply to real sediments. Thus, it is relevant to examine the aging effect of HgS on the bioavailability under more environmentally relevant conditions.

In this study, we conducted sediment slurry microcosm experiments to investigate whether the 'aging' states of mercuric sulfides is correlated with net MeHg production, as we observed in pure cultures of SRB. We also sought to understand how environmental variables (e.g., salinity) could influence the partitioning of mercury between various phases (e.g. dissolved, nanoparticulate, microparticulate) and the consequence of these changes for MeHg production. The microcosms were constructed with sediments and water collected at three locations in the San Francisco Bay-Delta estuary (California, U.S.A.) to represent sediment conditions ranging from freshwater to brackish settings. The slurries were amended with one of three forms of mercury: dissolved $Hg(NO_3)_2$ and Na_2S, HgS nanoparticles, and HgS microparticles. The slurry experiments were performed twice under variable microbial growth conditions: with added pyruvate as a carbon and energy substrate and without additional carbon. We compared net MeHg production and other water quality parameters relevant for microbial activity and mercury speciation.

4.2 Materials and Methods

Sediment and water collection. Sediment samples were collected in August 2011 as part of the biennial sediment survey conducted by the San Francisco Estuary Institute (SFEI) for their Regional Monitoring Program. Site 1 (BG30, based on SFEI's site identification number) is a freshwater location in the San Joaquin River (38.023° N, 121.808° W). Site 2 (SU044S, 38.076° N, 122.057° W) is located in Suisun Bay, connecting the confluence of the Sacramento and San Joaquin Rivers to San Pablo Bay. Site 3 (LSB129S) is a brackish water location at the southern section of the San Francisco Bay area near the city of San Jose (37.487° N, 122.101° W). Triplicate samples were collected from the top 5 cm of sediment with Van Veen samplers and packed into acid-cleaned polyethylene jars with Teflon-lined caps. The sediment samples were covered with a thin layer of overlaying water from the site, and the sample jars were sealed with no headspace. At the same sampling sites, surface water was also collected using acid-cleaned polyethylene jugs filled to capacity. Sediment and water samples were transported on ice to the laboratory and stored at 4°C. A portion of each sediment samples was analyzed for total mercury, MeHg, acid volatile sulfide (AVS) and water content. Surface water samples were analyzed for pH, total organic carbon (TOC), sulfate (SO_4^{2-}), ferrous iron (Fe(II)), total Fe, and total mercury content. Procedures for all chemical analyses are described in the SI.

Pore water characterization. Pore waters, as defined for this study, were extracted from the samples by centrifuging the sediments at 3000 *g* for 20 min. The supernatant was analyzed for total mercury concentration and pH. Aliquots for analysis of AVS were preserved with 0.01 N zinc sulfate ($ZnSO_4$) and 0.01 N potassium hydroxide (KOH, trace metal grade), and stored at 4°C. Particulate, colloidal, and dissolved mercury in pore waters were quantified by fractionating the porewater samples using centrifugation and ultracentrifugation[212]. In summary, we defined particulate fraction as the mercury species that settled from the water after centrifugation at 6,700 *g* for 5 min. The mercury in the supernatant was further fractionated by ultracentrifugation at 370,000 *g* for 1 h. After ultracentrifugation, the mercury remaining in the supernatant was considered to be nominally dissolved, while mercury in the pellet after ultracentrifugation was defined as colloidal mercury (including nanoparticulate HgS). The ability of this procedure to approximate size fractionation was tested and verified with solutions that comprised of either dissolved Hg, nanoparticulate HgS, or microparticulate HgS (Figure 4.1a).

Pore water samples were also filtered through 0.2 μm nylon syringe filters in an anaerobic chamber and analyzed for Hg, TOC, SO_4^{2-} , Fe(II) and total Fe concentrations.

HgS particle preparation. Stock solutions of $Hg(NO_3)_2$, Na_2S, HgS nanoparticles and suspension of microparticulate HgS were prepared according to Zhang et al.[212]. The nano-HgS stock solution was allowed to age for 16 h at room temperature prior to use in the methylation experiments. Our previous study[212] indicated that the nanoparticulate HgS comprised primarily of metacinnabar-like particles with an average diameter of 3.2 ± 0.8 nm (based on transmission electron microscopy, TEM) and geometric surface area of 264 ± 72 $m^2\ g^{-1}$. The microparticulate HgS was a mixture of metacinnabar and cinnabar particles (based on X-ray diffraction) with an average diameter of 530 ± 367 nm (based on TEM) and geometric surface area of 2.5 ± 1.8 $m^2\ g^{-1}$.

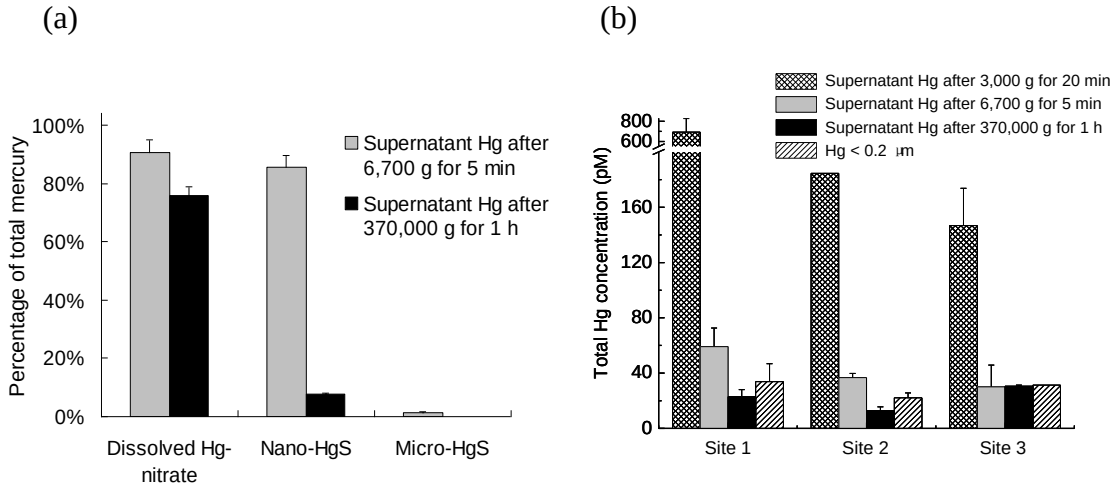

Figure 4.1. Mercury fractionation using centrifugation and ultracentrifugation. **(a)** Simulated water, consisting of 5 mM $NaHCO_3$, 50 mM NaCl and 1 mg-C/L Pony Lake fulvic acid (PLFA, International Humic Substances Society), was amended with 1 nM dissolved $Hg(NO_3)_2$, HgS nanoparticles or HgS microparticles, and (ultra)centrifuged immediately (less than 10 min) after mercury addition. **(b)** Pore water was first collected from the supernatant after centrifugation of the sediments at 3,000 *g* for 20 min. This pore water was further centrifuged at 6,700 g for 5 min or 370,000 for 1 h, or filtered with 0.2-μm filters. "Hg < 0.2 μm" represents the fraction of total mercury that passed through 0.2-μm filters. The error bars represent 1 s.d. for duplicate samples.

Table 4.1. Procedures utilized to construct sediment slurry microcosm for two different experiments. The objective was to test the effects of microbial activity and type of added mercury on net production of methylmercury.

	Experiment 1	Experiment 2
Source of sediment and water	Site 1, Site 2, Site 3	Site1, Site 3
Sediment wet weight	50 g	20 g
Water volume	120 mL	140 mL
Additional carbon source	10 mM Na-pyruvate	None
Pre-incubation time under anaerobic conditions (prior to Hg addition)	7.5 days	2.5 day
Mercury added (as dissolved Hg+S, nano-HgS, and microparticulate HgS)	50 nmol	50 nmol

Sediment slurry preparation. For slurry preparation, sediments were stirred to homogenize the samples, apportioned into 200-mL acid-cleaned serum bottles, and mixed with the N_2-purged surface water sample obtained from the same site (see Table 4.1 for details). A redox indicator, resazurin, was added to a final concentration of 2 mg/L. The serum bottles were then capped with butyl rubber stoppers and crimped with aluminum seals. The slurries were pre-incubated in the dark at room temperature (20-22°C) to deplete residual oxygen. The slurries were not utilized for mercury methylation experiments until resazurin became clear. Slurry experiments with sediments from Site 1 and Site 3 were performed two times (experimental conditions summarized in Table 4.1). These two separate experiments involved alterations to the solid-to-water ratio, pre-incubation period (prior to mercury addition), and an external carbon source (added in Experiment 1 only). Sediment from Site 2 was utilized only in Experiment 1.

Mercury methylation experiments. After pre-incubation, sediment slurries were spiked with 50 nmol of mercury as one of the following: dissolved Hg+S (i.e., equimolar amounts of dissolved $Hg(NO_3)_2$ and Na_2S added from their respective stock solutions), HgS nanoparticles, and HgS microparticles. Three sets of controls were also incubated in parallel with the methylation experiments: (1) a blank consisting of sediment slurries without added mercury (i.e., Hg blank); (2) a control slurry amended with 20 mM sodium molybdate, a specific inhibitor of sulfate reduction, added one day prior to dosing with dissolved Hg+S (later referred as the molybdate control); (3) a slurry that was autoclaved (121 °C, 30 min) prior to amending with dissolved Hg+S (later referred as the autoclaved control). In the dissolved Hg+S exposure, the micro-HgS exposure, and the three controls, Suwannee River humic acid (International Humic Substances Society), $NaNO_3$ and sodium 4-(2-hydroxyethyl) piperazine-1-ethanesulfonate (HEPES) were added to the slurries to account for the chemical carryover from the HgS nanoparticle stock in the nano-HgS treatment. After the addition of mercury, all the slurry microcosms were incubated statically for up to 7 days in the dark at room temperature (20-22°C).

Experiments 1 and 2 lasted 7.1 and 2.8 days, respectively, during which replicate serum bottles (n=2-3) were sacrificed periodically for chemical and biological analyses. At the time of sample collection, the slurries were first mixed end-over-end, and 1 mL of gas was collected from the headspace using a gas-tight syringe. The gaseous mercury content (e.g., Hg^0) in these samples was analyzed by injecting the sample into a gas-tight vial filled with ultrapure water (Barnstead Nanopure, >18 MΩ-cm) containing 2% (v/v) BrCl. These samples were stored and equilibrated for at least 3 days at room temperature prior to total mercury analysis in the liquid.

After collection of the headspace sample, liquid aliquots were withdrawn from the water overlaying the sediment, filtered through 0.2 μm nylon syringe filters and preserved for chemical analysis, including total Hg, AVS, TOC, major anions (e.g., SO_4^{2-} and Cl^-) and major cations concentrations. A drop of the 0.2-μm filtered water samples was placed on a 200-mesh copper TEM grid with lacey carbon support film (Electron Microscopy Sciences, PA), and then, allowed to evaporate in an anaerobic chamber (Coy Lab Products). The samples were later analyzed by a FEI Titan 80-300 field emission TEM operated at 200 keV and equipped with an energy dispersive X-ray (EDX) spectrometer for chemical analysis. pH and dissolved Fe(II) concentration were also measured immediately after collection of these liquid samples. Aliquots of the sediment-water mixture were fractionated using the (ultra)centrifugation method (as described in section "Pore water characterization") to separate particulate, colloidal, and dissolved forms of Hg. The remainder of the slurries were frozen (-80°C) until extraction for DNA and analysis for MeHg and total mercury content. All sample collection operations were conducted in an anaerobic chamber.

Equilibrium speciation calculations. Dissolved phase Hg speciation for Site 3 slurries in Experiment 1 was estimated using equilibrium speciation models. The calculations utilized equilibrium constants shown in Table S1 and were performed with MINEQL+ (v. 4.5)[213]. The calculations utilized the measured Hg concentration in the supernatant of ultracentrifuged pore water samples. Values for pH, Fe(II), AVS, Cl^- and thiol concentrations were based on data for filtered (<0.2 μm) pore water samples. Thiol concentrations were estimated from the TOC measurements of slurries that did not have added pyruvate, assuming 73 μmol thiol per gram TOC[214]. The ionic strength was estimated from the salinity of the water samples.

The potential presence of colloidal metal sulfides in Site 1 and Site 3 slurries was assessed through calculations of saturation indices for metacinnabar ($HgS_{(s)}$), mackinawite ($FeS_{(s)}$) and pyrite ($FeS_{2(s)}$) in the 0.2-μm filtered fraction. Hg, Fe(II) and AVS concentrations measured in filtered pore water samples were entered as total dissolved concentrations in the model. In all calculations, equilibrium with solid phases was not considered.

4.3 Results and Discussion

Sediment and pore water characteristics. The composition of samples from the three sites represented a typical gradient found in an estuarine setting (Table 4.2), with salinity varied from 0.44 to 24 psu and dissolved SO_4^{2-} concentration from 0.69 to 22 mM in surface water. Total Hg content were relatively low in both sediment (190-1900 pmol g^{-1}) and pore water (150-690 pmol L^{-1}) samples and fell within the range of previous measurements for the San Francisco Bay-Delta region[215]. Although the ambient total Hg concentrations in sediments from Site 1 and Site 3 were close to each other, the percentage of total Hg as MeHg was much higher for Site 3 (0.90%), relative to Site 1 (0.11%). In comparison, sediment from Site 2 contained approximately 10 times less total Hg, yet the proportion as MeHg in this sediment was relatively high (0.84%). Organic matter content of pore water from three sites were similar, while AVS concentration of whole sediment and pore water samples from Site 2 and Site 3 was 10 times greater than at Site 1. Total Fe was detected at 0.018 to 0.27 mM in pore waters, with Fe(II) representing 83% and 52% of total Fe at Site 1 and Site 3. Fe(II) concentration in sediment pore water from Site 2 was below the detection limit.

Table 4.2. Characteristics of sediment pore water, whole sediment and surface water samples used for slurry microcosm experiments.

Sample type	Parameters	Sample site		
		Site 1 (BG30)	Site 2 (SU044S)	Site 3 (LSB129S)
Pore water [a]	pH	7.4	7.5	7.7
	TOC (mg L^{-1})	20±0.2	9.2±0.3	16±0.1
	SO_4^{2-} (mM)	0.40±0.09	9.0±0.7	20±0.5
	AVS (μmol L^{-1})	1.0±0.2	11±2	21±4
	Fe(II) (mM)	0.10±0.003	<DL [d]	0.14±0.001
	Total Fe (mM)	0.12±0.002	0.018±0.0004	0.27±0.01
	Total Hg (pmol L^{-1})	694±134	185±24	147±27
Whole sediment [b]	AVS (μmol g^{-1})	1.3±0.3	8.2±0.9	13±2
	Total Hg (pmol g^{-1})	1943±104	188±14	1477±57
	MeHg (pmol g^{-1})	2.2±0.6	1.6±0.3	13±1
Surface water [c]	Salinity (psu) [e]	0.44±0.02	7.0±0.02	24±0.2
	pH	7.6	7.7	7.9
	TOC (mg L^{-1})	2.8±0.5	4.0±0.2	4.1±0.1
	SO_4^{2-} (mM)	0.69±0.02	8.9±0.4	22±0.1
	Fe(II) (mM)	<DL [d]	<DL [d]	<DL [d]
	Total Fe (mM)	0.0055±0.0001	0.0090±0.0004	0.011±0.0004
	Total Hg (pmol L^{-1})	0.020±0.008	0.017±0.008	0.011±0.0007

[a] Pore water was collected from the supernatant of whole sediment samples that were centrifuged at 3000 *g* for 20 min .The values represent mean ± standard deviation of triplicate samples.
[b]The values represent mean ± standard deviation of triplicate samples and are expressed on a dry weight (dw) basis.
[c]The values represent mean ± standard deviation of duplicate samples.
[d]< DL: values below the detection limit of Fe(II), 0.004 mM.
[e]The salinity data were provided by the Regional Monitoring Program at the San Francisco Estuary Institute.

Size fractionation of the mercury by centrifugation revealed that the majority of the mercury was associated with bulk-scale particles (i.e., the fraction removed from pore waters after centrifugation at 6,700 *g* for 5 min, Figure 4.1b). The colloidal fraction (i.e., the difference

between supernatant Hg after centrifugation at 6,700 g for 5 min and supernatant Hg after ultracentrifugation at 370,000 *g* for 1 h) was approximately 24-36 pmol L^{-1} in pore water from Site 1 and 2 but negligible (<1.6 pmol L^{-1}) in pore water from Site 3 (Figure 4.1b). This result is consistent with the aggregation of colloidal particles under high salinity (Site 3) to form large aggregates that settled from solution after mild centrifugation[216,217]. Similar patterns have been observed in mercury fractionation experiments with surface waters[218-220]. The concentrations of Hg in filtered pore waters from Site 1 and Site 2 was greater than dissolved Hg concentration as defined by ultracentrifugation (Figure 4.1b). Filtration with 0.2 or 0.45 μm filters is often used to define the dissolved mercury fraction in environmental samples, and our data demonstrate that a significant portion of this mercury can be associated with colloidal particles.

Net MeHg production in sediment slurry microcosms. Net production of MeHg in the microcosm experiments was dependent on the type of mercury added (i.e. dissolved, nanoparticulate, microparticulate) (Figures 4.2 and S1), consistent with our previous study with pure culture[212]. In Experiment 1, which involved a carbon amendment to promote anaerobic growth, the three forms of mercury were added at a concentration (2 nmol g^{-1}(dw)) that corresponded to 1.0, 10.6 and 1.4 times the concentration of the ambient total mercury in sediments from Site 1, Site 2, and Site 3, respectively (Table 4.2). The resulting MeHg concentration at the end of the experiment in dissolved and nano-HgS amended slurries was 17 to 1400 times and 16 to 364 times greater than the "Hg blank" (i.e., slurries without Hg addition and only contained Hg species from the original sediment, Figure 4.2). In slurries amended with microparticulate HgS, net production of MeHg was minimal and similar to the Hg blank (Figure 4.2). These observations indicate that more 'aged' forms of mercury (i.e., microparticulate HgS, native Hg in the sediments) have lower methylation potential compared to the added dissolved and nano-HgS. In the Site 2 and Site 3 slurry samples for Experiment 1, higher net MeHg production was obtained from slurries amended with dissolved $Hg(NO_3)_2$ and Na_2S than slurries amended with nano-HgS. (Figure 4.2b and 4.2c). This trend did not appear in the sediment slurry for Site 1 (Figure 4.2a): no difference in net MeHg production was observed between microcosms amended with dissolved Hg+S and nano-HgS. The comparisons between dissolved Hg+S and nano-HgS amendments were explored further by investigating how microbial activity could be controlling net MeHg production.

Sulfate reducing bacteria (SRB) appeared to be the primary methylators of mercury in these microcosms, as indicated by experiments performed with the addition of molybdate, a specific metabolic inhibitor of SRB. In slurries treated with molybdate, the concentrations of MeHg at the end of the incubation for Site 1, Site 2, and Site 3 were 7.1 ± 0.6%, 2.1 ± 0.1%, and 7.3 ± 1.1%, respectively, of MeHg in slurries without molybdate but amended with the same type of mercury (i.e., dissolved Hg+S) (Figure 4.2). This result is consistent with the dominant role of SRB for the production of MeHg, as demonstrated by many other studies[221-224].

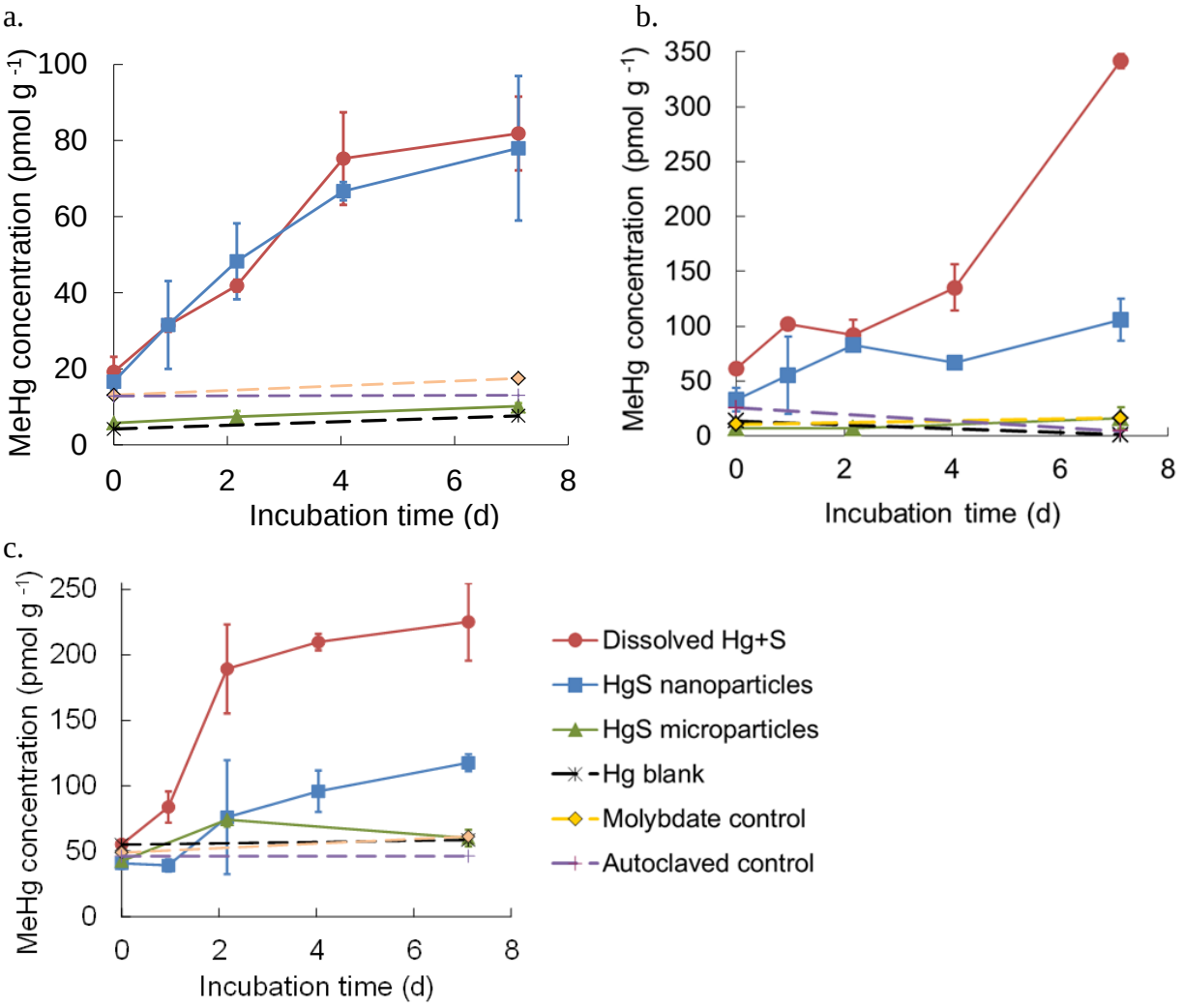

Figure 4.2. Net MeHg production in the slurry microcosms after the addition of 2 nmol Hg g^{-1} (dw sediment) in the form of dissolved $Hg(NO_3)_2$ and Na_2S, HgS nanoparticles or HgS microparticles in Experiment 1. The slurries were prepared with sediments from **(a)** Site 1, **(b)** Site 2 and **(c)** Site 3. The MeHg concentration was normalized to the dry sediment mass in each serum bottle. Incubation time represents the time after Hg amendments. The error bars represent 1 s.d. for duplicate samples in the test groups. Single replicate of slurries were incubated for the controls.

The number of the sulfite reductase *dsr*A gene copies and the abundance of *dsr*A relative to 16s rRNA genes did not yield significant differences ($p > 0.1$) in comparisons of microcosms amended with the three different forms of mercury (Figure S2). This result indicates that the difference in MeHg production (Figure 4.2) could not be explained by the abundance of SRB as determined by the abundance of *dsr*A genes, even though molybdate inhibition suggested the importance of sulfate reducers for mercury methylation. This discrepancy may be due to a poor correlation of the *dsr*A gene with SRB activity and with net MeHg production for these microcosm experiments.

The activity of SRB was also evaluated by the rate of sulfate loss in the microcosms. In the slurry samples with relatively high sulfate abundance (i.e., Site 2 and Site 3), sulfate concentration decreased at similar rates in all mercury sulfide exposures (Figure S3b and S3c). Thus, mercury methylation in these microcosms was most likely controlled by the speciation and bioavailability of inorganic mercury. However, in the low sulfate slurries (i.e., Site 1), sulfate was nearly completely consumed (i.e., close to the 0.01 mM detection limit) after the 7.5-day pre-incubation prior to Hg addition (Figure S3a). As a result, microbial activity most likely became the limiting factor for MeHg production, particularly in the presence of abundant bioavailable mercury species (i.e., slurries treated with dissolved and nano-HgS, Figure 4.2a).

In addition to sulfate abundance, net MeHg production also appeared to be affected by the availability of organic carbon in our experiments. Net MeHg production was calculated as the difference between the starting and final MeHg concentration in the slurry microcosms during a 52-h incubation in the initial course of Experiment 1 and 68-h incubation in Experiment 2 (which did not include an additional carbon amendment). As shown in Figure 3, net MeHg production was greater in Experiment 1 than in Experiment 2 regardless of which form of mercury was added to the slurry microcosms. Despite the higher inorganic mercury loading per sediment mass and longer incubation with mercury, net MeHg production in Experiment 2 was apparently limited by the bacterial activity, indicated by the minimal sulfate reduction (Figure S4). The availability of labile organic carbon for microbial metabolism is known to be an important factor for microbial MeHg production[225,226]. The addition of pyruvate in Experiment 1 enhanced methylation of all three forms of mercury (Figure 4.3) without significantly affecting the relative abundance of the sedimentary SRB community (the ratio of *dsr*A/16s rRNA remained similar during the 7-day incubation, Figure 4.2). In Experiment 2, TOC did not appear to decrease during the incubation (Figure S5), possibly due to the limited bioavailability of the native organic carbon for microbial metabolism.

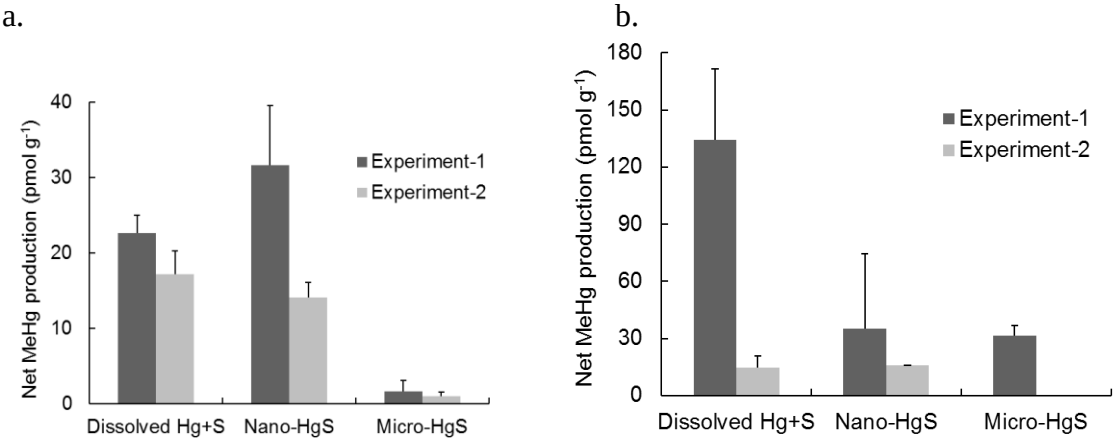

Figure 4.3. Net MeHg production in sediment slurries 52 h (Experiment 1) and 68 h (Experiment 2) after amendment of 50 nmol mercury (either dissolved $Hg(NO_3)_2$ + Na_2S, HgS nanoparticles or HgS microparticles). The slurries were prepared with sediments from **(a)** Site 1 and **(b)** Site 3. The MeHg concentration was normalized to the dry sediment mass. In Experiment 1, slurries consisted of 50 g wet sediment, 120 mL surface water and 10 mM sodium pyruvate, and pre-incubated for 7.5 days prior to Hg addition. In Experiment 2, slurries consisted of 20 g wet sediment and 140 mL surface water and no added pyruvate, and pre-incubated for 2.5 days prior to mercury addition. The error bars represent 1 s.d. of replicate samples (n=2-3). The net MeHg production from micro-HgS exposed Site 3 slurries in Experiment 2 was below the detection limit (0.2 pmol g^{-1}).

Mercury fractionation, speciation, and methylation potential in sediment slurry microcosms. The microcosm experiments demonstrated that in most cases, net production of MeHg depended on the type of mercury added. To further explore the relationship between mercury speciation and its methylation potential, mercury in the Site 1 and Site 3 slurries in Experiment 1 was quantified in different fractions of the microcosms. The highest concentration of Hg detected in the headspace of these samples accounted for <0.1% of total Hg spiked in the microcosms. Hence, the production of gaseous Hg was not significant in our experiments.

Fractionation of the porewaters using sequential centrifugation indicated that the nominally dissolved mercury contents in the slurries amended with dissolved Hg+S and nano-HgS were larger than dissolved mercury in micro-HgS amended slurries and the "Hg blank". However, more than 98% of the added Hg partitioned into the large particle fraction within 15 min of addition (regardless of the type of mercury added).

In our previous research with pure cultures, the concentration of dissolved Hg (defined by the same approach) was consistent with trends in MeHg production[212]. Thus, the higher concentration of dissolved Hg may explain the greater amount of MeHg production in slurries that were amended with dissolved and nano-HgS relative to the other slurries (Figure 4.2).

However, in the microcosm experiments the dissolved Hg fraction alone did not explain the MeHg production in Site 3 slurries amended with dissolved Hg+S and HgS nanoparticles. In these samples, the dissolved Hg contents and speciation were similar in the two mercury exposures (Figures 4.4c, 4.4d, and S6), while the net MeHg production differed significantly (Figure 4.2c). Previous researchers have hypothesized that neutrally charged Hg species represent the bioavailable forms of Hg[226,227]. However for Site 3 slurries, the sum of the concentrations of neutral Hg complexes in the nano-HgS treatment exceeded that in the dissolved Hg+S treatment (Figure S7), a pattern that is inconsistent with the trend in net MeHg production (Figure 4.2c). The discrepancy is probably caused by the bulk-scale sedimentary particles in the microcosms. The majority of the mercury added as dissolved Hg or nanoparticles was not observed in the dissolved or colloidal phase of the slurry microcosms (only 0.3-1.3% of the added mercury remained in the supernatant after centrifugation at 6,700 *g* for 5 min) and probably sorbed to or deposited onto large particles and microorganisms in the slurries.

Microorganisms tend to attach to the surface of mineral particles via sorption or biofilm formation[228]. Hence, sedimentary particles are the likely sites of MeHg production, and Hg bioavailability will increase in scenarios where weakly sorbed or highly soluble particulate Hg species closely associate with sites of methylation.

The relative amounts of dissolved and colloidal mercury in the microcosms depended on the type of sediment and salinity. A substantial amount of colloidal mercury was detected in Site 1 slurries (the freshwater site) amended with dissolved Hg+S and nano-HgS, and this colloidal fraction increased during the 7-day incubation period (Figure 4.4a and 4.4b). In contrast, the colloidal mercury concentration in the Site 3 slurries (the brackish water site) was less than the dissolved fraction and decreased to undetectable levels after 7 days (Figure 4.4c and 4.4d). These results suggest that dispersed HgS nanoparticles may exist for a relatively long time in the pore water of freshwater settings, likely via stabilization by natural organic matter[216], and perhaps produce a source of mercury for microbial methylation. In high salinity waters, these nanoparticles are subject to aggregation and partitioning to the larger particle fraction.

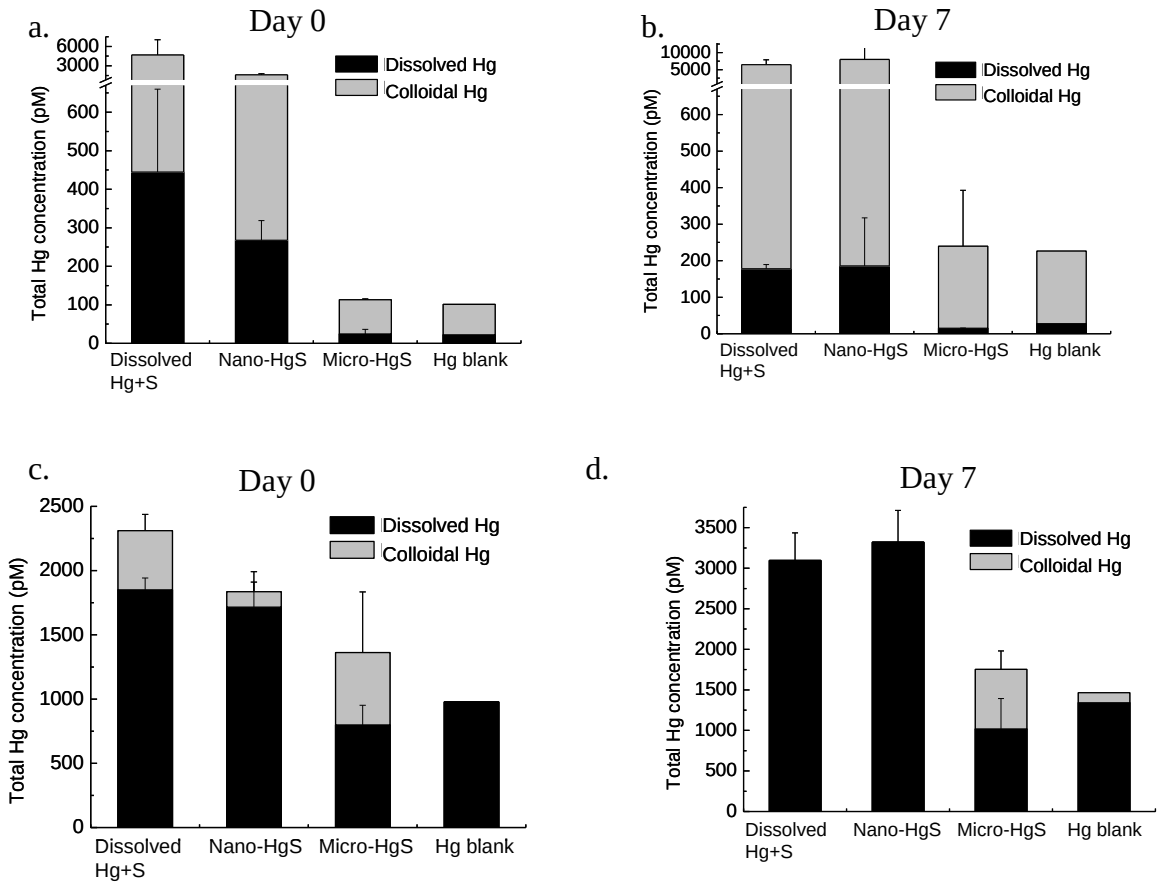

Figure 4.4. Hg fractionation in sediment slurries amended with 2 nmol g^{-1} (dw) added as dissolved $Hg(NO_3)_2$ and Na_2S, HgS nanoparticles or HgS microparticles in Experiment 1. This Hg spike corresponded to 345 nmol Hg per L of water was added into the slurries. The slurries were prepared with sediments from Site 1 (**a and b**) and Site 3 (**c and d**). (Ultra) centrifugation was performed within 15 min (**a and c**) and 7 days (**b and d**) after mercury amendments. 'Dissolved Hg' represents the total Hg that remained in the supernatant after ultracentrifugation at 370,000 *g* for 1 h. 'Colloidal Hg' represents the concentration difference of supernatant Hg after centrifugation at 6,700 *g* for 5 min and ultracentrifugation at 370,000 *g* for 1 h. 'Hg blank' represents slurries without mercury addition. The error bars represent 1 s.d. for duplicate samples in the test groups. Single replicate of slurries were incubated for the Hg blank control.

Potential influence of iron sulfide minerals. In sedimentary environments, other sulfide-complexing metals, such as Zn, Fe and Cu, often coexist at much higher levels relative to Hg. In particular, due to the high abundance of iron in pore waters, Fe(II) likely controls the sulfide speciation and thus indirectly influences the speciation and bioavailability of inorganic Hg. In sediment pore waters from Site 1 and Site 3, Fe(II) was detected at micromolar quantities (Table 2). Also, we observed a black layer on the sediment surface of the Site 3 slurry microcosms, indicative of FeS precipitates.

Equilibrium calculations were performed for the 0.2 μm-filtered fraction to evaluate whether metal sulfide precipitation was thermodynamically possible. The solubility product K_{s0} for

metacinnabar ($HgS_{(s)} + H^+ = Hg^{2+} + HS^-$) varies by 4 orders of magnitude in a database of critically selected stability constants[229]. Here, we utilized two values at the high and low end of this range (10^{-36} and 10^{-40}) for our calculations.

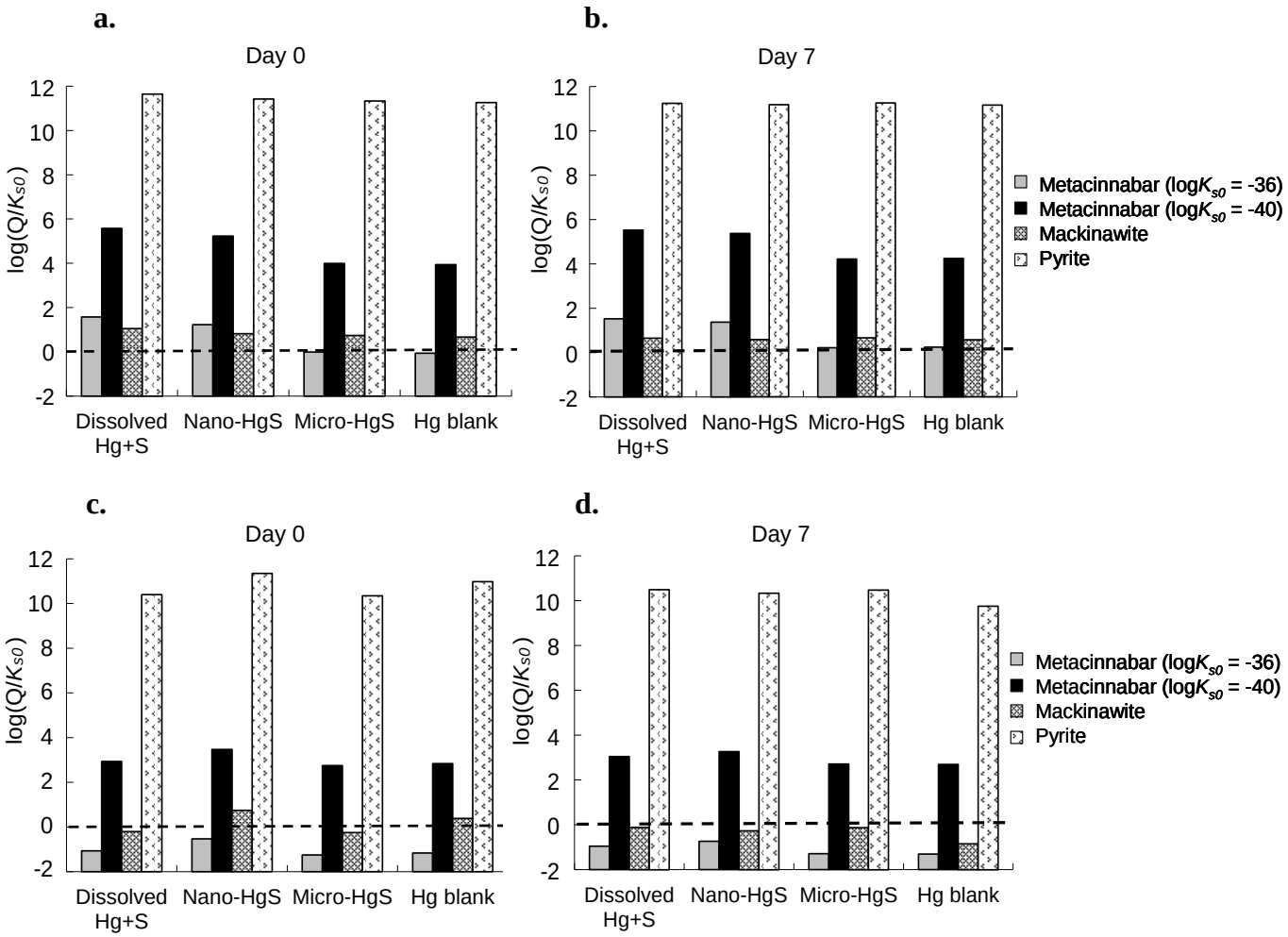

Figure 4.5. Calculated saturation indices for 0.2-μm filtered water samples withdrawn from the sediment slurries amended with 2 nmol g^{-1} (dw) dissolved $Hg(NO_3)_2$ and Na_2S, HgS nanoparticles or HgS microparticles in Experiment 1. The slurries were prepared with sediments from Site 1 (**a and b**) and Site 3 (**c and d**). Saturation indices of metacinnabar (β-$HgS_{(s)}$), mackinawite ($FeS_{(s)}$) and pyrite ($FeS_{2(s)}$) were calculated using measured pH, Hg, Fe(II), AVS, Cl^- and DOC concentrations in 0.2-μm filtered water samples collected at two time points during the methylation experiments: **(a and c)** Immediately (less than 10 min) and **(b and d)** 7 days.

The results of the calculations indicated that the precipitation of metal sulfide particles, including metacinnabar, pyrite and mackinawite was thermodynamically favored in the 0.2 μm-filtered fraction of most microcosms (Figure 4.5). For the Site 1 slurries, the speciation calculations indicated that the $HgS_{(s)}$ saturation index (defined by log Q/K_{s0}) was greater than zero in slurries treated with dissolved Hg+S and nano-HgS for both values of K_{s0} (Figure 4.5a and 4.5b). This result indicated that $HgS_{(s)}$ was above saturation, and precipitation of metacinnabar was

thermodynamically favored in these filtered samples. In the Site 1 slurries amended with micro-HgS or no Hg (i.e., Hg blank), oversaturation of $HgS_{(s)}$ could also occur, particularly at the end of the incubation (Figure 4.5b). Nanoparticles are small enough to pass through the 0.2-μm filters, although a portion may adsorb or deposit on the filter membrane surface. These calculations point to the possibility that nanoparticulate mercury species existed in the pore water of Site 1 slurry microcosms, consistent with our observations in the fractionation data (Figure 4.4a and 4.4b). In contrast, the speciation calculations indicated smaller (negative, if $K_{s0} = 10^{-36}$) saturation indices of metacinnabar in Site 3 samples (Figure 4.5c and 4.5d), suggesting a lower thermodynamic driving force for HgS precipitation and particle formation.

The saturation indices for pyrite were +10 to +11 in all the samples (Figure 4.5), indicating a high potential for $FeS_{2(s)}$ formation if S^0 was present in the sediments. Moreover, all Site 1 samples were oversaturated with respect to mackinawite, while the saturation indices of $FeS_{(s)}$ was near or below zero in most Site 3 samples.

Examination of the slurry samples with TEM revealed that amorphous nano-scale particles were present in the 0.2-μm filtered water from the Site 1 slurry microcosms amended with dissolved and nano-HgS (Figures S8a and S8b). According to the EDX analysis, these nanoparticles mainly contained Fe and S (Figures S8c and S8d). Although the mercury concentration in these 0.2-μm filtered water samples was too low to be detected by TEM-EDX, these results suggested that the colloidal mercury fraction in the slurry samples (Figure 4a and 4b) was likely associated with FeS via aggregation, adsorption to or coprecipitation with FeS nanoparticles[230,231]. A recent study with estuarine sediments has demonstrated that mercury associated with mackinawite has a greater methylation potential compared to metacinnabar and cinnabar[211]. Therefore, colloidal HgS/FeS species may play an important role in microbial mercury methylation, especially at settings where sulfate and iron reducing bacteria coexist[232].

Environmental implications. The results of the slurry microcosm experiments confirmed the major observation from our previous study with pure cultures[212]: the aging of mercury (from dissolved Hg to nanoparticulate HgS and then crystalline micro-HgS) decreased the bioavailability of mercury for microbial methylation. The microcosms also provided new insights regarding the complexity of and interconnected relationships between mercury speciation, microbial productivity, and mercury methylation potential. For example, mercury added as dissolved species and as nanoparticulate HgS did not always result in different rates of MeHg production. In these cases, microbial productivity was likely the limiting factor for methylation. Furthermore, most of the dissolved and nanoparticulate species added to the microcosms partitioned to the large particle fraction. Even so, MeHg production was greater in these microcosms than in microcosms receiving microparticulate HgS. This result highlights the weakness in directly relating the 'dissolved' fraction (defined by filtration or ultracentrifugation techniques) to methylation potential. Instead, consideration should be given to the chemical reactivity of mercury that is weakly sorbed to mineral particles or comprised of nanostructured particles that may fall in the colloidal or large particle fraction.

Results from the slurry microcosm experiments also indicated the importance of nano-scale FeS as the potential carrier of inorganic mercury (as a sorbent for Hg(II) molecules or aggregated with HgS nanoparticles). Previous researchers have proposed the use of Fe(II)-based sediment amendments as a strategy for preventing MeHg accumulation, based on the idea that Fe(II) can reduce the solubility (and subsequent bioavailability) of mercury by decreasing the concentration of dissolved sulfide[233,234]. This result has been demonstrated at high Fe(II) doses but not at low

doses of Fe(II)[233-235]. Perhaps the reason for this inconsistency is that Fe(II) amendments decrease mercury bioavailability by coagulation of colloidal HgS and low doses of Fe(II) result in stable occurrence of FeS nanoparticles[236,237] that facilitated mercury bioavailability and methylation. Future research, however, is needed to understand the importance of nano-FeS on microbial mercury methylation.

Overall this study has demonstrated that MeHg production in the sediment microcosms was largely governed by two factors, the productivity of the methylating bacteria and the availability of inorganic mercury. Environmental parameters, such as labile carbon, sulfate, salinity and iron, were observed to influence MeHg production by regulating one or both of these factors. Most previous mercury methylation studies[207,225,226,234,238-240] have used only actively growing bacteria and/or tested only one type of mercury (typically dissolved Hg) without a full understanding of Hg-sulfide speciation. This study, however, utilized different geochemical conditions (e.g., high and low carbon or sulfate content) and inorganic mercury species with different bioavailability to simultaneously assess the importance of various environmental parameters for MeHg production. Results from this study indicate that the differentiation of factors influencing MeHg production (i.e., mercury bioavailability versus microbial activity) can be achieved by experiments that control for both microbial production and the initial Hg-sulfide speciation. With this approach, measurement methods for mercury bioavailability and methylation potential could be developed and applied towards real environmental settings.

Chapter 5

Conclusions

Considering the complexity of the mercury biogeochemical cycle, the intention of this project was not to suggest a specific mechanism and exclude the others. Instead, this study aimed to bridge the knowledge gap between the speciation and availability/reactivity of mercury in the processes controlling MeHg concentrations in aquatic ecosystems. The implications of the research are summarized below.

5.1 Towards an understanding of mercury methylation potential

The results in Chapter 2 demonstrated that the equilibrium speciation of 'dissolved' aqueous mercury (defined by a 0.2-μm filter) cannot accurately predict the production of MeHg because this mercury fraction (<0.2 μm) contains a continuum of mercury species that include dissolved molecules, polynuclear clusters, and amorphous nanoparticles. These different forms of mercury exhibited distinct methylation potential. The transformation reactions involving these mercury species, such as cluster formation, monomer aggregation and crystal ripening, are often times kinetically-hindered in the presence of DOM[1]. Therefore, the bioavailability and methylation potential of mercury is most likely related to the 'slow' kinetics of these processes that control the relative abundance of various mercury species (i.e., those falling through a 0.2-μm filter), rather than the equilibrium chemistry. Future modeling efforts for predicting mercury bioavailability will need to consider the rate of transformations involving mercury species. Such an approach would require a series of rate constants for the geochemical reactions that dictate the concentration of the available forms of inorganic mercury for microbial methylation.

Chapters 2 and 4 provide the first documentation of HgS nanoparticles serving as an important, but previously unrecognized source of available mercury for biomethylation. The enhanced methylation of the nanoparticles (relative to bulk-scale HgS particles) cannot be simply explained by their greater surface area, and is likely caused by the unique reactivity at the nanoscale. The exact mechanism for microbial methylation of HgS nanoparticles was not thoroughly elucidated with the available data on my dissertation. In particular, this project did not provide a clear reason for the decreased availability of nano-HgS during aging. Future research is needed to address two main questions. First, the properties that change during the aging of mercury sulfides (particularly at the nanoscale) should be indentified and related to methylation potential. The structural changes of HgS nanoparticles aged for different length of time could not be reflected in the DLS, TEM or XRD results in the present study, probably because these methods are probing the more crystalline phases in the nano-HgS stock solution and are less sensitive towards amorphous materials. Additional techniques that better probe short scale atomic structure, such as small angle X-ray scattering (SAXS) and X-ray absorption spectroscopy (XAS), should be applied and complemented with bulk scale mercury speciation analysis (e.g., CLE-SPE) to assess the evolving properties of HgS during aging. Secondly, the environmental conditions, including pH, salinity (ionic strength), the concentration and type of DOM and metal:sulfide ratio, are known to control the formation and stability of metal sulfide nanoparticles[134,160,216,241,242]. The influence of these factors on the properties of mercury sulfide that change during aging and result in lower MeHg production needs to be investigated. The information from these works will possibly link the measurable environmental parameters to the amount of bioavailable mercury in sediments and ultimately to MeHg production.

The understanding of how the geochemical speciation determines the availability of inorganic mercury for methylation will be tremendously improved if future research in the field of microbiology and molecular biology can fully address the microbiological mechanism of mercury methylation. For example, the mechanism of mercury uptake by the methylating bacteria is poorly understood, even though bacterial uptake is believed to be the rate-limiting step of intracellular mercury methylation[243]. A few recent studies have proposed that methylating bacteria may preferentially take up Hg(II)-thiol complexes through an active transport system[244,245] and also that other metals such as Zn and Cd may compete for Hg at cell membrane transport sites[246]. Our results in Chapter 2 agree with this observation by showing that the susceptibility of mercury to thiol ligand exchange correlated with the methylation potential of these mercury species. If future studies further corroborate the notion that methylating microbes take up mercury through an active transport mechanism, our research then provides a methodology (i.e., CLE-SPE) to quantify the availability of inorganic mercury for microbial uptake and subsequent methylation.

Additionally, the biochemical pathway and the enzymes that are responsible for mercury methylation have been largely unknown until recently[53]. Although sulfate reduction rate has been widely used as a measure of microbial activity in mercury methylation studies[221,247] due to the dominant role of SRB in sedimentary MeHg production[248,249], our study, among others[106,250,251], has shown that MeHg production can occur to a significant extent under sulfate-limited conditions, suggesting that mercury methylation may not be directly coupled with sulfate reduction activity. Thus, further research is needed to determine a better measure of biological activity pertaining to MeHg production. This information will help design the experiments for assessing the bioavailability of inorganic mercury by ensuring that mercury methylation is not limited by microbial activity (e.g., enzyme, methyl donor molecules) and thus MeHg production solely reflects the availability of inorganic mercury.

Because of the complexity of environmental samples, the results from the pure culture study (Chapter 2) and the kinetic modeling of this dataset (Chapter 3) should be applied to real sediment systems with caution. Additional factors need to be taken into account when assessing mercury methylation in natural sediments. In Chapter 4, results showed that mercury had a high propensity to partition onto bulk sediment particles. The importance of this process for bioavailability would largely depend on the relative distribution of mercury and methylating bacteria. For instance, mercury bound to sediment particles may be directly available for the methylating bacteria that are also attached to the sediment solid phase. Thus, the biogeochemical reactions occurring at the microbe-sediment particle interfaces (e.g., adsorption, complexation, dissolution, precipitation, aggregation, *etc.*) may be important for determining MeHg production in real sediments. Analytical tools with both high spatial resolution and chemical sensitivity are required to investigate these interfacial processes, since these reactions involve nano-scale and mercury often occurs at relatively low concentrations in natural samples. High-resolution electron microscopy, synchrotron-based X-ray microscopy, and microprobe mapping have been utilized to examine the distribution of mercury and other trace elements and to identify the 'hot spots' of these elements in biological samples[171,252,253]. These techniques can also be coupled with metal speciation analysis, including X-ray absorption spectroscopy, X-ray diffraction, electron diffraction, and energy dispersive X-ray spectroscopy, and have shown great promise in elucidating the mechanisms of nanoparticle-microbe transformation processes[172].

5.2. Other metal sulfide nanoparticles

In the sediment environment, an array of sulfide-complexing metals, such as Fe, Mn, Zn and Cu, often exist and possibly affect mercury speciation. In particular, iron sulfides are the most abundant sulfide minerals and thus tend to control the fate of other metals[254], including mercury. Sulfate reduction and iron reduction are both commonly encountered electron-accepting processes in anaerobic sediments. Therefore, the products of these reactions (i.e., S^{2-} and Fe^{2+}) are expected to precipitate in sediments as $FeS_{(s)}$. Amorphous mackinawite is the initial product of FeS precipitation. This mineral phase slowly transforms into well-crystalline iron-sulfide minerals, such as pyrite ($FeS_{2(s)}$) under ambient conditions[255]. $FeS_{(s)}$ is known to scavenge metals from aqueous phase and renders them less available for biogeochemical reactions via three mechanisms: surface adsorption, co-precipitation and metathesis (surface metal exchange)[254].

In the case of mercury, amendment of wetland sediment with Fe(II) has been suggested as a strategy for preventing MeHg accumulation, based on the idea that Fe(II) can reduce the solubility (and subsequent availability for microbial methylation) of mercury by decreasing the concentration of dissolved sulfide[256,257]. This appeared to be true at high Fe(II) doses, but it has also been repeatedly shown that low doses of Fe(II) enhanced mercury methylation[256-258], which cannot be explained by equilibrium speciation. Instead, this phenomenon may be due to the 'slow' kinetics of FeS precipitation, and as a result, the stable occurrence of polynuclear cluster and nano-scale particles of FeS[236,237,259] (as suggested in Chapter 4).

Future research is needed to prove the promoting effect of nano-FeS on mercury methylation and more importantly, to elucidate why this occurs. A few studies have been conducted to investigate the interaction between Hg^{2+} and FeS nanoparticles[260-262]. However, the influence of FeS-Hg interaction on the availability of mercury for microbial methylation has yet to be evaluated. Moreover, pre-synthesized FeS nanoparticles were utilized in these studies, which do not necessarily simulate all the environmental conditions. For example, instead of reacting with pre-formed nanoparticulate FeS, Hg^{2+} may co-precipitate with Fe^{2+} and S^{2-} in natural sediments, especially during redox oscillation at the sediment-water interface, where mercury methylation often occurs. As suggested in this project, the initial precipitation products of HgS (e.g., polynuclear clusters) are likely more bioavailable than the nanoparticles. Thus, the clusters formed during the initial stage of co-precipitation of Fe^{2+}, S^{2-} and Hg^{2+} may be a potentially important source of available mercury for biomethylation.

It is interesting to note that the proposed mechanism of the interaction between Hg^{2+} and nano-FeS changed from Hg adsorption onto nano-FeS surface to surface precipitation of metacinnabar as the concentration ratio of Hg^{2+} to nano-FeS increased[261]. Also, natural organic matter (NOM) appeared to compete with disordered mackinawite for binding with Hg^{2+} through thiol complexation[262]. These parameters (Fe, S, Hg and NOM content) may significantly vary in natural settings and thus affect reactions involving Fe, S and Hg. Therefore, future research should focus on: 1) characterizing the structure (e.g., size, crystallinity, surface chemical composition, *etc.*) of the stable products of Hg, S and Fe co-precipitation; 2) quantifying the methylation potential of these products in relation to their structural characteristics; 3) assessing how environmental conditions (e.g., redox oscillation, pH, salinity, NOM, Fe, S and Hg content) affect the structure and methylation potential of these materials.

5.3 Predictive model for methylmercury

The prevailing theme throughout this research effort was the role of chemical speciation of mercury for methylation protential. The knowledge gained from this research will significantly

improve our understanding of how MeHg is generated in aquatic ecosystems. The results from this project and proposed future research contribute a pathway towards a quantitative model that link the kinetics of MeHg formation and degradation to environmental conditions. This model will include speciation-dependent rate constants and measurable environmental parameters that are known to determine mercury speciation. This model could enable an accurate prediction of MeHg accumulation in response to ecosystem alterations, such as accidental mercury contamination (e.g., industrial wastewater spill, atmospheric deposition, *etc.*), acid deposition, wetland restoration and sediment remediation. This information could also facilitate the development of effective cleanup strategies and proper policies for the regulation of mercury sources, and ultimately reducing the human exposure to MeHg.

References

1. Aiken, G. R.; Hsu-Kim, H.; Ryan, J. N., Influence of dissolved organic matter on the environmental fate of metals, nanoparticles, and colloids. *Environ. Sci. Technol.* **2011,** *45*, (8), 3196-3201.

2. Lindberg, S.; Bullock, R.; Ebinghaus, R.; Engstrom, D.; Feng, X. B.; Fitzgerald, W.; Pirrone, N.; Prestbo, E.; Seigneur, C., A synthesis of progress and uncertainties in attributing the sources of mercury in deposition. *Ambio* **2007,** *36*, (1), 19-32.

3. Clarkson, T. W., The three modern faces of mercury. *Environ. Health Persp.* **2002,** *110*, 11-23.

4. Mergler, D.; Anderson, H. A.; Chan, L. H. M.; Mahaffey, K. R.; Murray, M.; Sakamoto, M.; Stern, A. H., Methylmercury exposure and health effects in humans: A worldwide concern. *Ambio* **2007,** *36*, (1), 3-11.

5. Clarkson, T. W., The toxicology of mercury. *Crit. Rev. Cl. Lab. Sci.* **1997,** *34*, (4), 369-403.

6. Committee on the Toxicological Effects of Methylmercury; Board on Environmental Studies Toxicology; National Research Council, *Toxicological Effects of Methylmercury*. The National Academies Press: 2000.

7. Mahaffey, K. R.; Clickner, R. P.; Bodurow, C. C., Blood organic mercury and dietary mercury intake: National Health and Nutrition Examination Survey, 1999 and 2000. *Environ. Health Persp.* **2004,** *112*, (5), 562-570.

8. U.S. Environmental Protection Agency National Listing of Fish Advisories: Technical Factsheet 2010. http://www.epa.gov/hg/advisories.htm (October 21, 2012),

9. Benoit, J. M.; Gilmour, C. C.; Heyes, A.; Mason, R. P.; Miller, C. L., Geochemical and biological controls over methylmercury production and degradation in aquatic ecosystems. In *Biogeochemistry of Environmentally Important Trace Elements*, Cai, Y.; Braids, O. C., Eds. 2003; Vol. 835, pp 262-297.

10. Munthe, J.; Bodaly, R. A.; Branfireun, B. A.; Driscoll, C. T.; Gilmour, C. C.; Harris, R.; Horvat, M.; Lucotte, M.; Malm, O., Recovery of mercury-contaminated fisheries. *Ambio* **2007,** *36*, (1), 33-44.

11. Lin, C.-C.; Yee, N.; Barkay, T., Microbial Transformations in the Mercury Cycle. In *Environmental Chemistry and Toxicology of Mercury*, John Wiley & Sons, Inc.: 2012; pp 155-191.

12. Mason, R. R.; Abbot, M. L.; Bodaly, R. A.; Bullock, O. R.; Driscoll, C. T.; Evers, D.; Lindberg, S. E.; Murray, M.; Swain, E. B., Monitoring the response to changing mercury deposition. *Environ. Sci. Technol.* **2005,** *39*, (1), 14A-22A.

13. Skyllberg, U., Chemical Speciation of Mercury in Soil and Sediment. In *Environmental Chemistry and Toxicology of Mercury*, John Wiley & Sons, Inc.: 2012; pp 219-258.

14. Morel, F. M. M.; Kraepiel, A. M. L.; Amyot, M., The chemical cycle and bioaccumulation of mercury. *Annu. Rev. Ecol. Syst.* **1998,** *29*, 543-566.

15. Deonarine, A.; Hsu-Kim, H., Precipitation of mercuric sulfide nanoparticles in NOM-containing water: Implications for the natural environment. *Environ. Sci. Technol.* **2009,** *43*, (7), 2368-2373.

16. Slowey, A. J., Rate of formation and dissolution of mercury sulfide nanoparticles: The dual role of natural organic matter. *Geochim. Cosmochim. Ac* **2010,** *74*, (16), 4693-4708.

17. Gerbig, C. A.; Kim, C. S.; Stegemeier, J. P.; Ryan, J. N.; Aiken, G. R., Formation of nanocolloidal metacinnabar in mercury-DOM-sulfide systems. *Environ. Sci. Technol.* **2011,** *45*, (21), 9180-9187.

18. Graham, A. M.; Aiken, G. R.; Gilmour, C. C., Dissolved organic matter enhances microbial mercury methylation under sulfidic conditions. *Environ. Sci. Technol.* **2012,** *46*, (5), 2715-2723.

19. Zhang, T.; Kim, B.; Levard, C.; Reinsch, B. C.; Lowry, G. V.; Deshusses, M. A.; Hsu-Kim, H., Methylation of mercury by bacteria exposed to dissolved, nanoparticulate, and microparticulate mercuric sulfides. *Environ. Sci. Technol.* **2012,** *46*, (13), 6950-6958.

20. Merritt, K. A.; Amirbahman, A., Mercury methylation dynamics in estuarine and coastal marine environments - A critical review. *Earth-Sci. Rev.* **2009,** *96*, (1-2), 54-66.

21. Fitzgerald, W. F.; Lamborg, C. H.; Hammerschmidt, C. R., Marine biogeochemical cycling of mercury. *Chem. Rev.* **2007,** *107*, (2), 641-662.

22. Selin, N. E., Global Biogeochemical Cycling of Mercury: A Review. In *Annual Review of Environment and Resources*, Annual Reviews: Palo Alto, 2009; Vol. 34, pp 43-63.

23. Pirrone, N.; Cinnirella, S.; Feng, X.; Finkelman, R. B.; Friedli, H. R.; Leaner, J.; Mason, R.; Mukherjee, A. B.; Stracher, G. B.; Streets, D. G.; Telmer, K., Global mercury emissions to the atmosphere from anthropogenic and natural sources. *Atmos. Chem. Phys.* **2010,** *10*, (13), 5951-5964.

24. Selin, N. E., Science and strategies to reduce mercury risks: a critical review. *J. Environ. Monit.* **2011,** *13*, (9), 2389-2399.

25. Renner, R., Mercury woes appear to grow. *Environ. Sci. Technol.* **2004,** *38*, (8), 144A-144A.

26. Hight, S. C.; Cheng, J., Determination of methylmercury and estimation of total mercury in seafood using high performance liquid chromatography (HPLC) and inductively coupled plasma-mass spectrometry (ICP-MS): Method development and validation. *Anal. Chim. Acta* **2006,** *567*, (2), 160-172.

27. Gong, Y. S.; Krabbenhoft, D. P.; Ren, L. P.; Egelandsdal, B.; Richards, M. P., Mercury Distribution and Lipid Oxidation in Fish Muscle: Effects of Washing and Isoelectric Protein Precipitation. *J. Agric. Food Chem.* **2011,** *59*, (20), 11050-11057.

28. Krystek, P.; Ritsema, R., Mercury speciation in thawed out and refrozen fish samples by gas chromatography coupled to inductively coupled plasma mass spectrometry and atomic fluorescence spectroscopy. *Anal. Bioanal. Chem.* **2005,** *381*, (2), 354-359.

29. Wiener, J. G.; Krabbenhoft, D. P.; Heinz, G. H.; Scheuhammer, A. M., Ecotoxicology of mercury. In *Handbook of Ecotoxicology (2nd ed.)*, Hoffman, D. J.; Rattner, B. A.; G.A. Burton, J.; Cairns, J., Eds. Lewis Publishers: Boca Raton, FL, 2003; pp 409-463

30. Siciliano, S. D.; O'Driscoll, N. J.; Tordon, R.; Hill, J.; Beauchamp, S.; Lean, D. R. S., Abiotic production of methylmercury by solar radiation. *Environ. Sci. Technol.* **2005,** *39*, (4), 1071-1077.

31. James H, W., Review of possible paths for abiotic methylation of mercury(II) in the aquatic environment. *Chemosphere* **1993,** *26*, (11), 2063-2077.

32. Hammerschmidt, C. R.; Fitzgerald, W. F., Iron-mediated photochemical decomposition of methylmercury in an arctic Alaskan lake. *Environ. Sci. Technol.* **2010,** *44*, (16), 6138-6143.

33. Lehnherr, I.; Louis, V. L. S., Importance of ultraviolet radiation in the photodemethylation of methylmercury in freshwater ecosystems. *Environ. Sci. Technol.* **2009,** *43*, (15), 5692-5698.

34. Zhang, T.; Hsu-Kim, H., Photolytic degradation of methylmercury enhanced by binding to natural organic ligands. *Nat. Geosci.* **2010,** *3*, (7), 473-476.

35. Hammerschmidt, C. R.; Fitzgerald, W. F., Photodecomposition of methylmercury in an arctic Alaskan lake. *Environ. Sci. Technol.* **2006,** *40*, (4), 1212-1216.

36. Barkay, T.; Wagner-Dobler, I., Microbial transformations of mercury: Potentials, challenges, and achievements in controlling mercury toxicity in the environment. In *Advances in Applied Microbiology, Vol 57*, Laskin, A. I.; Bennett, J. W.; Gadd, G. M., Eds. Elsevier Academic Press Inc: San Diego, 2005; Vol. 57, pp 1-52.

37. Jensen, S.; Jernelov, A., Biological methylation of mercury in aquatic organisms. *Nature* **1969,** *223*, (5207), 753-&.

38. Yamada, M.; Tonomura, K., Formations of methylmercury compounds from inorganic mercury by *Clostridium cochlearium*. *J. Ferment. Technol.* **1972,** *50*, (3), 159-&.

39. Wood, J. M., Biological cycles for toxic elements in environment *Science* **1974,** *183*, (4129), 1049-1052.

40. Williams, J. W.; Morrison, J. F., The kinetics of reversible tight-binding inhibition. *Method. Enzymol.* **1979,** *63*, 437-67.

41. Zhao, X.; Rockne, K. J.; Drummond, J. L.; Hurley, R. K.; Shade, C. W.; Hudson, R. J. M., Characterization of methyl mercury in dental wastewater and correlation with sulfate-reducing bacterial DNA. *Environ. Sci. Technol.* **2008,** *42*, (8), 2780-2786.

42. Devereux, R.; Winfrey, M. R.; Winfrey, J.; Stahl, D. A. A., Genus-specific and groups-pecific hybridization probes for determinative and environmental studies of sulfate-reducing bacteria. *Syst. Appl. Microbiol.* **1992,** *15*, (4), 601-609.

43. Gilmour, C. C.; Elias, D. A.; Kucken, A. M.; Brown, S. D.; Palumbo, A. V.; C.W., S.; Wall, J. D., Sulfate-reducing bacterium *Desulfovibrio desulfuricans* ND132 as a model for understanding bacterial mercury methylation. *Appl. Environ. Microbiol.* **2011**, (77), 3938-3951.

44. Ranchou-Peyruse, M.; Monperrus, M.; Bridou, R.; Duran, R.; Amouroux, D.; Salvado, J. C.; Guyoneaud, R., Overview of mercury methylation capacities among anaerobic bacteria including representatives of the sulphate-reducers: Implications for environmental studies. *Geomicrobiol. J.* **2009,** *26*, (1), 1-8.

45. Acha, D.; Pabon, C. A.; Hintelmann, H., Mercury methylation and hydrogen sulfide production among unexpected strains isolated from periphyton of two macrophytes of the Amazon. *Fems Microbiol. Ecol.* **2012,** *80*, (3), 637-645.

46. Compeau, G. C.; Bartha, R., Sulfate-reducing bacteria: Principal methylators of mercury in anoxic estuarine sediment *Appl. Environ. Microbiol.* **1985,** *50*, 498-502.

47. Fleming, E. J.; Mack, E. E.; Green, P. G.; Nelson, D. C., Mercury methylation from unexpected sources: Molybdate-inhibited freshwater sediments and an iron-reducing bacterium. *Appl. Environ. Microbiol.* **2006,** *72*, (1), 457-464.

48. Hamelin, S.; Amyot, M.; Barkay, T.; Wang, Y. P.; Planas, D., Methanogens: Principal methylators of mercury in lake periphyton. *Environ. Sci. Technol.* **2011,** *45*, (18), 7693-7700.

49. Kerin, E. J.; Gilmour, C. C.; Roden, E.; Suzuki, M. T.; Coates, J. D.; R.P., M., Mercury methylation by dissimilatory iron-reducing bacteria. *Appl. Environ. Microbiol.* **2006,** *72*, (12), 7919-7921.

50. Eckley, C. S.; Hintelmann, H., Determination of mercury methylation potentials in the water column of lakes across Canada. *Sci. Total Environ.* **2006,** *368*, (1), 111-125.

51. Achá, D.; Hintelmann, H.; Yee, J., Importance of sulfate reducing bacteria in mercury methylation and demethylation in periphyton from Bolivian Amazon region. *Chemosphere* **2011,** *82*, (6), 911-916.

52. Gilmour, C. C.; Henry, E. A.; Mitchell, R., Sulfate stimulation of mercury methylation in fresh-water sediments. *Environ. Sci. Technol.* **1992,** *26*, (11), 2281-2287.

53. Parks, J. M.; Johs, A.; Podar, M.; Bridou, R.; Hurt, R. A.; Smith, S. D.; Tomanicek, S. J.; Qian, Y.; Brown, S. D.; Brandt, C. C.; Palumbo, A. V.; Smith, J. C.; Wall, J. D.; Elias, D. A.; Liang, L., The genetic basis for bacterial mercury methylation. *Science* **2013**, DOI:10.1126/science.1230667.

54. Berman, M.; Chase, T.; Bartha, R., Carbon flow in mercury biomethylation by *Desulfovibrio desulfuricans*. *Appl. Environ. Microbiol.* **1990,** *56*, (1), 298-300.

55. Choi, S. C.; Chase, T.; Bartha, R., Metabolic pathways leading to mercury methylation in *Desulfovibrio desulfuricans* LS. *Appl. Environ. Microbiol.* **1994,** *60*, (11), 4072-4077.

56. Schaefer, J. K.; Rocks, S. S.; Zheng, W.; Liang, L.; Gu, B.; Morel, F. M. M., Active transport, substrate specificity, and methylation of Hg(II) in anaerobic bacteria. *P. Natl. Acad. Sci. USA* **2011,** *108*, (21), 8714-8719.

57. Schaefer, J. K.; Morel, F. M. M., High methylation rates of mercury bound to cysteine by *Geobacter sulfurreducens*. *Nat. Geosci.* **2009,** *2*, (2), 123-126.

58. Bridou R., M. M., Gonzalez P.R., Guyoneaud R., Amouroux D., Simultaneous determination of mercury methylation and demethylation capacities of various sulfate-reducing bacteria using species-specific isotopic tracers. *Environ. Toxicol. Chem.* **2011,** *30*, 337-344.

59. Mason, R. P.; Reinfelder , J. R.; Morel, F. M. M., Uptake, toxicity, and trophic transfer of mercury in a coastal diatom. *Environ. Sci. Technol.* **1996,** *30*, (6), 1835-1845.

60. Barkay, T.; Gillman, M.; Turner, R. R., Effects of dissolved organic carbon and salinity on bioavailability of mercury. *Appl. Environ. Microbiol.* **1997,** *63*, (11), 4267-4271

61. Najera I., L. C. C., Kohbodi G.A., Jay J.A., Effect of chemical speciation on toxicity of mercury to *Escherichia coli* biofilms and planktonic cells. *Environ. Sci. Technol.* **2005,** *39*, 3116-3120.

62. Benoit, J. M.; Gilmour, C. C.; Mason, R. P.; Heyes, A., Sulfide controls on mercury speciation and bioavailability to methylating bacteria in sediment pore waters. *Environ. Sci. Technol.* **1999,** *33*, (6), 951-957.

63. Benoit, J. M.; Mason, R. P.; Gilmour, C. C., Estimation of mercury-sulfide speciation in sediment pore waters using octanol-water partitioning and implications for availability to methylating bacteria. *Environ. Toxicol. Chem.* **1999,** *18*, (10), 2138-2141.

64. Benoit, J. M.; Gilmour, C. C.; Mason, R. P., The influence of sulfide on solid phase mercury bioavailability for methylation by pure cultures of *Desulfobulbus propionicus* (1pr3). *Environ. Sci. Technol.* **2001,** *35*, (1), 127-132.

65. Graham, A. M.; Bullock, A. L.; Maizel, A. C.; Elias, D. A.; Gilmour, C. C., A detailed assessment of the kinetics of Hg-cell association, Hg methylation, and MeHg degradation in several *Desulfovibrio* species. *Appl. Environ. Microbiol.* **2012,** *78*, (20), 7337-7346.

66. Pedrero, Z.; Bridou, R.; Mounicou, S.; Guyoneaud, R.; Monperrus, M.; Amouroux, D., Transformation, localization, and biomolecular binding of Hg species at subcellular level in methylating and nonmethylating sulfate-reducing bacteria. *Environ. Sci. Technol.* **2012,** *46*, (21), 11744-11751.

67. Moberly, J. G.; Miller, C. L.; Brown, S. D.; Biswas, A.; Brandt, C. C.; Palumbo, A. V.; Elias, D. A., Role of Morphological Growth State and Gene Expression in Desulfovibrio africanus Strain Walvis Bay Mercury Methylation. *Environ. Sci. Technol.* **2012,** *46*, (9), 4926-4932.

68. Barkay, T.; Miller, S. M.; Summers, A. O., Bacterial mercury resistance from atoms to ecosystems. *Fems Microbiol. Rev.* **2003,** *27*, (2-3), 355-384.

69. Choi, S. C.; Bartha, R., Cobalamin-mediated mercury methylation by *Desulfovibrio desulfuricans* LS. *Appl. Environ. Microbiol.* **1993,** *59*, (1), 290-295.

70. Ekstrom, E. B.; Morel, F. M. M., Cobalt limitation of growth and mercury methylation in sulfate-reducing bacteria. *Environ. Sci. Technol.* **2008,** *42*, (1), 93-99.

71. Ekstrom, E. B.; Morel, F. M. M.; Benoit, J. M., Mercury methylation independent of the acetyl-coenzyme a pathway in sulfate-reducing bacteria. *Appl. Environ. Microbiol.* **2003,** *69*, (9), 5414-5422.

72. Landner, L., Biochemical model for the biological methylation of mercury suggested from methylation studies in vivo with *Neurospora crassa*. *Nature* **1971,** *230*, 452-454.

73. Rodionov, D. A.; Vitreschak, A. G.; Mironov, A. A.; Gelfand, M. S., Comparative genomics of the methionine metabolism in Gram-positive bacteria: a variety of regulatory systems. *Nucleic Acids Res.* **2004,** *32*, (11), 3340-3353.

74. Larose, C.; Dommergue, A.; De Angelis, M.; Cossa, D.; Averty, B.; Marusczak, N.; Soumis, N.; Schneider, D.; Ferrari, C., Springtime changes in snow chemistry lead to new insights into mercury methylation in the Arctic. *Geochim. Cosmochim. Ac* **2010,** *74*, (22), 6263-6275.

75. Bentley, R.; Chasteen, T. G., Environmental VOSCs—formation and degradation of dimethyl sulfide, methanethiol and related materials. *Chemosphere* **2004,** *55*, (3), 291-317.

76. Reisch, C. R.; Moran, M. A.; Whitman, W. B., Dimethylsulfoniopropionate-Dependent Demethylase (DmdA) from Pelagibacter ubique and Silicibacter pomeroyi. *J. Bacteriol.* **2008,** *190*, (24), 8018-8024.

77. Oremland, R. S.; Culbertson, C. W.; Winfrey, M. R., Methylmercury decomposition in sediments and bacterial cultures - Involvement of methanogens and sulfate reducers in oxidative demethylation. *Appl. Environ. Microbiol.* **1991,** *57*, (1), 130-137.

78. Choe, K. Y.; Gill, G. A.; Lehman, R., Distribution of particulate, colloidal, and dissolved mercury in San Francisco Bay estuary. 1. Total mercury. *Limnol. Oceanogr.* **2003,** *48*, (4), 1535-1546.

79. Babiarz, C. L.; Hurley, J. P.; Hoffmann, S. R.; Andren, A. W.; Shafer, M. M.; Armstrong, D. E., Partitioning of total mercury and methylmercury to the colloidal phase in freshwaters. *Environ. Sci. Technol.* **2001,** *35*, (24), 4773-4782.

80. Lee, S.; Han, S.; Gill, G. A., Estuarine mixing behavior of colloidal organic carbon and colloidal mercury in Galveston Bay, Texas. *J. Environ. Monit.* **2011,** *13*, (6), 1703-1708.

81. Ravichandran, M.; Aiken, G. R.; Ryan, J. N.; Reddy, M. M., Inhibition of precipitation and aggregation of metacinnabar (mercuric sulfide) by dissolved organic matter isolated from the Florida Everglades. *Environ. Sci. Technol.* **1999,** *33*, (9), 1418-1423.

82. Babiarz, C. L.; Hoffmann, S. R.; Shafer, M. M.; Hurley, J. P.; Andren, A. W.; Armstrong, D. E., A critical evaluation of tangential-flow ultrafiltration for trace metal studies in freshwater systems. 2. Total mercury and methylmercury. *Environ. Sci. Technol.* **2000,** *34*, (16), 3428-3434.

83. Miller, C. L.; Mason, R. P.; Gilmour, C. C.; Heyes, A., Influence of dissolved organic matter on the complexation of mercury under sulfidic conditions. *Environ. Toxicol. Chem.* **2007,** *26*, (4), 624-633.

84. Jassby, D.; Chae, S. R.; Hendren, Z.; Wiesner, M., Membrane filtration of fullerene nanoparticle suspensions: Effects of derivatization, pressure, electrolyte species and concentration. *J. Colloid Interface Sci.* **2010,** *346*, (2), 296-302.

85. Divis, P.; Leermakers, M.; Docekalova, H.; Gao, Y., Mercury depth profiles in river and marine sediments measured by the diffusive gradients in thin films technique with two different specific resins. *Anal. Bioanal. Chem.* **2005,** *382*, (7), 1715-1719.

86. Divis, P.; Szkandera, R.; Brulik, L.; Docekalova, H.; Matus, P.; Bujdos, M., Application of New Resin Gels for Measuring Mercury by Diffusive Gradients in a Thin-films Technique. *Anal. Sci.* **2009,** *25*, (4), 575-578.

87. Merritt, K. A.; Amirbahman, A., Mercury mobilization in estuarine sediment porewaters: A diffusive gel time-series study. *Environ. Sci. Technol.* **2007,** *41*, (3), 717-722.

88. Hong, Y. S.; Rifkin, E.; Bouwer, E. J., Combination of Diffusive Gradient in a Thin Film Probe and IC-ICP-MS for the Simultaneous Determination of CH3Hg+ and Hg2+ in Oxic Water. *Environ. Sci. Technol.* **2011,** *45*, (15), 6429-6436.

89. Fernandez-Gomez, C.; Dimock, B.; Hintelmann, H.; Diez, S., Development of the DGT technique for Hg measurement in water: Comparison of three different types of samplers in laboratory assays. *Chemosphere* **2011,** *85*, (9), 1452-1457.

90. Pesavento, M.; Alberti, G.; Biesuz, R., Analytical methods for determination of free metal ion concentration, labile species fraction and metal complexation capacity of environmental waters: A review. *Anal. Chim. Acta* **2009,** *631*, (2), 129-141.

91. Hsu, H.; Sedlak, D. L., Strong Hg(II) complexation in municipal wastewater effluent and surface waters. *Environ. Sci. Technol.* **2003,** *37*, (12), 2743-2749.

92. Han, S. H.; Gill, G. A., Determination of mercury complexation in coastal and estuarine waters using competitive ligand exchange method. *Environ. Sci. Technol.* **2005,** *39*, (17), 6607-6615.

93. Gasper, J. D.; Aiken, G. R.; Ryan, J. N., A critical review of three methods used for the measurement of mercury (Hg^{2+})-dissolved organic matter stability constants. *Appl. Geochem.* **2007,** *22*, (8), 1583-1597.

94. Haitzer, M.; Aiken, G. R.; Ryan, J. N., Binding of mercury(II) to dissolved organic matter: the role of the mercury-to-DOM concentration ratio. *Environ. Sci. Technol.* **2002,** *36*, (16), 3564-3570.

95. Khwaja, A. R.; Bloom, P. R.; Brezonik, P. L., Binding constants of divalent mercury (Hg^{2+}) in soil humic acids and soil organic matter. *Environ. Sci. Technol.* **2006,** *40*, (3), 844-849.

96. Black, F. J.; Bruland, K. W.; Flegal, A. R., Competing ligand exchange-solid phase extraction method for the determination of complexation of dissolved inorganic mercury(II) in natural waters. *Anal. Chim. Acta* **2007,** *598*, 318-333.

97. Dong, W. M.; Bian, Y. R.; Liang, L. Y.; Gu, B. H., Binding constants of mercury and dissolved organic matter determined by a modified ion exchange technique. *Environ. Sci. Technol.* **2011,** *45*, (8), 3576-3583.

98. Han, S. H.; Gill, G. A.; Lehman, R. D.; Choe, K. Y., Complexation of mercury by dissolved organic matter in surface waters of Galveston Bay, Texas. *Mar. Chem.* **2006,** *98*, (2-4), 156-166.

99. Nagy, K. L.; Manceau, A.; Gasper, J. D.; Ryan, J. N.; Aiken, G. R., Metallothionein-like multinuclear clusters of mercury(II) and sulfur in peat. *Environ. Sci. Technol.* **2011,** *45*, (17), 7298-7306.

100. Hesterberg, D.; Chou, J. W.; Hutchison, K. J.; Sayers, D. E., Bonding of Hg(II) to reduced organic, sulfur in humic acid as affected by S/Hg ratio. *Environ. Sci. Technol.* **2001,** *35*, (13), 2741-2745.

101. Skyllberg, U.; Bloom, P. R.; Qian, J.; Lin, C. M.; Bleam, W. F., Complexation of mercury(II) in soil organic matter: EXAFS evidence for linear two-coordination with reduced sulfur groups. *Environ. Sci. Technol.* **2006,** *40*, (13), 4174-4180.

102. Xia, K.; Skyllberg, U. L.; Bleam, W. F.; Bloom, P. R.; Nater, E. A.; Helmke, P. A., X-ray absorption spectroscopic evidence for the complexation of Hg(II) by reduced sulfur in soil humic substances. *Environ. Sci. Technol.* **1999,** *33*, (2), 257-261.

103. Hsu-Kim, H.; Sedlak, D. L., Similarities between inorganic sulfide and the strong Hg(II)-complexing ligands in municipal wastewater effluent. *Environ. Sci. Technol.* **2005,** *39*, 4035-4041.

104. Mitchell, C. P. J.; Gilmour, C. C., Methylmercury production in a Chesapeake Bay salt marsh. *J. Geophys. Res-Biogeo.* **2008,** *113*.

105. Drott, A.; Lambertsson, L.; Bjorn, E.; Skyllberg, U., Importance of dissolved neutral mercury sulfides for methyl mercury production in contaminated sediments. *Environ. Sci. Technol.* **2007,** *41*, (7), 2270-2276.

106. Drott, A.; Lambertsson, L.; Bjorn, E.; Skyllberg, U., Do potential methylation rates reflect accumulated methyl mercury in contaminated sediments? *Environ. Sci. Technol.* **2008,** *42*, (1), 153-158.

107. Benoit, J. M.; Gilmour, C. C.; Mason, R. P., Aspects of bioavailability of mercury for methylation in pure cultures of *Desulfobulbus propionicus* (1pr3). *Appl. Environ. Microbiol.* **2001,** *67*, (1), 51-58.

108. Merritt, K. A.; Amirbahman, A., Methylmercury cycling in estuarine sediment pore waters (Penobscot River estuary, Maine, USA). *Limnol. Oceanogr.* **2008,** *53*, (3), 1064-1075.

109. Mehrotra, A. S.; Horne, A. J.; Sedlak, D. L., Reduction of net mercury methylation by iron in *Desulfobulbus propionicus* (1pr3) cultures: Implications for engineered wetlands. *Environ. Sci. Technol.* **2003,** *37*, (13), 3018-3023.

110. Mehrotra, A. S.; Sedlak, D. L., Decrease of net mercury methylation rates following iron amendments to anoxic wetland sediment slurries. *Environ. Sci. Technol.* **2005,** *39*, (8), 2564-2570.

111. Goulet, R. R.; Holmes, J.; Page, B.; Poissant, L.; Siciliano, S. D.; Lean, D. R. S.; Wang, F.; Amyot, M.; Tessier, A., Mercury transformations and fluxes in sediments of a riverine wetland. *Geochim. Cosmochim. Ac* **2007,** *71*, (14), 3393-3406.

112. Dyrssen, D.; Wedborg, M., The sulfur-mercury(II) system in natural-waters. *Water Air Soil Poll.* **1991,** *56*, 507-519.

113. Skyllberg, U., Competition among thiols and inorganic sulfides and polysulfides for Hg and MeHg in wetland soils and sediments under suboxic conditions: Illumination of controversies and implications for MeHg net production. *J. Geophys. Res-Biogeo.* **2008,** *113*.

114. Smith, R. D.; Martell, A. E., *NIST Critical Stability Constants of Metal Complexes Database v. 2.0*. 1993.

115. Paquette, K. E.; Helz, G. R., Inorganic speciation of mercury in sulfidic waters: the importance of zero-valent sulfur. *Environ. Sci. Technol.* **1997,** *31*, (7), 2148-2153.

116. Haitzer, M.; Aiken, G. R.; Ryan, J. N., Binding of mercury(II) to aquatic humic substances: Influence of pH and source of humic substances. *Environ. Sci. Technol.* **2003,** *37*, (11), 2436-2441.

117. Ravichandran, M., Interactions between mercury and dissolved organic matter—a review. *Chemosphere* **2004,** *55*, (3), 319-331.

118. Miller, C. L.; Southworth, G.; Brooks, S.; Liang, L.; Gu, B., Kinetic controls on the complexation between mercury and dissolved organic matter in a contaminated environment. *Environ. Sci. Technol.* **2009,** *43*, (22), 8548-8553.

119. Manceau, A.; Nagy, K. L., Quantitative analysis of sulfur functional groups in natural organic matter by XANES spectroscopy. *Geochim. Cosmochim. Ac* **2012,** *In Press*, http://dx.doi.org/10.1016/j.gca.2012.09.033.

120. Kramer, J. R.; Bell, R. A.; Smith, D. S., Determination of sulfide ligands and association with natural organic matter. *Appl. Geochem.* **2007,** *22*, (8), 1606-1611.

121. Wolfenden, S.; Charnock, J. M.; Hilton, J.; Livens, F. R.; Vaughan, D. J., Sulfide species as a sink for mercury in lake sediments. *Environ. Sci. Technol.* **2005,** *39*, (17), 6644-6648.

122. Barnett, M. O.; Harris, L. A.; Turner, R. R.; Stevenson, R. J.; Henson, T. J.; Melton, R. C.; Hoffman, D. P., Formation of mercuric sulfide in soil. *Environ. Sci. Technol.* **1997,** *31*, (11), 3037-3043.

123. Ravichandran, M.; Aiken, G. R.; Reddy, M. M.; Ryan, J. N., Enhanced dissolution of cinnabar (mercuric sulfide) by dissolved organic matter isolated from the Florida Everglades. *Environ. Sci. Technol.* **1998,** *32*, (21), 3305-3311.

124. Hintelmann, H.; Keppel-Jones, K.; Evans, R. D., Constants of mercury methylation and demethylation rates in sediments and comparison of tracer and ambient mercury availability. *Environ. Toxicol. Chem.* **2000,** *19*, (9), 2204-2211.

125. Merritt, K. A.; Amirbahman, A., Mercury dynamics in sulfide-rich sediments: Geochemical influence on contaminant mobilization within the Penobscot River estuary, Maine, USA. *Geochim. Cosmochim. Ac* **2007,** *71*, (4), 929-941.

126. Ullrich, S. M.; Tanton, T. W.; Abdrashitova, S. A., Mercury in the aquatic environment: A review of factors affecting methylation. *Crit. Rev. Environ. Sci. Technol.* **2001,** *31*, (3), 241-293.

127. Lambertsson, L.; Nilsson, M., Organic material: The primary control on mercury methylation and ambient methyl mercury concentrations in estuarine sediments. *Environ. Sci. Technol.* **2006,** *40*, (6), 1822-1829.

128. Hammerschmidt, C. R.; Fitzgerald, W. F.; Balcom, P. H.; Visscher, P. T., Organic matter and sulfide inhibit methylmercury production in sediments of New York/New Jersey Harbor. *Mar. Chem.* **2008,** *109*, (1-2), 165-182.

129. Hammerschmidt, C. R.; Fitzgerald, W. F., Geochemical controls on the production and distribution of methylmercury in near-shore marine sediments. *Environ. Sci. Technol.* **2004,** *38*, (5), 1487-1495.

130. Furutani, A.; Rudd, J. W. M., Measurement of mercury methylation in lake water and sediment samples. *Appl. Environ. Microbiol.* **1980,** *40*, (4), 770-776.

131. Schartup, A. T.; Mason, R. P.; Balcom, P. H.; Hollweg, T. A.; Chen, C. Y., Methylmercury production in estuarine sediments: Role of organic matter. *Environ. Sci. Technol.* **2013,** *47*, (2), 695-700.

132. Sunderland, E. M.; Gobas, F.; Branfireun, B. A.; Heyes, A., Environmental controls on the speciation and distribution of mercury in coastal sediments. *Mar. Chem.* **2006,** *102*, (1-2), 111-123.

133. Waples, J. S.; Nagy, K. L.; Aiken, G. R.; Ryan, J. N., Dissolution of cinnabar (HgS) in the presence of natural organic matter. *Geochim. Cosmochim. Ac* **2005,** *69*, (6), 1575-1588.

134. Deonarine, A.; Lau, B. L. T.; Aiken, G. R.; Ryan, J. N.; Hsu-Kim, H., Effects of humic substances on precipitation and aggregation of zinc sulfide nanoparticles. *Environ. Sci. Technol.* **2011,** *45*, (8), 3217-3223.

135. Hochella, M. F.; Lower, S. K.; Maurice, P. A.; Penn, R. L.; Sahai, N.; Sparks, D. L.; Twining, B. S., Nanominerals, mineral nanoparticles, and Earth systems. *Science* **2008,** *319*, (5870), 1631-1635.

136. Wigginton, N. S.; Haus, K. L.; Hochella, M. F., Aquatic environmental nanoparticles. *J. Environ. Monit.* **2007,** *9*, (12), 1306-1316.

137. Waychunas, G. A.; Zhang, H. Z., Structure, chemistry, and properties of mineral nanoparticles. *Elements* **2008,** *4*, (6), 381-387.

138. Labrenz, M.; Druschel, G. K.; Thomsan-Ebert, T.; Gilbert, B.; Welch, S. A.; Kemner, K. M.; Logan, G. A.; Summons, R. E.; De Stasio, G.; Bond, P. L.; Lai, B.; Kelly, S. D.; Banfield, J. F., Formation of sphalerite (ZnS) deposits in natural biofilms of sulfate-reducing bacteria. *Science* **2000,** *290*, 1744-1747.

139. Hochella, M. F.; Moore, J. N.; Putnis, C. V.; Putnis, A.; Kasama, T.; Eberl, D. D., Direct observation of heavy metal-mineral association from the Clark Fork River Superfund Complex: Implications for metal transport and bioavailability. *Geochim. Cosmochim. Ac* **2005,** *69*, (7), 1651-1663.

140. Rozan, T. F.; Lassman, M. E.; Ridge, D. P.; Luther, G. W., Evidence for iron, copper and zinc complexation as multinuclear sulphide clusters in oxic rivers. *Nature* **2000,** *406*, (24), 879-882.

141. Weber, F.-A.; Voegelin, A.; Kaegi, R.; Kretzschmar, R., Contaminant mobilization by metallic copper and metal sulphide colloids in flooded soil. *Nature Geosci* **2009,** *2*, (4), 267-271.

142. International Union of Pure and Applied Chemistry, *Compendium of Chemical Terminology; Gold Book; version 2.3.1*. 2012.

143. Jeong, H. Y.; Klaue, B.; Blum, J. D.; Hayes, K. F., Sorption of mercuric ion by synthetic nanocrystalline mackinawite (FeS). *Environ. Sci. Technol.* **2007,** *41*, (22), 7699-7705.

144. Patty, C.; Barnett, B.; Mooney, B.; Kahn, A.; Levy, S.; Liu, Y. J.; Pianetta, P.; Andrews, J. C., Using X-ray microscopy and Hg L-3 XANES to study Hg binding in the rhizosphere of spartina cordgrass. *Environ. Sci. Technol.* **2009,** *43*, (19), 7397-7402.

145. Lowry, G. V.; Shaw, S.; Kim, C. S.; Rytuba, J. J.; Brown, G. E., Macroscopic and microscopic observations of particle-facilitated mercury transport from New Idria and Sulphur Bank mercury mine tailings. *Environ. Sci. Technol.* **2004,** *38*, (19), 5101-5111.

146. Auffan, M.; Rose, J.; Bottero, J. Y.; Lowry, G. V.; Jolivet, J. P.; Wiesner, M. R., Towards a definition of inorganic nanoparticles from an environmental, health and safety perspective. *Nat. Nanotechnol.* **2009,** *4*, (10), 634-641.

147. Bosch, J.; Heister, K.; Hofmann, T.; Meckenstock, R. U., Nanosized Iron Oxide Colloids Strongly Enhance Microbial Iron Reduction. *Appl. Environ. Microbiol.* **2010,** *76*, (1), 184-189.

148. Bonneville, S.; Van Cappellen, P.; Behrends, T., Microbial reduction of iron(III) oxyhydroxides: effects of mineral solubility and availability. *Chem. Geol.* **2004,** *212*, (3-4), 255-268.

149. Glasauer, S.; Langley, S.; Beveridge, T. J., Sorption of Fe (hydr)oxides to the surface of *Shewanella putrefaciens*: Cell-bound fine-grained minerals are not always formed de novo. *Appl. Environ. Microbiol.* **2001,** *67*, (12), 5544-5550.

150. Bonneville, S.; Behrends, T.; Van Cappellen, P.; Hyacinthe, C.; Roling, W. F. M., Reduction of Fe(III) colloids by *Shewanella putrefaciens*: A kinetic model. *Geochim. Cosmochim. Ac* **2006,** *70*, (23), 5842-5854.

151. Grantham, M. C.; Dove, P. M.; DiChristina, T. J., Microbially catalyzed dissolution of iron and aluminum oxyhydroxide mineral surface coatings. *Geochim. Cosmochim. Ac* **1997,** *61*, (21), 4467-4477.

152. Hotze, E. M.; Phenrat, T.; Lowry, G. V., Nanoparticle aggregation: Challenges to understanding transport and reactivity in the environment. *J. Environ. Qual.* **2010,** *39*, (6), 1909-1924.

153. Liu, J.; Aruguete, D. A.; Jinschek, J. R.; Rimstidt, J. D.; Hochella, M. F., The non-oxidative dissolution of galena nanocrystals: Insights into mineral dissolution rates as a function of

grain size, shape, and aggregation state. *Geochim. Cosmochim. Ac* **2008,** *72*, (24), 5984-5996.

154. Liu, J.; Aruguete, D. M.; Murayama, M.; Hochella, M. F., Influence of size and aggregation on the reactivity of an environmentally and industrially relevant nanomaterial (PbS). *Environ. Sci. Technol.* **2009,** *43*, (21), 8178-8183.

155. Cutting, R. S.; Coker, V. S.; Fellowes, J. W.; Lloyd, J. R.; Vaughan, D. J., Mineralogical and morphological constraints on the reduction of Fe(III) minerals by *Geobacter sulfurreducens*. *Geochim. Cosmochim. Ac* **2009,** *73*, (14), 4004-4022.

156. Horzempa, L. M.; Helz, G. R., Controls on the stability of sulfide sols - colloidal covellite as an example. *Geochim. Cosmochim. Ac* **1979,** *43*, (10), 1645-1650.

157. Helz, G. R.; Horzempa, L. M., EDTA as a kinetic inhibitor of copper(II) sulfide precipitation. *Water Res.* **1983,** *17*, (2), 167-172.

158. Shea, D.; Helz, G. R., Kinetics of inhibited crystal growth: precipitation of CuS from solutions containing chelated copper(II). *J. Colloid Interface Sci.* **1987,** *116*, (2), 373-383.

159. Gondikas, A. P.; Jang, E. K.; Hsu-Kim, H., Influence of amino acids cysteine and serine on aggregation kinetics of zinc and mercury sulfide colloids. *J. Colloid Interface Sci.* **2010,** *347*, (2), 167-171.

160. Mullaugh, K. M.; Luther, G. W., Spectroscopic determination of the size of cadmium sulfide nanoparticles formed under environmentally relevant conditions. *J. Environ. Monit.* **2010,** *12*, (4), 890-897.

161. Benning, L. G.; Waychunas, G. A., Nucleation, Growth, and Aggregation of Mineral Phases: Mechanisms and Kinetic Controls. In *Kinetics of Water-Rock Interactions*, Brantley, S. L.; Kubicki, J. D.; White, A. F., Eds. Springer: New York, 2008; pp 259-333.

162. Bligh, M. W.; Waite, T. D., Role of Heterogeneous Precipitation in Determining the Nature of Products Formed on Oxidation of Fe(II) in Seawater Containing Natural Organic Matter. *Environ. Sci. Technol.* **2010,** *44*, (17), 6667-6673.

163. Vilge-Ritter, A.; Rose, J.; Masion, A.; Bottero, J. Y.; Laine, J. M., Chemistry and structure of aggregates formed with Fe-salts and natural organic matter. *Colloid Surface A* **1999,** *147*, (3), 297-308.

164. Charnock, J. M.; Moyes, L. N.; Pattrick, R. A. D.; Mosselmans, J. F. W.; Vaughan, D. J.; Livens, F. R., The structural evolution of mercury sulfide precipitate: an XAS and XRD study. *Am. Mineral.* **2003,** *88*, (8-9), 1197-1203.

165. Bell, A. M. T.; Charnock, J. M.; Helz, G. R.; Lennie, A. R.; Livens, F. R.; Mosselmans, J. F. W.; Pattrick, R. A. D.; Vaughan, D. J., Evidence for dissolved polymeric mercury(II)-sulfur complexes? *Chem. Geol.* **2007,** *243*, 122-127.

166. Gondikas, A. P.; Mason, A.; Auffan, M.; Lau, B. L. T.; Hsu-Kim, H., Early-stage precipitation kinetics of cysteine-capped zinc sulfide nanoclusters. *Chem. Geol.* **2012,** *329*, 10-17.

167. Brown, G. E.; Sturchio, N. C., An overview of synchrotron radiation applications to low temperature geochemistry and environmental science. In *Applications of Synchrotron Radiation in Low-Temperature Geochemistry and Environmental Sciences*, Fenter, P. A.; Rivers, M. L.; Sturchio, N. C.; Sutton, S. R., Eds. 2002; Vol. 49, pp 1-115.

168. Andrews, J. C., Mercury speciation in the environment using X-ray absorption spectroscopy. In *Recent Developments in Mercury Science*, 2006; Vol. 120, pp 1-35.

169. Jonsson, S.; Skyllberg, U.; Nilsson, M. B.; Westlund, P.-O.; Shchukarev, A.; Lundberg, E.; Björn, E., Mercury methylation rates for geochemically relevant Hg^{II} species in sediments. *Environ. Sci. Technol.* **2012,** *In press.*

170. Kim, B.; Park, C.-S.; Murayama, M.; Hochella, M. F., Jr., Discovery and Characterization of Silver Sulfide Nanoparticles in Final Sewage Sludge Products. *Environ. Sci. Technol.* **2010,** *44*, (19), 7509-7514.

171. Kemner, K. M.; Kelly, S. D.; Lai, B.; Maser, J.; O'Loughlin, E. J.; Sholto-Douglas, D.; Cai, Z. H.; Schneegurt, M. A.; Kulpa, C. F.; Nealson, K. H., Elemental and redox analysis of single bacterial cells by X-ray microbeam analysis. *Science* **2004,** *306*, (5696), 686-687.

172. Suzuki, Y.; Kelly, S. D.; Kemner, K. M.; Banfield, J. F., Radionuclide contamination - Nanometre-size products of uranium bioreduction. *Nature* **2002,** *419*, (6903), 134-134.

173. Ahmadian, A.; Gharizadeh, B.; Gustafsson, A. C.; Sterky, F.; Nyrén, P.; Uhlén, M.; Lundeberg, J., Single-nucleotide polymorphism analysis by pyrosequencing. *Anal. Biochem.* **2000,** *280*, (1), 103-110.

174. Daniel, R., The metagenomics of soil. *Nat. Rev. Microbiol.* **2005,** *3*, (6), 470-478.

175. Tringe, S. G.; von Mering, C.; Kobayashi, A.; Salamov, A. A.; Chen, K.; Chang, H. W.; Podar, M.; Short, J. M.; Mathur, E. J.; Detter, J. C.; Bork, P.; Hugenholtz, P.; Rubin, E. M., Comparative metagenomics of microbial communities. *Science* **2005,** *308*, (5721), 554-557.

176. Ogunseitan, O., Soil Proteomics: Extraction and Analysis of Proteins from Soils Nucleic Acids and Proteins in Soil. In Nannipieri, P.; Smalla, K., Eds. Springer Berlin Heidelberg: 2006; Vol. 8, pp 95-115.

177. Polacco, B. J.; Purvine, S. O.; Zink, E. M.; LaVoie, S. P.; Lipton, M. S.; Summers, A. O.; Miller, S. M., Discovering mercury protein modifications in whole proteomes using natural isotope distributions observed in liquid chromatography-tandem mass spectrometry. *Mol. Cell. Proteomics* **2011,** *10*, (8).

178. Lowry, O. H.; Rosebrough, N. J.; Farr, A. L.; Randall, R. J., Protein measurement with the folin phenol reagent. *J. Biol. Chem.* **1951,** *193*, (1), 265-275.

179. Gilmour, C. C.; Elias, D. A.; Kucken, A. M.; Brown, S. D.; Palumbo, A. V.; Schadt, C. W.; Wall, J. D., The sulfate-reducing bacterium *Desulfovibrio desulfuricans* ND132 as a model for understanding bacterial mercury methylation. *Appl. Environ. Microbiol.* **2011**, In press.

180. Institute of Experimental Mineralogy, Russian Academy of Science. *Crystallographic and Crystallochemical Database for Minerals and their Structural Analogues* **Created 1997, Updated 2009**.

181. Reinsch, B. C.; Forsberg, B.; Penn, R. L.; Kim, C. S.; Lowry, G. V., Chemical Transformations during Aging of Zerovalent Iron Nanoparticles in the Presence of Common Groundwater Dissolved Constituents. *Environmental Science & Technology* **2010,** *44*, (9), 3455-3461.

182. Birks, L. S.; Friedman, H., Particle size determination from X-ray line broadening. *J. Appl. Phys.* **1946,** *17*, (8), 687-691.

183. Kim, C. S.; Bloom, N. S.; Rytuba, J. J.; Brown, G. E., Mercury speciation by X-ray absorption fine structure spectroscopy and sequential chemical extractions: A comparison of speciation methods. *Environ. Sci. Technol.* **2003,** *37*, (22), 5102-5108.

184. U.S., Environmental Protection Agency. Method 1630: Methyl Mercury in water by Distillation, Aqueous Ethylation, Purge and Trap, and CVAFS. *Washington, DC* **2001**.

185. U.S., Environmental Protection Agency. Method 1631, Revision D: Mercury in Water by Oxidation, Purge and Trap, and Cold Vapor Atomic Fluorescence Spectroscopy. *Washington, D.C.* **2001**.

186. Hsu-Kim, H.; Sedlak, D. L., Similarities between inorganic sulfide and the strong Hg(II) - Complexing ligands in municipal wastewater effluent. *Environ. Sci. Technol.* **2005,** *39*, (11), 4035-4041.

187. King, J. K.; Saunders, F. M.; Lee, R. F.; Jahnke, R. A., Coupling mercury methylation rates to sulfate reduction rates in marine sediments. *Environ. Toxicol. Chem.* **1999,** *18*, (7), 1362-1369.

188. Pak, K. R.; Bartha, R., Mercury methylation and demethylation in anoxic lake sediments and by strictly anaerobic bacteria. *Appl. Environ. Microbiol.* **1998,** *64*, (3), 1013-1017.

189. Bridou, R.; Monperrus, M.; Gonzalez, P. R.; Guyoneaud, R.; Amouroux, D., Simultaneous determination of mercury methylation and demethylation capacities of various sulfate-reducing bacteria using species-specific isotopic tracers. *Environ. Toxicol. Chem.* **2011,** *30*, (2), 337-344.

190. Dehner, C. A.; Barton, L.; Maurice, P. A.; Dubois, J. L., Size-dependent bioavailability of hematite (alpha-Fe_2O_3) nanoparticles to a common aerobic bacterium. *Environ. Sci. Technol.* **2011,** *45*, (3), 977-983.

191. Mishra, B.; Fein, J.; Yee, N.; Beverridge, T.; Myneni, S., Hg(II) adsorption and speciation on bacterial surfaces. *Geochim. Cosmochim. Acta* **2010,** *74*, (12), A713-A713.

192. Harris, R. C.; Rudd, J. W. M.; Amyot, M.; Babiarz, C. L.; Beaty, K. G.; Blanchfield, P. J.; Bodaly, R. A.; Branfireun, B. A.; Gilmour, C. C.; Graydon, J. A.; Heyes, A.; Hintelmann, H.; Hurley, J. P.; Kelly, C. A.; Krabbenhoft, D. P.; Lindberg, S. E.; Mason, R. P.; Paterson, M. J.; Podemski, C. L.; Robinson, A.; Sandilands, K. A.; Southworth, G. R.; Louis, V. L. S.; Tate, M. T., Whole-ecosystem study shows rapid fish-mercury response to changes in mercury deposition. *Proc. Nat. Acad. Sci. USA* **2007,** *104*, (42), 16586-16591.

193. Patty, C.; Barnett, B.; Mooney, B.; Kahn, A.; Levy, S.; Liu, Y. J.; Pianetta, P.; Andrews, J. C., Using X-ray microscopy and Hg L-3 XAMES to study Hg binding in the rhizosphere of *Spartina* cordgrass. *Environ. Sci. Technol.* **2009,** *43*, (19), 7397-7402.

194. Bessinger, B. A.; Vlassopoulos, D.; Serrano, S.; O'Day, P. A., Reactive transport modeling of subaqueous sediment caps and implications for the long-term fate of arsenic, mercury, and methylmercury. *Aquat. Geochem.* **2012,** *18*, (4), 297-326.

195. Ndungu, K., Model predictions of copper speciation in coastal water compared to measurements by analytical voltammetry. *Environ. Sci. Technol.* **2012,** *46*, (14), 7644-7652.

196. Graham, A. M.; Bullock, A. L.; Maizel, A. C.; Elias, D. A.; Gilmour, C. C., A detailed assessment of the kinetics of Hg-cell association, Hg methylation, and MeHg degradation in several *Desulfovibrio* species. *Appl. Environ. Microbiol.* **2012,** *78*, 7337-7346.

197. Hsu-Kim, H., Kucharzyk, K.H., Zhang, T., Deshusses, M.A., Mechanisms regulating mercury bioavailability for methylating microorganisms in the aquatic environment: A critical review. *Environ. Sci. Technol.* **2013,** *47*, (6), 2441-2456.

198. Guentzel, J. L.; Powell, R. T.; Landing, W. M.; Mason, R. P., Mercury associated with colloidal material in an estuarine and an open-ocean environment. *Mar. Chem.* **1996,** *55*, (1-2), 177-188.

199. Diaz, X.; Johnson, W. P.; Fernandez, D.; Naftz, D. L., Size and elemental distributions of nano- to micro-particulates in the geochemically-stratified Great Salt Lake. *Appl. Geochem.* **2009,** *24*, (9), 1653-1665.

200. Powell, K. J.; Brown, P. L.; Byrne, R. H.; Gajda, T.; Hefter, G.; Sjoberg, S.; Wanner, H., Chemical speciation of environmentally significant metals with inorganic ligands – Part 1: The Hg^{2+}-Cl^-, OH^-, CO_3^{2-}, SO_4^{2-}, and PO_4^{3-} aqueous systems. *Pure Appl. Chem.* **2005,** *77*, (4), 739-800.

201. Morel, F. M. M.; Hering, J. G., *Principles and applications of aquatic chemistry*. John Wiley & Sons, Inc.: New York, 1993.

202. Jonsson, S.; Skyllberg, U.; Nilsson, M. B.; Westlund, P.-O.; Shchukarev, A.; Lundberg, E.; Björn, E., Mercury methylation rates for geochemically relevant Hg^{II} species in sediments. *Environ. Sci. Technol.* **2012,** *46*, 11653-11659.

203. King, J. K.; Kostka, J. E.; Frischer, M. E.; Saunders, F. M.; Jahnke, R. A., A quantitative relationship that demonstrates mercury methylation rates in marine sediments are based on the community composition and activity of sulfate-reducing bacteria. *Environ. Sci. Technol.* **2001,** *35*, (12), 2491-2496.

204. Xu, X. N., Brownlow, W.J., Kyriacou, S.V., Wan, Q., Viola, J.J., Real-time probing of membrane transport in living microbial cells using single nanoparticle optics and living cell imaging. *Biochemistry* **2004,** *43*, 10400-10413.

205. Xu, X. N.; Chen, J.; Jeffers, R. B.; Kyriacou, S., Direct measurement of sizes and dynamics of single living transporters using nanooptics. *Nano Letters* **2002,** *2*, (3), 175-182.

206. Nallathamby, P. D.; Lee, K. J.; Xu, X. N., Study of multidrug membrane transporter of single living Pseudomonas aeruginosa cells using size-dependent plasmonic nanoparticle optical probes. *Biochemistry* **2010,** *49*, (28), 5942-5953.

207. Bridou R., M. M., Gonzalez P.R., Guyoneaud R., Amouroux D., Simultaneous determination of mercury methylation and demethylation capacities of various sulfate-reducing bacteria using species-specific isotopic tracers. *Environ. Toxicol. Chem.* **2011,** *30*, 337-344.

208. Kerin, E. J.; Gilmour, C. C.; Roden, E.; Suzuki, M. T.; Coates, J. D.; Mason, R. P., Mercury methylation by dissimilatory iron-reducing bacteria. *Appl. Environ. Microbiol.* **2006,** *72*, (12), 7919-7921.

209. Oremland, R. S.; Culbertson, C. W.; Winfrey, M. R., Methylmercury decomposition in sediments and bacterial cultures: Involvement of methanogens and sulfate reducers in oxidative demethylation. *Appl. Environ. Microbiol.* **1991,** *57*, (1), 130-137.

210. Behra, P.; Bonnissel-Gissinger, P.; Alnot, M.; Revel, R.; Ehrhardt, J. J., XPS and XAS study of the sorption of Hg(II) onto pyrite. *Langmuir* **2001,** *17*, (13), 3970-3979.

211. Jonsson, S.; Skyllberg, U.; Nilsson, M. B.; Westlund, P. O.; Shchukarev, A.; Lundberg, E.; Bjorn, E., Mercury methylation rates for geochemically relevant Hg-II species in sediments. *Environ. Sci. Technol.* **2012,** *46*, (21), 11653-11659.

212. Zhang, T.; Kim, B.; Leyard, C.; Reinsch, B. C.; Lowry, G. V.; Deshusses, M. A.; Hsu-Kim, H., Methylation of mercury by bacteria exposed to dissolved, nanoparticulate, and microparticulate mercuric sulfides. *Environ. Sci. Technol.* **2012,** *46*, (13), 6950-6958.

213. Schecher, W. D., MINEQL+: A chemical equilibrium program for personal computers, 4.5 ed.; Environmental Research Software, Hallowell, ME. **2001**.

214. Waples, J. S.; Nagy, K. L.; Aiken, G. R.; Ryan, J. N., Dissolution of cinnabar (HgS) in the presence of natural organic matter. *Geochim. Cosmochim. Acta* **2005,** *69*, (6), 1575-1588.

215. San Francisco Estuary Institute Regional Monitoring Program data; San Francisco Estuary Institute: San Francisco, CA; accessed at www.sfei.org on Feb 19, 2012.

216. Deonarine, A.; Hsu-Kim, H., Precipitation of mercuric sulfide nanoparticles in NOM-containing water: implications for the natural environment. *Environ. Sci. Technol.* **2009,** *43*, (7), 2368-2373.

217. Gondikas, A. P.; Jang, E. K.; Hsu-Kim, H., Influence of amino acids cysteine and serine on aggregation kinetics of zinc and mercury sulfide colloids. *J. Colloid Interface Sci.* **2010,** *347*, (2), 167-171.

218. Choe, K. Y.; Gill, G. A.; Lehman, R., Distribution of particulate, colloidal, and dissolved mercury in San Francisco Bay estuary. 1. Total mercury. *Limnol. Oceanogr.* **2003,** *48*, (4), 1535-1546.

219. Babiarz, C. L.; Hurley, J. P.; Hoffmann, S. R.; Andren, A. W.; Shafer, M. M.; Armstrong, D. E., Partitioning of total mercury and methylmercury to the colloidal phase in freshwaters. *Environ. Sci. Technol.* **2001,** *35*, (24), 4773-4782.

220. Lee, S.; Han, S.; Gill, G. A., Estuarine mixing behavior of colloidal organic carbon and colloidal mercury in Galveston Bay, Texas. *J. Environ. Monit.* **2011,** *13*, (6), 1703-1708.

221. King, J. K.; Saunders, F. M.; Lee, R. F.; Jahnke, R. A., Coupling mercury methylation rates to sulfate reduction rates in marine sediments. *Environ. Toxicol. Chem.* **1999,** *18*, (7), 1362-1369.

222. Devereux, R.; Winfrey, M. R.; Winfrey, J.; Stahl, D. A., Depth profile of sulfate-reducing bacterial ribosomal RNA and mercury methylation in an estuarine sediment. *Fems Microbiol. Ecol.* **1996,** *20*, (1), 23-31.

223. Gilmour, C. C.; Henry, E. A.; Mitchell, R., Sulfate stimulation of mercury methylation in fresh-water sediments. *Environ. Sci. Technol.* **1992,** *26*, (11), 2281-2287.

224. Compeau, G. C.; Bartha, R., Sulfate-reducing bacteria - principal methylators of mercury in anoxic estuarine sediment. *Appl. Environ. Microbiol.* **1985,** *50*, (2), 498-502.

225. King, J. K.; Kostka, J. E.; Frischer, M. E.; Saunders, F. M., Sulfate-reducing bacteria methylate mercury at variable rates in pure culture and in marine sediments. *Appl. Environ. Microbiol.* **2000,** *66*, (6), 2430-2437.

226. Drott, A.; Lambertsson, L.; Bjorn, E.; Skyllberg, U., Importance of dissolved neutral mercury sulfides for methyl mercury production in contaminated sediments. *Environ. Sci. Technol.* **2007,** *41*, (7), 2270-2276.

227. Benoit, J. M.; Gilmour, C. C.; Mason, R. P.; Heyes, A., Sulfide controls on mercury speciation and bioavailability to methylating bacteria in sediment pore waters. *Environ. Sci. Technol.* **1999,** *33*, (6), 951-957.

228. Long, G. Y.; Zhu, P. T.; Shen, Y.; Tong, M. P., Influence of extracellular polymeric substances (EPS) on deposition kinetics of bacteria. *Environ. Sci. Technol.* **2009,** *43*, (7), 2308-2314.

229. Smith, R. D.; Martell, A. E., NIST Critical Stability Constants of Metal Complexes Database v. 2.0. **1993**.

230. Jeong, H. Y.; Klaue, B.; Blum, J. D.; Hayes, K. F., Sorption of mercuric ion by synthetic manocrystalline mackinawite (FeS). *Environ. Sci. Technol.* **2007,** *41*, (22), 7699-7705.

231. Morse, J. W.; Luther, G. W., Chemical influences on trace metal-sulfide interactions in anoxic sediments. *Geochim. Cosmochim. Acta* **1999,** *63*, (19-20), 3373-3378.

232. Yu, R. Q.; Flanders, J. R.; Mack, E. E.; Turner, R.; Mirza, M. B.; Barkay, T., Contribution of coexisting sulfate and iron reducing bacteria to methylmercury production in freshwater river sediments. *Environ. Sci. Technol.* **2012,** *46*, (5), 2684-2691.

233. Ulrich, P. D.; Sedlak, D. L., Impact of iron amendment on net methylmercury export from tidal wetland microcosms. *Environ. Sci. Technol.* **2010,** *44*, (19), 7659-7665.

234. Mehrotra, A. S.; Sedlak, D. L., Decrease in net mercury methylation rates following iron amendment to anoxic wetland sediment slurries. *Environ. Sci. Technol.* **2005,** *39*, (8), 2564-2570.

235. Han, S.; Obraztsova, A.; Pretto, P.; Deheyn, D. D.; Gieskes, J.; Tebo, B. M., Sulfide and iron control on mercury speciation in anoxic estuarine sediment slurries. *Mar. Chem.* **2008,** *111*, (3-4), 214-220.

236. Luther, G. W.; Rozan, T. F.; Taillefert, M.; Nuzzio, D. B.; Di Meo, C.; Shank, T. M.; Lutz, R. A.; Cary, S. C., Chemical speciation drives hydrothermal vent ecology. *Nature* **2001,** *410*, (6830), 813-816.

237. Rozan, T. F.; Lassman, M. E.; Ridge, D. P.; Luther, G. W., Evidence for iron, copper and zinc complexation as multinuclear sulphide clusters in oxic rivers. *Nature* **2000,** *406*, (6798), 879-882.

238. Gilmour, C. C.; Elias, D. A.; Kucken, A. M.; Brown, S. D.; Palumbo, A. V.; C.W., S.; Wall, J. D., Sulfate-reducing bacterium Desulfovibrio desulfuricans ND132 as a model for understanding bacterial mercury methylation. *Appl. Environ. Microbiol.* **2011**, (77), 3938-3951.

239. Hintelmann, H.; Keppel-Jones, K.; Evans, R. D., Constants of mercury methylation and demethylation rates in sediments and comparison of tracer and ambient mercury availability. *Environ. Toxicol. Chem.* **2000,** *19*, (9), 2204-2211.

240. Harmon, S. M.; King, J. K.; Gladden, J. B.; Newman, L. A., Using sulfate-amended sediment slurry batch reactors to evaluate mercury methylation. *Arch. Environ. Contam. Toxicol.* **2007,** *52*, (3), 326-331.

241. Horzempa, L. M.; Helz, G. R., Controls on the stability of sulfide sols-colloidal covellite as an example. *Geochimica et Cosmochimica Acta* **1979,** *43*, (10), 1645-1650.

242. Lau, B. L. T.; Hsu-Kim, H., Precipitation and growth of zinc sulfide nanoparticles in the presence of thiol-containing natural organic ligands. *Environmental Science & Technology* **2008,** *42*, (19), 7236-7241.

243. Bridou, R.; Monperrus, M.; Gonzalez, P. R.; Guyoneaud, R.; Amouroux, D., Simultaneous determination of mercury methylation and demethylation capacities of various sulfate-reducing bacteria using species-specific isotopic tracers. *Environ. Toxicol. Chem.* **2011,** *30*, (2), 337-344.

244. Schaefer, J. K.; Morel, F. M. M., High methylation rates of mercury bound to cysteine by Geobacter sulfurreducens. *Nature Geosci.* **2009,** *2*, (2), 123-126.

245. Schaefer, J. K.; Rocks, S. S.; Zheng, W.; Liang, L. Y.; Gu, B. H.; Morel, F. M. M., Active transport, substrate specificity, and methylation of Hg(II) in anaerobic bacteria. *Proceedings of the National Academy of Sciences of the United States of America* **2011,** *108*, (21), 8714-8719.

246. Schaefer, J. K.; Szczuka, A.; Morel, F. M. M., Effect of Divalent Metals on Hg(II) Uptake and Methylation by Bacteria. *Environ. Sci. Technol.* **2014**.

247. King, J. K.; Kostka, J. E.; Frischer, M. E.; Saunders, F. M.; Jahnke, R. A., A quantitative relationship that remonstrates mercury methylation rates in marine sediments are based on the community composition and activity of sulfate-reducing bacteria. *Environmental Science & Technology* **2001,** *35*, (12), 2491-2496.

248. Devereux, R.; Winfrey, M. R.; Winfrey, J.; Stahl, D. A., Depth profile of sulfate-reducing bacterial ribosomal RNA and mercury methylation in an estuarine sediment. *Fems Microbiol. Ecol.* **1996,** *20*, (1), 23-31.

249. Compeau, G. C.; Bartha, R., Sulfate-reducing bacteria - principal methylators of mercury in anoxic estuarine sediment. *Appl. Environ. Microbiol.* **1985,** *50*, (2), 498-502.

250. Benoit, J. M.; Gilmour, C. C.; Mason, R. P., Aspects of bioavailability of mercury for methylation in pure cultures of *Desulfobulbus propionicus* (1pr3). *Appl. Environ. Microbiol.* **2001,** *67*, (1), 51-58.

251. Gilmour, C. C.; Elias, D. A.; Kucken, A. M.; Brown, S. D.; Palumbo, A. V.; Schadt, C. W.; Wall, J. D., Sulfate-Reducing Bacterium Desulfovibrio desulfuricans ND132 as a Model for Understanding Bacterial Mercury Methylation. *Applied and Environmental Microbiology* **2011,** *77*, (12), 3938-3951.

252. Patty, C.; Barnett, B.; Mooney, B.; Kahn, A.; Levy, S.; Liu, Y. J.; Pianetta, P.; Andrews, J. C., Using X-ray microscopy and Hg L-3 XAMES to study Hg binding in the rhizosphere of *Spartina* cordgrass. *Environ. Sci. Technol.* **2009,** *43*, (19), 7397-7402.

253. Kim, B.; Park, C. S.; Murayama, M.; Hochella, M. F., Discovery and Characterization of Silver Sulfide Nanoparticles in Final Sewage Sludge Products. *Environmental Science & Technology* **2010,** *44*, (19), 7509-7514.

254. Morse, J. W.; Luther, G. W., Chemical influences on trace metal-sulfide interactions in anoxic sediments. *Geochimica et Cosmochimica Acta* **1999,** *63*, (19-20), 3373-3378.

255. Rickard, D.; Luther, G. W., Kinetics of pyrite formation by the H2S oxidation of iron(II) monosulfide in aqueous solutions between 25 and 125 degrees C: The mechanism. *Geochimica et Cosmochimica Acta* **1997,** *61*, (1), 135-147.

256. Mehrotra, A. S.; Sedlak, D. L., Decrease in net mercury methylation rates following iron amendment to anoxic wetland sediment slurries. *Environmental Science & Technology* **2005,** *39*, (8), 2564-2570.

257. Ulrich, P. D.; Sedlak, D. L., Impact of Iron Amendment on Net Methylmercury Export from Tidal Wetland Microcosms. *Environmental Science & Technology* **2010,** *44*, (19), 7659-7665.

258. Han, S.; Obraztsova, A.; Pretto, P.; Deheyn, D. D.; Gieskes, J.; Tebo, B. M., Sulfide and iron control on mercury speciation in anoxic estuarine sediment slurries. *Marine Chemistry* **2008,** *111*, (3-4), 214-220.

259. Luther, G. W.; Ferdelman, T. G., Voltammetric characterization of iron (II) sulfide complexes in laboratory solutions and in marine waters and porewaters. *Environmental Science & Technology* **1993,** *27*, (6), 1154-1163.

260. Jeong, H. Y.; Sun, K.; Hayes, K. F., Microscopic and Spectroscopic Characterization of Hg(II) Immobilization by Mackinawite (FeS). *Environmental Science & Technology* **2010,** *44*, (19), 7476-7483.

261. Jeong, H. Y.; Klaue, B.; Blum, J. D.; Hayes, K. F., Sorption of mercuric ion by synthetic manocrystalline mackinawite (FeS). *Environmental Science & Technology* **2007,** *41*, (22), 7699-7705.

262. Skyllberg, U.; Drott, A., Competition between Disordered Iron Sulfide and Natural Organic Matter Associated Thiols for Mercury(II)-An EXAFS Study. *Environmental Science & Technology* **2010,** *44*, (4), 1254-1259.

263. Bloom, N. S.; Colman, J. A.; Barber, L., Artifact formation of methyl mercury during aqueous distillation and alternative techniques for the extraction of methyl mercury from environmental samples. *Fresenius Journal of Analytical Chemistry* **1997,** *358*, (3), 371-377.

264. U.S. Environmental Protection Agency. Method 1630: Methyl mercury in water by distillation, aqueous ethylation, purge and trap, and CVAFS. *Washington, DC* **2001**.

265. U.S. Environmental Protection Agency. Method 1631, Revision D: Mercury in water by oxidation, purge and trap, and cold vapor atomic fluorescence spectroscopy. *Washington, D.C.* **2001**.

266. U.S. Environmental Protection Agency. Method 7473: Mercury in solids and solutions by thermal decomposition, amalgamation, and atomic absorption spectrophotometry. **1998**.

267. Allen, H. E.; Fu, G. M.; Deng, B. L., Analysis of acid-volatile sulfide (AVS) and simultaneously extracted metals (SEM) for the estimation of potential toxicity in aquatic sediments *Environ. Toxicol. Chem.* **1993,** *12*, (8), 1441-1453.

268. Cline, J. D., Spectrophotometric determination of hydrogen sulfide in natural waters. *Limnol. Oceanogr.* **1969,** *14*, (3), 454-458.

269. Olson, R. V.; Ellis Jr., R., Iron, In: Methods of Soil Analysis, Part 2, Agronomy Monograph no. 9, Soil Science Society of America, Madison, WI, USA, pp. 301-312. **1982**.

270. Denman, S. E.; McSweeney, C. S., Development of a real-time PCR assay for monitoring anaerobic fungal and cellulolytic bacterial populations within the rumen. *Fems Microbiol. Ecol.* **2006,** *58*, (3), 572-582.

271. Kondo, R.; Nedwell, D. B.; Purdy, K. J.; Silva, S. D., Detection and enumeration of sulphate-reducing bacteria in estuarine sediments by competitive PCR. *Geomicrobiology Journal* **2004,** *21*, (3), 145-157.

272. Acha, D.; Hintelmann, H.; Yee, J., Importance of sulfate reducing bacteria in mercury methylation and demethylation in periphyton from Bolivian Amazon region. *Chemosphere* **2011,** *82*, (6), 911-916.

273. Lee, Z. M. P.; Bussema, C.; Schmidt, T. M., rrnDB: documenting the number of rRNA and tRNA genes in bacteria and archaea. *Nucleic Acids Research* **2009,** *37*, D489-D493.

274. Dyrssen, D.; Wedborg, M., The sulfure-mercury(II) system in natural waters. *Water Air and Soil Pollution* **1991,** *56*, 507-519.

275. Haitzer, M.; Aiken, G. R.; Ryan, J. N., Binding of mercury(II) to aquatic humic substances: Influence of pH and source of humic substances. *Environ. Sci. Technol.* **2003,** *37*, (11), 2436-2441.

276. Khwaja, A. R.; Bloom, P. R.; Brezonik, P. L., Binding constants of divalent mercury (Hg2+) in soil humic acids and soil organic matter. *Environ. Sci. Technol.* **2006,** *40*, (3), 844-849.

277. Wei, D. W.; Osseoasare, K., Formation of iron monosulfide - A spectrophotometric study of the reaction between ferrous and sulfide ions in aqueous-solutions. *J. Colloid Interface Sci.* **1995,** *174*, (2), 273-282.

Supporting Information

Chapter 2 Supporting Information

Data for Figure 2.1										
1pr3										
MeHg Concentration (pM)			Dissolved Hg+S (1 nM)		HgS nanoparticles (aged for 16 h, 1 nM		HgS nanoparticles (aged for 3 days or		HgS microparticles (6 nM)	
Hrs	mins	Mean	STD	Mean	STD	Mean	STD	Mean	STD	
0	0	0	0	0	0	0	0	0	0	
0.5	30	35.04	0.07	22.88	3.40	15.98	0.75	4.89	1.82	
1.5	30	59.67	8.25	33.03	2.46	21.76	1.58	3.50	4.94	
4.5	30	64.51	6.70	41.82	2.77	25.89	1.25	6.94	2.10	
10	0	71.06	2.08	54.92	6.45	32.93	2.93	7.04	1.28	
23	0	91.14	10.22	62.35	7.60	35.93	1.99	4.89	0.69	
ND132										
MeHg Concentration (pM)			Dissolved Hg-sulfide		HgS nanoparticles (aged for 16 hrs)		HgS nanoparticles (aged for 1 week)		Metacinnabar	
Hrs	mins	Mean	STD	Mean	STD	Mean	STD	Mean	STD	
0	0	7.7	6.0	6.4	4.3	0.0	0.0	3.1	4.4	
0.25	15	119.1	27.7	55.1	2.4	7.0	3.8	9.9	5.0	
0.5	30	181.5	41.5	68.4	17.7	9.7	1.0	5.7	3.5	
1.5	30	177.5	27.6	69.7	11.5	13.6	1.6	1.8	2.5	
4.5	30	207.0	46.6	83.4	9.6	20.2	4.2	0.4	0.6	
10	0	236.2	61.6	98.1	4.7	21.0	9.4	2.4	3.3	
23	0	243.8	62.3	92.5	8.1	18.7	3.9	6.9	4.0	
1pr3 - surface area normalized										
MeHg Concentration (pM)			HgS nanoparticles		HgS microparticles (56 nM, 3×10-5 m2L		HgS microparticles (227 nM, 11×10-5 m2L-1)			
Hrs	mins	Mean	STD	Mean	STD	Mean	STD			
0	0	0	0	0	0	0	0			
0.5	30	22.9	3.4	3.9	1.4	13.1	10.4			
1.5	30	33.0	2.5	7.3	5.4	14.0	11.9			
4.5	30	41.8	2.8	8.6	2.3	11.9	1.1			
10	0	54.9	6.4	10.0	4.2	18.8	10.0			
23	0	62.3	7.6	12.7	1.6	22.2	7.9			

Data for Figure 2.8				
Filtration				
Dissolved H	Hg < 0.02 µm		0.02 µm < Hg < 0.22 µm	
Time (hours)	Mean	STD	Mean	STD
0	74.7%	2.3%	12.0%	8.0%
4.4	31.6%	6.3%	37.4%	2.6%
20.6	16.7%	0.8%	18.7%	12.9%
HgS nanopa	Hg < 0.02 µm		0.02 µm < Hg < 0.22 µm	
Time	Mean	STD	Mean	STD
0	6.9%	0.2%	82.4%	7.4%
4.4	9.6%	0.2%	65.0%	11.6%
20.6	14.0%	7.6%	26.4%	6.2%
Metacinnaba	Hg < 0.02 µm		0.02 µm < Hg < 0.22 µm	
Time	Mean	STD	Mean	STD
0	0.26%	0.02%	0.6%	0.2%
4.4	0.37%	0.01%	2.6%	0.4%
20.6	1.6%	1.8%	5.0%	0.2%

Data for Figure 2.9				
	Dissolved Hg-sulfide			
	Hg < 0.02 µm		0.02 µm < Hg < 0.22 µm	
Time (hrs)	Mean	STD	Mean	STD
0	89.9%	4.9%	5.7%	4.5%
0.5	84.5%	3.4%	8.7%	7.2%
1.5	78.9%	5.3%	12.3%	10.1%
4.5	61.9%	3.9%	27.5%	3.4%
10	55.9%	11.6%	32.6%	13.5%
23	50.6%	7.3%	28.1%	13.0%
HgS nanoparticles				
	Hg < 0.02 µm		0.02 µm < Hg < 0.22 µm	
Time (hrs)	Mean	STD	Mean	STD
0	7.3%	1.3%	83.2%	2.2%
0.5	11.8%	2.7%	80.9%	1.3%
1.5	12.0%	5.1%	86.4%	5.3%
4.5	18.4%	7.8%	81.7%	0.7%
10	16.9%	3.1%	71.1%	11.9%
23	20.7%	8.9%	70.9%	7.7%
Metacinnabar				
	Hg < 0.02 µm		0.02 µm < Hg < 0.22 µm	
Time (hrs)	Mean	STD	Mean	STD
0	0.3%	0.1%	0.1%	0.1%
0.5	1.4%	0.7%	2.6%	2.5%
1.5	1.1%	0.2%	1.3%	0.5%
4.5	1.8%	0.4%	1.8%	0.3%
10	1.8%	0.5%	2.7%	3.6%
23	0.8%	0.3%	6.2%	2.5%

Data for Figure 2.13								
Time-0	Control	Dissolved Hg	Nano-HgS	Micro-HgS	Control	Dissolved Hg	HgS nanopar	Metacinnabar
Time	Mean	Mean	Mean	Mean	STD	STD	STD	STD
No treatment	37.5%	34.0%	4.9%	0.7%	4.8%	5.3%	0.8%	0.1%
0.1 mM GSH	88.0%	75.2%	13.8%	5.3%	7.2%	7.7%	2.4%	1.2%
0.1 mM DED	13.2%	2.6%	3.1%	0.3%	1.3%	0.1%	0.3%	0.0%
Time-1	Control	Dissolved Hg	HgS nanopar	Metacinnabar	Control	Dissolved Hg	HgS nanopar	Metacinnabar
Time	Mean	Mean	Mean	Mean	STD	STD	STD	STD
No treatment	26.4%	22.7%	16.8%	0.3%	2.1%	2.9%	3.9%	0.2%
0.1 mM GSH	71.8%	53.2%	24.0%	5.7%	7.5%	5.1%	4.2%	2.9%
0.1 mM DED	6.5%	1.4%	2.0%	0.2%	0.1%	0.1%	0.2%	0.1%

Chapter 3 Supporting Information

Materials and Methods

Dissolved Mercury Complexation Kinetics. The formation rates of dissolved complexes were modeled with kinetic expressions. The formation rate constant is composed of two terms: the water exchange rate constant for mercury (k_w) and the equilibrium constant for outer sphere association (K_{OS}). The measured water exchange rate constant for mercury is 2×10^9 s^{-1} (1). The equilibrium constant for outer sphere association was calculated using the following theoretical expression described in Morel and Hering[1] and is based on the electrostatic interactions between ion pairs:

$$K_{OS} = \frac{4000\pi\mathcal{N}a^3}{3}\exp\left[\frac{-z_M z_L e^2}{4\pi\varepsilon_0\varepsilon\boldsymbol{k}Ta}\right] exp\left[\frac{-z_M z_L e^2\kappa}{4\pi\varepsilon_0\varepsilon\boldsymbol{k}T(1+\kappa a)}\right]$$

Where the term κ is the Debye-Hückel ion atmosphere parameter calculated as:

$$\kappa^2 = \frac{2000e^2\mathcal{N}I}{\varepsilon_0\varepsilon\boldsymbol{k}T}$$

The above equations contain SI units and represent the following constants: e (elementary charge) in Coulombs, $\boldsymbol{k}$ (Boltzmann constant) in $J\cdot K^{-1}$, $\mathcal{N}$ (Avogadro constant) in mol^{-1}, ε_0 (vacuum permittivity) 8.854 x 10^{-12} $J^{-1}C^2m^{-1}$, T (absolute temperature) in K, ε (relative permittivity of the medium) 78.54 for water at 25°C, a (distance of closest approach of the ions) usually 5 x 10^{-10} m, z_M and z_L (charge of the metal and ligand ions), and I (ionic strength) in mol L^{-1}.

For the model calculations, the following values were used: K_{OS0} = -0.50 for z_Mz_L =0; K_{OS-1} = 0.12 for z_Mz_L = -1; K_{OS-2} = 0.74 for z_Mz_L = -2; K_{OS-4} = 1.98 for z_Mz_L = -4.

HgS Nanoparticle Preparation. A dissolved Hg stock solution (1.96 mM) was prepared with $Hg(NO_3)_2$ dissolved in 0.1 N HNO_3. The Na_2S stock solution (10 mM) was prepared by dissolving freshly washed and dried crystals of $Na_2S\cdot 9H_20$ (Fischer Scientific) in N_2-purged nanopure water. The sulfide stock was utilized within 2 hours of preparation. All chemicals used in this study were ACS reagent grade and were purchased from Sigma Aldrich, unless otherwise noted. Filtered (<0.2 μm) ultrapure water (Barnstead Nanopure) was used to prepare all stocks. Acid cleaned 20 mL glass vials with butyl rubber stoppers sealed with screw caps were utilized for all dissolution experiments. Other glassware for stock solutions were cleaned by overnight soak in phosphate-free soap, overnight soak in 1 M HCl, and rinsed three times with ultrapure water.

HgS nanoparticles were synthesized as in our previous study (2). In summary, nanoparticles stock solutions were prepared by adding dissolved Hg and sulfide from their respective stock solutions to a final concentration of 50 μM each in a buffer solution containing 10 mg-C L^{-1} Suwannee River Humic Acid (SRHA, International Humic Substances Society), 4 mM sodium 4-(2-hydroxyethyl) piperazine-1-ethanesulfonate (HEPES), and 0.1 M $NaNO_3$. Prior to the addition of Hg and sulfide, the buffer solution pH was adjusted to 7.5 with the addition of trace metal grade hydrochloric acid and filtered to <0.1 μm (EMD Millipore Isopore Polycarbonate). After the addition of Hg and sulfide, the Hg-S-humic acid solution was allowed to age for 16 hours prior to use in the dissolution experiments.

HgS Nanoparticle Characterization. Particles were characterized by measuring the average hydrodynamic diameter using dynamic light scattering (DLS) (Malvern Zetasizer NS) at 25 °C. The hydrodynamic diameter was estimated from the scattering of the incident light (663 nm) at 173° and averaged over 20 individual 10 s measurements. The nanoparticles used for this

experiment had an average hydrodynamic diameter of 29 nm, similar to results reported in our previous study (2). Our previous work also indicated that these nanoparticles are aggregates of smaller particles (3 ± 1 nm diameter) with metacinnabar-like composition.

Rate Equations for Dissolved Hg Species

$$d[Hg^{2+}]/dt = K_{OS\text{-}2}k_w/K_{eq1}[HgOH^+] - K_{OS\text{-}2}k_w[Hg^{2+}][OH^-] - K_{OS\text{-}2}k_w[Hg^{2+}][Cl^-] + K_{OS\text{-}2}k_w/K_{eq4}[HgCl^+] - K_{OS\text{-}2}k_w[Hg^{2+}][HS^-] + K_{OS\text{-}2}k_w/K_{eq7}[HgHS^+] - K_{OS\text{-}4}k_w[Hg^{2+}][RS_2^{2-}] + k_{d,NOM}[RS_2^{2-}]$$

$$d[HgOH^+]/dt = -K_{OS\text{-}2}k_w/K_{eq1}[HgOH^+] + K_{OS\text{-}2}k_w[Hg^{2+}][OH^-] + K_{OS\text{-}1}k_w/K_{eq2}[Hg(OH)_2] - K_{OS\text{-}1}k_w[HgOH^+][OH^-] + K_{OS\text{-}1}k_w[HgCl^+][OH^-] - K_{OS\text{-}1}k_w/(K_{eq1}/K_{eq3})[HgOH^+][Cl^-] + K_{OS\text{-}1}k_w/K_{eq5}[HgOHCl] - K_{OS\text{-}1}k_w[HgOH^+][Cl^-] + K_{OS\text{-}1}k_w/(K_{eq7}/K_{eq1})[HgHS^+][OH^-] - K_{OS\text{-}1}k_w[HgOH^+][HS^-]$$

$$d[HgCl^+]/dt = -K_{OS\text{-}2}k_w/K_{eq3}[HgCl^+] + K_{OS\text{-}2}k_w[Hg^{2+}][Cl^-] + K_{OS\text{-}1}k_w/K_{eq4}[HgCl_2] - K_{OS\text{-}1}k_w[HgCl^+][Cl^-] + K_{OS\text{-}1}k_w/(K_{eq1}/K_{eq3})[HgOH^+][Cl^-] - K_{OS\text{-}1}k_w[HgCl^+][OH^-] + K_{OS\text{-}1}k_w/K_{eq6}[HgOHCl] - K_{OS\text{-}1}k_w[HgCl^+][OH^-] + K_{OS\text{-}1}k_w/(K_{eq7}/K_{eq3})[HgHS^+][Cl^-] - K_{OS\text{-}1}k_w[HgCl^+][HS^-]$$

$$d[HgHS^+]/dt = -K_{OS\text{-}2}k_w/K_{eq7}[HgHS^+] + K_{OS\text{-}2}k_w[Hg^{2+}][HS^-] + K_{OS\text{-}1}k_w/K_{eq8}[Hg(HS)_2] - K_{OS\text{-}1}k_w[HgHS^+][HS^-] + K_{OS\text{-}1}k_w[HgOH^+][HS^-] - K_{OS\text{-}1}k_w/(K_{eq7}/K_{eq1})[HgHS^+][OH^-] + K_{OS\text{-}1}k_w[HgCl^+][HS^-] - K_{OS\text{-}1}k_w/(K_{eq7}/K_{eq3})[HgHS^+][Cl^-] + K_{OS\text{-}1}k_w/K_{eq9}[HgS_2H^-][H^+] - K_{OS\text{-}1}k_w[HgHS^+][HS^-] + K_{OS\text{-}1}k_w/K_{eq10}[HgS_2^{2}][H^+]^2 - K_{OS\text{-}1}k_w[HgHS^+][HS^-]$$

$$d[HgRS_2]/dt = -K_{OS\text{-}4}k_w/K_{eq11}[HgRS_2] + K_{OS\text{-}4}k_w[Hg^{2+}][RS_2^{2-}]$$

$$d[HgOHCl]/dt = -K_{OS\text{-}1}k_w/K_{eq5}[HgOHCl] + K_{OS\text{-}1}k_w[HgOH^+][Cl^-] - K_{OS\text{-}1}k_w/K_{eq6}[HgOHCl] + K_{OS\text{-}1}k_w[HgCl^+][OH^-] - K_{OS0}k_w/(K_{eq6}/K_{eq4})[HgOHCl][Cl^-] + K_{OS0}k_w[HgCl_2][OH^-] - K_{OS0}k_w/(K_{eq5}/K_{eq2})[HgOHCl][OH^-] + K_{OS0}k_w[Hg(OH)_2][Cl^-]$$

$$d[Hg(OH)_2]/dt = -K_{OS\text{-}1}k_w/K_{eq2}[Hg(OH)_2] + K_{OS\text{-}1}k_w[HgOH^+][OH^-] - K_{OS0}k_w[Hg(OH)_2][Cl^-] + K_{OS0}k_w/(K_{eq5}/K_{eq2})[HgOHCl][OH^-]$$

$$d[HgCl_2]/dt = -K_{OS\text{-}1}k_w/K_{eq4}[HgCl_2] + K_{OS\text{-}1}k_w[HgCl^+][Cl^-] - K_{OS0}k_w[HgCl_2][OH^-] + K_{OS0}k_w/(K_{eq6}/K_{eq4})[HgOHCl][Cl^-]$$

$$d[Hg(HS)_2]/dt = -K_{OS\text{-}1}k_w/K_{eq8}[Hg(HS)_2] + K_{OS\text{-}1}k_w[HgHS^+][HS^-]$$

$$d[HgS_2H^-]/dt = -K_{OS\text{-}1}k_w/K_{eq9}[HgS_2H^-][H^+] + K_{OS\text{-}1}k_w[HgHS^+][HS^-]$$

$$d[HgS_2^{2-}]/dt = -K_{OS\text{-}1}k_w/K_{eq10}[HgS_2^{2-}][H^+]^2 + K_{OS\text{-}1}k_w[HgHS^+][HS^-]$$

Table S1. Equilibrium formation constants Keq (I = 0, T = 25°C) for dissolved Hg-ligand complexes considered in the speciation calculations. The constants were used in both chemical equilibrium calculations and in calculations for ligand exchange rates.

Reaction		**Reference**
$Hg^{2+} + OH^- \leftrightarrow HgOH^+$	$\log K_{eq1} = 10.60$	(SI 3)
$HgOH^+ + OH^- \leftrightarrow Hg(OH)_2$	$\log K_{eq2} = 11.42$	(SI 3)
$Hg^{2+} + Cl^- \leftrightarrow HgCl^+$	$\log K_{eq3} = 7.31$	(SI 3)
$HgCl^+ + Cl^- \leftrightarrow HgCl_2$	$\log K_{eq4} = 6.69$	(SI 3)
$HgOH^+ + Cl^- \leftrightarrow HgOHCl$	$\log K_{eq5} = 7.67$	(SI 3)
$HgCl^+ + OH^- \leftrightarrow HgOHCl$	$\log K_{eq6} = 10.96$	(SI 3)
$Hg^{2+} + HS^- \leftrightarrow HgHS^+$	$\log K_{eq7} = 30.20$	(SI 4)
$HgHS^+ + HS^- \leftrightarrow Hg(HS)_2$	$\log K_{eq8} = 7.50$	(SI 5)
$HgHS^+ + HS^- \leftrightarrow HgS_2H^- + H^+$	$\log K_{eq9} = 1.30$	(SI 5)
$HgHS^+ + HS^- \leftrightarrow HgS_2^{2-} + 2H^+$	$\log K_{eq10} = -7.00$	(SI 5)
$Hg^{2+} + RS_2^{2-} \leftrightarrow HgRS_2$	$\log K_{eq11} = 28.70$	(SI 6)

Table S2. Comparison of dissolved Hg(II) speciation in the kinetic model and equilibrium model (using the constants in Table 1 and entered into MINEQL+). Kinetic model simulations were run to 0.1 hours at which point an approximate steady state was reached.

Species	$[Cl^-]$ = 1 mM $[HS^-]_{total}$ = 1 µM $[Hg]_{total}$ = 1 nM		**Species**	$[Cl^-]$ = 1 mM $[HS^-]_{total}$ = 1 mM $[Hg]_{total}$ = 1 nM	
	Kinetic Model (Conc, M)	**Equilibrium (Conc, M)**		**Kinetic Model (Conc, M)**	**Equilibrium (Conc, M)**
Hg^{2+}	2.8×10^{-36}	1.5×10^{-36}	Hg^{2+}	1.9×10^{-42}	1.5×10^{-42}
$HgOH^+$	3.9×10^{-34}	1.9×10^{-32}	$HgOH^+$	1.1×10^{-38}	1.9×10^{-38}
$Hg(OH)_2$	8.5×10^{-36}	1.5×10^{-27}	$Hg(OH)_2$	2.7×10^{-41}	1.5×10^{-33}
$HgCl^+$	9.4×10^{-33}	3.0×10^{-32}	$HgCl^+$	4.5×10^{-38}	3.0×10^{-38}
$HgCl_2$	4.6×10^{-29}	1.5×10^{-28}	$HgCl_2$	5.4×10^{-35}	1.5×10^{-34}
HgOHCl	4.7×10^{-36}	8.7×10^{-28}	HgOHCl	7.1×10^{-42}	8.6×10^{-34}
$HgHS^+$	9.0×10^{-13}	1.3×10^{-12}	$HgHS^+$	9.0×10^{-16}	1.8×10^{-15}
$Hg(HS)_2$	9.0×10^{-12}	4.1×10^{-11}	$Hg(HS)_2$	9.0×10^{-12}	4.2×10^{-11}
$HgHS_2^{-1}$	9.0×10^{-10}	8.3×10^{-10}	$HgHS_2^{-1}$	9.0×10^{-10}	8.3×10^{-10}
HgS_2^{-2}	9.0×10^{-11}	1.3×10^{-10}	HgS_2^{-2}	9.0×10^{-11}	1.3×10^{-10}

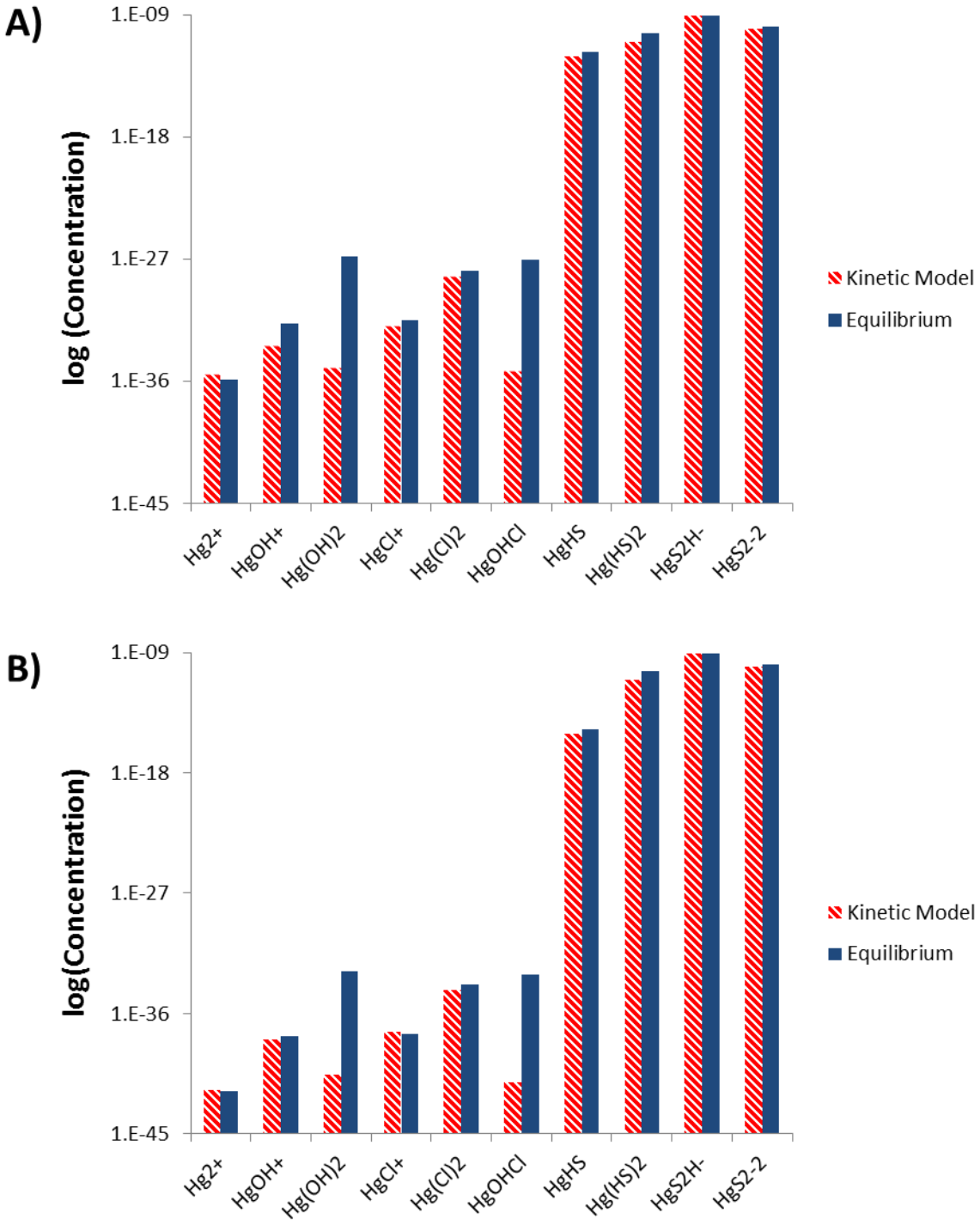

Figure S1. Comparison of dissolved Hg-ligand concentrations (in moles L^{-1}) calculated from the kinetic model and equilibrium model. Water chemistry conditions for the simulations are A) 1 mM Cl^-, 1 µM total dissolved HS^-, 1 nM total dissolved Hg ; B) 1 mM Cl^-, 1 mM total dissolved HS^-, 1 nM total dissolved Hg. Concentrations from the kinetic model correspond to the 0.1 hour time point.

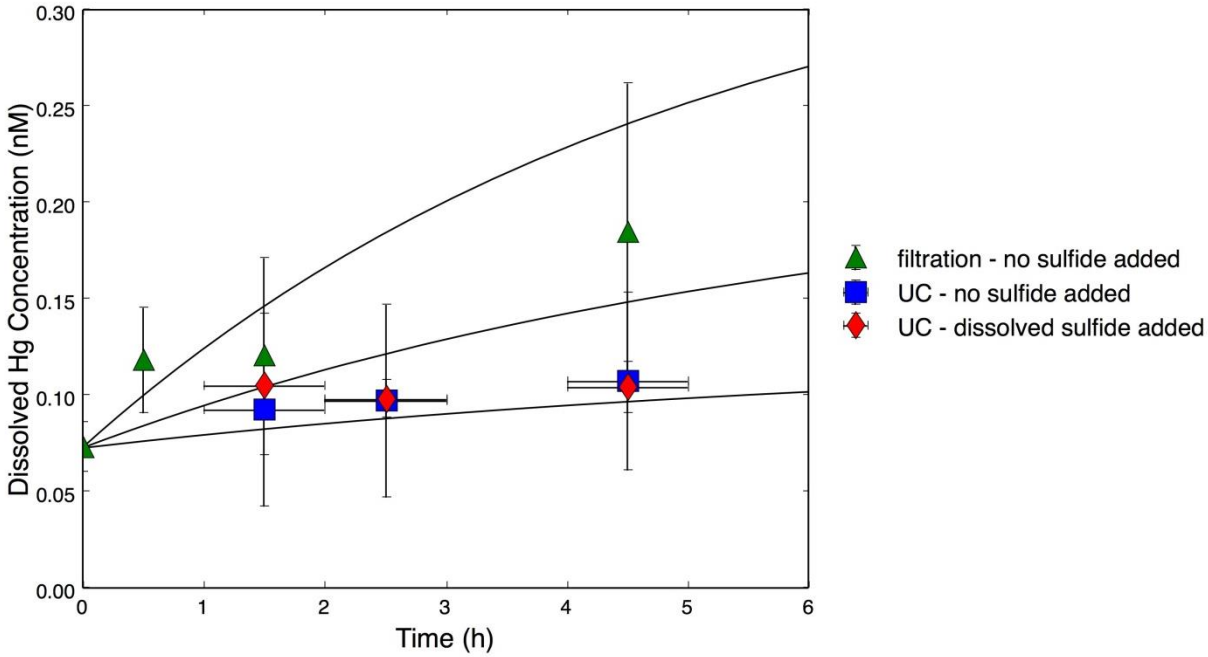

Figure S2. Dissolution of mercury in batch experiments (symbols) comprising of 1 nM of nanoparticulate HgS added to sterile N_2-purged fermentative culture media and model calculations (lines) of dissolved Hg concentration. The dissolution experiments utilized two methods to quantify dissolved Hg concentration: filtration with a 0.02-μm filter (data from Zhang *et al.*[2]) and ultracentrifugation (UC), both under anaerobic conditions. An additional dissolution experiment was performed for a mixture of 1 nM nanoparticulate HgS added to culture media with 10 μM additional sulfide. The vertical error bars correspond to the standard deviation associated with concentration measurements while the horizontal bars correspond to uncertainties in time (± 30 minutes for UC). The data points for UC measurements correspond to the midpoint centrifugation time (i.e., 0.5 hours after the start of the centrifugation process). Model calculations were performed assuming nHgS dissolution rate constant $k_{dis,nHgS}$ value of 0.037 h^{-1} (the best fit for the filtration data) and $k_{dis,nHgS}$ values that were 2-times greater and smaller.

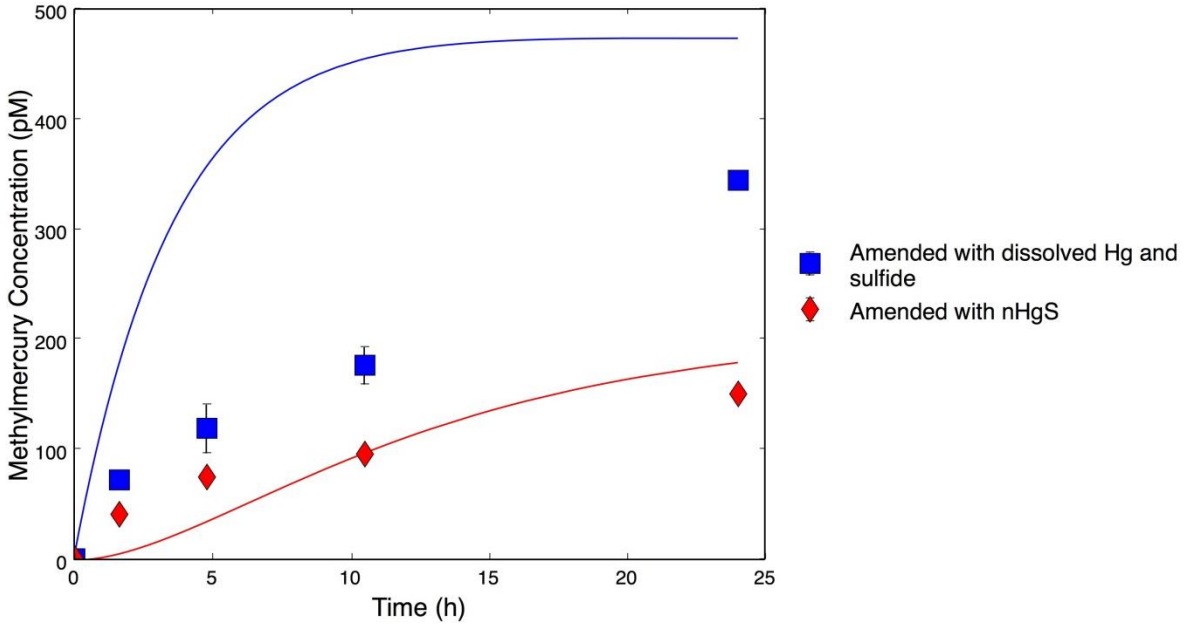

Figure S3. Simulation of methylmercury production (lines) for *D. propionicus* 1pr3 pure cultures exposed to dissolved Hg+S and HgS nanoparticles (data points) described in Zhang *et al.*[2]. The experiments comprised of 5 nM mercury (added as dissolved Hg+S or nanoparticles). Error bars represent ± 1 SD for replicate samples. Data points represent Figure S1-A in Zhang *et al.*[2].

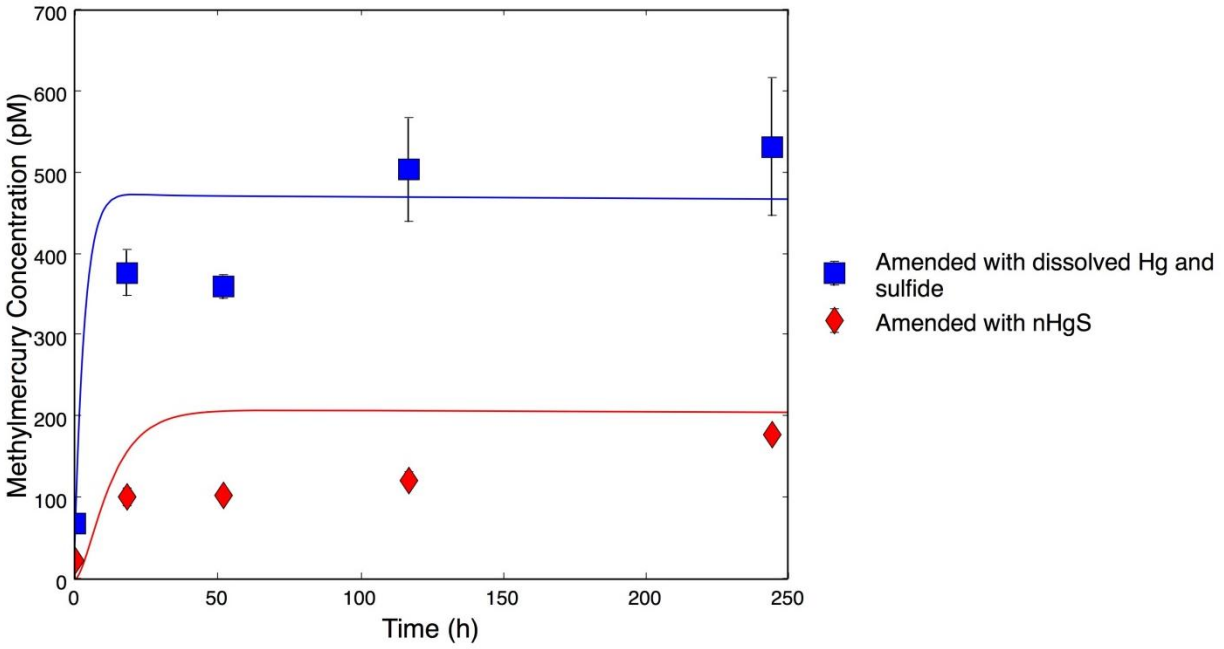

Figure S4. Simulation of methylmercury production (lines) for *D. propionicus* 1pr3 pure cultures exposed to dissolved Hg+S and HgS nanoparticles (data points) described in Zhang *et al.*[2]. The experiments comprised of 5 nM mercury (added as dissolved Hg+S or nanoparticles). Error bars represent ± 1 SD for replicate samples. Data points represent Figure S1-B in *Zhang et al.*[2].

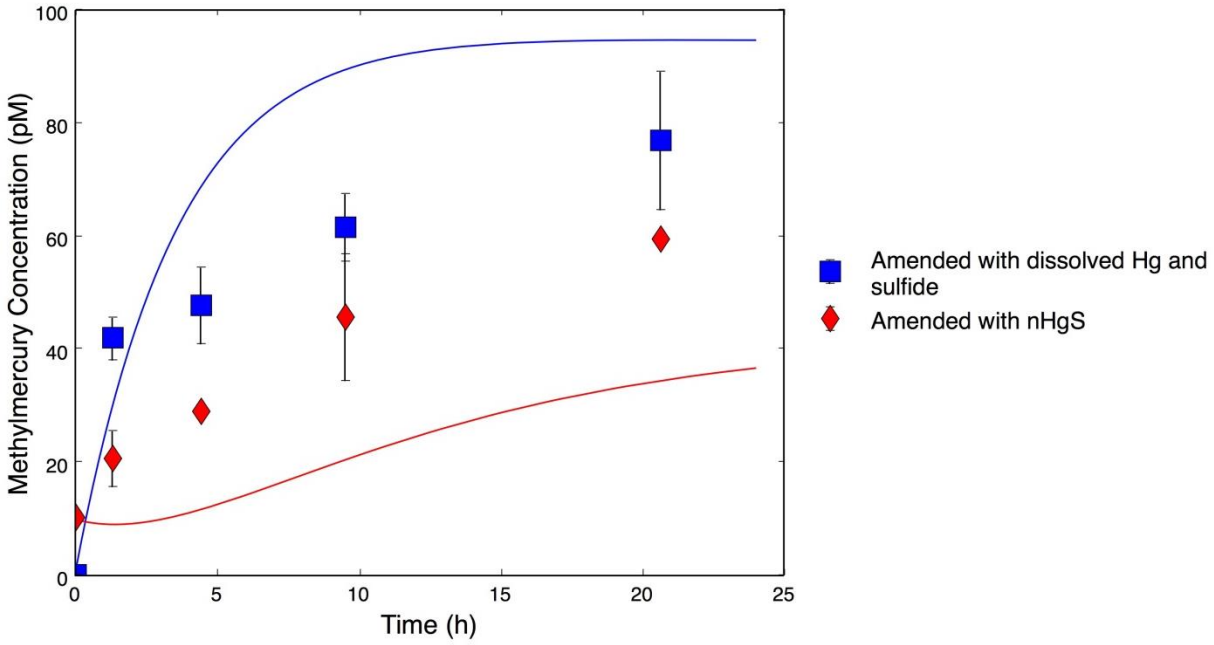

Figure S5. Simulation of methylmercury production (lines) for *D. propionicus* 1pr3 pure cultures exposed to dissolved Hg+S and HgS nanoparticles (data points) described in Zhang *et al.*[2]. The experiments comprised of 1 nM mercury (either as dissolved Hg+S or nanoparticles). Error bars represent ± 1 SD for replicate samples. Data points represent Figure S8 in Zhang *et al.*[2].

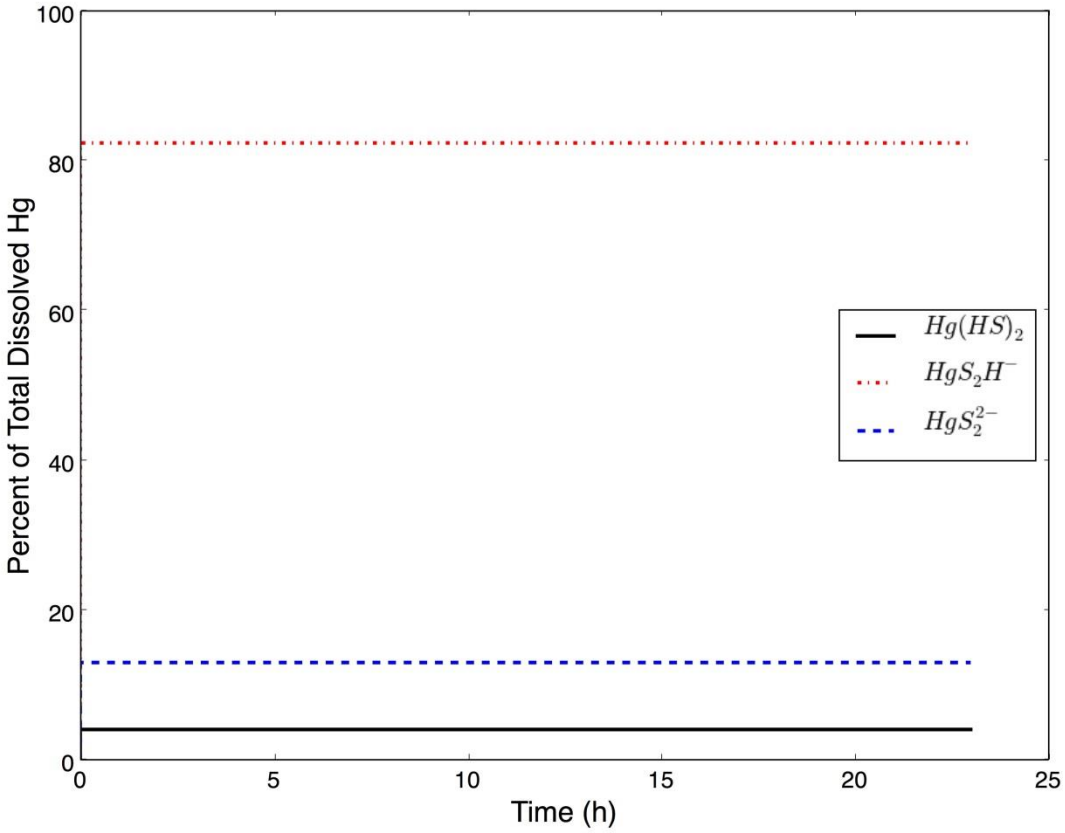

Figure S6. Relative distribution of the top three dissolved Hg species. Lines for both dissolved and nanoparticulate HgS treatments overlap, and thus were plotted as a single line. The three major species account for >99% of the total dissolved Hg in the experimental system.

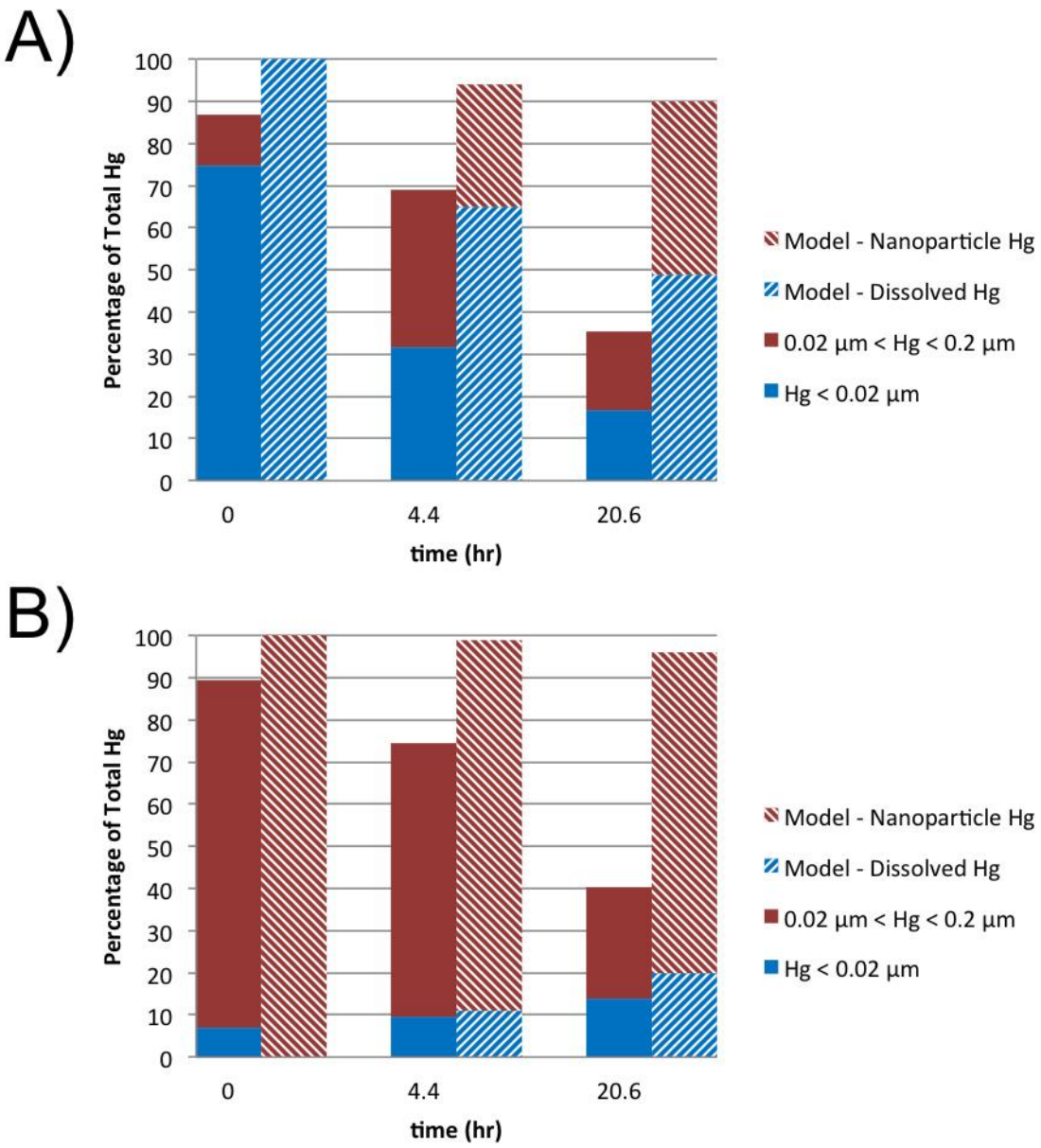

Figure S7. Mercury fractionation comparison of experimental data (Zhang *et al.*[2]) and model output for *D. propionicus* 1pr3 cultures exposed to dissolved (A) and nanoparticulate (B) mercury. From Zhang *et al.*[2], dissolved Hg was defined as Hg passing through a 0.02 µm filter and nanoparticulate Hg was defined as that passing through a 0.2 µm filter but not through a 0.02 µm filter. The kinetic model did not consider sorption to cells, which could be an important mechanism for Hg removal from solution.

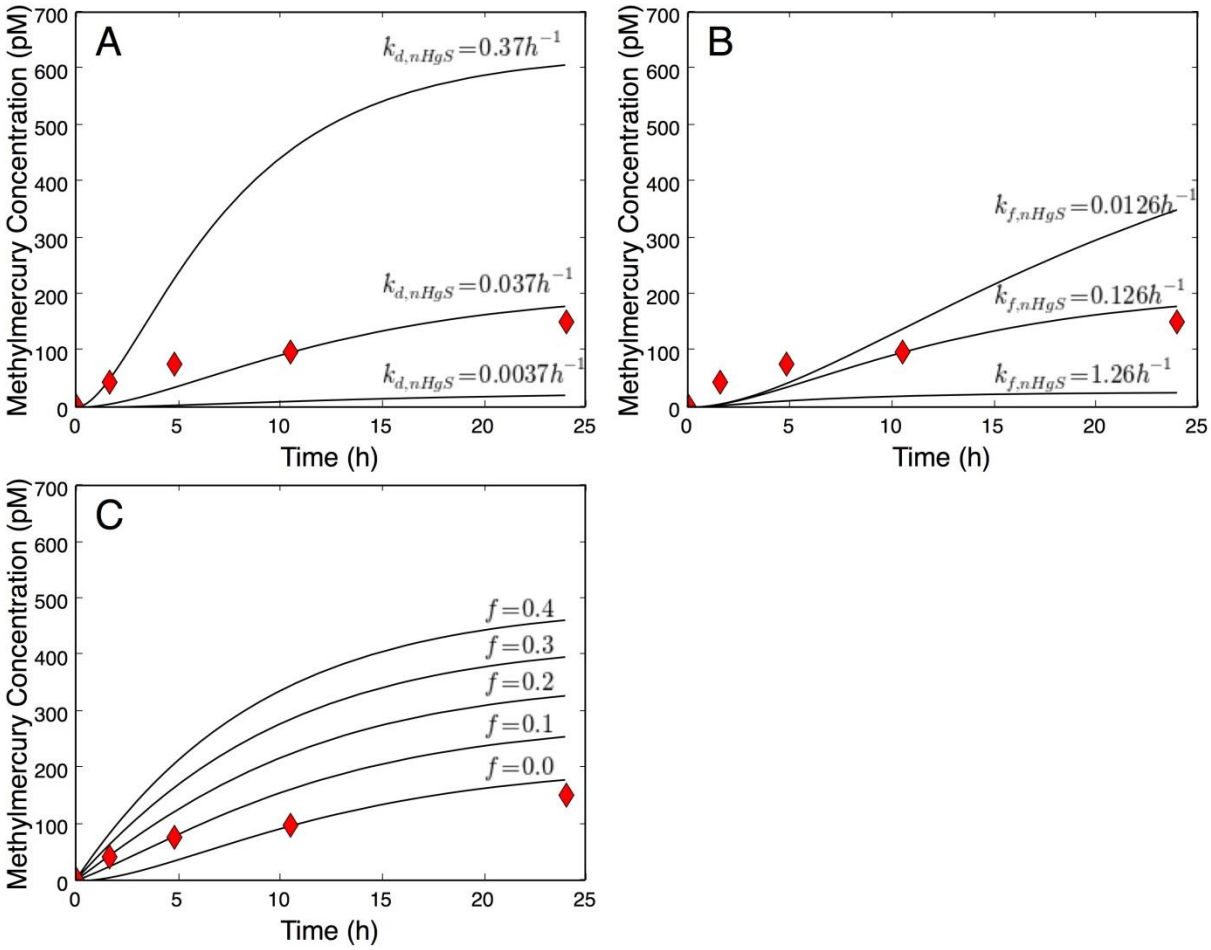

Figure S8. Parametric sensitivity analysis for 5 nM Hg experiments with *D. propionicus* 1 pr3, where A) adjustment of dissolution rate constant ($k_{dis,nHgS}$); B) adjustment of formation rate constant ($k_{f,nHgS}$) ± 1 order of magnitude from fitted parameter value; C) fraction of HgS nanoparticles available for the enhance methylation pathway (f = 0 – 0.4). The data points correspond to data from Zhang *et al.*[2] as well as those plotted in Figure S4.

SI References

1. Morel, F.M.M.; Hering, J.G. *Principles and Applications of Aquatic Chemistry*; John Wiley and Sons, Inc.: New York, **1993**.

2. Zhang T.; Kim, B.; Levard, C.; Reinsch, B.C.; Lowry, G.V.; Deshusses, M.A.; Hsu-Kim, H., Methylation of mercury by bacteria exposed to dissolved, nanoparticulate, and microparticulate mercuric sulfides. *Environ. Sci. Technol.* **2012**, *46*, 6950-6958.

3. Powell, K. J.; Brown, P. L.; Byrne, R. H.; Gajda, T.; Hefter, G.; Sjoberg, S.; Wanner, H., Chemical speciation of environmentally significant metals with inorganic ligands – Part 1: The Hg^{2+}-Cl^-, OH^-, CO_3^{2-}, SO_4^{2-}, and PO_4^{3-} aqueous systems. *Pure Appl. Chem.* **2005,** *77*, (4), 739-800.

4. Benoit, J. M.; Gilmour, C. C.; Mason, R. P.; Heyes, A., Sulfide controls on mercury speciation and bioavailability to methylating bacteria in sediment pore waters. *Environ. Sci. Technol.* **1999,** *33*, (6), 951-957.

5. Dyrssen, D.; Wedborg, M., The sulfur-mercury(II) system in natural-waters. *Water Air Soil Poll.* **1991,** *56*, 507-519.

6. Haitzer, M.; Aiken, G. R.; Ryan, J. N., Binding of mercury(II) to aquatic humic substances: Influence of pH and source of humic substances. *Environ. Sci. Technol.* **2003,** *37*, (11), 2436-2441.

Chapter 4 Supporting Information

Materials and Methods

HgS particle preparation. The mercury stock solution consisted of $Hg(NO_3)_2$ dissolved in 0.1 N HNO_3. Na_2S stocks were prepared by dissolving freshly washed and dried crystals of $Na_2S{\cdot}9H_2O$ in N_2-purged water and were utilized within 20 h of preparation. HgS nanoparticles were synthesized by dissolving 50 μM $Hg(NO_3)_2$ and 50 μM Na_2S with 10 mg-C L^{-1} Suwannee River humic acid (SRHA, International Humic Substances Society) in a solution of 0.1 M $NaNO_3$ and 4 mM sodium 4-(2-hydroxyethyl) piperazine-1-ethanesulfonate (HEPES, pH 7.5, filtered to <0.1 μm). A microparticulate HgS stock suspension was prepared by adding a commercially-purchased metacinnabar powder (β-HgS, Alfa Aesar) into nanopure-filtered water (>18 MΩ-cm). This suspension was mixed end-over-end prior to taking an aliquot for the experiments.

Chemical analysis. MeHg concentration in the slurry samples was analyzed using a modified version of a previous method [263]. In summary, MeHg was extracted from an aliquot of the slurries (containing ~1 g wet sediment) by adding 5 mL of a potassium bromide (KBr) extraction solution, 1 mL of 1 M $CuSO_4$, and 10 mL dichloromethane (CH_2Cl_2) into the slurry samples. The KBr extraction solution consisted of 18% KBr (w/v), 5% concentrated 36 M H_2SO_4 (v/v, trace metal grade) and 0.02% $NH_2OH{\bullet}HCl$ (w/v). The sediment-CH_2Cl_2 mixture was held under static conditions for 1 h and then continuously mixed for 1 h. The CH_2Cl_2 phase of this mixture was then separated from the sediments. MeHg that partitioned in the CH_2Cl_2 was back-extracted into nanopure-filtered water while heating at 70°C for 2 h. At the end of the heating, CH_2Cl_2 was purged from the sample with ultrapure N_2 for 5 min. MeHg concentration in the aqueous phase was quantified by aqueous phase ethylation, gas chromatographic separation, and atomic fluorescence spectrometry (Brooks Rand Model III) [264]. Sediment MeHg concentrations were corrected for extraction efficiency using a standard reference material (CC580) and reported on a dry weight basis.

For total mercury analysis, water samples were first digested with 0.5-2% (v/v) BrCl and analyzed by $SnCl_2$ reduction, gold amalgamation, and cold vapor atomic fluorescence spectrometry [265]. Total mercury in sediment slurries was measured by atomic absorption spectrometry (Milestone DMA-80) [266].

Acid volatile sulfide (AVS) was quantified using acid leaching with 1 N HCl, volatilization of H_2S and subsequent trapping in 0.5 N NaOH, followed by colorimetric detection of sulfide by the Cline method [267,268]. Dissolved Fe(II) concentration was determined using a phenanthroline colorimetric method [269]. SO_4^{2-} and Cl^- concentrations were determined by a Dionex ICS-2000 ion chromatograph (IC) equipped with an AS18 analytical column, ASRS 300 suppressor and KOH eluent generator (Dionex, Sunnyvale, CA). TOC concentration was measured by a TOC-V CPH total organic carbon analyzer (Shimadzu, Kyoto, Japan). Water samples for analysis of major cations were treated with 0.5% (v/v) hydrochloric acid (HCl, trace metal grade) and 2% (v/v) nitric acid (HNO_3, trace metal grade), and analyzed using ICP-MS (Agilent Technologies, Santa Clara, CA). The water content in sediment samples was determined by overnight drying of 4 to 5 g wet sediments at 100°C.

DNA extraction. The genomic DNA from tested sediment samples was extracted using the PowerLyzer Power Soil DNA extraction kit (MoBio Laboratories, Inc., Carlsbad, CA), following the manufacturer's instructions with modifications. In summary, 200 μl of 0.1 M $AlNH_4(SO_4)_2$ was added to 2 g of sediment to remove potential PCR inhibitors, such as humic acids. The modifications of the protocol further consisted of DNA extraction with

phenol/chloroform/isoamyl alcohol (15:24:1) (Sigma-Aldrich, St.Louis, MO), followed by one volume of chloroform/isoamyl alcohol (24:1) extraction procedure. Subsequently, the cells were lysed by a combination of detergents and mechanical disruption with bead beating. In addition, DNA extracts were further purified and concentrated using Genomic DNA Clean & Concentrator (Zymo Research, Irvine, CA). The released DNA was bound to a silica spin filter. The filter was washed, and the DNA was recovered in Milli-Q water. The extracted DNA was examined on 0.8 % (wt/vol) agarose gels in Tris-Acetate-EDTA (TAE) solution after staining with ethidium bromide. Images were obtained using the Gel Doc 2000 system (Bio-Rad, Hercules, CA). The quality of extracted DNA was assessed by measuring A260/A280 ratios using a ND-1000 Spectrophotometer (NanoDrop Products, Wilmington, DE). Measured A260/280 and A260/280 ratios of extracted DNA were mostly > 1.8 and yields averaged in 24.7 - 30 μg g^{-1} sediment wet weight (n=3) for all sites. All samples were subject to cleanup with Qiagen (Qiagen Inc., Valencia, CA) DNA cleanup kits. Following biomass extraction, cell pellets for DNA analysis were stored at −20 ^{o}C for no more than two weeks before further processing.

PCR of total 16S rRNA and *dsrA* gene fragments. Universal primers that amplify the 16S rRNA gene from all bacteria[270] as well as specific primers designed to amplify dissimilatory sulfite reductase *dsrA*[271] unit were employed in quantitative PCR with SYBR green. PCR amplification was performed on StepOne™ Real-Time PCR System (Applied Biosystems, Grand Island, NY) using SYBR® Green Supermix with ROX (Bio-Rad Laboratories, Inc., Hercules, CA). Amplification of the extracted DNA was performed in a 25 μL final volume with 12.5 μL Master Mix QIAGEN (QIAGEN, Hilden, Germany), $MgCl_2$ (final concentration of 1.75 mM), and 1 μL (final concentration of 300 nM) of primer DSR-1F+ (5'-ACSCACTGGAAGCACGCCGG-3') and DSR-R (5'-GTGGMRCCGTGCAKRTTGG-3). The following PCR conditions were used: (1) 15 min at 95 °C; (2) 35 cycles, with 1 cycle consisting of 95 °C for 30 s, 58 °C for 30 s, and 72 °C for 30 s; and (3) a final extension at 72 °C for 7 min.

Amplification of 1114 F (5'-CGGCAACGAGCGCAACCC-3') and 1275 R (5'-CCATTGTAGCACGTGTGTAGCC-3') primer pair was performed in a 25 μL final volume with 12.5 μL Master Mix QIAGEN (QIAGEN, Hilden, Germany), $MgCl_2$ (final concentration of 1.5 mM), and 1 μL (final concentration of 400 nM) of primers. The PCR procedure consisted of 15 min of initial denaturation at 95 °C, followed by 35 cycles denaturation at 94 °C for 30 s, annealing at 60 °C for 30s, and extension at 72 °C for 30s. All samples were amplified in triplicates. The dissociation curve was used to detect the presence of primer dimers or non-specific amplification products in the PCR reactions. The absence of primer dimers or other non-specific amplicons in these reactions were further confirmed by visualizing the PCR samples on an 0.8 % (wt/vol) agarose gel.

Genomic DNA of *E.coli* K12 and *Desulfobulbus propionicus* strain1pr3 (ATCC 33891), isolated using PureLink Genomic DNA extraction kit (Invitrogen, Carlsbad, CA) were used as a positive control for the presence of bacteria and SRB. Standard curves were generated with purified PCR products of the individual genes targeted against the fluorescence corresponding to initial DNA concentration in PCR reactions. Ratios of expressions of *dsrA* and 16S rRNA genes per gram of sediment within one particular sample were reported in the results. It is important to note that this calculation estimates that the copy number of the 16S rRNA gene per genome is the same[272]. Since, different bacteria groups may have 1-15 copies of the 16S rRNA gene per genome[273], the calculation performed supports only relative abundance and not the absolute quantity of bacteria in the sample.

Table S1. Stability constants utilized to calculate saturation indices for $HgS_{(s)}$ (metacinnabar), $FeS_{(s)}$ (mackinawite) and $FeS_{2(s)}$ (pyrite).

	log *K* (I = 0 M, 25°C)	Reference
$H_2S \Leftrightarrow HS^- + H^+$	-7.02	213
$HS^- \Leftrightarrow S^{2-} + H^+$	-17.3	213
$\beta\text{-}HgS_{(s)} + H^+ \Leftrightarrow Hg^{2+} + HS^-$	log K_{s0} = -38 ± 2	229
$Hg^{2+} + HS^- \Leftrightarrow HgSH^+$	30.2	227
$Hg^{2+} + 2HS^- \Leftrightarrow Hg(SH)_2^0$	37.7	274
$Hg^{2+} + 2HS^- \Leftrightarrow HgHS_2^- + H^+$	31.5	274
$Hg^{2+} + 2HS^- \Leftrightarrow HgS_2^{2-} + 2H^+$	23.2	274
$Hg^{2+} + RS_2^{2-} \Leftrightarrow Hg(RS_2)$	log K_{DOM} = 28.7 (aquatic humic)	275
$RS_2^{2-} + H^+ \Leftrightarrow RS_2H^-$	8.4	276
$RS_2H^- + H^+ \Leftrightarrow RS_2H_2$	8.4	276
$Hg^{2+} + H_2O \Leftrightarrow HgOH^+ + H^+$	-3.4	229
$Hg^{2+} + 2H_2O \Leftrightarrow Hg(OH)_2^0 + 2H^+$	-6.2	229
$Hg^{2+} + 3H_2O \Leftrightarrow Hg(OH)_3^- + 3H^+$	-21.1	229
$Hg^{2+} + Cl^- \Leftrightarrow HgCl^+$	7.3	229
$Hg^{2+} + 2Cl^- \Leftrightarrow Hg(Cl)_2^0$	14.0	229
$Hg^{2+} + 3Cl^- \Leftrightarrow Hg(Cl)_3^-$	15.0	229
$Hg^{2+} + Cl^- + H_2O \Leftrightarrow HgOHCl^0 + H^+$	4.2	229
$Fe^{2+} + HS^- \Leftrightarrow FeS_{(s),\ mackinawite} + H^+$	3.6	213
$Fe^{2+} + HS^- + S^0_{(s)} \Leftrightarrow FeS_{2(s),\ pyrite} + H^+$	14.2	236
$Fe^{2+} + HS^- \Leftrightarrow Fe(HS)^+$	4.34	277
$Fe^{2+} + 2HS^- \Leftrightarrow Fe(HS)_{2(aq)}$	8.95	213
$Fe^{2+} + 3HS^- \Leftrightarrow Fe(HS)_3^-$	10.99	213
$Fe^{2+} + H_2O \Leftrightarrow FeOH^+ + H^+$	-9.40	213
$Fe^{2+} + 2H_2O \Leftrightarrow Fe(OH)_{2(aq)} + 2H^+$	-20.49	213
$Fe^{2+} + 3H_2O \Leftrightarrow Fe(OH)_3^- + 3H^+$	-28.99	213
$Fe^{2+} + Cl^- \Leftrightarrow FeCl^+$	-0.20	213

a.

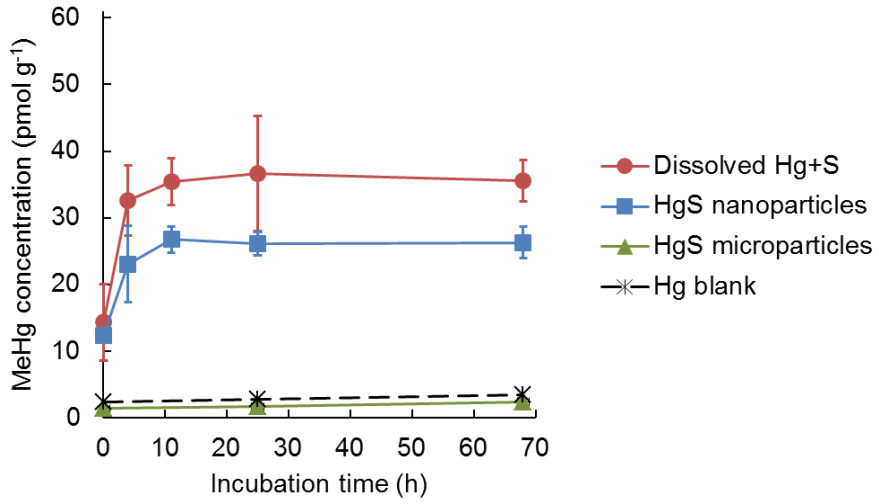

b.

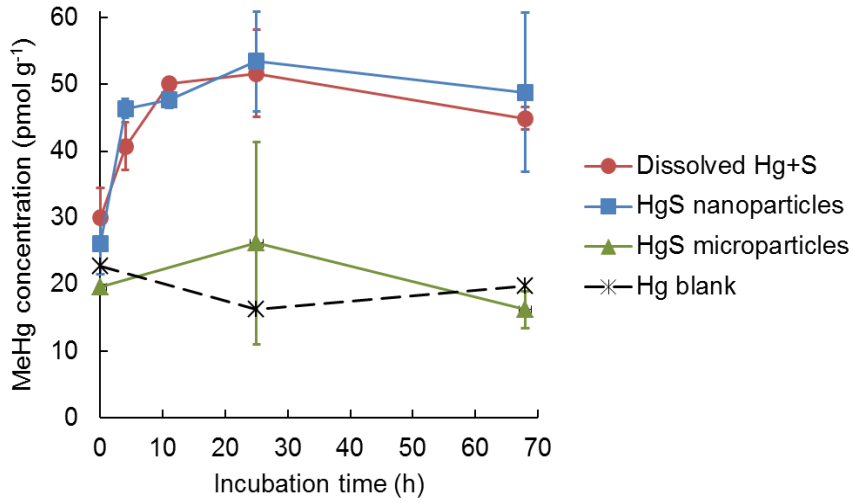

Figure S1. Net MeHg production in the slurry microcosms after the addition of 5 nmol Hg g-1 (dw sediment) in the form of dissolved $Hg(NO_3)_2$ and Na_2S, HgS nanoparticles or HgS microparticles in Experiment 2. The slurries were prepared with sediments from **(a)** Site 1 and **(b)** Site 3. The MeHg concentration was normalized to the dry sediment mass in each serum bottle. Incubation time represents the time after Hg amendments. The error bars represent 1 s.d. for replicate samples (n=2-3) in the test groups. Single replicate of slurries were incubated for the Hg blank control.

a.

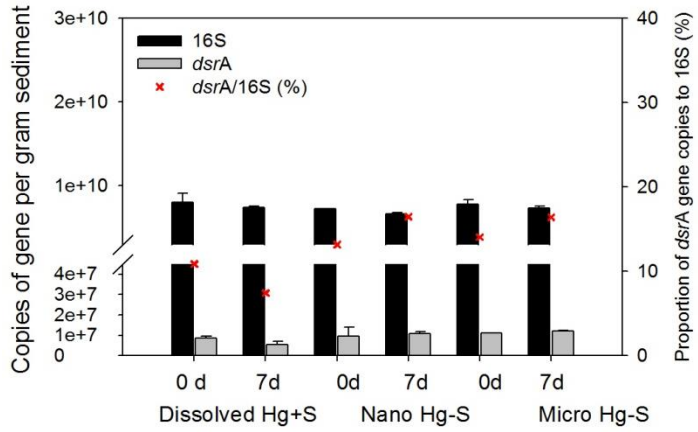

b.

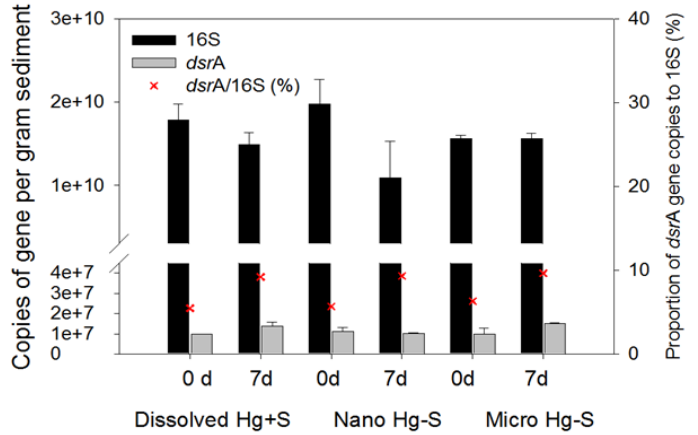

c.

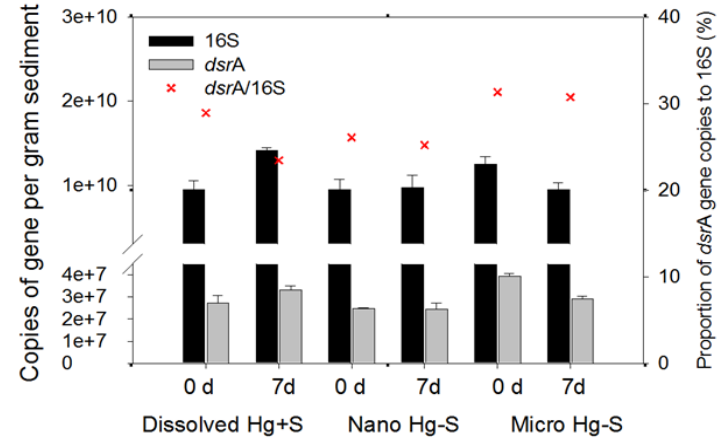

Figure S2. Abundance of 16S rRNA and *dsr*A genes in the slurry microcosms exposed to 2 nmol g^{-1} (dw) dissolved $Hg(NO_3)_2$ and Na_2S, HgS nanoparticles or HgS microparticles in Experiment 1. The slurries were prepared with sediments from **(a)** Site 1, **(b)** Site 2 and **(c)** Site 3. The copy numbers of 16S rRNA and *dsr*A genes were normalized to the dry sediment mass in each serum bottle. Slurry samples were collected at two time points during the methylation experiments: 0 day (Immediately after Hg addition) and 7 days. The error bars represent 1 s.d. for duplicate samples.

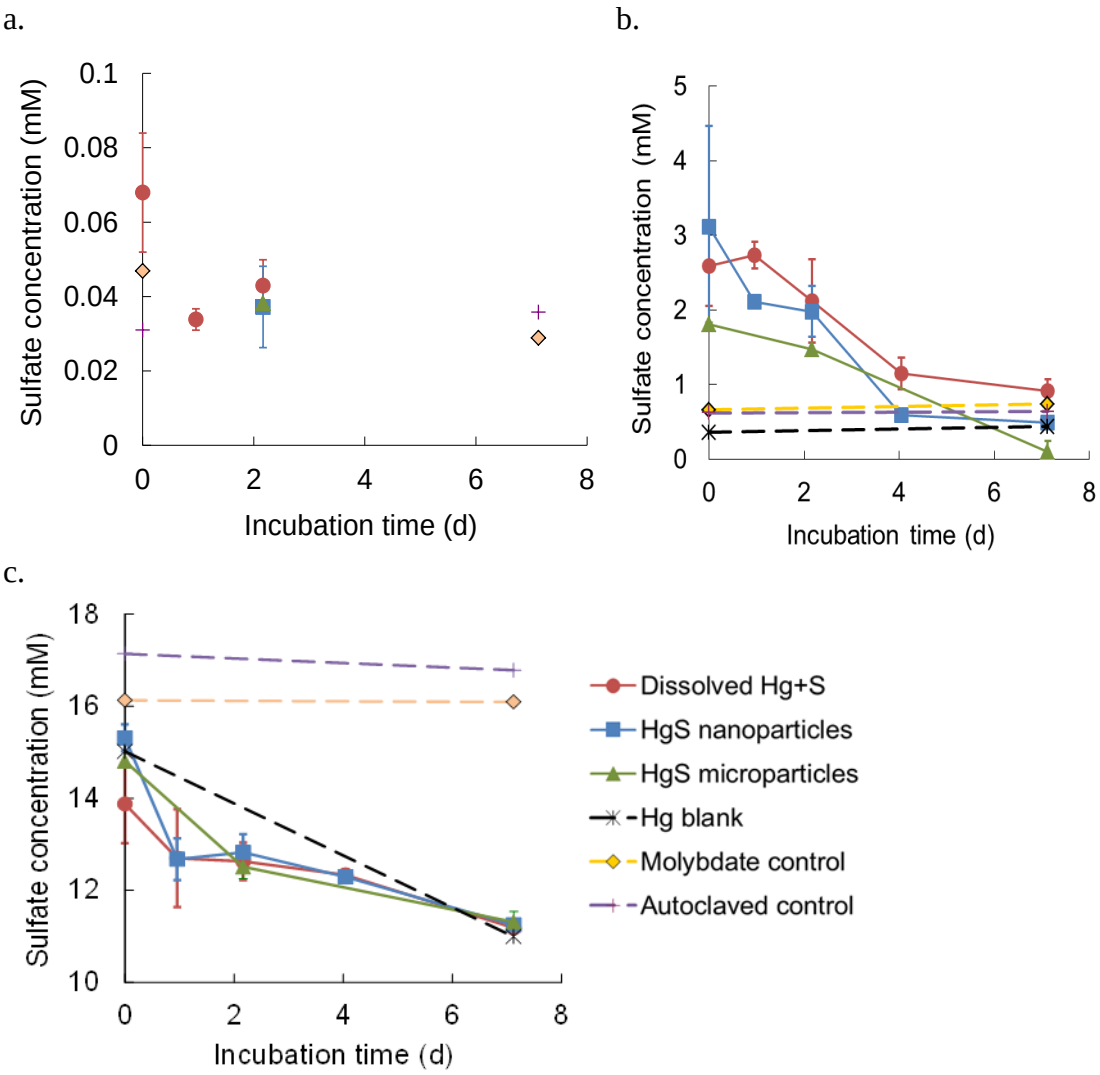

Figure S3. Sulfate concentrations in slurry microcosms exposed to 2 nmol g^{-1} (dw) dissolved $Hg(NO_3)_2$ and Na_2S, HgS nanoparticles or HgS microparticles in Experiment 1. The slurries were prepared with sediments and water from **(a)** Site 1, **(b)** Site 2 and **(c)** Site 3. The original water samples used to prepare the slurries contained 0.69, 8.9, and 22 mM sulfate, respectively (see Table 2). The error bars represent 1 s.d. for duplicate samples in the test groups. Single replicate of slurries were incubated for the controls. After 2.2-day incubation, sulfate was only detected in the samples collected from molybdate-treated and autoclaved slurries with sediment from Site 1 (**a**).

a.

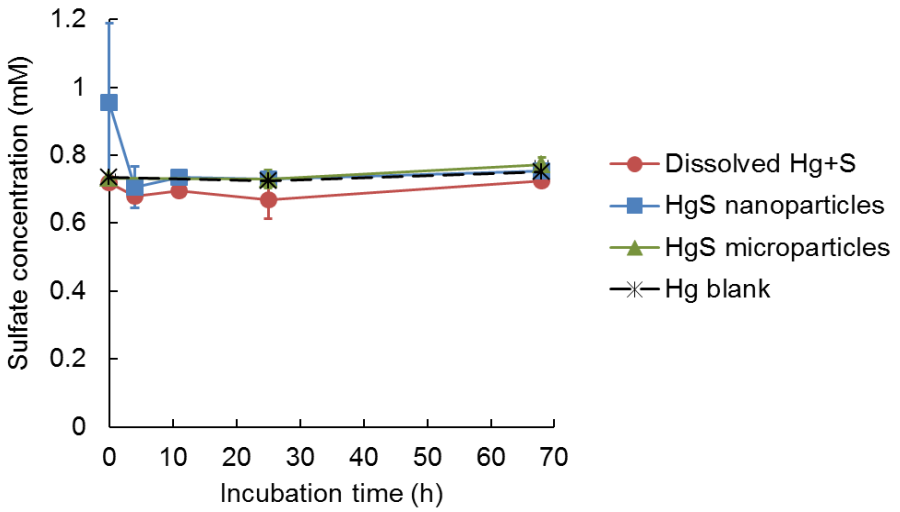

b.

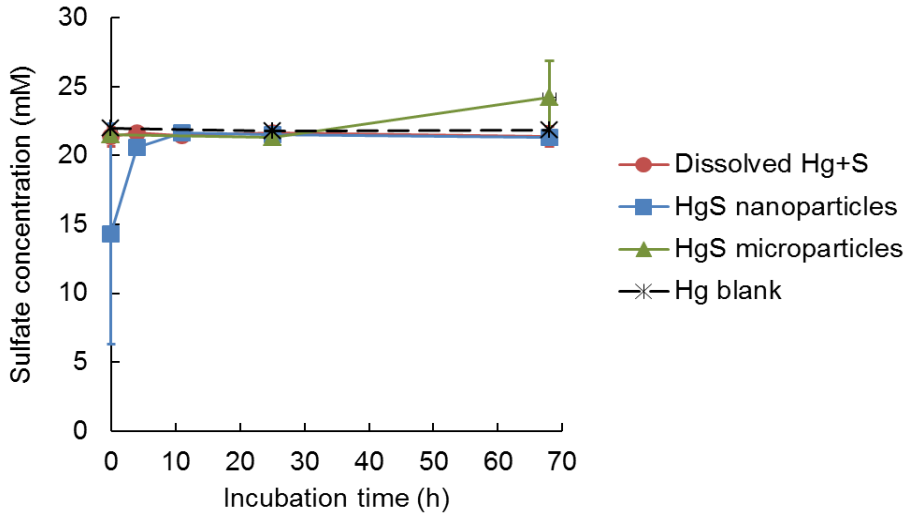

Figure S4. Sulfate concentrations in slurry microcosms exposed to 5 nmol g^{-1} (dw) dissolved $Hg(NO_3)_2$ and Na_2S, HgS nanoparticles or HgS microparticles in Experiment 2. The slurries were prepared with sediments from **(a)** Site 1 and **(b)** Site 3. The error bars represent 1 s.d. for replicate samples (n=2-3) in the test groups. Single replicate of slurries were incubated for the Hg blank control.

a.

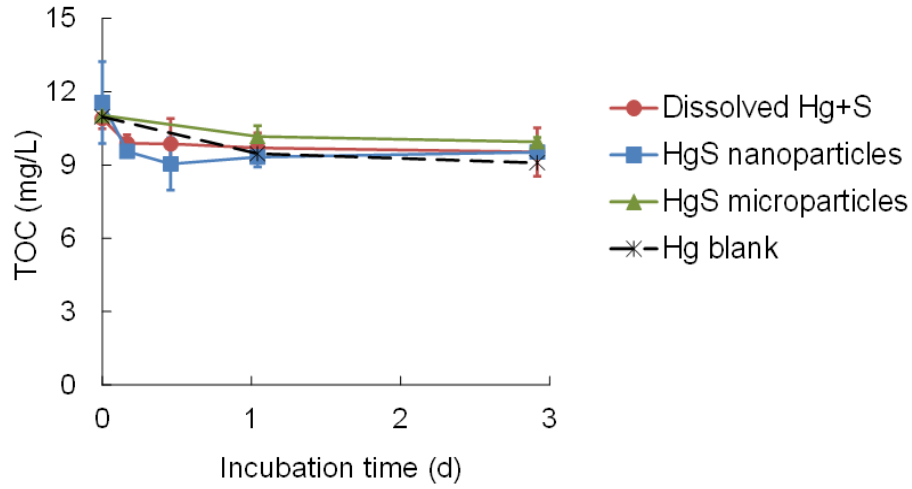

b.

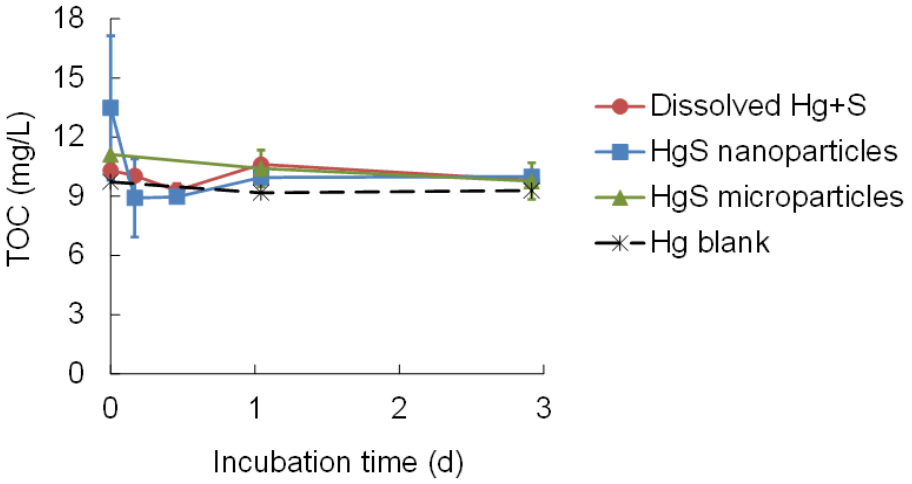

Figure S5. Total organic carbon (TOC) concentrations in water samples withdrawn from the sediment slurries exposed to 50 nmol mercury (either dissolved $Hg(NO_3)_2$ and Na_2S, HgS nanoparticles or HgS microparticles) in Experiment 2. The slurries were prepared with sediments from **(a)** Site 1 and **(b)** Site 3. The error bars represent 1 s.d. of replicate samples (n=2-3). Single replicate of slurries were incubated for the controls.

a.

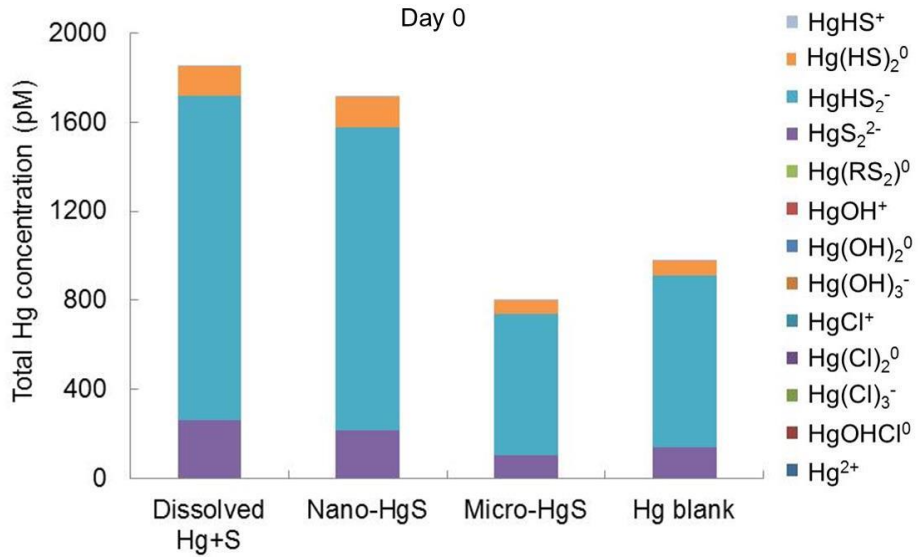

b.

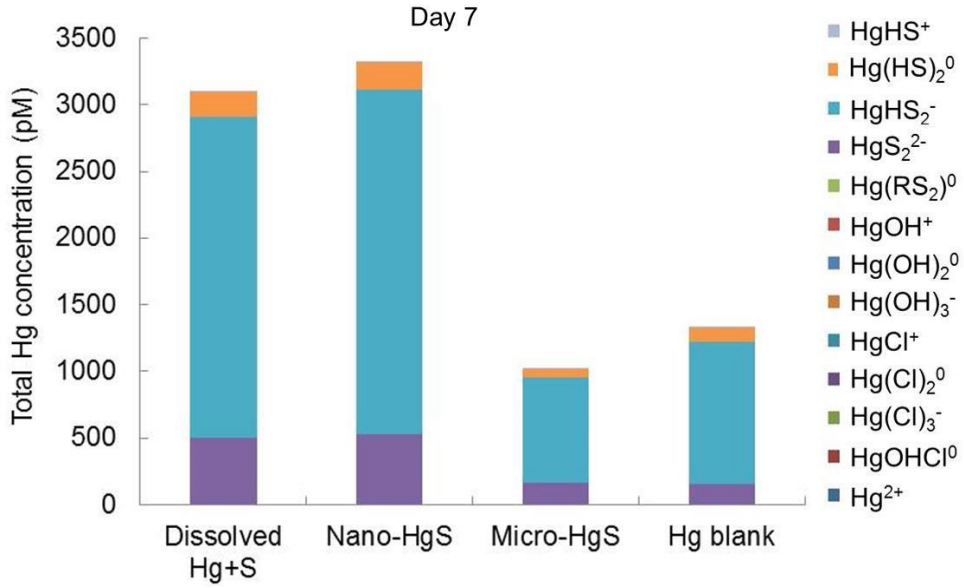

Figure S6. Speciation of dissolved Hg (i.e., total Hg remained in the aqueous phase after ultracentrifugation at 370,000 *g* for 1 h) in sediment slurries amended with 2 nmol g^{-1} (dw) (345 nmol Hg per L of water was added into the slurries) dissolved $Hg(NO_3)_2$ and Na_2S, HgS nanoparticles or HgS microparticles in Experiment 1. The slurries were prepared with sediments from Site 3. Samples were collected immediately (**a**) and 7 days (**b**) after mercury amendments. 'Hg blank' represents slurries without mercury addition.

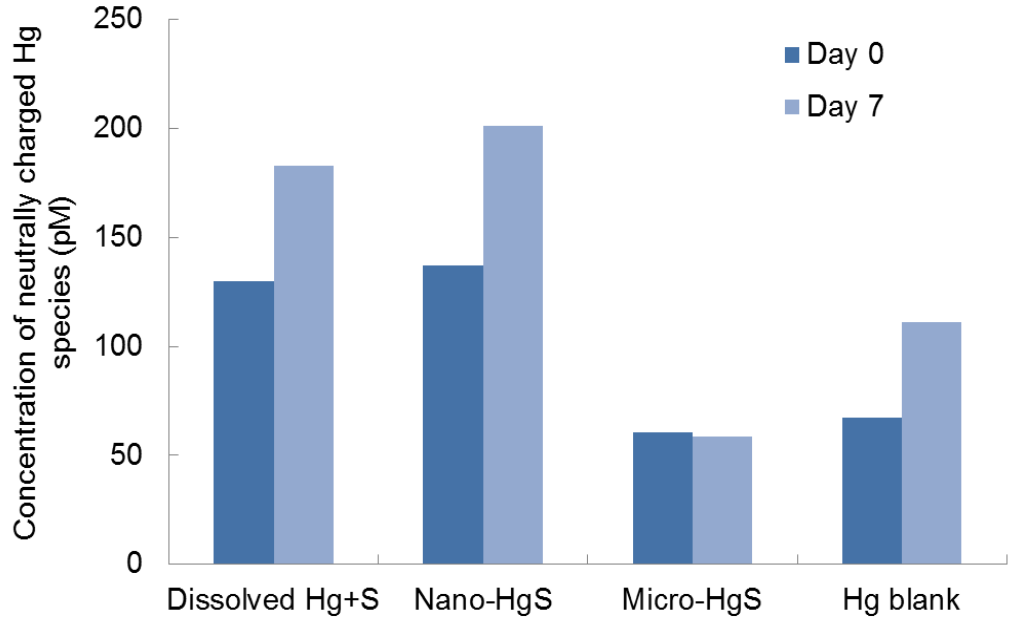

Figure S7. Concentration of neutrally charged Hg species (i.e., $HgOHCl^0$, $Hg(Cl)_2^0$, $Hg(OH)_2^0$, $Hg(RS_2)^0$, $Hg(HS)_2^0$) in the aqueous phase after ultracentrifugation (at 370,000 *g* for 1 h) of sediment slurries amended with 2 nmol g^{-1} (dw) (345 nmol Hg per L of water was added into the slurries) dissolved $Hg(NO_3)_2$ and Na_2S, HgS nanoparticles or HgS microparticles in Experiment 1. The slurries were prepared with sediments from Site 3. Samples were collected immediately and 7 days after mercury amendments. 'Hg blank' represents slurries without mercury addition.

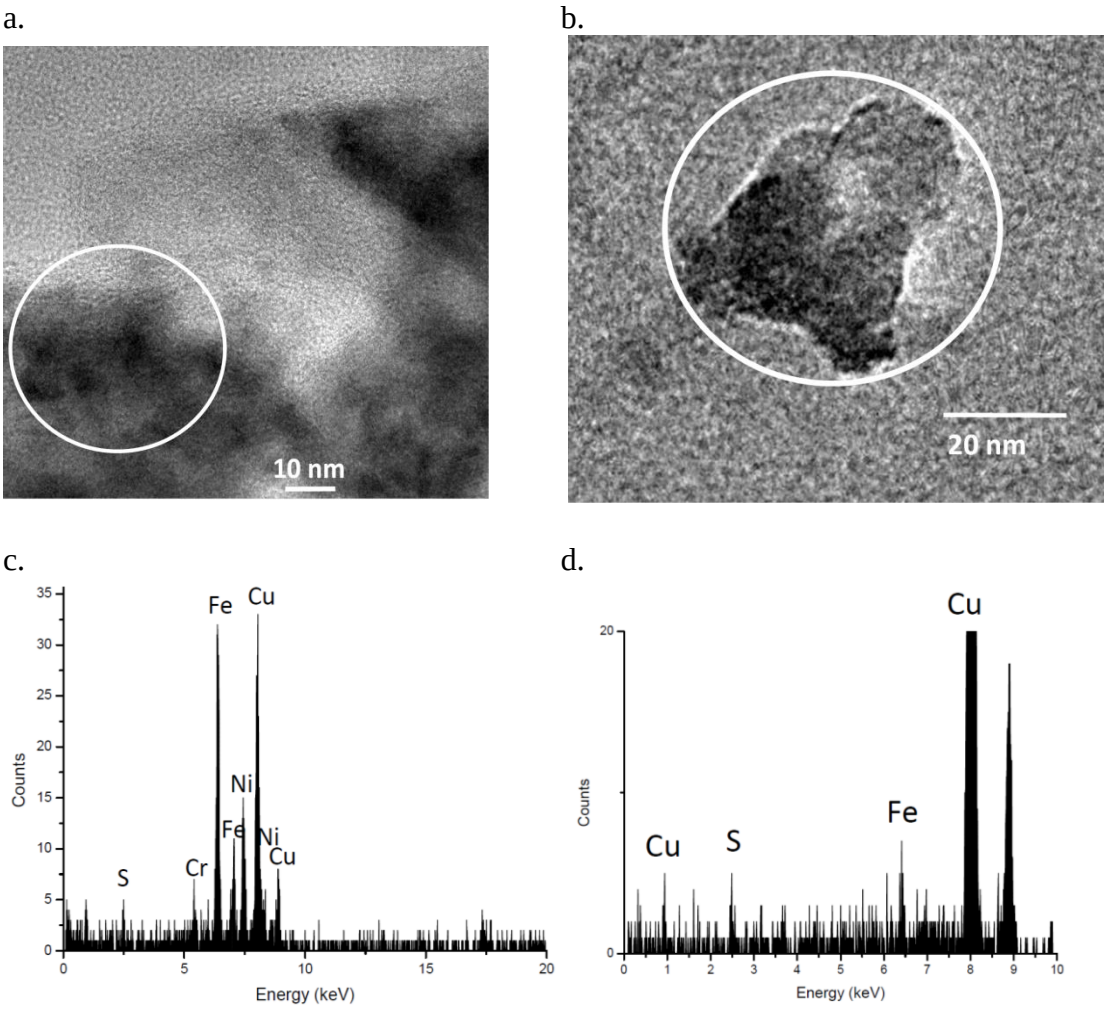

Figure S8. TEM images **(a and b)** and EDX spectra **(c and d)** of 0.2-µm filtered water samples withdrawn from the Site 1 slurries amended with 2 nmol g^{-1} (dw) dissolved $Hg(NO_3)_2$ and Na_2S **(a and c)** or HgS nanoparticles **(b and d)** in Experiment 1. Elemental composition of the particles in white circles was determined by EDX. The Cu peaks are from the sample grid.

Fig. 4.1a								
	Supernatant Hg after 6,700 g for 5 min		Supernatant Hg after 370,000 g for 1 h					
% Total Hg	Mean	Error	Mean	Error				
Dissolved Hg-	90.7%	3.1%	75.9%	2.1%				
Nano-HgS	85.5%	2.8%	7.7%	0.2%				
Micro-HgS	1.5%	0.2%	<1 %	<1 %				
Fig. 4.1b								
Total Hg	Supernatant Hg after 3000 g, 20 min		Supernatant Hg after 6700 g, 5 min		Supernatant Hg after 370,000 g, 1 hr		< 0.2 um nylon	
(pM)	Mean	Error	Mean	Error	Mean	Error	Mean	Error
Site 1	693.6	94.9	59.1	9.5	22.9	3.7	33.9	9.1
Site 2	184.5	16.8	36.7	2.2	12.7	2.1	22.1	2.5
Site 3	146.8	19.0	30.1	11.1	30.4	0.6	31.4	0.0

Fig. 4.2a - Site 1												
MeHg in sediment (pmol/g)	Dissolved Hg+S		HgS nanoparticles		HgS microparticles		Hg blank		Molybdate control		Autoclaved control	
Days	Mean	Error	Mean	Error	Mean	Error	Mean	Error	Mean	Error	Mean	Error
0.0	19.2	2.8	16.6	1.5	5.8	0.0	4.2		13.1		12.8	
1.0	31.4	1.2	31.5	8.2								
2.2	41.8	1.1	48.3	7.1	7.4	1.0						
4.0	75.3	8.6	66.7	1.7								
7.1	81.8	6.9	78.0	13.4	10.2	0.6	7.6		17.5		13.0	
Fig.4.2b - Site 2												
MeHg in sediment (pmol/g)	Dissolved Hg+S		HgS nanoparticles		HgS microparticles		Hg blank		Molybdate control		Autoclaved control	
Days	Mean	Error	Mean	Error	Mean	Error	Mean	Error	Mean	Error	Mean	Error
0.0	61.3	2.6	33.0	7.5	7.2	0.4	13.6		25.6		10.6	
1.0	101.7	1.4	55.1	24.8								
2.2	91.8	10.1	82.7	1.2	6.9	0.0						
4.0	135.2	15.0	66.7	3.7								
7.1	341.6	4.7	106.0	13.7	16.4	6.7	1.2		4.7		16.4	
Fig. 4.2c - Site 3												
MeHg in sediment (pmol/g)	Dissolved Hg+S		HgS nanoparticles		HgS microparticles		Hg blank		Molybdate control		Autoclaved control	
Days	Mean	Error	Mean	Error	Mean	Error	Mean	Error	Mean	Error	Mean	Error
0.0	55.2	2.5	40.8	3.0	42.6	0.0	55.0		48.9		46.2	
1.0	83.7	8.5	39.2	3.3								
2.2	189.4	24.0	76.0	30.8	74.2	3.7						
4.0	209.9	4.5	95.8	11.2								
7.1	225.3	20.9	117.6	4.5	60.0	4.5	58.6		61.3		46.3	

Fig. 4.4a: Site 1-Day 0				
Total Hg	Dissolved Hg		Colloidal Hg	
(pM)	Mean	Error	Mean	Error
Dissolved Hg+S	444.6	152.2	4232.8	1671.6
Nano-HgS	267.7	36.1	1341.0	99.3
Micro-HgS	8.0		84.5	
Hg blank	22.0		80.7	
Fig. 4.4b: Site 1-Day 7				
Total Hg	Dissolved Hg		Colloidal Hg	
(pM)	Mean	Error	Mean	Error
Dissolved Hg+S	177.9	8.2	6285.3	997.6
Nano-HgS	185.6	93.1	7793.3	3469.4
Micro-HgS	15.4	0.2	246.1	130.0
Hg blank	32.7		187.2	
Fig. 4.4c: Site 3-Day 0				
Total Hg	Dissolved Hg		Colloidal Hg	
(pM)	Mean	Error	Mean	Error
Dissolved Hg+S	1856.8	71.8	464.5	97.9
Nano-HgS	1725.4	178.0	115.8	59.7
Micro-HgS	797.2	129.2	568.3	358.9
Hg blank	977.8		0.0	
Fig. 4.4d: Site 3-Day 7				
Total Hg	Dissolved Hg		Colloidal Hg	
(pM)	Mean	Error	Mean	Error
Dissolved Hg+S	3095.1	241.3	1.0	241.5
Nano-HgS	3320.3	278.2	1.7	278.1
Micro-HgS	1017.3	265.6	735.5	160.2
Hg blank	1332.3		119.8	

Fig. 4.5a: Site 1-Day 0				
$\log(Q/K_{S0})$	Metacinnabar ($\log K_{s0}$=-36)	Metacinnabar ($\log K_{s0}$=-40)	Mackinawite	Pyrite
Dissolved Hg+S	1.517	5.517	1	11.6
Nano-HgS	1.177	5.177	0.769	11.369
Micro-HgS	-0.055	3.945	0.678	11.278
Hg blank	-0.105	3.895	0.607	11.207
Fig. 4.5b: Site 1-Day 7				
$\log(Q/K_{S0})$	Metacinnabar ($\log K_{s0}$=-36)	Metacinnabar ($\log K_{s0}$=-40)	Mackinawite	Pyrite
Dissolved Hg+S	1.468	5.468	0.589	11.189
Nano-HgS	1.321	5.321	0.536	11.136
Micro-HgS	0.168	4.168	0.607	11.207
Hg blank	0.198	4.198	0.517	11.117
Fig. 4.5c: Site 3-Day 0				
$\log(Q/K_{S0})$	Metacinnabar ($\log K_{s0}$=-36)	Metacinnabar ($\log K_{s0}$=-40)	Mackinawite	Pyrite
Dissolved Hg+S	-1.042	2.958	-0.182	10.418
Nano-HgS	-0.511	3.489	0.757	11.357
Micro-HgS	-1.23	2.77	-0.232	10.368
Hg blank	-1.142	2.858	0.397	10.997
Fig. 4.5d: Site 3-Day 7				
$\log(Q/K_{S0})$	Metacinnabar ($\log K_{s0}$=-36)	Metacinnabar ($\log K_{s0}$=-40)	Mackinawite	Pyrite
Dissolved Hg+S	-0.93	3.07	-0.093	10.507
Nano-HgS	-0.714	3.286	-0.247	10.353
Micro-HgS	-1.266	2.734	-0.107	10.493
Hg blank	-1.282	2.718	-0.823	9.777

Scientific/Technical Publications

Journal Papers

Hsu-Kim, H.; Kucharzyk, K.H.; Zhang, T.; Deshusses, M.A. (2013). Mechanisms regulating mercury bioavailability for methylating microorganisms in the aquatic environment: A critical review. *Environ. Sci. & Technol*. 47(6), 2441-2456. DOI: 10.1021/es304370g.

Zhang, T.; Kim, B.; Levard, C.; Reinsch, B.C.; Lowry, G.V.; Deshusses, M.A.; Hsu-Kim, H. (2012). Methylation of mercury by bacteria exposed to dissolved, nanoparticulate, and microparticulate mercuric sulfides. *Environ. Sci. & Technol*. 46(13), 6950-6958. DOI: 10.1021/es203181m

Zhang, T.; Kucharzyk, K.H.; Kim, B.; Deshusses, M.A.; Hsu-Kim, H. (2014). Net methylation of mercury in estuarine sediment microcosms amended with dissolved, nanoparticulate, and microparticulate mercuric sulfides. Manuscript submitted to *Environ. Sci. & Technol*. DOI: 10.1021/es500336j.

Ticknor, J.L.; Zhang, T.; Deshusses, M.A.; Hsu-Kim, H. Kinetic Modeling of Mercury Speciation and Methylation in Bacterial Cultures Exposed to Dissolved and Nanoparticulate Mercuric Sulfides. Manuscript submitted to *Environmental Modeling*.

Conference presentations

Hsu-Kim H., Zhang T., Kucharzyk K., Ticknor J., Pham A., Deshusses M.A. Nanoscale mercury-sulfide-organic matter interactions: Implications for mercury bioavailability and methylation potential. International Conference on Mercury and a Global Pollutant. Edinburg, UK. July 29 – August 2, 2013.

Zhang T., M.A. Deshusses, H. Hsu-Kim. Production of methylmercury by sulfate-reducing bacteria exposed to mercuric sulfide nanoparticles. 243rd ACS National Meeting, San Diego, CA. March 25-29, 2012.

Hsu-Kim H., Zhang T., Kucharyzyk K.H., Ticknor J., Pham A.L.T., Deshusses M.A. Nanogeochemistry of a neurotoxin: Reactivity and microbial methylation potential of nanoscale mercury sulfides. 245th National Spring Meeting of the American-Chemical-Society. New Orleans, LA. April 7-11, 2013.

Zhang T., Hsu-Kim H., Deshusses M.A. Biomethylation potential of mercury depends on the kinetics of HgS precipitation. 21th Annual V.M. Goldschmidt Conference Prague, Czech Republic. August 15-19, 2011.

Zhang T., Hsu-Kim H., Deshusses M.A. The influence of kinetically-limited mercury sulfide precipitation on mercury bioavailability for methylation by pure cultures of sulfate reducing bacteria. International Conference on Mercury as a Global Pollutant., Halifax, Nova Scotia. July 25-29, 2011.

Hsu-Kim H., Deonarine A., Gondikas A., Zhang T., Lau B.L.T., Aiken G.R., Ryan J.N., Mason A., Auffan M., Deshusses M.A. Nanoscale Metal Sulfide-Organic Matter Interactions: Implications for Mercury Speciation and Methylation Potential. International Conference on Mercury as a Global Pollutant., Halifax, Nova Scotia. July 25-29, 2011.

Hsu-Kim H., Deonarine A., Gondikas A., Zhang T., Deshusses M.A. Natural organic matter interactions with metal-based nanomaterials: Implications for aggregation, dissolution, and bioavailability. AEESP Education and Research Conference. Tampa, FL. July 10-12, 2011.

Zhang T., Hsu-Kim H. Deshusses M.. Microbial methylation of mercury sulfide nanoparticles: Influence of particle size and crystallinity on methylation potential. 3rd Annual International Conference on the Environmental Implications of NanoTechnology. Durham, NC. May 9-11, 2011.

Zhang T., Hsu-Kim H., Deshusses M.A. (2010). Microbial methylation of mercury sulfides: comparison between dissolved Hg-sulfides, nanoparticulate and bulk scale HgS. Partners in Environmental Technology Technical Symposium & Workshop. Washington, DC. November 30 – December 2, 2010.

Zhang T., Hsu-Kim H., Deshusses M.A. (2010). Microbial methylation of mercury sulfides: comparison between dissolved Hg-sulfides, nanoparticulate and bulk scale HgS. SETAC North America 31st Annual Meeting. Portland, OR. November 7-11, 2010.

Deshusses M.A., Zhang T., Hsu-Kim H. (2010). Microbial methylation of mercury sulfides: comparison between dissolved Hg-sulfides, nanoparticulate and bulk scale HgS. 20th Annual V.M. Goldschmidt Conference Knoxville, TN. June 21-25, 2010.